

MULTIFUNCTIONAL POLYETHER ARCHITECTURES:

Versatile Materials for Surface Attachment and Functionalization

Dissertation
zur Erlangung des Grades
„Doktor der Naturwissenschaften“

im Promotionsfach Makromolekulare Chemie

im Fachbereich Chemie, Pharmazie und Geowissenschaften
der Johannes Gutenberg-Universität
in Mainz

Valerie Sophie Wilms (geb. Reuß)

geboren in Mainz

Mainz, den 12. Oktober 2012

JOHANNES GUTENBERG
UNIVERSITÄT MAINZ



Dekan: [REDACTED]

Prodekan: [REDACTED]

1. Berichterstatter: [REDACTED]

2. Berichterstatter: [REDACTED]

Tag der mündlichen Prüfung: 14.11.2012

Hiermit versichere ich gemäß § 10 Abs. 3d der Promotionsordnung vom 24.07.2007, dass ich die als Dissertation vorgelegte Arbeit selbst angefertigt und alle benutzten Hilfsmittel (Literatur, Apparaturen, Material) in der Arbeit angegeben habe.

Die als Dissertation vorgelegte Arbeit wurde in der Zeit von Oktober 2009 bis Oktober 2012 am Institut für Organische Chemie der Johannes Gutenberg-Universität Mainz im Arbeitskreis von Univ.-Prof. Dr. Holger Frey angefertigt.

TABLE OF CONTENTS

Motivation and Objectives	4
Abstract	7
Graphical Abstract	10
1) Introduction	13
1.1) Aminofunctional Polyethers: Smart Materials for Applications in Solution and on Surfaces	14
2) Multiaminofunctional Polyethers	49
2.1) Thermoresponsive Copolymers of Ethylene Oxide and <i>N,N</i> -Diethyl Glycidyl Amine: Polyether Polyelectrolytes and PEGylated Gold Nanoparticle Formation	50
Supporting Information	61
2.2) <i>N,N</i> -Diallylglycidylamine: A Key Monomer for Amino-Functional Poly(ethylene glycol) Architectures.....	71
Supporting Information	91
3) Multifunctional PEGs for Surface Functionalization	106
3.1) Catechol-initiated Polyethers: Multifunctional Hydrophilic Ligands for PEGylation and Functionalization of Metal Oxide Nanoparticles	107
Supporting Information	125
3.2) Novel Cationic Polyether Block Copolymers for Passivation and Functionalization of Glass Surfaces.....	134
4) Investigation of Thermoresponsive Polyethers with EPR Spectroscopy	148
4.1) How Structure-Related Collapse Mechanisms Determine Nanoscale Inhomogeneities in Thermoresponsive Polymers	149
Supporting Information	179
4.2) Impact of Amino-Functionalization on PEG Response to External Stimuli.....	190
Supporting Information	199
5) Cyclic Polymers	206
5.1) Efficient Approach to Poly(ethylene glycol) Macrocycles via Ring-Closing Metathesis	207
Appendix	214
A.1) Multihydroxy-Functional Polysilanes via an Acetal Protecting Group Strategy	215
Curriculum Vitae	226

MOTIVATION AND OBJECTIVES

Multi-aminofunctional polymers are found in a plethora of everyday applications. These materials induce wet-strength in paper, support adhesion of coatings to substrates, and represent useful auxiliaries in waste water management. Further prominent applications play a key role in the home and personal care industry as conditioners or components of hair sprays. In addition, multi-aminofunctional polymers are frequently mentioned in scientific publications dealing with heavy metal-ion removal via ultrafiltration, functionalization of planar or nanoparticle surfaces, and complexation of DNA, i.e., formation of polyplexes, for gene transfection purposes.

Materials used are often combinations of poly(ethylene glycol) (PEG) with multi-aminofunctional compounds such as poly(ethylene imine) (PEI, linear or hyperbranched), poly(dimethylaminoethyl methacrylate) (PDMAEMA), and poly(diethylaminoethyl methacrylate) (PDEAEMA). Up to date, two distinct, tedious strategies have been predominantly employed to unite PEG and a multi-aminofunctional polymer in one macromolecule: Either both polymers were synthesized individually and coupled together in a third step, or one polymer – usually PEG – was synthesized first before switching the polymerization method and subsequently polymerizing the amino monomer.

Interest in finding new, easier ways to combine these aminofunctional polymers with polyethers has emerged in recent years, caused by the intriguing properties of PEG: i) PEG can induce water-solubility; ii) PEG can serve as “stealth” material, shielding compounds in the body from detection by the immune system, thus ensuring longer circulation times in the blood stream; iii) PEG is biocompatible and can reduce cytotoxicity of bound materials. This unique set of polymer properties is exploited in several applications, such as nanoparticle solubilization, drug delivery, and design of anti-fouling surfaces, e.g., for use in the sensing of biomolecules.

This thesis addresses the following questions:

*Is there an easier, straight-forward route to multi-aminofunctional polyethers?
Is it possible to obtain multi-aminofunctional polyether architectures in one step and/or one pot syntheses?*

Are the copolymers obtained useful for surface functionalization applications?

Aiming at these issues, a rather neglected class of comonomers for anionic ring-opening polymerization (AROP), glycidyl amine derivatives, are further developed. These compounds,

accessible via reaction of commercially available epichlorohydrin and dialkylamines, possess an epoxide ring, perfectly suited for random or block copolymerization with ethylene oxide (EO), the building block of PEG. Furthermore, they contain a tertiary amino moiety, akin, e.g., DEAEMA.

The polymer syntheses and characterization of the materials obtained hereby address the following objectives:

1) *Insight into copolymer microstructure*: Materials obtained from concurrent copolymerization of EO and different glycidyl amine derivatives are analyzed regarding their relative reactivities of both comonomers under the applied reaction conditions. Tools that are employed for this purpose include online ^1H NMR kinetics, ^{13}C NMR triad sequence analysis, and differential scanning calorimetry (DSC).

2) *Investigation of stimuli-responsive behavior*: PEG itself exhibits a lower critical solution temperature (LCST) in aqueous solution, albeit at temperatures close to or above the boiling point of water, depending on molecular weight. Upon introduction of different amounts of less polar glycidyl amine comonomers (*N,N*-diethyl glycidyl amine, DEGA; *N,N*-diallyl glycidyl amine, DAGA), this LCST should become tailorable. Additionally, the amino groups should render the materials not only temperature-, but simultaneously pH-responsive. These properties are analyzed using turbidimetry and electron paramagnetic resonance (EPR) spectroscopy (the latter study is carried out in cooperation with the group of Dariush Hinderberger, MPI for Polymer Research, Mainz).

3) *Introduction of primary amines*: A monomer with cleavable protecting groups bound to the amine, i.e., DAGA, is analyzed regarding its ability to copolymerize with EO via AROP and the dependence of double bond isomerization on polymerization temperature and counterion. Furthermore, isomerization of the double bonds to propenyl moieties under homogeneous conditions in presence of a transition metal catalyst as well as liberation of primary amines upon acidic work-up are studied. Addressability of the amines at the backbone is probed in a model reaction.

In the second part of the thesis, building upon the synthesis of these novel functional polymers, multifunctional polyethers are tested for applicability in functionalization of different surfaces in two cooperative research projects:

1) *Solubilization and functionalization of MnO nanoparticles* (in cooperation with the group of Prof. Tremel, Department of Inorganic and Analytical Chemistry, JGU Mainz): Employing an acetal-protected catechol initiator, EO has been copolymerized either with DAGA or with ethylene glycol vinyl glycidyl ether (EVGE), releasing primary amines or hydroxyl groups along the chain, respectively. After deprotection, the L-DOPA-inspired catechol is thought to be able to bind to a large variety of

metal oxide surfaces. The promising potential of the resulting multifunctional ligands is highlighted by demonstrating the ability to render MnO nanoparticles water-soluble. MnO nanoparticles are candidates for novel T_1 contrast agents in magnetic resonance imaging (MRI). Reactivity of the primary amines in the polymer shell is studied in a model reaction with fluoresceine isothiocyanate (FITC). The additional functionalities bear potential for targeted delivery of the MnO nanoparticles to specific tissues.

2) *Passivation and functionalization of glass surfaces* (in cooperation with the group of Prof. Sönnichsen, Department of Physical Chemistry, JGU Mainz): PEG-*b*-PDEGA diblock copolymers are quaternized to yield polyether polyelectrolytes PEG-*b*-PqDEGA. Subsequently, the positively charged PqDEGA block is used for attachment of the polymers to negatively charged glass surfaces. The pending PEG chains are assumed to reach into the aqueous environment. Thus, attachment of gold nanorods to the glass shall be prevented. The success of this approach is analyzed by dark field microscopy. Targeted functionalization of the glass surfaces is introduced by use of a disulfide initiator for the synthesis of PqDEGA-*b*-PEG-SS-PEG-*b*-PqDEGA copolymers, cleavable in reductive environment and suitable for attachment of gold nanoparticles via strong Au-S linkages.

ABSTRACT

Chapter 1 of this thesis comprises the first review of polyether polyamines, i.e., linear or branched, random or block-like combinations of polyether scaffolds with polymers bearing multiple amino moieties. Focus is laid on controlled or living polymerization methods leading to well-defined materials. This includes atom transfer radical polymerization (ATRP), reversible addition fragmentation transfer (RAFT) polymerization, group transfer polymerization (GTP), and anionic polymerization (AP). Use of (meth)acrylates, both amino- or polyether-functional, and epoxide derivatives as monomers is presented. Furthermore, fields in which the combination of cationic, complexing, and pH-sensitive properties of the polyamines and biocompatibility and water-solubility of polyethers promise enormous potential are presented. Applications include stimuli-responsive polymers with a lower critical solution temperature (LCST) and/or the ability to gel, preparation of shell cross-linked (SCL) micelles, complexation of DNA into polyplexes for gene transfection purposes, and functionalization of planar and nanoparticle surfaces.

In **Chapter 2**, novel multiaminofunctional polyethers relying on the class of glycidyl amine comonomers for anionic ring-opening polymerization (AROP) are presented. In **Chapter 2.1**, *N,N*-diethyl glycidyl amine (DEGA) is introduced for copolymerization with ethylene oxide (EO) in a concurrent or step-wise fashion. Copolymer microstructure is assessed using online ^1H NMR kinetics, ^{13}C NMR triad sequence analysis, and differential scanning calorimetry (DSC). The concurrent copolymerization of EO and DEGA is found to result in macromolecules with a gradient structure. The LCSTs of the resulting copolymers can be tailored by adjusting DEGA fraction or pH value of the environment. Quaternization of the amino moieties by methylation results in polyelectrolytes with a mere polyether backbone. Block copolymers are used as dual reducing and capping agents for PEGylated gold nanoparticle formation. **Chapter 2.2** deals with a glycidyl amine monomer with a removable protecting group at the amino moiety, for liberation of primary amines at the polyether backbone, which is *N,N*-diallyl glycidyl amine (DAGA). Its allyl groups are able to withstand the harsh basic conditions of AROP, but can be cleaved homogeneously after polymerization. Gradient as well as block copolymers poly(ethylene glycol)-PDAGA (PEG-PDAGA) are obtained. They are analyzed regarding their microstructure, LCST behavior, and cleavage of the protecting groups. Addressability of the primary amines is demonstrated for all architectures.

Chapter 3 describes applications of multi(amino)functional polyethers for functionalization of inorganic surfaces. In **Chapter 3.1**, they are combined with an acetal-protected catechol initiator,

leading to well-defined poly(ethylene glycol) and heteromultifunctional PEG analogues. After deprotection, multifunctional PEG-ligands capable of attaching to a variety of metal oxide surfaces are obtained. In a cooperative project with the group of Prof. Tremel (Department of Inorganic and Analytical Chemistry, JGU Mainz), their potential is demonstrated on MnO nanoparticles, which are promising candidates as T_1 contrast agents in magnetic resonance imaging. The MnO nanoparticles are solubilized in aqueous solution upon ligand exchange. Functionalization of the polymer shell is possible, as shown in a model reaction with the fluorescent dye fluoresceine isothiocyanate (FITC). In **Chapter 3.2**, a concept for passivation and functionalization of glass surfaces towards gold nanorods is developed. Quaternized mPEG-*b*-PqDEGA diblock copolymers are attached to negatively charged glass surfaces via the cationic PqDEGA blocks. The PEG blocks are able to suppress gold nanorod adsorption on the glass in the flow cell, analyzed by dark field microscopy. Further functionality is introduced to PEG by using a disulfide bond, capitalizing on the strong Au-S interaction.

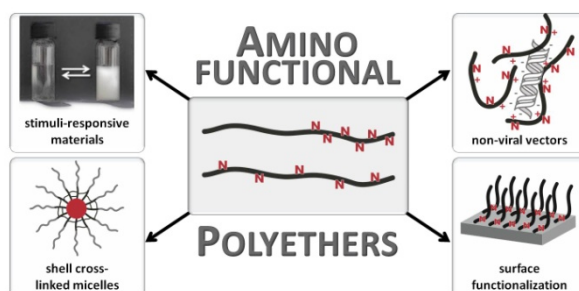
In **Chapter 4**, studies of the temperature-dependent water-solubility of polyether copolymers, carried out in cooperation with the group of PD Dr. Hinderberger (Max Planck Institute for Polymer Research, Mainz), are presented. PEG-*co*-PDEGA and PEG-*b*-PDEGA copolymers of varying composition are analyzed in **Chapter 4.1**. Macroscopic cloud points, determined by turbidimetry, are compared with microscopic aggregation phenomena, monitored by continuous wave electron paramagnetic resonance (CW EPR) spectroscopy in presence of the amphiphilic spin probe and model drug (2,2,6,6-tetramethylpiperidin-1-yl)oxyl (TEMPO). Distinct collapse mechanisms for the two architectures are proposed, supported by MD simulations. These thermoresponsive polymers are promising candidates for molecular transport applications. The principles of host-guest interactions derived from these measurements may serve as guides for the design of materials with specific release profiles. The same techniques are applied in **Chapter 4.2** to explore the pH-dependence of the cloud points of PEG-PDEGA copolymers in further detail. It is shown that the introduction of amino moieties at the PEG backbone leads to the emergence of distinguished physico-chemical properties that allow for precise manipulation of complex phase transition modes by adjusting the polymer topology and the environmental conditions.

Chapter 5 highlights a straightforward approach to poly(ethylene glycol) macrocycles. Starting from commercially available bishydroxy-PEG, cyclic polymers are available by perallylation and ring-closing metathesis in presence of Grubbs' catalyst. Purification of cyclic PEG is carried out using α -cyclodextrin. This cyclic sugar derivative forms inclusion complexes with remaining unreacted linear PEG in aqueous solution. Simple filtration leads to pure macrocycles, as evidenced by SEC and MALDI-ToF mass spectrometry. Cyclic polymers from biocompatible precursors are interesting materials regarding their increased blood circulation time compared to their linear counterparts.

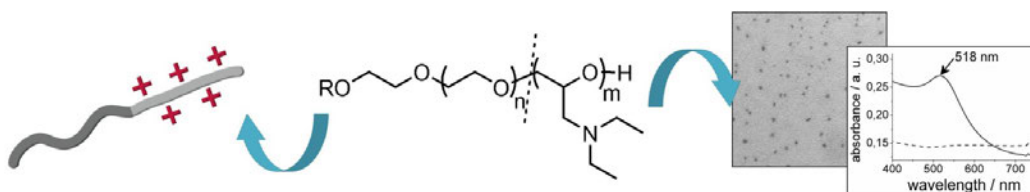
In the **Appendix**, novel multi-hydroxyfunctional polymers with a mere silicon backbone, i.e., polysilanes, are presented. They are obtained via Wurtz-type copolymerization of the acetal-protected dichloro(isopropylidene glyceryl propyl ether)methylsilane monomer with dichlorodi-*n*-hexylsilane. The random character of the copolymer microstructure is confirmed by ^{29}Si NMR spectroscopy and DSC measurements. The hydroxyl groups are liberated through acidic work-up, yielding versatile access to new multifunctional polysilanes and unusual polysilane-based structures, such as hydrogels and cross-linked nanoparticles.

GRAPHICAL ABSTRACT

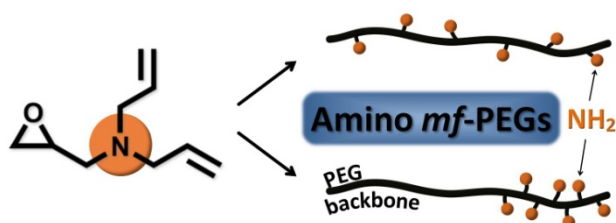
- 1.1) **Aminofunctional Polyethers:**
Smart Materials for Applications in Solution and on Surfaces 14



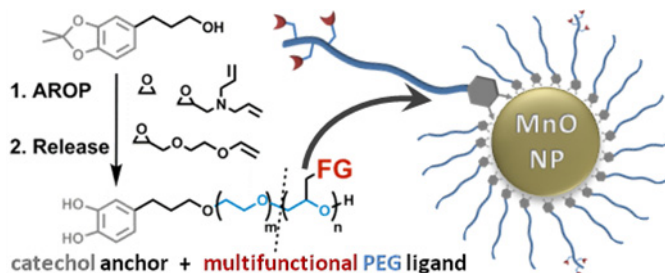
- 2.1) **Thermoresponsive Copolymers of Ethylene Oxide and *N,N*-Diethyl Glycidyl Amine:**
Polyether Polyelectrolytes and PEGylated Gold Nanoparticle Formation 50



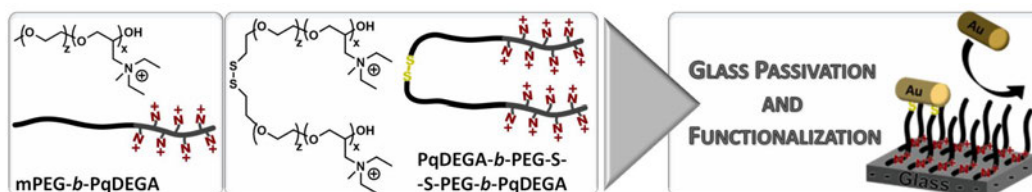
- 2.2) ***N,N*-Diallylglycidylamine:**
A Key Monomer for Amino-Functional Poly(ethylene glycol) Architectures..... 71



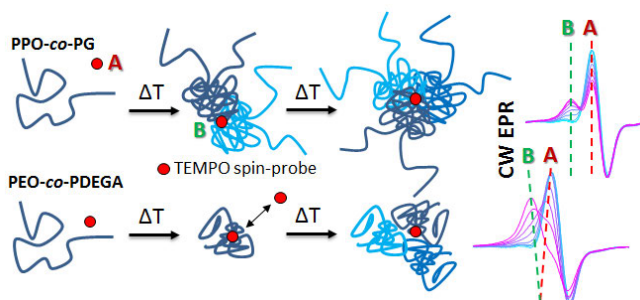
3.1) **Catechol-initiated Polyethers:**
Multifunctional Hydrophilic Ligands for PEGylation and Functionalization of Metal Oxide Nanoparticles..... 107



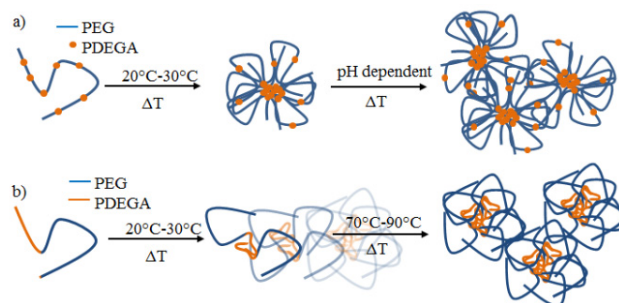
3.2) **Novel Cationic Polyether Block Copolymers for Passivation and Functionalization of Glass Surfaces 134**



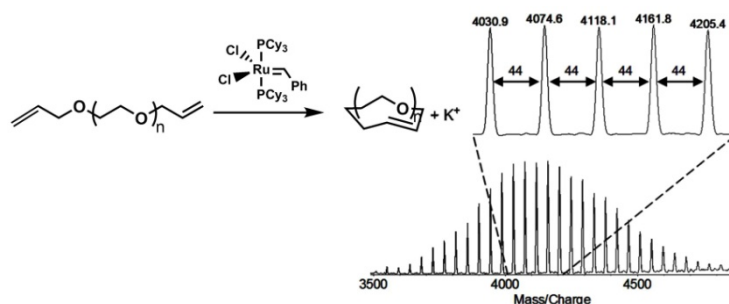
4.1) **How Structure-Related Collapse Mechanisms Determine Nanoscale Inhomogeneities in Thermoresponsive Polymers 149**



4.2) Impact of Amino-Functionalization on PEG Response to External Stimuli..... 190



5.1) Efficient Approach to Poly(ethylene glycol) Macrocycles via Ring-Closing Metathesis..... 207



1) INTRODUCTION

1.1) Aminofunctional Polyethers: Smart Materials for Applications in Solution and on Surfaces

Valerie S. Wilms and Holger Frey

To be submitted to Polymer International.

Abstract

In this minireview, the state of the art of materials combining the properties of biocompatible polyethers with multi-aminofunctionality is presented. Synthetic strategies for polymerization of the respective amine and ether monomers are discussed, focusing on controlled polymerization leading to defined materials of linear or branched, random or block-like architecture. This includes atom transfer radical polymerization (ATRP), reversible addition fragmentation transfer (RAFT) polymerization, group transfer polymerization (GTP), and anionic polymerization (AP). Approaches employing linear poly(ethylene glycol) (PEG), ethylene oxide (EO), or (meth)acrylate monomers with pendant oligo- or poly(ethylene glycol) chains as ether building block, and aminofunctional monomers based on methacrylic acid or epoxide derivatives are addressed. Applications in the fields of double stimuli-responsive polymers, shell cross-linked micelles, gene transfection, and surface functionalization are summarized.

1. Introduction

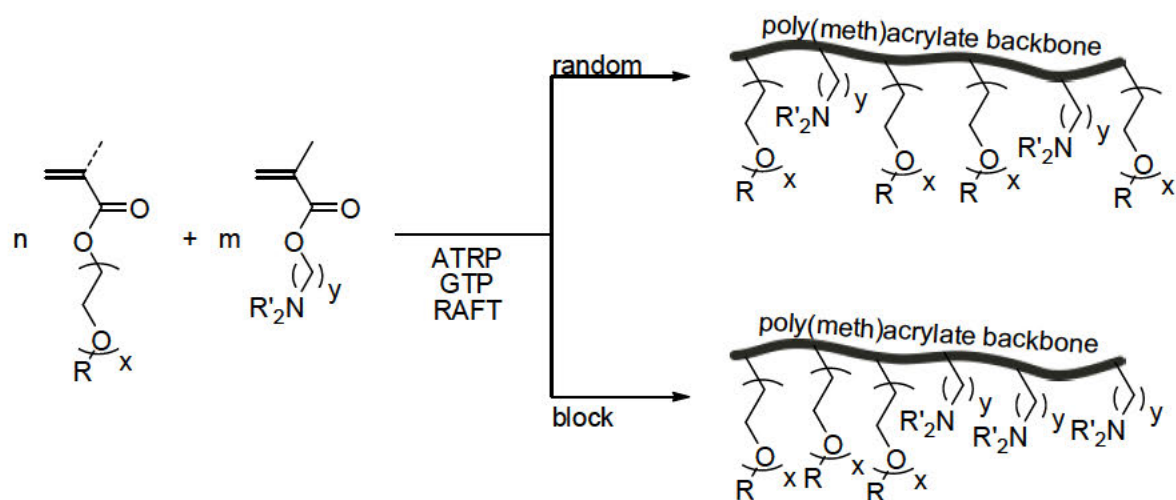
Multi-aminofunctional polymers are used in a vast variety of applications, including every day uses like waste water management,¹ personal care products,² and as flocculation aids in paper industry.¹ More sophisticated projects deal with functionalization of flat and nanoparticle surfaces,³ heavy metal-ion removal via ultrafiltration,⁴ and the complexation of DNA for gene transfection.⁵

Poly(ethylene glycol) (PEG) and its derivatives, such as oligo(ethylene glycol) methacrylate (OEGMA) and poly(ethylene glycol) methacrylate (PEGMA) are representatives of the highly versatile class of polyethers, covering applications from fields as diverse as biomedicine to non-ionic surfactants, and soluble polymeric supports for catalysts and reagents (irrespective of different names used, such as DEGMEMA [di(ethylene glycol) methyl ether methacrylate], these monomers will be called OEGMA due to their structural similarity).⁶⁻¹⁰ Approved by the US-American Food and Drug Administration (FDA) for use in the human body,¹¹ PEG is known for its “stealth effect” and biocompatibility; showing no immunogenicity, antigenicity, or toxicity.¹² These properties are accompanied by excellent solubility in both organic and aqueous solvents, as well as high flexibility and pronounced hydration of the main chain. As a result, PEG has left behind its former task as a simple additive in cosmetic and skin care formulations, now being the “gold standard” for use in sophisticated biomedical applications such as “PEGylation” of pharmaceutically active drugs and peptides.¹²

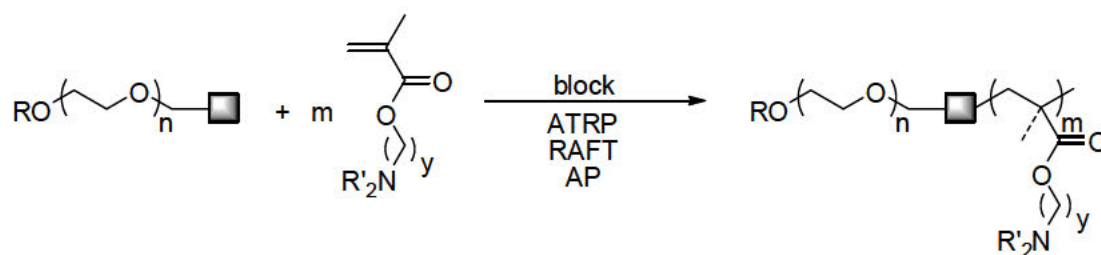
In this short review, we would like to summarize the state of the art of materials that combine the properties of biocompatible polyethers with multi-aminofunctionality. Synthetic strategies for polymerization of the respective amine and ether monomers will be discussed, focusing on controlled polymerization leading to defined materials exclusively. First, approaches employing (meth)acrylate monomers with pendant oligo- or poly(ethylene glycol) chains will be addressed, leading to graft copolymers (Figure 1, i). In the following, syntheses leading to linear polymers will be presented (Figure 1, ii and iii). The synthetic part will be accompanied by an overview over applications of the compounds obtained in this manner as stimuli-responsive materials, non-viral vectors, in shell cross-linked micelles, and for surface functionalization.

Comprehensive reviews of branched and linear poly(ethylene imine)-based materials as well as syntheses and properties of poly(2-oxazoline)s have been published recently.¹³⁻¹⁶ Therefore, these polymers will not be topics of this article.

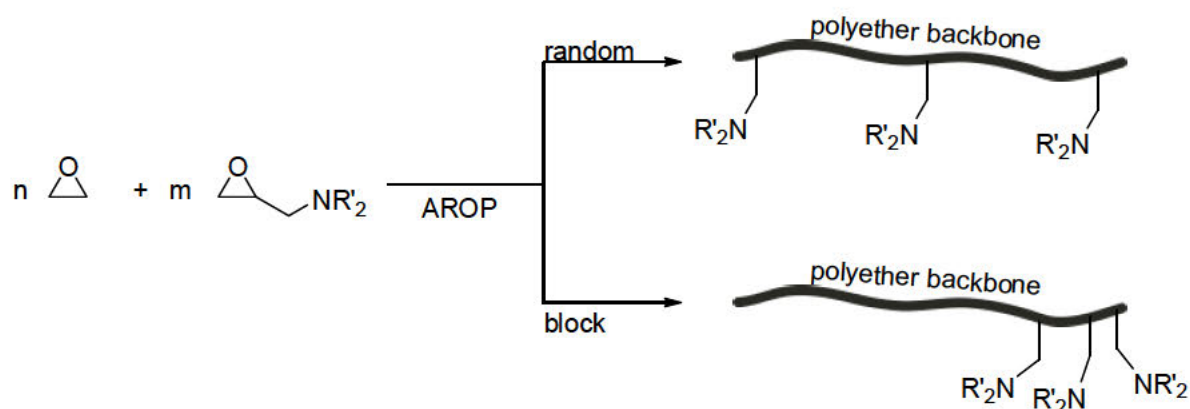
i) Graft structures with poly(meth)acrylate backbone and pendant polyether side chains:



ii) Block copolymers from linear PEG macroinitiator:



iii) Random and block polyethers:



Scheme 1. General synthetic strategies for the combination of polyethers with multiple amine moieties: (i) Controlled radical copolymerization of oligo(ethylene glycol) (meth)acrylates and amine-bearing methacrylates; (ii) use of mPEG macroinitiator for polymerization of amine-bearing methacrylates leading to block copolymers; (iii) anionic ring-opening copolymerization of ethylene oxide with glycidyl amine derivatives.

2. Synthesis

2.1 Polyether Polyamines via Controlled/Living Copolymerization of Oligo(ethylene glycol) Acrylates and Methacrylates (OEGA/OEGMA)

In this chapter, strategies involving polymerization of oligo(ethylene glycol) acrylates (OEGA) and oligo- or poly(ethylene glycol) methacrylates (OEGMA/PEGMA) will be discussed. With this approach, graft copolymer structures consisting of a poly(meth)acrylate backbone with pending oligo- or polyether side chains (Figure 1, i) are obtained.

2.2.1 Atom Transfer Radical Polymerization (ATRP)

Because of its versatility and ease of use, ATRP is very popular in the polymerization of aminofunctional methacrylates, since first studies on the ATRP of dimethylaminoethyl methacrylate (DMAEMA) were carried out in the group of Matyjaszewski.¹⁷ Nevertheless, possible interactions between copper catalyst and amino groups in both monomer and polymer as well as difficulties concerning catalyst removal have to be kept in mind.¹⁸

ABA triblock copolymers with PDMAEMA or poly(diethylaminoethyl methacrylate) (PDEAEMA) as A blocks and POEGMA as B block have been prepared by Haddleton and coworkers.¹⁹ The synthesis was carried out in toluene in a one-pot reaction, started by the bifunctional initiator bis(bromoisobutyryloxy)benzene (BIBB). The reactivity ratios of DMAEMA and DEAEMA versus OEGMA were determined, using the integrated expression of the Mayo equation, as developed by Jaacks. The relative rates of consumption of the monomers were monitored using ¹H NMR of the vinyl region, using mesitylene as an internal standard. They were found to be similar for the monomers used. Consequently, it is important to achieve as high a conversion as possible for the central POEGMA block in order to avoid random copolymerization in the outer A blocks. The second monomer (DMAEMA or DEAEMA) was added at 89% or 72% conversion of the central block, respectively. Polydispersities remained narrow throughout the reaction with values in the range of 1.14 – 1.31. Similar syntheses were carried out by Liu et al.^{20,21} starting from an aliphatic bifunctional initiator.

Asymmetric triblock copolymers have been obtained in a one-pot synthesis by Liu and Armes.²² From a poly(propylene oxide) (PPO) macroinitiator, DMAEMA was polymerized in bulk up to a conversion of about 99%, then after cooling, an aqueous solution of OEGMA was added, resulting in a PPO-*b*-PDMAEMA-*b*-POEGMA triblock copolymer with a molecular weight distribution of 1.20. Little to no evidence for PPO macroinitiator contamination was found.

Starting from β -cyclodextrin, a cyclic oligosaccharide, star block copolymers with four arms on average could be obtained in a core-first approach.²³ In sequential polymerizations, PDMAEMA-*b*-PPEGMA arms were formed. Following the same route, Schmalz et al.²⁴ synthesized 4-arm stars PDMAEMA-*b*-POEGMA, showing a low extent of star-star coupling caused by nucleophilic attack of an amine on the chain end halogen. By quaternization of the tertiary amines, a strong polyelectrolyte block was formed. In order to determine the polydispersity of the arms, i.e., the blocking efficiency, they were cleaved off the core by alkaline ester hydrolysis at elevated temperatures. A non-aqueous environment was chosen to circumvent insolubility issues stemming from the lower critical solution temperature (LCST) of the OEGMA block. At the same time, the PDMAEMA block was degraded to poly(methacrylic acid) (PMAA) and subsequently converted to poly(methyl methacrylate) (PMMA), facilitating SEC analysis.

A graft approach was developed by Huang and coworkers:²⁵ after ATRP of OEGA, a series of ATRP initiators was installed along the polyacrylate backbone using lithium diisopropylamine for abstraction of the methine proton and subsequent reaction with 2-bromopropionyl chloride. Then, grafting-from of DMAEMA was carried out using a high feed ratio of monomer to initiator and low conversion of the monomer in order to suppress intermolecular coupling. Via ¹H NMR, degrees of polymerization of the POEGA backbone and per PDMAEMA arm were found to be 20 and 8.6 – 24.4, respectively. From another point of view, this elegant strategy allows for the synthesis of unusual, densely double-grafted polyacrylates with PEG and PDMAEMA side chains.

2.1.2 Reversible addition/fragmentation chain transfer polymerization (RAFT)

Although being well-suited for the polymerization of both OEGMAs and dialkylaminoethyl methacrylates, RAFT polymerization is used less frequently in this process than ATRP. Nevertheless, well-defined homopolymers of DMAEMA were already obtained in early studies²⁶ and polymerization parameters were optimized by Sahnoun et al.²⁷

In the group of Schubert,²⁸ an automated synthesizer was later utilized for the establishment of a library of statistical copolymers of PEGMA (approx. 300 g mol⁻¹) and DMAEMA. As a chain transfer agent (CTA), 2-cyano-2-butyl dithiobenzoate (CBDB) in toluene was applied, in the presence of azobisisobutyronitrile (AIBN) as a radical source. Comonomer contents were varied from 0 – 100% in steps of 10 mol%. The obtained polymers were relatively well-defined with PDIs in the range of 1.11 – 1.30, values increasing with increasing PEGMA content caused by a high-molecular weight shoulder. The macromolecular structure of the copolymer was assessed by determination of the monomer reactivity ratios via the Kelen-Tüdös method^{29,30} in order to be able to achieve high

conversions. Under the chosen reaction conditions, DMAEMA was incorporated preferentially in the early phase of the RAFT polymerization ($r_{\text{DMAEMA}} = 0.93$, $r_{\text{PEGMA}} = 0.66$), resulting in a gradient copolymer composition. Recently, statistical copolymerization of DMAEMA and OEGMA was also realized from a poly(*tert*-butyl acrylate) (PtBA) macro-RAFT agent.³¹ Selective cleavage of the *tert*-butyl ester led to a poly(acrylic acid)-P(DMAEMA-*co*-OEGMA) block copolymer.

Aiming at stable micelles, Stenzel and coworkers³² synthesized block copolymers P(DMAEMA)-*b*-P(PEGMA) in a two-step reaction, suitable for shell cross-linking via the thiocarbonylthio group. Consequently, the more hydrophobic core block PDMAEMA was synthesized first using 4-cyanopentanoic acid dithiobenzoate as CTA in methanol. The polymerization was found to proceed according to first-order kinetics, with narrow molecular weight distributions below 1.2 throughout the course of the reaction. Similar to the observations for concurrent copolymerization of these monomers, chain extension of the resulting macromolecular RAFT agent with PEGMA in toluene results in a slight elevation of the polydispersity up to 1.3 at higher conversions. Some molecular weight tailing pointing to incomplete PEGMA chain extension was observed in SEC. However, molecular weight increased linearly with conversion. Also functional RAFT agents carrying, e.g., α -phosphonic acid groups suitable as anchors for attachment to the surface of iron oxide nanoparticles, have been applied, giving similar results.³³

Block copolymers with one block consisting of a mixture of OEGMAs of different lengths, tuning the solubility properties, and a second block of poly(aminoethyl methacrylate) (PAEMA) has been the focus of a recent work by Dai et al.³⁴ In a two-pot reaction sequence, the OEGMAs have been polymerized first, followed by addition of aminoethyl methacryloyl hydrochloride (AEMA-HCl). In a second step, pyrene carboxaldehyde was attached to the PAEMA block by Schiff base formation and critical micelle concentrations (CMCs) were measured employing the pyrene method. Release of pyrene, a model compound for drug molecules, was studied depending on the pH of the surrounding medium.

2.1.3 Group Transfer Polymerization (GTP)

As expected, OEGMA is less reactive in GTP than the sterically less demanding DMAEMA. Hence, in order to allow both monomers to randomly copolymerize, Vamvakaki et al.³⁵ drip-fed solutions of both monomers at different speeds into the reaction vessel. Comonomer fractions were varied widely from 10 – 90 mol% while maintaining a total molecular weight of 10,000 – 20,000 g mol⁻¹. Terpolymers were prepared by simply adding *n*-butyl methacrylate (*n*BuMA) to the DMAEMA solution, assuming similar reactivities for both low molecular weight monomers. In contrast to GTP

homopolymerizations of OEGMA, almost quantitative conversions were obtained with polydispersities < 1.2. Similar reaction conditions were used for block copolymers PDMAEMA-*b*-POEGMA.³⁶ DMAEMA was polymerized first in THF, following the course of polymerization via monitoring of the exotherm. After abatement of the exotherm, i.e., complete conversion of DMAEMA, an OEGMA solution was added dropwise for formation of the second block. Further versatility of GTP has been demonstrated in the synthesis of terpolymers of OEGMA and DMAEMA with *n*BuMA, exploring influence of block sequence and length ratios on physical properties and behavior in solution.^{37,38}

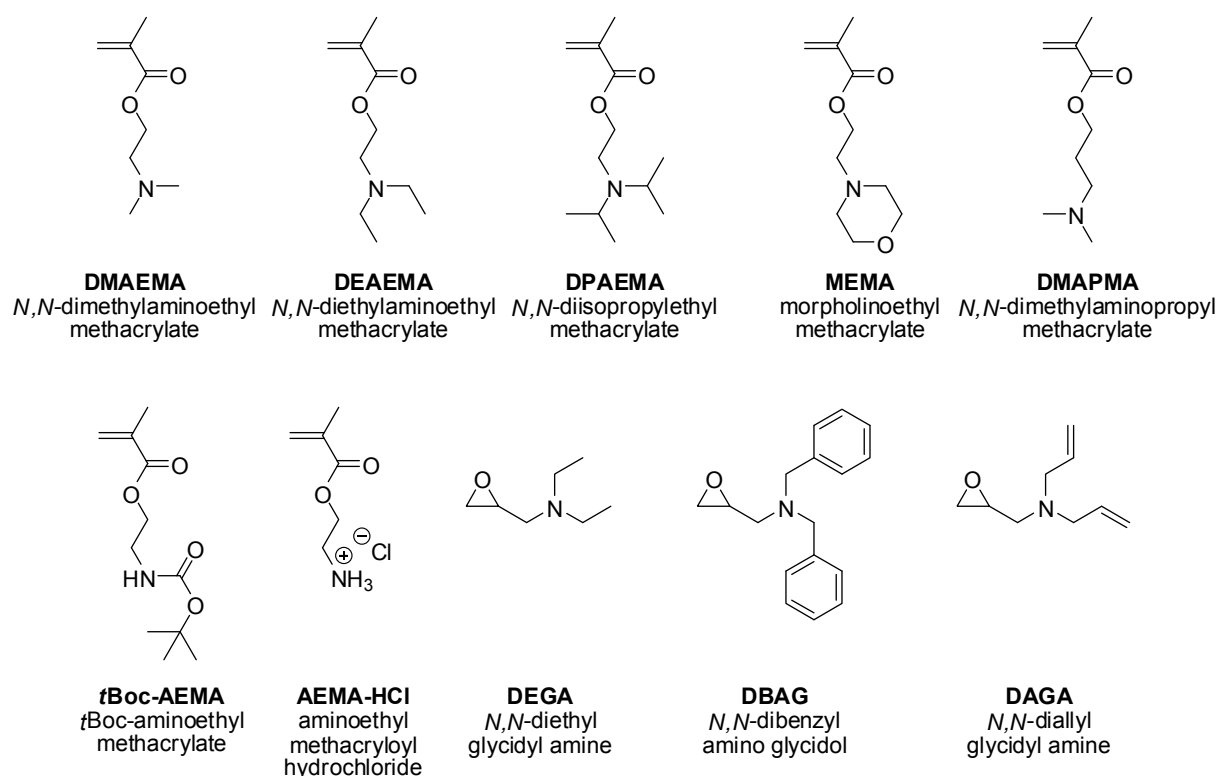


Figure 1. Amine-containing monomers for controlled/living polymerization methods.

2.2 Polyether Polyamines Containing Linear PEG via Controlled/Living Polymerization

In chapter 2.2, synthetic approaches starting from polyether macroinitiators for the polymerization of mostly methacrylic amino-functional monomers via anionic or controlled radical polymerization will be discussed first (Figure 1, ii). In the following, advantages of anionic ring-opening polymerization regarding versatility and variety of the resulting polymer structures will be presented (Figure 1, iii).

2.2.1 Atom Transfer Radical Polymerization

PEG monomethyl ether (mPEG) is commercially readily available over a wide range of molecular weights. Simple esterification with 2-bromoisobutyryl bromide converts it to a macroinitiator for ATRP, a road frequently traveled for syntheses of diblock copolymers. Symmetric triblock and pentablock copolymers are equally easy available through similar derivatization of commercial dihydroxy-PEG or PEO-*b*-PPO-*b*-PEO, also known under the tradename Pluronics.

Diblock copolymers following the strategy described above were explored employing DMAEMA, DEAEMA, and Boc-protected aminoethyl methacrylate (*t*Boc-AEMA).³⁹ Based on this approach, also primary amines could be liberated in an acidic environment. Buffering capacities of the polymers were determined. Potentiometric titrations gave pK_a values of 7.13, 6.58, and 6.75 for PEG-*b*-PAEMA, PEG-*b*-PDMAEMA, and PEG-*b*-PDEAEMA, respectively. Furthermore, AB block copolymers were subjects of later studies, focusing on short aminofunctional B blocks.^{40,41} Telechelic diblock copolymers were obtained by Tan et al.⁴² by installation of a biotinyl residue at one terminus of PEG and further esterification of the second terminus for use as macroinitiator in the ATRP of DEAEMA. PEG-*b*-PDMAEMA became cleavable under acidic conditions through installation of a scissile ortho-ester linkage between the blocks.⁴³ For this purpose, an acetal-containing macroinitiator was prepared in a five step synthesis, starting from 3-amino-1,2-propanediol and mPEG, and was used for DMAEMA polymerization.

As mentioned above, ABA triblocks are similarly available, as demonstrated by Peng et al.⁴⁴ Initiation efficiency of the bifunctional PEG macroinitiator for DMAEMA was estimated to about 87 wt%. Moderate yields were ascribed to the high viscosity of the reaction solution. Successive ATRP of different aminoethyl methacrylate comonomers from a PEG macroinitiator is a route to ABC triblock copolymers forming stable micelles in aqueous solution. Capitalizing on the absence of the usual termination under monomer-starved conditions observed for hydrophilic methacrylates in water, Liu et al.⁴⁵ carried out a one-pot synthesis of PEG-*b*-PDMAEMA-*b*-PDEAEMA, following unsuccessful attempts of block formation in two steps. For polymerization of the second block, methanol was added because of the insolubility of DEAEMA in water. This property of DEAEMA also allowed for a detailed tailoring of the hydrophilic/hydrophobic balance of the terpolymer and its self-assembly in water at varying pH values. A zwitterionic triblock copolymer was obtained in a similar one-pot synthesis protocol using DEAEMA and 2-hydroxyethyl methacrylate (HEMA). Post-polymerization functionalization with succinic anhydride gave PEG-*b*-PDEAEMA-*b*-poly(2-succinyloxyethyl methacrylate) (PEG-*b*-PDEAEMA-*b*-PSEMA) with multiple amines and carboxylic acid moieties in the B and C block, respectively. Synthesis in two steps was chosen for mPEG-initiated ABC triblocks of DMAEMA and BuMA,⁴⁶ irrespective of a tailing towards low molecular weight and slightly bimodal

molecular weight distributions, pointing to termination during polymerization. In the same work, PEG-*b*-(PDMAEMA-*co*-PBuMA) and PEG-*b*-(PDMAEMA-*grad*-PBuMA) terpolymers with second “blocks” of random or gradient composition were obtained by simultaneous addition of both monomers or constant feeding of one monomer to the ATRP of the second monomer, relying on almost identical reactivities of DMAEMA and BuMA. Pentablock copolymers of propylene oxide (PO), EO, and several amine-containing methacrylates were started from derivatized Pluronics as bifunctional initiator.⁴⁷ Optimization of reaction conditions by selection of solvent and catalyst concentration was studied.

Sophisticated architectures generated by ATRP are also found in literature, including a PEG-*b*-PDEAEMA four-arm star⁴⁸ and H-shaped (PNIPAM/PDMAEMA)-*b*-PEG-*b*-(PNIPAM/PDMAEMA) via combination of ATRP and azide/alkyne click chemistry.⁴⁹ Anionic ring-opening polymerization of EO and ethoxy ethyl glycidyl ether (EEGE) and acidic work-up is a route to random PEG-*co*-linear poly(glycerol) (PEG-*co*-*lin*PG) polymers. The pending hydroxyl groups were esterified with 2-bromoisobutyryl bromide, and DMAEMA was grafted-from by the group of Li.⁵⁰ PEG-*g*-PDMAEMA with tailing towards low molecular weights resulting in elevated polydispersities was prepared. Cyclic homologues *c*-PEG-*g*-PDMAEMA were also available through ring-closure of bishydroxy-PEG-*co*-PEEGE in diluted alkaline solution, deprotection and derivatization of the in-chain hydroxyl groups, and ATRP of DMAEMA.⁵¹

2.2.2 Reversible Addition/Fragmentation Chain Transfer Polymerization

Transformation of mPEG into a macro-RAFT agent is possible via esterification with a carboxy-functional low molecular weight dithiobenzoate.^{52,53} Such, diblocks PEG-*b*-PDMAEMA with polymerization degrees of about 50 per block and low polydispersities (< 1.18) were obtained. Furthermore, in a three-step synthesis starting from bishydroxy-PEG, including activation with *p*-nitrophenyl chloroformate, and reactions with cystamine hydrochloride and cyanopentanoic acid dithionaphthalenoate, a bifunctional macro-chain transfer agent (macro-CTA) has been created.⁵⁴ By polymerization of DMAEMA to form the outer multi-aminofunctional blocks, Zhu et al. obtained an ABA triblock PDMAEMA-SS-PEG-SS-PDMAEMA which was cleavable in-between the blocks by reduction of the introduced disulfide linkages. Non-reducible PDMAEMA-*b*-PEG-*b*-PDMAEMA served as a control, showing considerably lower polydispersity (< 1.35) than the reducible, scissile counterparts (< 1.85). A monomer with a slightly varied architecture, namely *N,N*-3-dimethylaminopropyl methacrylate (DMAPMA), was used by Zhuo and coworkers⁵⁵ for the preparation of tercopolymers. Again, mPEG was transformed into a macro-CTA via the well-known

route and concurrent copolymerization of preformed HEMA-poly(ϵ -caprolactone) (HEMA-PCL) macromonomers and DMAPMA was carried out. The ratio of CL/DMAPMA repeating units was varied from 2.5 to 0.6. Unfortunately, the question of the microstructure of the resulting macromolecules, i.e., the ordering along the chain of the monomers differing considerably in size, was not addressed. CMC determination via the pyrene method indicated formation of micellar structures in aqueous solution, with PCL forming the hydrophobic core. As expected, CMC values increased with decreasing PCL content.

2.2.3 Anionic Polymerization (AP)

Methacrylate monomers. For a long time, it was part of common knowledge that alkali metal alkoxides cannot initiate the anionic polymerization of methacrylate monomers because of the low nucleophilicity of the alkoxide anion. However, Iijima et al.⁵⁶ found that a methacrylic ester possessing a siloxy group at the β -position of the ester moiety is polymerizable by a simple alkoxide such as potassium ethoxide. The increased reactivity of the initiator was ascribed to chelation of the initiator by the monomer, although the exact mechanism remained unclear. This polymerization was also termed "oxyanionic polymerization" because of the nature of its initiator.⁵⁷ In following work, this concept was expanded to other methacrylic monomers exhibiting chelating groups in the ester side chain, such as the amino moiety in DEAEMA⁵⁸ and structurally similar disubstituted aminoethyl methacrylates.^{57,59-61} It was not long until the synthesis of block copolymers by the use of deprotonated monohydroxy-functional PEG as macroinitiator for the anionic polymerization of the respective methacrylates was reported. The first study of the synthesis of diblock copolymers was published by the group of Armes.⁵⁹ After deprotonation of mPEG of a molecular weight of 1,000 g mol⁻¹ or 2,000 g mol⁻¹ with potassium naphthalenide, DMAEMA, DEAEMA, diisopropylaminoethyl methacrylate (DPAEMA), or *N*-morpholinoethyl methacrylate (MEMA) were polymerized. For all tertiary amine monomers, high yields >95% and good control over molecular weight was possible, while polydispersities were somewhat elevated compared to other anionic polymerizations (PDI: 1.23 – 1.35). Concerning polydispersities and molecular weights of multi-aminofunctional polymers determined by SEC in general, one has to always keep in mind occurring interactions between amino groups and the column packing as well as relatively high molecular weight of the pendent groups in the amine monomers. Capitalizing on the lower critical solution temperature (LCST) of the resulting diblock copolymers in alkaline aqueous solution (60 – 80 °C), contamination of the product with unreacted mPEG macroinitiator was removed via filtration of this solution at 90 °C. While mPEG remained soluble under these conditions, the block copolymer precipitated quantitatively.

Micellization behavior in aqueous solution was further investigated by means of dynamic light scattering and ^1H NMR.

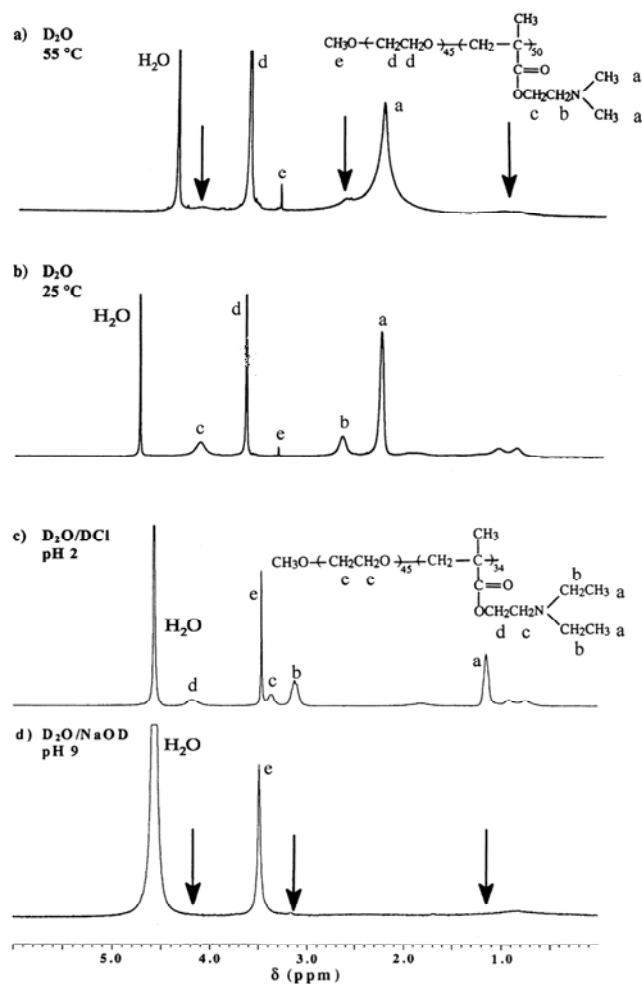


Figure 2. ^1H NMR spectra (D_2O) for a) a micellar solution of a $\text{PEG}_{45}\text{-}b\text{-PDMAEMA}_{50}$ diblock copolymer at $55\text{ }^\circ\text{C}$, b) the same $\text{PEG}_{45}\text{-}b\text{-PDMAEMA}_{50}$ diblock copolymer at $25\text{ }^\circ\text{C}$ (note the increased relative intensities of the re-solvated DMAEMA residues); c) a $\text{PEG}_{45}\text{-}b\text{-PDEAEMA}_{34}$ diblock copolymer in $\text{DCI}/\text{D}_2\text{O}$ at $\text{pH } 2$, and d) a micellar solution of the same $\text{PEG}_{45}\text{-}b\text{-PDEAEMA}_{34}$ copolymer at $\text{pH } 8$ (note the complete disappearance of the DEAEMA residues, indicating fully dehydrated micelle cores). Reproduced from Vamvakaki et al.⁵⁹

In the latter, measurements of $\text{PEG}\text{-}b\text{-PDMAEMA}$ in D_2O were carried out at $25\text{ }^\circ\text{C}$ and $55\text{ }^\circ\text{C}$ (Figure 2, a and b). Upon temperature increase, a broadening of the signals of the PDMAEMA block was observed. The fact that these signals did not disappear completely pointed to some retained degree of hydration inside the micelles. For $\text{PEG}\text{-}b\text{-PDEAEMA}$, influence of pH on the solution state

was studied (Figure 2, c and d). In acidic aqueous environment (pH 2), the macromolecule was in its unimer state. The amino groups were protonated and both blocks fully hydrated. On the other hand, in alkaline solution (pH 9), the DEAEMA residues became deprotonated and hydrophobic. Hence, the signals in NMR disappeared completely, indicating fully dehydrated micellar cores.

Further functionality can be introduced by use of a (protected) functional initiator for the anionic ring-opening polymerization (AROP) of ethylene oxide (EO), thus resulting in telechelic PEG with initiator functionality and hydroxyl function at the termini, the latter being suitable for the above-mentioned "oxyanionic" polymerization of aminofunctional methacrylates. This was demonstrated by Nagasaki and coworkers⁶⁰ using potassium 3,3-diethoxypropanolate, an α -acetal-protected aldehyde, as initiator. The diblock copolymer α -acetal-PEG-*b*-PDMAEMA was obtained in one pot by subsequent addition of EO and DMAEMA monomers. Here, a different work-up was chosen for removal of α -acetal-PEG homopolymer contamination: an aqueous solution of the crude product was treated batchwise with an ion-exchange resin at pH 5. Only the block copolymer adsorbed on the resin surface and was desorbed in acetate buffer/sodium chloride solution (pH 5). Thus, monomodal molecular weight distributions below 1.41 could be determined in SEC. Similar results concerning blocking efficiency and polydispersity were also obtained using a different initiator/deprotonating agent system in a one pot synthesis, namely 1,1-diphenyl-3-methylpentyllithium in combination with the phosphazene base *t*-BuP₄, allowing for the polymerization of EO in presence of the counterion lithium.⁶¹ In near infrared (NIR) spectra recorded during polymerization, initiation upon addition of DMAEMA to the living PEG chains was found to be slow, probably accounting for the broadening of the molecular weight distribution. After a monomer conversion of approximately 20%, a living character was proven by linearity of the first-order plot.

Self assembly of ABC triblock copolymers PEG-*b*-PDMAEMA-*b*-PBAEMA from successive one pot reactions of mPEG macroinitiator with DMAEMA and *t*-butylaminoethyl methacrylate (BAEMA) in aqueous solution was confirmed by ¹H NMR studies.⁶² Three-layer onion micelles with relatively hydrophobic BAEMA in the dehydrated core region were found in aqueous solution, with no visible signals for this block, while PEG constituted the hydrated corona.

pH-sensitive Pluronic analogues should be obtained through the polymerization of DMAEMA starting from bishydroxyfunctional PPO, yielding PDMAEMA-*b*-PPO-*b*-PDMAEMA ABA triblock copolymers.⁶³ Again, reversible micellar assembly with PPO as core upon changes in pH and temperature were visible in ¹H NMR measurements. In dynamic light scattering, micelles were found to grow upon heating and finally, LCST behavior was observed. Pluronics themselves have also served as macroinitiators for DEAEMA,⁶⁴ resulting in well-defined pentablock copolymers. Micellization temperatures (T_m) and endothermic enthalpies (ΔH) from differential scanning calorimetry (DSC) of

aqueous solutions decreased with increasing PDEAEMA block length. It was assumed that the PDEAEMA block partitions into the hydrophobic core of the micelle consisting of the PPO central block under these conditions. Thus, entropic advantage of micellization is reduced, causing the observed changes in T_m and ΔH with increasing PDEAEMA fraction. The pentablocks formed non-crosslinked hydrogels with incorporated Nile blue chloride (NBCI). This dye is a suitable model drug for release studies because of its moderate water-solubility and low molecular weight. Release rates were monitored in a UV/Vis spectrometer at the absorbance maximum at 636 nm (Figure 3). At high pH values, the gel was relatively insoluble. Lowering the pH effected dissolution of the non-crosslinked molecules upon protonation of amines, accompanied by an increased release rate of NBCI. In comparison, the diblocks PEG-*b*-PDEAEMA did not form hydrogels, but were pressed into tablets by compression-molding of a solid polymer/dye mixture. Also, release behavior was pH-dependent. PEG and Pluronic controls showed release rates independent of solution pH.

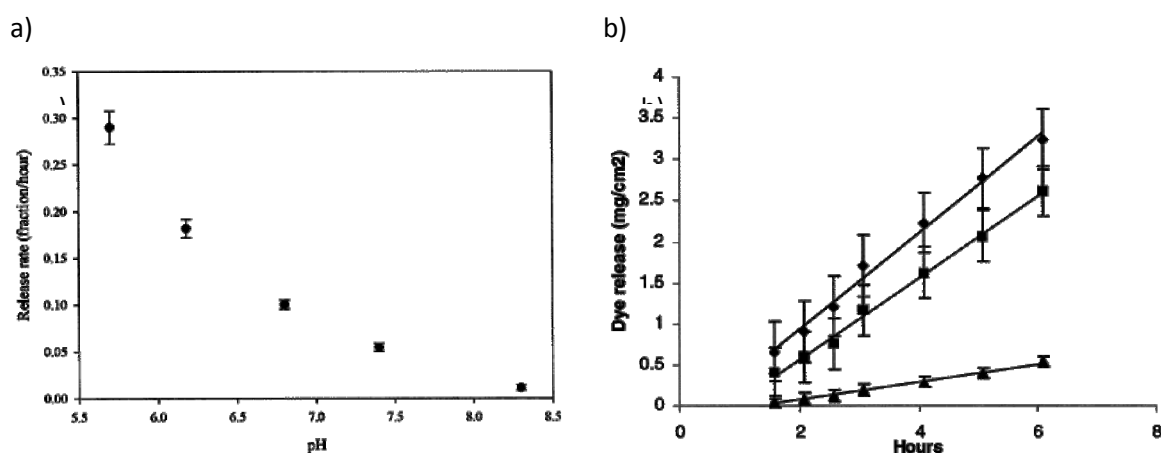


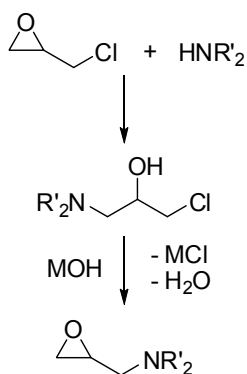
Figure 3. a) Release rate of Nile blue chloride from PEG-*b*-PDEAEMA diblock copolymer tablets as a function of pH. Dye loading was 30 mg/cm³. b) Release of Nile blue chloride from PDEAEMA-*b*-PEG-*b*-PPO-*b*-PEG-*b*-PDEAEMA pentablock copolymer gels at a pH of 6.2 (◆), 7.4 (■), and 8.2 (▲). Reproduced from Anderson et al.⁶⁴

Epoxide monomers. While oxyanionic polymerization has proven beneficial in the synthesis of diblock polyether polyamines in a one pot reaction, random structures are not accessible using aminofunctional methacrylates. Furthermore, self-catalyzed degradation of methacrylate-based structures has been an issue.⁶⁵ Other strategies had to be developed, involving functional epoxide comonomers for the concurrent or successive copolymerization with EO, leading to so-called multifunctional PEGs (*mf*-PEGs).^{6,7} First steps towards multi-aminofunctionality were made by

Koyama et al.⁶⁶ in the 1990s. By random copolymerization of EO with allyl glycidyl ether (AGE) and subsequent thiol-ene click of aminoethanethiol to the double bond, the first polyether with amino groups distributed along the polyether backbone was created. Addressability of the primary amines was demonstrated in a model reaction with acetic anhydride leading to the corresponding amide. Other possible candidates for covalent attachment, i.e., conjugation, to the PEG backbone are low molecular weight drugs. The aminated PEG was able to solubilize lauric acid in aqueous solution. Assembly behavior was investigated with the pyrene method, pointing to secondary aggregation of the aminated PEG and the fatty acid into a microdomain structure, trapping the pyrene molecules in the hydrophobic domains. PEG with multiple pendant amino groups was able to stabilize solutions with fatty acid and pyrene over a long period of time, while use of PEG with primary amines only at the termini led to precipitation already after one day.

Recently, a new strategy for incorporation of amino functionalities along the polyether backbone has been explored by the group of Frey.⁶⁷⁻⁶⁹ The new class of glycidyl amine comonomers for anionic ring-opening copolymerization with EO in a concurrent or step-wise manner has been introduced, after first attempts of Tsvetanov and coworkers in 2001.⁷⁰ Thus, multi-aminofunctional polyether architectures have become available in one-step syntheses.

In general, glycidyl amines are accessible via reaction of epichlorohydrin with the corresponding secondary amine (Scheme 2). The reactive pathway proceeds in two consecutive steps: i) nucleophilic attack of nitrogen on the methylene group in the three-membered ring of epichlorohydrin, accompanied by an opening of the ring and formation of a chlorohydrins; ii) ring-closure to reform the epoxide moiety promoted by alkaline catalysis and formal removal of HCl. These reactions are carried out in one or two pots, depending on the amine used.



Scheme 2. General synthesis of glycidyl amine derivatives.

Such, a monomer exhibiting the same diethylamino motif known from DEAEMA has been obtained: *N,N*-diethyl glycidyl amine (DEGA).⁶⁹ In both concurrent and block copolymerization with EO, well-defined materials were obtained (PDI: 1.03 – 1.13). The monomer's reaction behavior in a concurrent copolymerization with EO initiated by an alkali metal alkoxide was analyzed using ¹³C NMR triad analysis, determination of the thermal properties in bulk and in aqueous solution, and via ¹H NMR online kinetic measurements. In the latter, solutions of a monomer mixture and of the initiator in deuterated DMSO were successively introduced into a conventional NMR tube and frozen in liquid nitrogen. Then, high vacuum was applied to the NMR tube and it was flame-sealed. Thus, it was possible to carry out the polymerization reaction inside a NMR spectrometer and follow the consumption of the monomers and growth of the polymer backbone through the measurement of NMR spectra at pre-set time intervals in the range of seconds. Quantification of the consumption of each monomer with time resulted in slower incorporation of DEGA at the beginning of the polymerization. Relative DEGA incorporation increased as the reaction progressed. Hence, the obtained copolymer did not possess a random, but rather a gradient structure. The probability to find a DEGA monomer in the chain increased with increasing distance from the initiator terminus. Formation of a block copolymer with extended stretches of only one repeating unit, EO or DEGA, could be excluded. This was further supported by increasing number and intensities of the signals of DEGA-centered triads in ¹³C NMR with increasing DEGA fraction, accompanied by decreasing melting temperatures as determined by dynamic scanning calorimetry (DSC). The existence of these gradient structures, i.e., absence of blocky copolymers, allowed for tailoring of stimuli-responsive properties such as the lower critical solution temperature (LCST, see application part). On the other hand, well-defined block copolymers with the amino moieties concentrated at one end were available by use of a mPEG macroinitiator. Further treatment with methyl iodide led to quaternization of the amines and formation of the first cationic polyelectrolyte with a backbone wholly constituted of a polyether.

A step further is the introduction of primary amines at the polyether backbone. This is not possible directly with glycidyl amine, since primary amines themselves are able to attack epoxide rings. A suitable protecting group had to be applied, which is able to withstand the harsh basic conditions of AROP, but can be cleaved subsequently in a quantitative manner. The first protective group which has been applied for this means is the benzyl moiety, resulting in the monomer *N,N*-dibenzyl amino glycidol (DBAG), obtainable from a two-pot synthesis.⁶⁷ In copolymerizations with EO, again a reaction behavior leading to gradient structures was found, which seemed to be an inherent property of all glycidyl amine comonomers investigated until today. Hydrogenolysis of the dibenzylamines in presence of Pearlman's catalyst (Pd(OH)₂/C) in an autoclave led to liberation of the primary amines after 1-8 days. PEG-poly(glycidyl amine) (PEG-PGA) copolymers were obtained without chain cleavage. However, this reaction was not successful for the synthesized block

copolymers, probably due to adhesion of PEG-*b*-PGA on the catalyst surface. This was probably also the reason for the moderate to low yields of the deprotection reaction of 30-50%. Amine accessibility was proven in a model reaction with acetic anhydride.

For the development of amino-functional PEG architectures, *N,N*-diallyl glycidyl amine (DAGA) was found to be a superior comonomer choice to DBAG. The allyl protecting groups are able to withstand the oxanionic conditions and the monomer was obtainable in a one-pot reaction. In contrast to DBAG, cleavage was carried out in a homogeneous manner: isomerization of the *N*-allyl to *N*-propenyl moieties using Wilkinson's catalyst ($\text{RhCl}[\text{PPh}_3]_3$) in toluene solution and acidic aqueous work-up releasing primary amines on the polymer and the volatile propanal. The time for deprotection was shortened from days to four hours and the yields improved considerably to over 85%. Most importantly, this monomer granted access not only to gradient but also to block copolymers of PEG and PGA. These materials offer vast opportunities concerning multiple conjugation of, e.g., biomolecules or low molecular weight drugs in PEGylation applications. In the area of soluble polymer-supported catalysts, especially the block copolymers can be of interest.

3. Applications

3.1 Stimuli-Responsive Materials

PEG and POEGMA themselves are materials with a temperature-dependent water-solubility, i.e., a lower critical solution temperature (LCST).^{71,72} Solubility of polymers with multiple amino groups in water is governed not only by temperature but also a second stimulus: pH value. In sufficiently acidic media, the amines become protonated and thus a cationic polyelectrolyte is obtained. Concerning the methacrylates, unprotonated PDMAEMA is still water-soluble, while this holds no longer true for the amino methacrylates with longer alkyl substituents. By choice of monomers, architecture, and composition of the polymers, the stimuli-responsive properties of the materials can be modified. This is particularly of interest in the area of stimuli-triggered drug release.

3.1.1 Towards Tailored Cloud Points

For all kinds of copolymers of polyethers and polymers with multiple amino groups, general trends have been observed for the LCST behavior.^{19,25,28,41,68,69,73,74} With increasing content of PEG or POEGMA, cloud point temperatures increase, since in these combinations the polyether serves as the more hydrophilic partner. Influence of linear PEG was found to be more pronounced in diblock than

in triblock copolymers.⁴¹ For same contents of different amino monomers, LCSTs decreased with increasing chain length of the substituents due to the more apolar character.^{19,69} With decreasing pH values, LCSTs increased due to increasing protonation. Often, solubility over the whole temperature range could be observed at pH values above the pK_a of the amine derivative present. Increase of salinity of the solution also lowered the LCST, because of a salting out effect.⁴¹ The best way to targeted cloud point temperatures were random copolymers, accessible through random copolymerization of either OEGMA and amino methacrylates²⁸ or EO and glycidyl amines.^{67-69,74} LCSTs depended almost linearly on amine comonomer fraction. As an example, turbidimetric measurements of PEG-co-PDEGA are depicted in Figure 2.

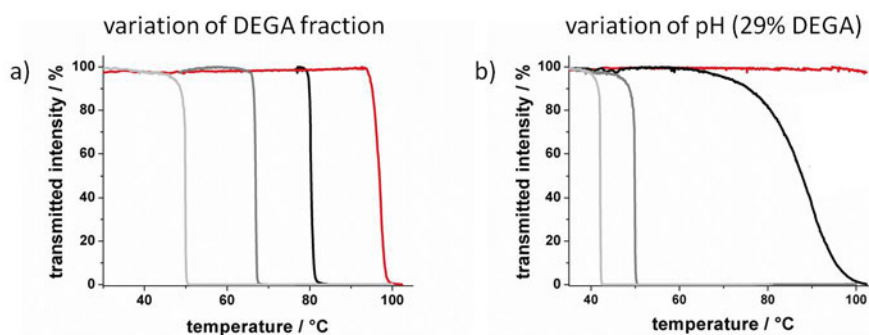


Figure 2. Turbidimetric measurements of PEG-co-PDEGA, demonstrating double stimuli-responsive behavior. a) Variation of DEGA fraction (red: 4%, black: 7%, dark gray: 15%, light gray: 29%). b) Influence of pH variation, measuring PEG-co-PDEGA with 29% DEGA fraction (red: pH 7, black: pH 9, dark gray: pH 11, light gray: pH 14). Data from Reuss et al.⁶⁹

¹H NMR measurements in D₂O varying both temperature and pH value gave a first hint what is happening upon heating or acidification of the aqueous polymer solutions. As an example, for mPEG-*b*-DMAEMA,⁵⁹ signals of both blocks were present at room temperature. For elevated temperatures near the cloud point, signals of the DMAEMA block broadened and became less intensive. This process was reversible and pointed to formation of micelles with DMAEMA cores and PEG coronas. Since the PDMAEMA signals did not disappear completely, the micelles were believed to retain some degree of hydration. For mPEG-*b*-PDEAEMA, exhibiting a PDEAEMA block insoluble in water in its unprotonated state, micelle formation could be induced at room temperature by adjusting the pH. At pH 2, signals for both blocks were visible. Here, the polymers existed as unimers in solution. At pH 9, PDEAEMA signals disappeared completely. Micelles with deprotonated, hydrophobic PDEAEMA cores

were formed, which were fully dehydrated. Similar observations were made for other polyether polyamine block and graft copolymers.^{25,46,59,63}

Another technique used to gain more insight into the polymer's behavior in aqueous solution before and at the cloud point, is electron paramagnetic resonance (EPR) spectroscopy. It has been applied to aqueous solutions of random and block PEG-PDEGA copolymers in a temperature range of 20 – 90 °C.⁷⁵ The amphiphilic spin probe (2,2,6,6-tetramethylpiperidin-1-yl)oxyl (TEMPO) was added to the solutions. The resonances of TEMPO in hydrophobic or hydrophilic surroundings differ and enable the microscopic analysis of formation of hydrophobic cavities in the polymers upon heating. For the PEG-*b*-PDEGA block copolymers with large PDEGA blocks, static inhomogeneities were found. The TEMPO radical became trapped in the micellar aggregates. For PEG-*b*-PDEGA with shorter PDEGA blocks, dynamic inhomogeneities were diagnosed, with increasing movement of TEMPO in and out of the micelles with increasing temperature and thus increasing kinetic energy. On the other hand, for PEG-*co*-PDEGA, probe exchange decreased with increasing temperature until it was no longer visible on the EPR timescale. The collapse mechanism of the gradient copolymers was believed to proceed in two steps: First, the unimer micelles, with DEGA units in the core and PEG loops as the outer shell, collapse. Only then, inter-chain aggregation takes place.

3.1.2 *Supramolecular Interaction: Micellization and Gelation*

Micellization of polyether polyamines has been the object of many studies in recent years, with focus on possible carrier applications in the field of biomedicine and capitalizing on the added value of pH-responsiveness included through the amines. Biotinylated and non-biotinylated PEG-*b*-PDEAEMA were shown to have identical micellization properties, irrespective of the added functional group at the micellar corona.⁴² In dynamic light scattering, a sharp micelle to unimer transition was observed upon a decent pH change from 7.3 to 7.0, again caused by complete deprotonation of the PDEAEMA core. Static light scattering revealed decreasing aggregation numbers with decreasing pH value and development of a Gaussian coil-like morphology. TEM showed uniform particles with a diameter of 50 nm at pH 11 and large, porous aggregates of 300 nm at pH 7.4. This was consistent with light scattering results, explained by existence of core-shell structures and aggregates of random Gaussian coil-like structures at pH 11 and 7.4, respectively. Critical micelle concentrations (CMC) were determined with a tensiometer. Similar CMC values were obtained for biotinylated and non-biotinylated samples, although the surface tensions of the biotinylated materials were generally higher.

Cai and Armes⁷⁶ observed a trinity of micelles from their zwitterionic ABC triblock copolymer PEG-*b*-PDEAEMA-*b*-poly(2-succinyloxyethyl methacrylate) (PEG-*b*-PDEAEMA-*b*-PSEMA). At low pH, PEG and protonated PSEMA formed a hydrogen-bonded complex core with a cationic PDEAEMA shell. Increasing the pH led to formation of a PSEMA/PDEAEMA interpolyelectrolyte complex core with PEG shell. Further increase of the pH resulted in hydrophobic PDEAEMA cores with an anionic PEG/PSEMA shell.

Self-assembly of (PEG-*co*-*lin*PG)-*g*-PDMAEMA at varying pH and ionic strength was studied in TEM.⁵⁰ At low pH, worm-like cylinder structures were formed. In presence of NaCl, fractals were observed. By adjusting both pH and salinity, fractal aggregates with different topologies were obtained. Furthermore, the graft copolymer solution showed shear thickening behavior. This graft copolymer was compared to its cyclized pendant by Huang and coworkers.⁵¹ The critical micellization pH value was lower for the cyclic than for the linear compound.

By reaction of double hydrophilic POEGMA-*b*-PAEMA with pyrene carboxaldehyde, the apolar pyrene moiety was bound as a Schiff base to the PAEMA block. This step induced micelle formation with pyrene in the core and allowed for CMC determination via the pyrene method. Release of pyrene from the micelles was monitored via fluorescence spectroscopy. At physiological pH 7.4, almost no pyrene was released. Release of almost 80% of the payload and cleavage of the imine bond was possible at pH 5.5 after 80 hours. Control experiments for determination of 100% release were carried out at pH 1.

Incorporation of a sufficient amount of hydrophobic comonomer BuMA in triblock copolymers with OEGMA and DMAEMA effected gelation in phosphate buffer solutions.^{37,38} This was not the case for the equivalent random terpolymers. Increasing molecular weight led to decreasing gel point temperatures because of decreasing LCSTs and more pronounced physical entanglement of the chains.

In concentrated aqueous solutions at high pH, PDMAEMA-*b*-PEG-*b*-PDMAEMA triblock copolymers caused gelation because of hydrophobic interactions of the deprotonated PDMAEMA blocks.⁴⁴ This was measured by rheological measurements on the 25 wt% solutions, with shear thinning above pH 13. Upon heating, the solutions changed from transparent to opaque and reversibly formed a gel at 80 °C. From non-crosslinked gels of PDEAEMA-*b*-PEG-*b*-PPO-*b*-PEG-*b*-PDEAEMA pentablock copolymers,^{64,77} pH-dependent release of the included model drug Nile blue chloride (NBCl) could be shown. At the same time, cytotoxicity of the gels was low. Thus, these materials offer potential for use as injectable hydrogels in medicine: once injected, a drug can be released from the hydrogel continuously over time.

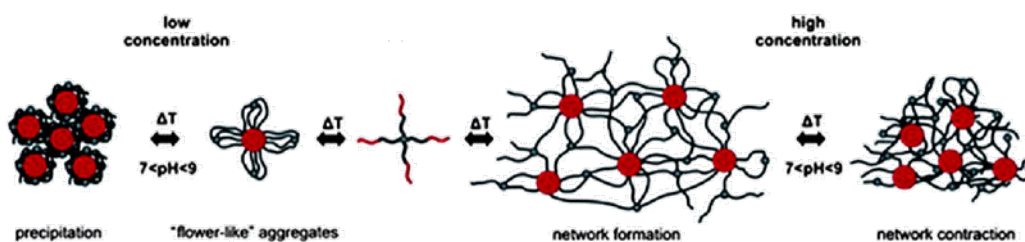


Figure 4. Aggregation and network formation of the dual temperature- and pH-responsive 4-arm star PDMAEMA-*b*-POEGMA copolymers in dependence of concentration (red: POEGMA, black: PDMAEMA). Slightly modified from Schmalz et al.²⁴

Furthermore, star block copolymers are suitable for micellar and gel applications.^{24,48} Schmalz et al.²⁴ obtained smart hydrogels from 4-arm star PDMAEMA-*b*-POEGMA copolymers. Flower-like aggregates were formed in dilute solution upon heating because of collapse of the outer POEGMA block (Figure 4). Further increase of temperature led to a response of the inner PDMAEMA block according to the pH. A sequential collapse starting with the outer block could be triggered at a suitable pH environment, and hydrogels were formed. Temperature control could be used for manipulation of the mechanical properties of the gels. Interestingly, gels formed at pH 8 did not show changes in their moduli at temperatures above the transition temperature of PDMAEMA. Thus, strong gels were obtained under these conditions. Gels made at pH 9 exhibited significantly reduced gel strengths and moduli drops above the cloud point of the PDMAEMA blocks. Quaternization of the inner PDMAEMA blocks led to loss of pH sensitivity but allowed for introduction of UV-sensitive, multivalent $[\text{Co}(\text{CN})_6]^{3-}$ counterions. Additionally, increased effective volume fraction of the polycation stars led to significant decreases of the critical gelation concentrations.

3.2 Shell Cross-Linked (SCL) Micelles

A fundamental problem of block copolymer micelles is their spontaneous disassembly at concentrations below their critical micelle concentration (CMC). Robust nanoparticles have been reported by Wooley's group⁷⁸ in 1996 after cross-linking of the micelle coronas at high dilution, leading to shell cross-linked (SCL) micelles. Since this first example, many other cross-linking strategies have been used, as reviewed by Read and Armes.⁷⁹ While SCL micelles from diblock copolymers have to be prepared at high dilution, ABC triblock copolymers containing an outer PEG block as steric stabilizer can be cross-linked at much higher copolymer concentrations (> 1% solids content) without inter-micellar cross-linking (Figure 5).

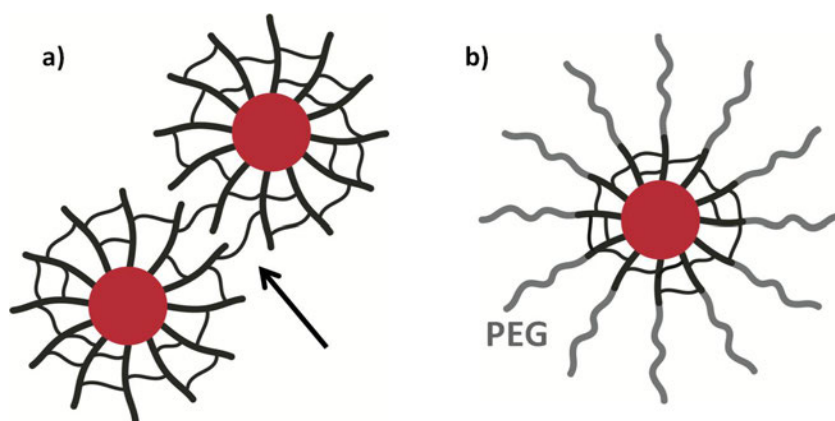
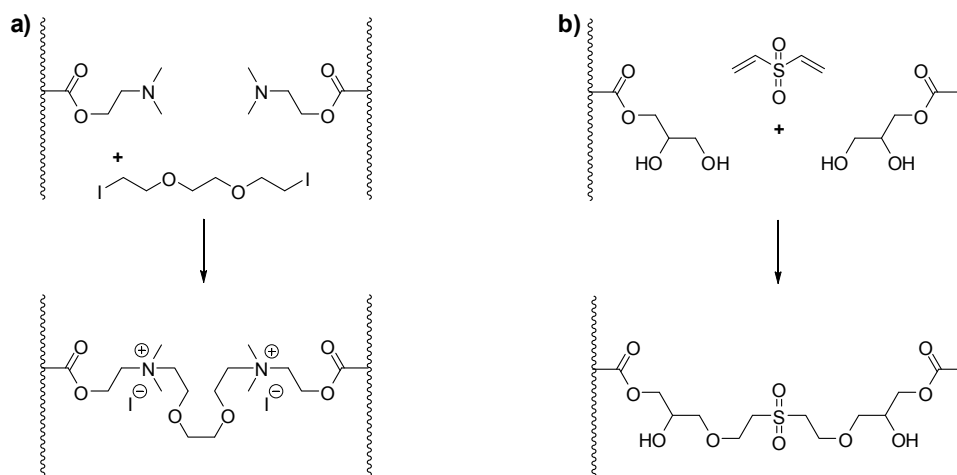


Figure 5. Schematic representation of intra- and inter-micellar cross-linking for a) diblock copolymer (arrow highlights inter-micellar cross-linking) and b) ABC triblock copolymer containing PEG as sterically stabilizing corona (only intra-micellar cross-linking).

This is the reason for use of polyether polyamines in SCL micelle chemistry. In most cases, cross-linking is carried out using the bifunctional agent 1,2-bis(2-iodoethoxy)ethane (BIEE) and proceeds via intermolecular quaternization of the amino moieties (Scheme 3, a). For ABC triblock copolymers, this concept was initially published by Bütün et al.⁸⁰ using PEG-*b*-PDMAEMA-*b*-PMEMA triblock copolymers synthesized by ATRP. The PMEMA block was selectively salted out by addition of sodium sulphate. In this procedure the triblock self-assembled into three-layer “onion” micelles in aqueous solution at 20 °C, with PMEMA core and PDMAEMA inner shell. PEG acted as stabilizing corona because of the energetically favorable PEG-water interactions. Cross-linking of the PDMAEMA layer with BIEE was possible at 10% solids content. In absence of the PEG block, macroscopic gelation occurred under these conditions, proving its stabilizing effect. Shell cross-linking was verified by dilution and acidification of the solution to pH 2. If no cross-linking had occurred, the micelles would have disassembled into individually solved triblock copolymer chains. However, in DLS measurements, micelles were still detected, proving successful formation of SCL micelles.

PPO-*b*-PDMAEMA-*b*-POEGMA ABC triblocks were also shown to self-assemble *in situ* into micelles at 40 °C at pH 8.5 in aqueous solution.²² The LCST of PPO is around 15 °C, so PPO formed the core at this temperature. At 60 – 70 °C, also the PDMAEMA block collapsed. Again, the PDMAEMA inner shell was cross-linked with BIEE. DLS studies at 20 °C indicated the existence of water-swollen SCL micelles. On heating of the micelles, the hydrodynamic radius decreased due to progressive dehydration of the micelle cores. This swelling behavior has shown to be reversible. Thus, these “nanogels” offer potential as delivery vehicles for temperature-controlled release applications.



Scheme 3. Cross-linking reactions of a) amino residues of DMAEMA with 1,2-bis(2-iodoethoxy)ethane (BIEE) and b) hydroxyl residues of GMA with divinylsulfone (DVS).

Also PEG-*b*-PDMAEMA-*b*-poly(*tert*-butylaminoethyl methacrylate) copolymers have been employed to prepare SCL micelles via BIEE cross-linking with solid contents up to 25%.⁶²

SCL micelles with pH-responsive cores have been synthesized from PEG-*b*-PDMAEMA-*b*-PDEAEMA.⁴⁵ While these triblocks were molecularly dissolved at low pH, unprotonated PDEAEMA formed a micelle core above pH 7.3. Robust SCL micelles were obtained after BIEE cross-linking. Abrupt changes in core hydrophilicity and water-uptake occurred between pH 7 and 8 due to protonation of the PDEAEMA units. The amount of swelling increased with increasing length of the PDEAEMA block and decreasing cross-linking degree. This should allow for pH-triggered release of hydrophobic drugs from the compartment.

Zwitterionic SCL micelles were the objective of a study by Ding et al.,³¹ starting from self-assembled poly(*tert*-butylacrylate)-*b*-P(PEGMA-*co*-DMAEMA) terpolymers. After cross-linking with BIEE and formation of ammonium groups in the shell, poly(*tert*-butylacrylate) was hydrolyzed with trifluoroacetic acid to give the corresponding carboxylic acid moieties in the core. The size of the micelles increased during this step because of the transformation of the hydrophobic into a hydrophilic poly(acrylic acid) (PAA) core. The short PEG chains sufficed to offer stabilization and suppress inter-micellar reactions. Positive zeta potentials were measured at all pH values, indicating a positive surface charge. However, an abrupt increase in surface charge is observed at pH 7 – 8, in line with expectation.

A cross-linking reaction for hydroxyl groups employs divinylsulfone (DVS) and is an example of a Michael addition reaction. It has been used for SCL micelles from PEG-*b*-poly(glycerol monomethacrylate)-*b*-PDEAEMA and PEG-*b*-PHEMA-*b*-PDEAEMA.⁸¹

Cross-linking was also achieved by chain extension of POEGMA-*b*-PDMAEMA diblock micelles, synthesized by RAFT polymerization, with ethylene glycol dimethacrylate (EGDMA).³² Since cross-linking occurred on the surface of the micelles, it again was carried out in high dilution and EGDMA was diluted with PEGMA to minimize inter-micellar reactions. After cross-linking, a distinctive CMC value was no longer detectable. Surface tension decreased almost linearly with the logarithm of the polymer concentration, as has been observed before. Particle sizes decreased with increasing pH value of the environment with a sudden collapse around pH 7. Furthermore, stability against ionic strength change has been demonstrated. Especially high ionic strengths limit the usage of some gene delivery systems because of unimer formation. In contrast, the investigated SCL micelles remained unaffected by high salt concentrations. Good binding properties with oligonucleotides were shown in ethidium bromide displacement assays. Cytotoxicity of fluorescence-labeled SCL micelles was tested using fibroblast L929 cell lines. Endocytosis was confirmed in fluorescence spectroscopy, although it seemed to be significantly less prominent than for the PDMAEMA homopolymer control. On the other hand, after 46 h of treatment, the PDMAEMA homopolymer-treated cells did not survive while SCL nanoparticles did not show any signs of cytotoxicity, thanks to the encapsulation of the toxic PDMAEMA in the POEGMA shell.

3.3 Non-viral Vectors for Gene Delivery

For the cure of many severe diseases such as cancer and genetic diseases, hopes are placed in gene therapy. A target gene is inserted into cells with the help of a carrier vector, either viral or non-viral. The vector has to be able to transport DNA in the blood stream, cross the cell membrane, and free the genetic material near the nucleus. Although viral vectors show high transfection efficiencies, they are not considered as being safe *in vivo*. Issues include immunogenicity and mutation of the host genome. Non-viral vectors are considered the more controllable alternative. Their synthesis is simple and properties are tunable by variation of composition, molecular weight, and architecture, but they suffer from inferior transfection efficiencies. DNA can be complexed by cationically charged polymers into small neutral or cationic polyplexes (Figure 6, A). These are able to cross the negatively charged cell membrane by endocytosis (B), either non-specific or receptor-mediated, depending on the existence of target molecules on the polyplex surface. After dissociation of the polyplex and release of the genetic material from the endosome (C), internalization of the DNA into the nucleus is

possible (D).⁸² The cationic polymers are often combined with PEG to reduce surface charge density and cytotoxicity of the resulting polyplexes. PEG has anti-fouling properties and shields the positively charged complexes from interactions with serum proteins and blood cells, improves colloidal stability, and prolongs the circulation time in the blood stream.⁸³ General synthetic strategies for polymeric vectors via controlled or living polymerization methods have been comprehensively reviewed recently.^{82,83}

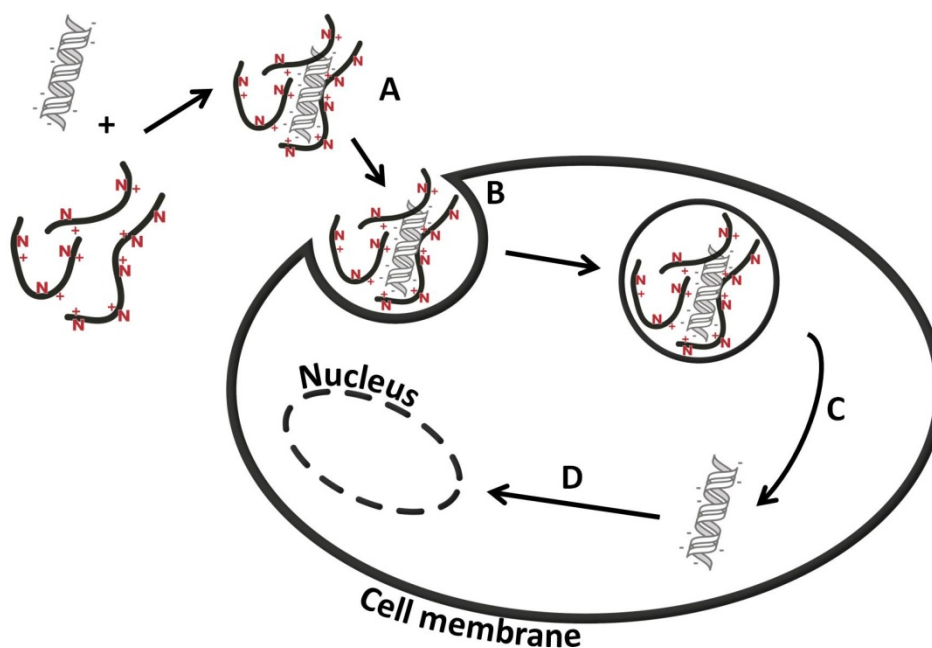


Figure 6. Pathways of gene transfection promoted by a cationic multi-aminofunctional polymer as non-viral vector. A) Complexation of DNA with cationic polymer, formation of polyplex; B) non-specific or receptor-mediated endocytosis; C) release of DNA; D) translocation to nucleus.

The influence of PEG architecture and molecular weight on gene transfection performance has been examined *in vitro*.^{36,52,84,85} For this purpose, PDMAEMA homopolymer, PEG-*b*-PDMAEMA, POEGMA-*b*-PDMAEMA, and PEGMA-*co*-PDMAEMA copolymers have been compared. All polymers were shown to bind and condense different kinds of DNA,³⁶ confirmed by gel electrophoresis, ethidium bromide displacement, and TEM. The presence of PEG improved the polymers' ability to bind DNA, colloidal stable complexes were obtained. In TEM, spherical objects of uniform size were observed and DLS resulted in diameters of 80 – 100 nm, suitable for endocytosis. On the other hand, PDMAEMA homopolymer gave agglomerated particles. However, transfection efficiencies of the PEG-containing copolymers were reduced compared to PDMAEMA. PEG increased the hydrophilicity of the polymer-DNA complexes, which was positive in terms of solubility and biocompatibility, but at

the same time made it difficult for them to bind and penetrate into cells. The above-mentioned polymer architectures were also compared concerning their potential as vectors for phosphorothioate antisense oligonucleotides (ISIS 5132).⁸⁵ All polymers showed good binding ability with the oligonucleotides (ON). PEGMA-*co*-PDMAEMA was found to have the highest binding ability and formed highly soluble complexes that did not phase separate from a buffer solution. PEG-*b*-PDMAEMA and POEGMA-*b*-PDMAEMA formed compact, colloiddally stable complexes with diameters of 80 – 150 nm and a micellar structure. All copolymers displayed lower cytotoxicity than poly(L-lysine) controls. In a study on the complexes of the same polymers with plasmid DNA using flow cytometry and laser confocal microscopy, different rates and extents of interaction with and internalization in cells depending on the polymer architecture were analyzed.⁸⁴ While introduction of polyether chains generally lowered interaction, the micelle-forming PEG-*b*-PDMAEMA and POEGMA-*b*-PDMAEMA were found superior to the statistical copolymer PEGMA-*co*-PDMAEMA. Cell associations generally increased over time and association of complexes with cells resulted in endocytosis, with the exception of the statistical copolymer. In another study,⁵² increase of molecular weight of statistical copolymers resulted in somehow improved gene expression efficiency. Furthermore, statistical copolymers were less cytotoxic than their blocky counterparts. Other studies employed star block copolymers, triblock, and pentablock copolymers.^{23,55,86,87}

Also polymerization degree and choice of aminofunctional monomer plays a role. Longer PAEMA segments in PEG-*b*-PAEMA gave better transfection results.⁸⁸ PEG-*b*-PDEAEMA exhibited much less tendency to condense DNA and to penetrate cells in comparison with PDMAEMA homopolymer and PEG-*b*-PDMAEMA.⁸⁹ This was attributed to the more amphiphilic character of PEG-*b*-PDEAEMA and the neutral charge of the resulting complexes. The positively charged PEG-*b*-PDMAEMA/DNA complexes penetrated cells more easily.

In order to still profit from the lower cytotoxicity of PEGylated polyamines in polyplex formation but still effect high transfection efficiencies, scissile copolymers have been created. Acid-labile PEG-*a*-PDMAEMA block copolymers with cyclic ortho-ester linkages at the junction point were prepared by Lin et al.⁴³ By changing the structure of the ortho-esters, hydrolytic stability could be tuned. The polymers effectively complexed DNA into PEGylated nanoparticles with low surface charges. At the physiological pH of blood (pH 7.4), the particles were stable and had lower cytotoxicity than without PEG. After endocytosis, the particles were subjected to the endosomal pH (pH 5.0). The acetal at the block junction was hydrolyzed and the PEG shield was removed. The resulting exposure of the positive surface charges facilitated membrane disruption and endosomal escape of the polyplexes. Gene transfection efficiencies were enhanced compared to the stable block copolymers.

Bioreducible PDMAEMA-SS-PEG-SS-PDMAEMA ABA triblock copolymers with disulfide linkages were designed by Zhong and coworkers recently.⁵⁴ After DNA condensation, small particles with diameters less than 120 nm and close to zero zeta potentials were obtained. In saline solution, the particles were colloidally stable. However, in the presence of the reducing agent dithiothreitol (DTT), the polyplexes were deshielded rapidly. Positive surface charges and particle sizes increased significantly and DNA release was proven in gel retardation assays. In vitro transfection efficacies of the reversibly shielded polyplexes were 28 times higher than of the stably shielded control complexes. Confocal laser scanning microscopy was used to show efficient delivery and release of plasmid DNA near and into the nuclei of the cells. Another way to incorporate reducible disulfide linkages into polymeric non-viral vector agents was explored by Tao et al.⁹⁰ Low molecular weight PDMAEMA chains were cross-linked using a disulfide dimethacrylate, yielding larger hyperbranched polymers. The positive charges on the surface were covered by PEGMA chains connected to the surface, at the same time decreasing the toxicity of the polymer. DNA could be bound efficiently and destruction of the hyperbranched polymer into oligomeric chains in a reducible environment was possible. A similar approach was chosen by Matyjaszewski and coworkers for the preparation of reducible cationic nanogels for nucleic acid delivery in inverse miniemulsion.⁹¹

Approaches to targeted delivery included the conjugation of lactose to PEG-*b*-PDMAEMA vectors by Wakebayashi et al.⁹² following a route published earlier, via reactive aldehyde groups at the PEG terminus.⁶⁰ The goal was selective transfection of hepatic cells. Lactosylated polyplexes with plasmid DNA were substantially more transfection efficient against HepG2 cells than non-lactosylated controls. These receptors possessed asialoglycoprotein (ASGP) receptors recognizing the β -D-galactose residues. ASGP receptor-mediated endocytosis was proposed to be a major route of the cellular uptake of the lactosylated micelles.

Polyether polyamine copolymers have also been used for micellization with heparin³⁹ and hydrophobic Re(phen) complexes.²⁰ The latter were used for in vitro cell imaging, capitalizing on the red emission of the organometallic complexes. Bifunctional particles with complexed Re(phen) and DNA have potential for simultaneous gene transfection and imaging purposes.

3.4 Surface Functionalization

PEG is often used as an anti-fouling surface-modification agent. First reports of Nagaoka and coworkers⁹³ date back to 1982, where a PEG polymer brush, i.e., PEG immobilized at the chain end on a substrate surface to form a tethered chain, was shown to improve anti-thrombogenicity. Both PEG chain length and grafting density are important parameters for the design of repellent surfaces. The

group of Nagasaki introduced the concept of surface functionalization with mixed PEGs of different chain lengths, e.g., 5000 g mol⁻¹ and 2000 g mol⁻¹, for improved passivation against protein interactions.^{3,94-96}

For attachment of PEG to gold surfaces, PEG-SH is commonly used because of the formation of strong Au-S linkages (47 kcal mol⁻¹).⁹⁷ However, under physiological conditions, the thiolate species are prone to oxidation and damage by exposure to light, high temperature, and oxygen. Additionally, exchange reactions with thiolated compounds inside the body occur.⁹⁵ On the other hand, long-term stability has been obtained by use of PEGs with multiple amino groups attached. These polyvalent interactions are stable even under physiological conditions,⁴⁰ although the coordination of one nitrogen lone pair to gold is fairly weak (3 – 6 kcal mol⁻¹).^{97,98} Nagasaki's group attached PEG to different surfaces either using pentaethylenehexamine-terminated PEG (N6-PEG),⁹⁹⁻¹⁰² PEG-*b*-PDMAEMA,¹⁰³⁻¹⁰⁵ or POEGMA-*co*-PDMAEMA¹⁰³ (co)polymers.

They were used, for example, in enzyme-linked immunosorbent assays. In these assays, immune complexes attached to a solid phase were quantified using microtiter plates or immunomagnetic beads.^{101,104} Densely packed mixed N6-PEG tethered chains surrounded the immobilized antibodies on magnetic surfaces. This resulted in low non-specific binding and high specific sensitivity, giving high signal-to-noise (S/N) ratios. Both S/N ratios as well as dispersion stabilities in cell lysate were much higher for the N6-PEG coated beads than for those using the conventional blocking agent bovine serum albumin (BSA). The dense PEG brushes were believed to also enhance orientation of the antibody and accessibility of the antigens.

Another tool in molecular biology is the sensitive and selective detection of target molecules on DNA-modified gold surfaces. For this purpose, single stranded DNA (ssDNA) is usually anchored on the surface via an Au-S linkage. However, amine groups of non-hybridized nucleobases in ssDNA are also able to interact with gold surfaces and thus become unavailable for hybridization with the target DNA on the surface. Hence, the remaining free gold surface has to be blocked. PEG-*b*-PDMAEMA and POEGMA-*co*-PDMAEMA of almost identical elemental composition were studied concerning their blocking ability using angle-resolved X-ray photoelectron spectroscopy (ARXPS, Figure 7).¹⁰³ In the case of the POEGMA-*co*-PDMAEMA copolymers, the ratio between nitrogen and carbon atomic composition (N/C ratio) was identical over all take-off angles (90 – 0°). For PEG-*b*-PDMAEMA copolymers, the N/C ratio was also stable for measurements at 90 – 45°, but decreased dramatically from 45 – 0°. Hence, nitrogen content in the upper part of the polymer layer was lowered. PDMAEMA segments were concentrated on the gold surface, shielded by PEG reaching into the solution. Using PEG-*b*-PDMAEMA of different chain lengths, ssDNA/PEG-*b*-PDMAEMA hybrid surfaces on gold substrates were constructed.¹⁰⁵ Hybridization behavior of the immobilized probe ssDNA was assessed

by SPR measurements. PEG-*b*-PDMAEMA inhibited the interaction of the gold surface with nucleobases in ssDNA and forced the immobilized ssDNA into a standing conformation, readily able to hybridize with the complementary ssDNA.

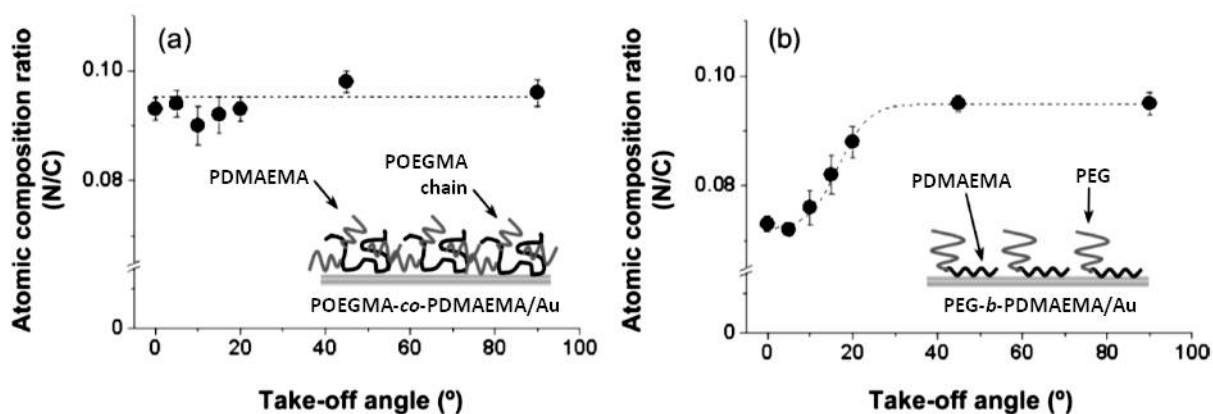


Figure 7. ARXPS data of a) POEGMA-co-PDMAEMA- and b) PEG-*b*-PDMAEMA-modified gold surfaces. The illustrations show possible structures of the PEG polyamine layers. This figure is reproduced from Yoshimoto et al.¹⁰³ and has been slightly modified.

In addition to flat gold surfaces, also gold nanoparticles have been modified with PEG-*b*-PDMAEMA.⁴⁰ Under alkaline conditions (pH > 10) and a ratio of [N] to gold nanoparticle (GNP) of more than 3,300, the PEGylated GNPs showed complete dispersion stability without coagulation. Coordination of the tertiary amino groups, fully deprotonated at pH 10 and above, was not electrostatic of nature, but a multipoint coordination. Zeta potentials of the PEG GNPs were shielded to almost 0 mV, regardless of chain length. However, too long PDMAEMA chain lengths resulted in coagulation after purification. Short PDMAEMA segments improved long-term stability. PEG density on the GNP surface increased as the PDMAEMA chain length decreased to three repeating units. Dispersion stability of the PEGylated GNPs was also retained in BSA solution and in 95% human serum. In addition, PEGylated GNPs containing thiol-siRNA (small interfering RNA) showed significant RNA interference activity, i.e., gene inhibition, in human hepatoma cells (HuH-7).¹⁰⁶

PEG-polyamine block copolymers, PEG-*b*-PDMAEMA and PEG-*b*-PDEGA, were also able to act as dual reducing and capping agents for the simultaneous reduction of auric cations in aqueous solution and PEGylation of the resulting gold colloids, without the need for additional reducing agents.^{69,107} Upon addition of the block copolymer to an aqueous solution of tetrachloroauric acid, a color change from colorless to bright red could be observed. This red color is typical for gold colloids in water and

is caused by the surface plasmon resonance of the metallic nanoparticles. The color change could be quantified by evolution of an absorption band in UV/Vis spectroscopy around 520 nm (Figure 8).⁶⁹ This was not the case for the gradient copolymers PEG-*co*-PDEGA, consistent with the belief that auric cation reduction takes place in the interior of the micelles formed by the block copolymers, with a DEGA core and a PEG corona. Transmission electron micrographs proved the formation of spherical gold nanoparticles with narrow size distributions. Also, thermo- and pH-sensitive gold nanoparticles were obtained from tetrachloroauric acid and H-shaped (PNIPAM/PDMAEMA)-*b*-PEG-*b*-(PNIPAM/PDMAEMA) copolymers.⁴⁹ The concept of PEGylation of particles by PEG-*b*-polyamines could be extended to materials such as CdS quantum dots¹⁰⁸ and inorganic nanoporous clay.¹⁰⁹

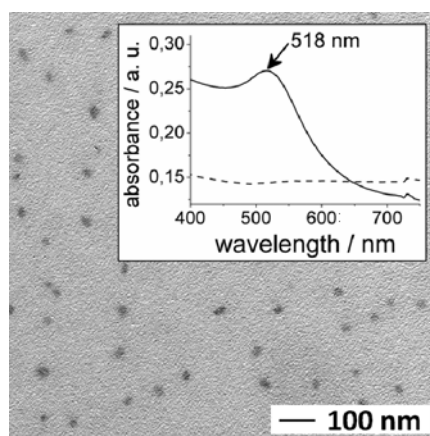


Figure 8. TEM of gold nanoparticles produced in PEG-*b*-PDEGA. Inset: Representative UV/Vis spectra of reaction solutions with PEG-*co*-PDEGA (dashed line) and PEG-*b*-PDEGA (solid line). Reproduced from Reuss et al.⁶⁹

Primary amines from deprotected PEG-PDAGA copolymers have been used not only for attachment of the polymer to the nanoparticle, but also for further functionalization and derivatization reactions.¹¹⁰ In this work, an acetal-protected catechol initiator was used for AROP of EO and DAGA. It was inspired by L-DOPA (L-dihydroxyphenylalanine), an important component in the mussel adhesive protein. This catechol moiety is well-known for its ability to strongly attach to several metal oxide surfaces. In the cited work, the obtained catechol-PEG-PGA copolymers were used for surface modification of oleate-capped MnO nanoparticles, rendering them water-soluble. MnO are promising candidates for use as T₁ contrast agents in magnetic resonance imaging (MRI), resulting in a positive contrast. The reactivity of the primary amines at the MnO nanoparticle-

polymer shell was proven in a model reaction with fluoresceine isothiocyanate (FITC), a fluorescent dye.

3.5 Other Applications

PEGMA-*co*-PDEAEMA has also been used as pH-responsive stabilization agent for emulsions of tetradecane in water and dispersions of carbendazim in water by Shahalom et al.¹¹¹ An important advantage of copolymer stabilizers over short-chain surfactants is the simple introduction of responsiveness within the surfactant layer in a homogeneous manner through structural variation. The copolymer chains themselves collapsed pH-triggered at pH values above the pK_a . The resulting droplet and particulate dispersions showed weak flocculation at pH values above the pK_a , the emulsions coalesced at low pH values. The best dispersion stabilities were obtained at pH values slightly below the pK_a . Potential for this concept is seen in applications for triggered release in the body, e.g., in injectable emulsions or particulate dispersions.

Poly(quarternary ammonium) salts have antimicrobial properties,¹¹² but introducing biocompatibility to such compounds has been a challenge. One strategy to combat haemolysis has been the incorporation of PEG.^{113,114} So, use of cationic copolymers of OEGMA and quaternized DMAEMA as antimicrobial materials has been explored by Venkataraman et al.¹¹⁵ Through the quaternization reaction of the dimethylamines with functional halides, moieties such as alkyl, primary alcohol, primary amine, and carboxylic acid were introduced. Furthermore, the amphiphilic balance could be varied by the choice of the functional halide. The antimicrobial activities were determined against Gram-positive bacteria, *Bacillus subtilis*. The polymer concentration needed to completely inhibit bacterial growth, i.e. the minimum inhibitory concentration (MIC), depended on both the nature of the functional group and the hydrophobicity of the compounds. Alkyl and alcohol substituents were found to be effective agents, with MICs in the range 20 – 80 mg L⁻¹. Additionally, haemolytic properties of the studied polymers were analyzed on mouse red blood cells. Again, polymers with short alkyl chains or hydroxyl groups effected only little haemolysis, but retained their antimicrobial activity.

4. Outlook

Polymeric structures combining polyethers in linear or graft form, i.e. PEG, OEG(M)A, or PEGMA, with multiple amino groups from acrylic, methacrylic, or epoxide monomers have attracted increasing interest in recent years. They show high potential in a wide variety of application areas.

1.1) AMINOFUNCTIONAL POLYETHERS

This is, first of all, due to the manifold possibilities to synthesize these polymers via controlled methods, leading to well-defined materials. Secondly, properties can be tailored for each purpose, such as dual temperature- and pH-responsive behavior and water-solubility. This behavior is introduced through both polyether and polyamine components and can thus be readily tuned by copolymer microstructure and composition. Amino functionalities can be employed for attachment of polyether copolymers to flat or nanoparticle surfaces, rendering them, e.g., anti-fouling. Such platforms for further functionalization and for bio-assays with high signal-to-noise ratios can be designed from polyether polyamines. Furthermore, the high level of control over synthesis and properties is promising for applications in areas as sensitive as the human body. Hopes are placed in stimuli-sensitive polymers, (injectable) hydrogels, and shell cross-linked micelles in terms of drug release upon an internal or external trigger or for long-term medication purposes.

References

- [1] Bolto, B. A. *Prog. Polym. Sci.* **1995**, *20*, 987-1041.
- [2] Feigenbaum, H. N. *Cosmet. Toiletries* **1993**, *108*, 73-77.
- [3] Nagasaki, Y. *Chem. Lett.* **2008**, *37*, 564-569.
- [4] Schacher, F.; Ulbricht, M.; Müller, A. H. E. *Adv. Funct. Mater.* **2009**, *19*, 1040-1045.
- [5] Jeong, J. H.; Kim, S. W.; Park, T. G. *Prog. Polym. Sci.* **2007**, *32*, 1239-1274.
- [6] Obermeier, B.; Wurm, F.; Mangold, C.; Frey, H. *Angew. Chem. Int. Ed.* **2011**, *50*, 7988-7997.
- [7] Mangold, C.; Wurm, F.; Frey, H. *Polym. Chem.* **2012**, *3*, 1714-1721.
- [8] Knop, K.; Hoogenboom, R.; Fischer, D.; Schubert, U. S. *Angew. Chem. Int. Ed.* **2010**, *49*, 6288-6308.
- [9] Lutz, J.-F. *Adv. Mater.* **2011**, *23*, 2237-2243.
- [10] Hu, Z.-B.; Cai, T.; Chi, C.-L. *Soft Matter* **2010**, *6*, 2115-2123.
- [11] Fuertges, F.; Abuchowski, A. *J. Controlled Release* **1990**, *11*, 139-148.
- [12] Pasut, G.; Veronese, F. M. *Adv. Drug Del. Rev.* **2009**, *61*, 1177-1188.
- [13] Jäger, M.; Schubert, S.; Ochrimenko, S.; Fischer, D.; Schubert, U. S. *Chem. Soc. Rev.* **2012**, *41*, 4755-4767.
- [14] Luxenhofer, R.; Han, Y.; Schulz, A.; Tong, J.; He, Z.; Kabanov, A. V.; Jordan, R. *Macromol. Rapid Commun.* **2012**, DOI: 10.1002/marc.201200354.
- [15] Schlaad, H.; Diehl, C.; Gress, A.; Meyer, M.; Demirel, A. L.; Nur, Y.; Bertin, A. *Macromol. Rapid Commun.* **2010**, *31*, 511-525.
- [16] Adams, N.; Schubert, U. S. *Adv. Drug Deliv. Rev.* **2007**, *59*, 1504-1520.
- [17] Zhang, X.; Xia, J.; Matyjaszewski, K. *Macromolecules* **1998**, *31*, 5167-5169.
- [18] Lad, J.; Harisson, S.; Mantovani, G.; Haddleton, D. M. *Dalton Trans.* **2003**, 4175-4180.
- [19] Munoz-Bonilla, A.; Fernandez-Garcia, M.; Haddleton, D. M. *Soft Matter* **2007**, *3*, 725-731.
- [20] Liu, L.; Li, X.; Hou, S.; Xue, Y.; Yao, Y.; Ma, Y.; Feng, X.; He, S.; Lu, Y.; Wang, Y.; Zeng, X. *Chem. Commun.* **2009**, 6759-6761.
- [21] Liu, L.; Yang, Y.-L.; Wang, C.; Yao, Y.; Ma, Y.-Z.; Hou, S.; Feng, X.-Z. *Colloids Surf., B* **2010**, *75*, 230-238.
- [22] Liu, S.; Armes, S. P. *J. Am. Chem. Soc.* **2001**, *123*, 9910-9911.
- [23] Xu, F. J.; Zhang, Z. X.; Ping, Y.; Li, J.; Kang, E. T.; Neoh, K. G. *Biomacromolecules* **2009**, *10*, 285-293.
- [24] Schmalz, A.; Schmalz, H.; Müller, A. H. E. *Soft Matter* **2012**, *8*, 9436-9445.
- [25] Gu, L.; Feng, C.; Yang, D.; Li, Y.; Hu, J.; Lu, G.; Huang, X. *J. Polym. Sci., Part A: Polym. Chem.* **2009**, *47*, 3142-3153.
- [26] Chiefari, J.; Chong, Y. K.; Ercole, F.; Krstina, J.; Jeffery, J.; Le, T. P. T.; Mayadunne, R. T. A.; Meijs, G. F.; Moad, C. L.; Moad, G.; Rizzardo, E.; Thang, S. H. *Macromolecules* **1998**, *31*, 5559-5562.
- [27] Sahnoun, M.; Charreyre, M.-T.; Veron, L.; Delair, T.; D'Agosto, F. *J. Polym. Sci., Part A: Polym. Chem.* **2005**, *43*, 3551-3565.
- [28] Fournier, D.; Hoogenboom, R.; Thijs, H. M. L.; Paulus, R. M.; Schubert, U. S. *Macromolecules* **2007**, *40*, 915-920.
- [29] Kelen, T.; Tüdös, F.; Turcsányi, B.; Kennedy, J. P. *J. Polym. Sci., Part A: Polym. Chem.* **1977**, *15*, 3047-3074.
- [30] Kennedy, J. P.; Kelen, T.; Tüdös, F. *J. Polym. Sci., Part A: Polym. Chem.* **1975**, *13*, 2277-2289.
- [31] Ding, Z.-L.; He, W.-D.; Tao, J.; Jiang, W.-X.; Li, L.-Y.; Pan, T.-T. *J. Polym. Sci., Part A: Polym. Chem.* **2011**, *49*, 2783-2789.

- [32] Zhang, L.; Nguyen, T. L. U.; Bernard, J.; Davis, T. P.; Barner-Kowollik, C.; Stenzel, M. H. *Biomacromolecules* **2007**, *8*, 2890-2901.
- [33] Boyer, C.; Priyanto, P.; Davis, T. P.; Pissuwan, D.; Bulmus, V.; Kavallaris, M.; Teoh, W. Y.; Amal, R.; Carroll, M.; Woodward, R.; St Pierre, T. *J. Mater. Chem.* **2010**, *20*, 255-265.
- [34] Dai, X.-H.; Hong, C.-Y.; Pan, C.-Y. *Macromol. Chem. Phys.* **2012**, n/a-n/a.
- [35] Vamvakaki, M.; Billingham, N. C.; Armes, S. P. *Polymer* **1999**, *40*, 5161-5171.
- [36] Rungsardthong, U.; Deshpande, M.; Bailey, L.; Vamvakaki, M.; Armes, S. P.; Garnett, M. C.; Stolnik, S. *J. Controlled Release* **2001**, *73*, 359-380.
- [37] Ward, M. A.; Georgiou, T. K. *J. Polym. Sci., Part A: Polym. Chem.* **2010**, *48*, 775-783.
- [38] Ward, M. A.; Georgiou, T. K. *Soft Matter* **2012**, *8*, 2737-2745.
- [39] Dufresne, M.-H.; Leroux, J.-C. *Pharm. Res.* **2004**, *21*, 160-169.
- [40] Miyamoto, D.; Oishi, M.; Kojima, K.; Yoshimoto, K.; Nagasaki, Y. *Langmuir* **2008**, *24*, 5010-5017.
- [41] Dong, A.; Zhai, Y.; Xiao, L.; Qi, H.; Tian, Q.; Deng, L.; Guo, R. *J. Polym. Sci., Part B: Polym. Phys.* **2010**, *48*, 503-508.
- [42] Tan, J. F.; Ravi, P.; Too, H. P.; Hatton, T. A.; Tam, K. C. *Biomacromolecules* **2005**, *6*, 498-506.
- [43] Lin, S.; Du, F.; Wang, Y.; Ji, S.; Liang, D.; Yu, L.; Li, Z. *Biomacromolecules* **2008**, *9*, 109-115.
- [44] Peng, Z.; Li, G.; Liu, X.; Tong, Z. *J. Polym. Sci., Part A: Polym. Chem.* **2008**, *46*, 5869-5878.
- [45] Liu, S.; Weaver, J. V. M.; Tang, Y.; Billingham, N. C.; Armes, S. P.; Tribe, K. *Macromolecules* **2002**, *35*, 6121-6131.
- [46] Lee, S. B.; Russell, A. J.; Matyjaszewski, K. *Biomacromolecules* **2003**, *4*, 1386-1393.
- [47] Determan, M. D.; Guo, L.; Thiyagarajan, P.; Mallapragada, S. K. *Langmuir* **2006**, *22*, 1469-1473.
- [48] He, E.; Ravi, P.; Tam, K. C. *Langmuir* **2007**, *23*, 2382-2388.
- [49] Li, L.-Y.; He, W.-D.; Li, W.-T.; Zhang, K.-R.; Pan, T.-T.; Ding, Z.-L.; Zhang, B.-Y. *J. Polym. Sci., Part A: Polym. Chem.* **2010**, *48*, 5018-5029.
- [50] Sui, K.; Zhao, X.; Wu, Z.; Xia, Y.; Liang, H.; Li, Y. *Langmuir* **2012**, *28*, 153-160.
- [51] Pang, X.; Jing, R.; Pan, M.; Huang, J. *Sci. China Chem.* **2010**, *53*, 1653-1662.
- [52] Venkataraman, S.; Ong, W. L.; Ong, Z. Y.; Joachim Loo, S. C.; Rachel Ee, P. L.; Yang, Y. Y. *Biomaterials* **2011**, *32*, 2369-2378.
- [53] Yan, L.; Tao, W. *Polymer* **2010**, *51*, 2161-2167.
- [54] Zhu, C.; Zheng, M.; Meng, F.; Mickler, F. M.; Ruthardt, N.; Zhu, X.; Zhong, Z. *Biomacromolecules* **2012**, *13*, 769-778.
- [55] Zhu, J.-L.; Cheng, H.; Jin, Y.; Cheng, S.-X.; Zhang, X.-Z.; Zhuo, R.-X. *J. Mater. Chem.* **2008**, *18*, 4433-4441.
- [56] Iijima, M.; Nagasaki, Y.; Kato, M.; Kataoka, K. *Polymer* **1997**, *38*, 1197-1202.
- [57] Lascelles, S. F.; Malet, F.; Mayada, R.; Billingham, N. C.; Armes, S. P. *Macromolecules* **1999**, *32*, 2462-2471.
- [58] Nagasaki, Y.; Sato, Y.; Kato, M. *Macromol. Rapid Commun.* **1997**, *18*, 827-835.
- [59] Vamvakaki, M.; Billingham, N. C.; Armes, S. P. *Macromolecules* **1999**, *32*, 2088-2090.
- [60] Kataoka, K.; Harada, A.; Wakebayashi, D.; Nagasaki, Y. *Macromolecules* **1999**, *32*, 6892-6894.
- [61] Schacher, F.; Müllner, M.; Schmalz, H.; Müller, A. H. E. *Macromol. Chem. Phys.* **2009**, *210*, 256-262.
- [62] de Paz Banez, M. V.; Robinson, K. L.; Bütün, V.; Armes, S. P. *Polymer* **2001**, *42*, 29-37.
- [63] Ni, P.-H.; Pan, Q.-S.; Zha, L.-S.; Wang, C.-C.; Elaïssari, A.; Fu, S.-K. *J. Polym. Sci., Part A: Polym. Chem.* **2002**, *40*, 624-631.
- [64] Anderson, B. C.; Cox, S. M.; Bloom, P. D.; Sheares, V. V.; Mallapragada, S. K. *Macromolecules* **2003**, *36*, 1670-1676.

- [65] Truong, N. P.; Jia, Z.; Burges, M.; McMillan, N. A. J.; Monteiro, M. J. *Biomacromolecules* **2011**, *12*, 1876-1882.
- [66] Koyama, Y.; Umehara, M.; Mizuno, A.; Itaba, M.; Yasukouchi, T.; Natsume, K.; Suginaka, A.; Watanabe, K. *Bioconjugate Chem.* **1996**, *7*, 298-301.
- [67] Obermeier, B.; Wurm, F.; Frey, H. *Macromolecules* **2010**, *43*, 2244-2251.
- [68] Reuss, V. S.; Obermeier, B.; Dingels, C.; Frey, H. *Macromolecules* **2012**, *45*, 4581-4589.
- [69] Reuss, V. S.; Werre, M.; Frey, H. *Macromol. Rapid Commun.* **2012**, *33*, 1556-1561.
- [70] Rangelov, S.; Tsvetanov, C. *Des. Monomers Polym.* **2001**, *4*, 39-43.
- [71] Weber, C.; Hoogenboom, R.; Schubert, U. S. *Prog. Polym. Sci.* **2012**, *37*, 686-714.
- [72] Lutz, J. F. *Adv. Mater.* **2011**, *23*, 2237-2243.
- [73] Triftaridou, A. I.; Vamvakaki, M.; Patrickios, C. S. *Polymer* **2002**, *43*, 2921-2926.
- [74] Mangold, C.; Obermeier, B.; Wurm, F.; Frey, H. *Macromol. Rapid Commun.* **2011**, *32*, 1930-1934.
- [75] Kurzbach, D.; Schömer, M.; Wilms, V. S.; Frey, H.; Hinderberger, D. *Macromolecules* **2012**, *45*, 7535-7548.
- [76] Cai, Y.; Armes, S. P. *Macromolecules* **2004**, *37*, 7116-7122.
- [77] Determan, M. D.; Guo, L.; Thiyagarajan, P.; Mallapragada, S. K. *Langmuir* **2005**, *22*, 1469-1473.
- [78] Thurmond, K. B.; Kowalewski, T.; Wooley, K. L. *J. Am. Chem. Soc.* **1996**, *118*, 7239-7240.
- [79] Read, E. S.; Armes, S. P. *Chem. Commun.* **2007**, 3021-3035.
- [80] Bütün, V.; Wang, X. S.; de Paz Báñez, M. V.; Robinson, K. L.; Billingham, N. C.; Armes, S. P.; Tuzar, Z. *Macromolecules* **2000**, *33*, 1-3.
- [81] Liu, S.; Ma, Y.; Armes, S. P.; Perruchot, C.; Watts, J. F. *Langmuir* **2002**, *18*, 7780-7784.
- [82] Heath, W. H.; Senyurt, A. F.; Layman, J.; Long, T. E. *Macromol. Chem. Phys.* **2007**, *208*, 1243-1249.
- [83] Xu, F. J.; Yang, W. T. *Prog. Polym. Sci.* **2011**, *36*, 1099-1131.
- [84] Deshpande, M. C.; Davies, M. C.; Garnett, M. C.; Williams, P. M.; Armitage, D.; Bailey, L.; Vamvakaki, M.; Armes, S. P.; Stolnik, S. *J. Controlled Release* **2004**, *97*, 143-156.
- [85] Deshpande, M. C.; Garnett, M. C.; Vamvakaki, M.; Bailey, L.; Armes, S. P.; Stolnik, S. *J. Controlled Release* **2002**, *81*, 185-199.
- [86] Agarwal, A.; Unfer, R.; Mallapragada, S. K. *J. Controlled Release* **2005**, *103*, 245-258.
- [87] Xu, F. J.; Li, H. Z.; Li, J.; Zhang, Z. X.; Kang, E. T.; Neoh, K. G. *Biomaterials* **2008**, *29*, 3023-3033.
- [88] Tang, R.; Palumbo, R. N.; Nagarajan, L.; Krogstad, E.; Wang, C. *J. Controlled Release* **2010**, *142*, 229-237.
- [89] Tan, J. F.; Hatton, T. A.; Tam, K. C.; Too, H. P. *Biomacromolecules* **2007**, *8*, 448-454.
- [90] Tao, L.; Chou, W. C.; Tan, B. H.; Davis, T. P. *Macromol. Biosci.* **2010**, *10*, 632-637.
- [91] Averick, S. E.; Paredes, E.; Irastorza, A.; Srinivasan, A.; Siegwart, D. J.; Magenau, A. J. D.; Cho, H. Y.; Shrivats, A. R.; Hsu, E.; Kim, J.; Liu, S.; Hollinger, J. O.; Das, S. R.; Matyjaszewski, K. *Biomacromolecules* **2012**.
- [92] Wakebayashi, D.; Nishiyama, N.; Yamasaki, Y.; Itaka, K.; Kanayama, N.; Harada, A.; Nagasaki, Y.; Kataoka, K. *J. Controlled Release* **2004**, *95*, 653-664.
- [93] Mori, Y.; Nagaoka, S.; Takiuchi, H.; Kikuchi, T.; Noguchi, N.; Tanzawa, H.; Noishiki, Y. *Trans. Am. Soc. Artif. Intern. Organs* **1982**, *28*, 459-463.
- [94] Nagasaki, Y. *Chem. Lett.* **2008**, *37*, 564-569.
- [95] Nagasaki, Y. *Polym. J.* **2011**, *43*, 949-958.
- [96] Nagasaki, Y. *Sci. Technol. Adv. Mater.* **2010**, *11*, 054505.
- [97] Di Felice, R.; Selloni, A. *J. Chem. Phys.* **2004**, *120*, 4906-4914.

- [98] Pong, B.-K.; Lee, J.-Y.; Trout, B. L. *Langmuir* **2005**, *21*, 11599-11603.
- [99] Kubota, M.; Yoshimoto, K.; Yuan, X.; Nagasaki, Y. *Polym. J.* **2011**, *43*, 493-496.
- [100] Yuan, X.; Yoshimoto, K.; Nagasaki, Y. *Anal. Chem.* **2009**, *81*, 1549-1556.
- [101] Nagasaki, Y.; Kobayashi, H.; Katsuyama, Y.; Jomura, T.; Sakura, T. *J. Colloid Interface Sci.* **2007**, *309*, 524-530.
- [102] Furusho, H.; Kitano, K.; Hamaguchi, S.; Nagasaki, Y. *Chem. Mater.* **2009**, *21*, 3526-3535.
- [103] Yoshimoto, K.; Nozawa, M.; Matsumoto, S.; Echigo, T.; Nemoto, S.; Hatta, T.; Nagasaki, Y. *Langmuir* **2009**, *25*, 12243-12249.
- [104] Yuan, X.; Fabregat, D. a.; Yoshimoto, K.; Nagasaki, Y. *Anal. Chem.* **2009**, *81*, 10097-10105.
- [105] Yoshimoto, K.; Matsumoto, S.; Asakawa, R.; Uchida, K.; Ishii, T.; Nagasaki, Y. *Chem. Lett.* **2007**, *36*, 1444-1445.
- [106] Oishi, M.; Nakaogami, J.; Ishii, T.; Nagasaki, Y. *Chem. Lett.* **2006**, *35*, 1046-1047.
- [107] Ishii, T.; Otsuka, H.; Kataoka, K.; Nagasaki, Y. *Langmuir* **2004**, *20*, 561-564.
- [108] Nagasaki, Y.; Ishii, T.; Sunaga, Y.; Watanabe, Y.; Otsuka, H.; Kataoka, K. *Langmuir* **2004**, *20*, 6396-6400.
- [109] Takahashi, T.; Yamada, Y.; Kataoka, K.; Nagasaki, Y. *J. Controlled Release* **2005**, *107*, 408-416.
- [110] Wilms, V. S.; Bauer, H.; Tonhauser, C.; Schilman, A.-M.; Müller, M.-C.; Tremel, W.; Frey, H. *to be submitted* **2012**.
- [111] Shahalom, S.; Tong, T.; Emmett, S.; Saunders, B. R. *Langmuir* **2006**, *22*, 8311-8317.
- [112] Kenawy, E.-R.; Worley, S. D.; Broughton, R. *Biomacromolecules* **2007**, *8*, 1359-1384.
- [113] Sellenet, P. H.; Allison, B.; Applegate, B. M.; Youngblood, J. P. *Biomacromolecules* **2007**, *8*, 19-23.
- [114] Allison, B. C.; Applegate, B. M.; Youngblood, J. P. *Biomacromolecules* **2007**, *8*, 2995-2999.
- [115] Venkataraman, S.; Zhang, Y.; Liu, L.; Yang, Y.-Y. *Biomaterials* **2010**, *31*, 1751-1756.

2) MULTIAMINOFUNCTIONAL POLYETHERS

2.1) Thermoresponsive Copolymers of Ethylene Oxide and *N,N*-Diethyl Glycidyl Amine: Polyether Polyelectrolytes and PEGylated Gold Nanoparticle Formation

Valerie S. Reuss, Mathias Werre, Holger Frey

Published in Macromol. Rapid Commun. 2012, 33, 1556-1561.

Abstract

The synthesis of diblock as well as gradient copolymers of *N,N*-diethyl glycidyl amine (DEGA) with ethylene oxide (EO) via anionic ring-opening polymerization is presented. The polymers exhibit low polydispersities (≤ 1.13) and molecular weights in the range of 3300–10 200 g mol⁻¹. In PEG-*co*-PDEGA copolymers, incorporation of 4%–29% DEGA results in tailorable cloud point temperatures in aqueous solution and melting points depending on DEGA content. mPEG-*b*-PDEGA block copolymers can be quaternized to generate cationic double-hydrophilic polyelectrolyte copolymers with polyether backbone. Furthermore, mPEG-*b*-PDEGA has been used as dual reducing and capping agent for gold nanoparticle synthesis.

1. Introduction

Poly(ethylene glycol) (PEG) and its recently developed multifunctional derivatives (*mf*-PEGs)¹⁻³ represent a highly versatile class of water-soluble polyether materials. Fields of application range from the simple additives in care products to soluble catalyst supports and bioconjugation, that is, PEGylation, for pharmaceutical purposes. Depending on the desired application and the relative reactivities of the monomers, graft, random, gradient, or block copolymers can be prepared.

Random or gradient multi-aminofunctional PEG copolymer structures have been obtained by concurrent anionic ring-opening polymerization (AROP) of ethylene oxide (EO) and glycidyl amine (GA) derivatives.⁴ Graft structures include poly(aminoethyl methacrylate)-poly(PEG methyl ether methacrylate) copolymers from free-radical copolymerization,⁵ poly(L-lysine)-*graft*-PEG,⁶⁻⁷ and poly(ethylene imine)-*graft*-PEG.⁸ PEG-polyamine block copolymers have been realized previously using end-group-modified PEG monomethyl ether (mPEG) as a macroinitiator for anionic or atom transfer radical polymerization of *N,N*-(dimethylamino)ethyl methacrylate (DMAEMA).⁹⁻¹¹ Quaternization results in cationic polyelectrolytes.

PEG-polyamine copolymers in neutral or cationic state have been used for various purposes such as the preparation of polyion complex micelles for drug delivery,^{11,12} stabilization of gold colloids under physiological conditions¹³⁻¹⁶ as well as one-step syntheses of PEGylated gold nanoparticles through polymer-induced reduction of auric cations and colloid stabilization.^{13,17}

Here, we report on the synthesis of new copolymer architectures utilizing *N,N*-diethyl glycidyl amine (DEGA) as a novel monomer building block for AROP (Figure 1). Polymerization is achieved in a single step, resulting in materials with a mere polyether backbone. Copolymerization has been studied using online ¹H NMR and turbidimetric as well as calorimetric measurements of the obtained compounds. Methylation of the polymers results in quaternized DEGA repeating units (qDEGA) and leads to the first reported completely polyether-based double-hydrophilic cationic polyelectrolyte block copolymer structure. Furthermore, mPEG-*b*-PDEGA can be applied in auric acid reduction, directly resulting in the formation of PEG-decorated gold nanoparticles.

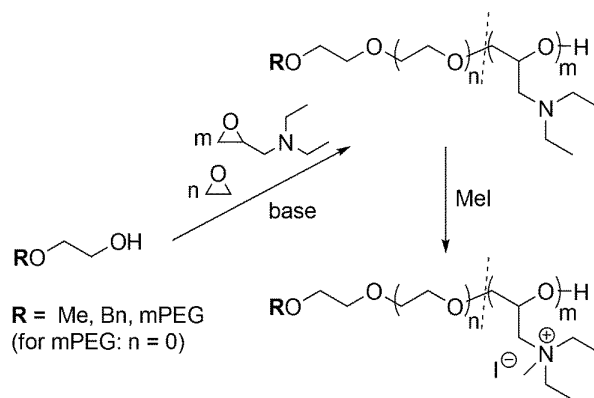


Figure 1. Synthesis of PEG-PDEGA block and gradient copolymers and subsequent quaternization to give cationic copolyelectrolytes.

2. Experimental Section

Instrumentation, reagent details, and monomer synthesis are given in the Supporting Information.

2.1. Block Copolymer Synthesis (mPEG-*b*-PDEGA)

mPEG (1 eq.), cesium hydroxide monohydrate (0.9 eq.), and 10 mL benzene were added sequentially to a dry Schlenk flask under argon atmosphere. Stirring at 60 °C for 30 min and evacuation at 90 °C for 3 h afforded the partially deprotonated macroinitiator. The respective amount of DEGA was syringed in and the reaction mixture was stirred for 12 h. After addition of 0.3 mL methanol and cooling, the polymer was dissolved in chloroform and filtered to remove salts. The solvents were removed under reduced pressure. Precipitation from methanol into cold diethyl ether and drying in high vacuum afforded the block copolymer in quantitative yields.

2.2. Random Copolymerization of Ethylene Oxide and *N,N*-Diethyl Glycidyl Amine (PEG-*co*-PDEGA)

In a dry Schlenk flask under argon atmosphere, 177 mg cesium hydroxide monohydrate (1.05 mmol, 1 eq.) was suspended in 5 mL benzene. After addition of 80 mg 2-methoxyethanol (1.05 mmol, 1 eq.), the mixture was stirred at 60 °C for 30 min and evacuated at 70 °C overnight, affording the cesium alkoxide. 5 mL DMSO and approximately 30 mL THF were added to the evacuated flask. The

flask was cooled to -80°C and EO was cryo-transferred from a graduated ampoule. DEGA was injected with a syringe. Polymerization was performed at 40°C for 12 h. Polymerizations were terminated by addition of methanol. Removal of THF under reduced pressure and precipitation in cold diethyl ether resulted in the pure polymer. Polymers were dried at 40°C in high vacuum or dissolved in water and lyophilized to give colorless to pale yellow materials in good yields (>90%).

2.3. Online ^1H NMR Kinetics

Polymerization in an NMR tube was carried out according to the literature⁴ with 19% DEGA at 40°C , recording spectra every 15 s.

2.4. Quaternization with Methyl Iodide (PEG-PqDEGA)

Quaternization of the tertiary amines to give the ammonium moieties (qDEGA) was carried out according to a literature procedure,¹⁸ adjusting the amount of reagents used to the number of amines present and taking the already tertiary character of these moieties in account.

2.5. Gold Nanoparticle Preparation

Aqueous solutions of tetrachloroaurate(III) hydrate ($\text{HAuCl}_4 \cdot 3 \text{H}_2\text{O}$, $2 \times 10^{-3} \text{ mol L}^{-1}$ in MilliQ water) and of the respective PEG-PDEGA polymer ($5 \times 10^{-3} \text{ mol L}^{-1}$ in MilliQ water) were mixed in a volume ratio of 1:9. After agitation by a vortex mixer for approximately 10 s, the reaction was allowed to proceed at room temperature for 3 h. During this time, a light red color was observed for the block copolymer-containing samples.

3. *Results and Discussion*

3.1. Monomer Synthesis

Via classic chemistry, the synthesis of DEGA can be realized in one step starting from epichlorohydrin and *N,N*-diethylamine in the presence of aqueous sodium hydroxide solution. A literature procedure has been adapted to give acceptable yields of 70% or more. Some loss of material during work-up can be observed, since distillation of the product is accompanied by

formation of a brownish viscous residue, which can most likely be ascribed to nucleophilic attack of the epoxide ring by the nitrogen atom, resulting in a polymeric by-product. This has not been observed for GA derivatives with bulkier substituents in previous work.^{4,19}

3.2. Copolymerization of EO and DEGA (PEG-co-PDEGA)

Initiated by cesium methoxy- or benzyloxy ethoxide, EO and DEGA have been copolymerized via AROP at 40 °C. Varying the DEGA fraction from 4% to 29%, well-defined PEG-co-PDEGA copolymers with molecular weights of approximately 6-8000 g mol⁻¹ and narrow molecular weight distributions with PDIs in the range of 1.09 to 1.13 have been obtained (Figure 2).

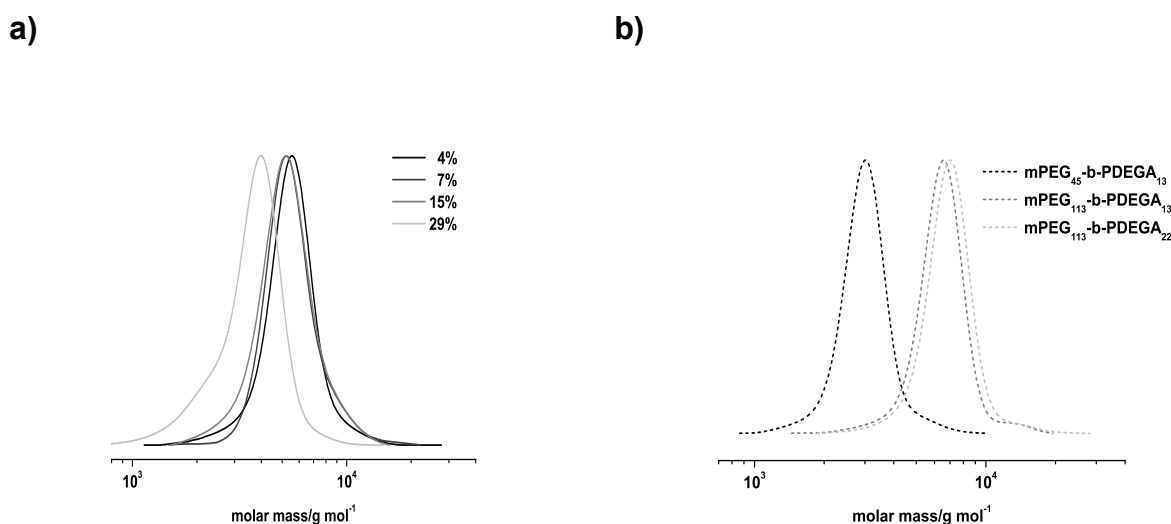


Figure 2. SEC elution traces (DMF, RI detection, PEG standards) of a) PEG-co-PDEGA (denoted as 4%, 7%, 15%, and 29% in the legend) and b) mPEG-b-PDEGA copolymers (denoted with polymer composition).

3.3. ¹³C NMR Triad Analysis

A first insight into copolymer microstructure is gained via ¹³C NMR analysis (Figure S5, Supporting Information). The chemical shift of the signal of the monitored repeating unit in the center of the monomer triad varies depending on the neighboring units. Following nomenclature in previous work on EO copolymers,^{4,20-22} the monomer units are denoted as D (DEGA) or E (EO), a and b representing first and second CH₂, respectively. As an example, focusing on the D_b signal in DEGA-centered triads at low field, new signals emerge with increasing amount of DEGA content in PEG-co-

PDEGA, while the signal for E-D_b-E remains the strongest resonance, indicating the absence of long blocks of D monomer at one chain end. On the other hand, EO units are less often observed at the terminus than would be expected from the EO percentage in the copolymer. For example, E-E_b-OH is only observed in the 4% copolymer. Although inverse gated experiments have not been carried out due to signal overlap, this is a first indication that reactivity ratios of the comonomers differ, with DEGA being less reactive, leading to increased incorporation of DEGA in the final stages of the copolymerization.

3.4. Online ¹H NMR Kinetics

In order to gain deeper insight into the distribution of DEGA comonomer at the backbone, polymerization has been carried out in DMSO-*d*₆ in a sealed NMR tube in the NMR spectrometer at 40 °C. By following the decrease of the monomer signal intensities and growth of the polymer backbone, the rate of consumption of EO and DEGA could be analyzed over time (Figure S7, Supporting Information). As has been observed for copolymerization of other GA derivatives with EO under these reaction conditions,^{4,19} the resulting copolymer exhibits a compositional drift. EO is incorporated at a higher rate, and therefore DEGA concentration increases from polymer initiator to terminus. Apparently, this effect is not governed by the steric demand of the groups at the tertiary amine, since the effect is of comparable magnitude in *N,N*-dibenzyl-, diallyl-, and the here presented diethyl-substituted GAs.^{4,19} It is also unlikely to be caused by the existence of two substituents in β-position to the epoxide, since attack of the epoxide ring takes place at the methylene position, and this would probably slow down propagation only. Possible causes include lower electronegativity of nitrogen versus oxygen as well as less effective coordination of the counterion with the GA, although this has only been described for potassium counterions in the rather unpolar THF before,²³ and not for the “soft” cesium cation in presence of DMSO used here.

3.5. Cloud Point Temperatures of Aqueous Polymer Solutions

PEG and its copolymers are known for their tunable lower critical solution temperature (LCST) behavior in water.² This holds also true for the synthesized PEG-*co*-PDEGA series, where the cloud point at a concentration of 20 mg mL⁻¹ spans the range from 55 °C for 29% DEGA fraction to 97 °C for 4% DEGA content (Figure S9, Supporting Information; Table 1). The LCSTs were found to be considerably higher than those observed for other GAs, for example, 6% DAGA (diallyl) results in a cloud point at 60 °C,¹⁹ 4% DBAG (dibenzyl) in 57 °C;² compared to 67 °C at a DEGA content as high as

15%. This again shows the expected less apolar and sterically less demanding character of DEGA compared to previously reported GA derivatives. Additionally, cloud points depend on pH, but not on the concentration of the aqueous solution at a certain pH (Figures S10 and S11, Table S1, Supporting Information), as has been observed for other functional polyethers.²

Table 1. Characterization data for the series of PEG-PDEGA copolymer structures.

compound	DEGA [%]	M _n (NMR) [g mol ⁻¹]	M _n (GPC) [g mol ⁻¹]	M _n /M _w	LCST [°C]	T _g [°C]	T _m [°C]	ΔH [J g ⁻¹]
PEG ₄₅ - <i>b</i> -PDEGA ₁₃	-	3700	2900	1.07	-	-	-	-
mPEG ₁₁₃ - <i>b</i> -PDEGA ₁₃	-	6700	5800	1.08	-	-	-	-
mPEG ₁₁₃ - <i>b</i> -PDEGA ₂₂	-	7900	6600	1.07	-	-	-	-
mPEG ₄₅ - <i>b</i> -PqDEGA ₁₃	-	5500	2900	1.05	-	-	-	-
mPEG ₁₁₃ - <i>b</i> -PqDEGA ₁₂	-	8200	3300	1.06	-	-	-	-
mPEG ₁₁₃ - <i>b</i> -PqDEGA ₁₇	-	10200	3300	1.03	-	-	-	-
PEG ₁₅₄ - <i>co</i> -PDEGA ₇	4	7700	5000	1.09	97	-66	40	89
PEG ₁₅₅ - <i>co</i> -PDEGA ₁₂	7	8400	4900	1.09	80	-65	43	77
PEG ₁₂₄ - <i>co</i> -PDEGA ₂₂	15	8300	4900	1.11	67	-70	23	43
PEG ₅₈ - <i>co</i> -PDEGA ₂₄	29	5700	3300	1.13	55	-71	-10	21

3.6. Thermal Properties by Differential Scanning Calorimetry

Thermal properties of the copolymers in bulk have been studied using DSC (Table 1). The glass transition temperature is hardly affected by copolymerization, with only a slight shift from -65°C (7%) to -71°C (29%), in the range of the literature value for PEG.²⁴ However, the melting temperatures decrease with increasing DEGA content in a nonlinear fashion. PEG has a melting temperature of 66 °C, which is already lowered considerably to 40°C upon incorporation of only 4% DEGA. Melting enthalpies show a more gradual decrease with increasing DEGA incorporation, indicating the effect of the comonomers to impede crystallization.

3.7. Block Copolymers (mPEG-*b*-PDEGA)

Block copolymers have been obtained in a single step initiated by partially deprotonated mPEG macroinitiators with molecular weights of 2000 or 5000 g mol⁻¹, respectively. Materials with narrow polydispersities < 1.1 have been obtained (Figure 2, Table 1). A certain extent of chain transfer to monomer was observed, resulting in lower degrees of polymerization and shorter DEGA block lengths than stoichiometrically expected. However, the low-molecular-weight side products can be removed easily via precipitation, giving well-defined mPEG-*b*-PDEGA compounds as analyzed by SEC and NMR.

3.8. Quaternization and Preparation of Polyether-Polyelectrolytes

Full methylation of PEG-*b*-PDEGA with methyl iodide resulted in a double-hydrophilic block copolymer consisting of a neutral hydrophilic PEG block and a cationically charged block. This polyelectrolyte can be obtained by anionic polymerization only without the need to switch the polymerization method in between the synthetic steps. To the best of our knowledge, it is the first compound of this kind which consists exclusively of a polyether backbone. This reaction can be followed by ¹H NMR spectroscopy, following the shift of the methylene protons of the diethylamino moiety under the backbone signals (Figure S4, Supporting Information). The methyl protons of ethyl and methyl groups remained visible separately and could be integrated to give the expected ratio of 6:3, indicating full conversion of all DEGA moieties to the quaternized units (qDEGA). In addition, a remarkable change in SEC elution behavior could be observed after quaternization (Table 1). SEC measurements had to be carried out in high dilution ($\approx 1/10$ of the usual sample concentration of 1 mg mL⁻¹). Despite the increase in molecular weight during this reaction, measured molecular weights were shifted considerably to lower values. This was not expected, since multiple positive charges on the backbone are believed to lead to a stiffening of the polymer chain and thus an increase in hydrodynamic volume. Nevertheless, the observed effect might be caused by attractive interaction of the neutral-charged polyether polyelectrolyte block copolymer with the column material, thereby decreasing the apparent molecular weight.

3.9. Gold Nanoparticle Synthesis

In several recent reports, PEG block copolymers have been shown to act directly both as dual reducing and capping agents for gold nanoparticle formation in aqueous solution by chemical reduction of hydrogen tetrachloroaurate(III) hydrate (HAuCl₄ · 3 H₂O).^{13,17,25} Amongst others, the

amphiphilic compounds Pluronic (PEO-PPO-PEO),^{26,27} Tetronics (X-shaped PEO-PPO block copolymer),²⁸ Surfamine (amino-terminated PEO-PPO)²⁹ and PEG-*b*-PDMAEMA¹⁰ have been used successfully for this purpose, while for PEG homopolymer particle aggregation has been observed in some cases.²⁶ The nonpolar blocks are believed to interact with the gold surface, while the hydrophilic PEG blocks extend into the aqueous environment, shielding the nanoparticles from aggregation.²⁷

The structurally analogous mPEG-*b*-PDEGA block copolymers were able to reduce HAuCl₄ at ambient temperature in the absence of energy input to give light red aqueous solutions with an absorption maximum centered at 518 nm (Figure 3, inset). This value lies within the typical range for the absorption of the surface plasmon of spherical gold nanoparticles.^{10,26} These particles could be visualized with TEM (Figure 3), using samples drop-cast onto copper grids. Only the gold nanospheres and not the polymer shell are visible in these images due to the low contrast of PEG. We assume the tertiary amines to become partially protonated upon addition of HAuCl₄, whereas the remaining non-protonated moieties reduce the AuCl₄⁻ counterion to metallic gold. The shape of the particle depends on the micellar shape, which in this case is obviously spherical. Solutions remained translucent after 2 months of storage at room temperature with no signs of precipitation, evidencing the excellent shielding properties of the novel polyether block copolymers. Control experiments with mPEG 5000 as well as PEG-*co*-PDEGA gradient copolymers did not produce gold nanoparticles under these conditions and remained colorless even after weeks without detectable UV absorption band or signs of precipitation.

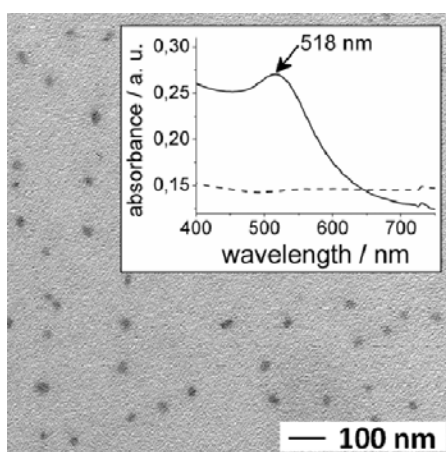


Figure 3. Transmission electron micrograph of gold nanoparticles produced in mPEG₁₁₃-*b*-PDEGA₁₃ (diameter: 21 ± 3 nm). Inset: Representative UV-Vis spectra of reaction solutions with PEG-*co*-PDEGA (dashed line) and mPEG-*b*-PDEGA (solid line, maximum at 518 nm indicates formation of gold nanospheres).

4. Conclusions

Employing the easily accessible DEGA as a new comonomer for AROP, versatile linear block and gradient polyether structures based on EO and DEGA (PEG-PDEGA) have been obtained. In online ^1H NMR kinetics and ^{13}C NMR triad analysis, copolymerization of DEGA with EO has been shown to lead to stimuli-responsive PEG-co-PDEGA copolymers of gradient microstructure with tailorable cloud points and melting temperatures depending on the fraction of apolar comonomer. Block copolymer synthesis is straightforward, resulting in mPEG-*b*-PDEGA suitable for use as dual reducing and capping agent in gold nanoparticle formation. Furthermore, quaternization of the DEGA block results in double hydrophilic neutral-charged cationic polyelectrolyte block copolymers representing the first examples of this type of structure with an exclusive polyether backbone. Clearly, the dialkyl GA structure offers vast further design possibilities for this class of well-defined polyether polyelectrolytes by variation of the alkyl chain structure.

Acknowledgments

The authors thank Dr. Mihail Mondeshki for online ^1H NMR measurements and Dennis Sauer for technical assistance. V.S.R. is grateful to the Fonds der Chemischen Industrie for a scholarship and to the Gutenberg-Akademie for funding. V.S.R. and M.W. thank the Graduate School “Materials Science in Mainz” for valuable financial support.

References

- [1] B. Obermeier, F. Wurm, C. Mangold, H. Frey, *Angew. Chem. Int. Ed.* **2011**, *50*, 7988.
- [2] C. Mangold, B. Obermeier, F. Wurm, H. Frey, *Macromol. Rapid Commun.* **2011**, *32*, 1930.
- [3] B. Obermeier, F. Wurm, H. Frey, *Macromolecules* **2010**, *43*, 2244.
- [4] L. Ionov, A. Synytska, E. Kaul, S. Diez, *Biomacromolecules* **2010**, *11*, 233.
- [5] N.-P. Huang, R. Michel, J. Voros, M. Textor, R. Hofer, A. Rossi, D. L. Elbert, J. A. Hubbell, N. D. Spencer, *Langmuir* **2000**, *17*, 489.
- [6] N.-P. Huang, J. Vörös, S. M. De Paul, M. Textor, N. D. Spencer, *Langmuir* **2002**, *18*, 220.
- [7] L. M. Bronstein, S. N. Sidorov, A. Y. Gourkova, P. M. Valetsky, J. Hartmann, M. Breulmann, H. Cölfen, M. Antonietti, *Inorg. Chim. Acta* **1998**, *280*, 348.
- [8] F. Schacher, M. Müllner, H. Schmalz, A. H. E. Müller, *Macromol. Chem. Phys.* **2009**, *210*, 256.
- [9] T. Ishii, H. Otsuka, K. Kataoka, Y. Nagasaki, *Langmuir* **2004**, *20*, 561.
- [10] K. Kataoka, A. Harada, D. Wakebayashi, Y. Nagasaki, *Macromolecules* **1999**, *32*, 6892.
- [11] N. Bayó-Puxan, M.-H. Dufresne, A. E. Felber, B. Castagner, J.-C. Leroux, *J. Controlled Release* **2011**, *156*, 118.
- [12] Y. Nagasaki, *Chem. Lett.* **2008**, *37*, 564.
- [13] D. Miyamoto, M. Oishi, K. Kojima, K. Yoshimoto, Y. Nagasaki, *Langmuir* **2008**, *24*, 5010.
- [14] M. Oishi, J. Nakaogami, T. Ishii, Y. Nagasaki, *Chem. Lett.* **2006**, *35*, 1046.
- [15] Y. Nagasaki, *Sci. Technol. Adv. Mater.* **2010**, *11*, 054505.
- [16] P. Alexandridis, *Chem. Eng. Technol.* **2011**, *34*, 15.
- [17] P. Mongondry, C. Bonnans-Plaisance, M. Jean, J. F. Tassin, *Macromol. Rapid Commun.* **2003**, *24*, 681.
- [18] V. S. Reuss, B. Obermeier, C. Dingels, H. Frey, *Macromolecules* **2012**, accepted.
- [19] T. Hamaide, A. Goux, M.-F. Llauro, R. Spitz, A. Guyot, *Angew. Makromol. Chem.* **1996**, *237*, 55.
- [20] F. Heatley, G. Yu, C. Booth, T. G. Blease, *Eur. Polym. J.* **1991**, *27*, 573.
- [21] V. Rejsek, D. Sauvanier, C. Billouard, P. Desbois, A. Deffieux, S. Carlotti, *Macromolecules* **2007**, *40*, 6510.
- [22] B. F. Lee, M. J. Kade, J. A. Chute, N. Gupta, L. M. Campos, G. H. Fredrickson, E. J. Kramer, N. A. Lynd, C. J. Hawker, *J. Polym. Sci., Part A: Polym. Chem.* **2011**, *49*, 4498.
- [23] J. Brandrup, E. H. Immergut, E. A. Grulke, *Polymer Handbook*, 4th edition, Wiley-Interscience, New York, **1999**, p. VI-253.
- [24] F. Dumur, A. Guerlin, E. Dumas, D. Bertin, D. Gimes, C. Mayer, *Gold Bull.* **2011**, *44*, 119.
- [25] T. Sakai, P. Alexandridis, *Langmuir* **2004**, *20*, 8426.
- [26] T. Sakai, P. Alexandridis, *J. Phys. Chem. B* **2005**, *109*, 7766.
- [27] S. Goy-López, P. Taboada, A. Cambón, J. Juárez, C. Alvarez-Lorenzo, A. Concheiro, V. Mosquera, *J. Phys. Chem. B* **2009**, *114*, 66.
- [28] T. Sakai, T. Mukawa, K. Tsuchiya, H. Sakai, M. Abe, *J. Nanosci. Nanotechnol.* **2009**, *9*, 461.
- [29] C. Mangold, F. Wurm, H. Frey, *Polym. Chem.* **2012**, DOI: 10.1039/C2PY00489E.

Supporting Information

Thermoresponsive Copolymers of Ethylene Oxide and N,N-Diethyl Glycidyl Amine: Polyether Polyelectrolytes and PEGylated Gold Nanoparticle Formation

Valerie S. Reuss, Mathias Werre, Holger Frey

Instrumentation

^1H NMR spectra (300 MHz and 400 MHz) and ^{13}C NMR spectra (75.5 MHz and 100 MHz) were recorded using a Bruker AC300 or a Bruker AMX400 spectrometer. All spectra were referenced internally to residual proton signals of the deuterated solvent. For SEC measurements in DMF (containing 0.25 g/L of lithium bromide as an additive), an Agilent 1100 Series was used as an integrated instrument, including a PSS HEMA column ($10^6/10^5/10^4$ g mol $^{-1}$), a UV (275 nm) and a RI detector. Calibration was carried out using poly(ethylene glycol) standards provided by Polymer Standards Service. DSC measurements were performed under nitrogen atmosphere using a PerkinElmer DSC 8500 with PerkinElmer CLN2 in the temperature range from -100 to 100 °C at heating rates of 20 and 10 K min $^{-1}$ for first and second heating run, respectively. Cloud points were determined in deionized water at a concentration of 20 mg mL $^{-1}$ and observed by optical transmittance of a light beam ($\lambda = 670$ nm). The measurements were performed in a Tepper turbidimeter TP1. The intensities of the transmitted light were recorded versus the temperature of the sample cell. The heating/cooling rate was 1 K min $^{-1}$. The cloud point temperatures of the sharp transitions from translucent to opaque solutions were defined as the values measured at 50% transmittance. Titration of pH values was performed using conc. HCl (aq.) and 50 wt.% NaOH (aq.), respectively. UV-Vis spectra were measured on a JASCO V-630 spectrometer in a quartz glass cuvette (diameter: 1 cm). Electron microscopy measurements were performed using a transmission electron microscope (FEI, XM12) with an acceleration voltage of 120 kV. Particle diameters were determined using ImageJ 1.45s.

Reagents

Poly(ethylene glycol) monomethyl ether (mPEG 5000, $M_n = 5000$ g mol $^{-1}$) was purchased from Fluka. Diallylamine, epichlorohydrin (99%), sodium hydroxide, ethylene oxide (99.5%), dimethylsulfoxide (puriss, over molecular sieve), and tetrachloroaurate(III) hydrate (99.999+%) were purchased from Aldrich. Deuterated chloroform- d_1 and DMSO- d_6 were purchased from Deutero GmbH. All other solvents and reagents were purchased from Acros Organics.

***N,N*-Diethyl Glycidyl Amine (DEGA, 1-diethylamino-2,3-epoxypropane)**

A modified literature procedure was applied.^[S1, S2] 39 g Epichlorohydrin (0.42 mol, 1.05 eq.), 29 g diethylamine (0.40 mol, 1 eq.), and a 50 wt.% aqueous solution of sodium hydroxide (1.75 eq.) were

added to a round-bottom flask and stirred vigorously at room temperature overnight. After centrifugation, the organic phase was separated and dried over sodium sulphate. Filtration and fractionating distillation (30 mbar, 60 °C) gave the product as a colorless liquid (yield: 70-80%). The compound was stored under argon at 8 °C and cryo-transferred from calcium hydride immediately prior to use. ¹H NMR (300 MHz, CDCl₃, δ): 3.04 (m, 1H, CH), 2.81-2.26 (m, 8H, CH₂), 1.02 (t, *J* = 7 Hz, 6H, CH₃).

[S1] H. Gilman, C. S. Sherman, C. C. Price, R. C. Elderfield, J. T. Maynard, R. H. Reitsema, L. Tolman, S. P. Massie, F. J. Marshall, L. Goldman, *J. Am. Chem. Soc.* **1946**, *68*, 1291.

[S2] *N,N*-Diethyl glycidyl amine is also commercially available from Evoblocks Inc. (EB14305).

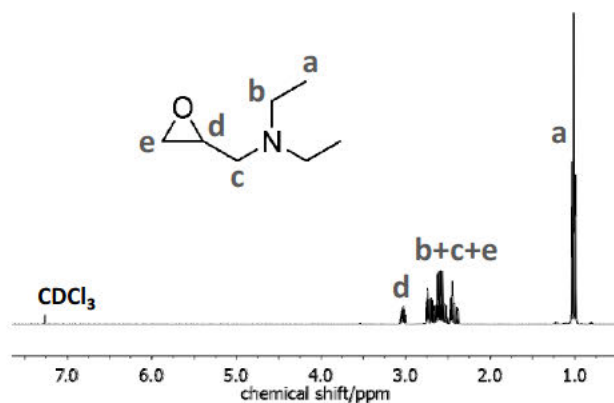


Figure S1. ^1H NMR spectrum (300 MHz, CDCl_3) of *N,N*-diethyl glycidyl amine (DEGA).

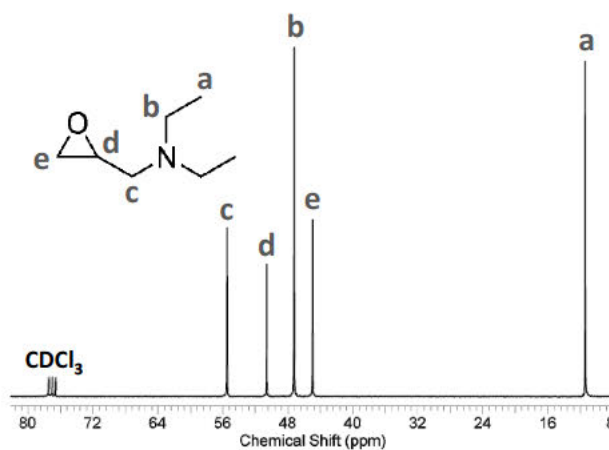


Figure S2. ^{13}C NMR spectrum (75.5 MHz, CDCl_3) of *N,N*-diethyl glycidyl amine (DEGA).

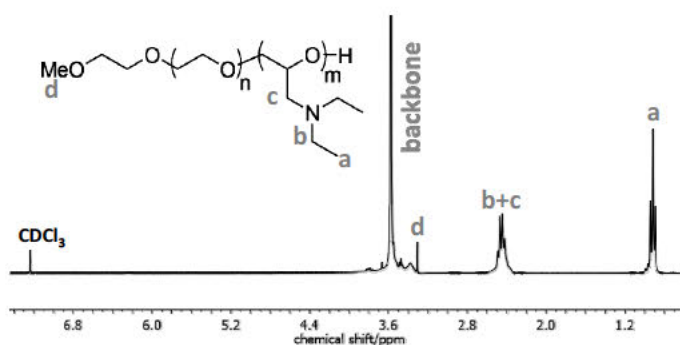


Figure S3. ^1H NMR spectrum (300 MHz, CDCl_3) of mPEG-*b*-PDEGA.

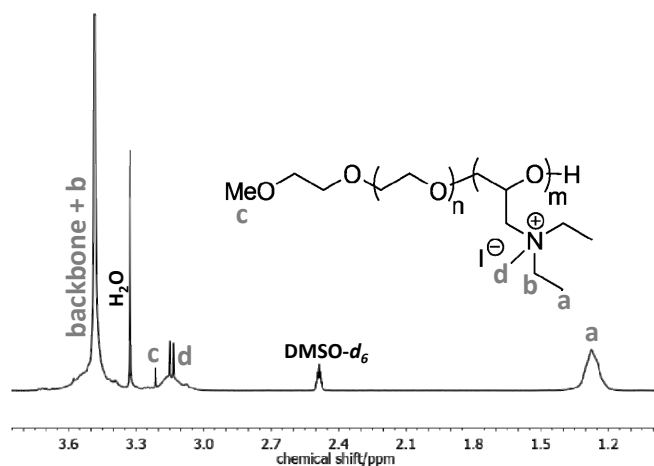


Figure S4. ^1H NMR spectrum (300 MHz, CDCl_3) of mPEG-*b*-PqDEGA.

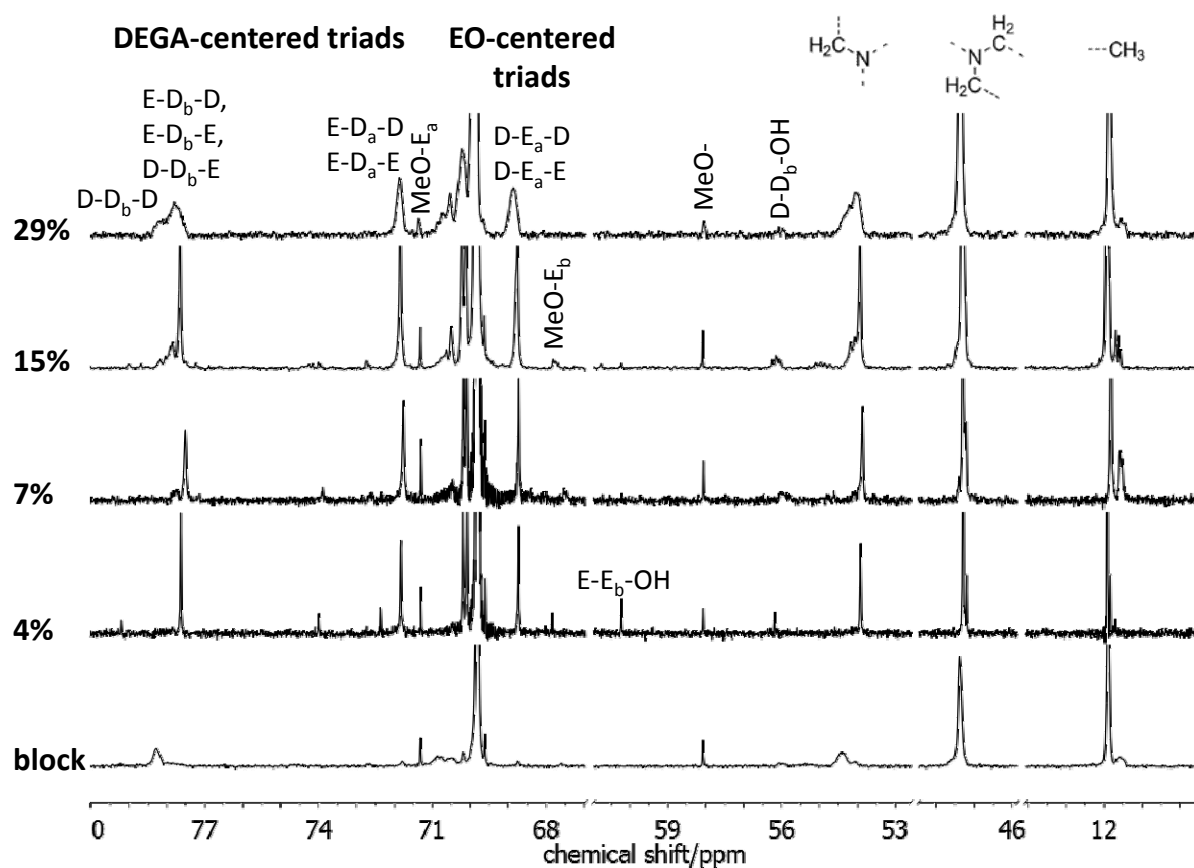


Figure S5. ^{13}C NMR spectra ($\text{DMSO-}d_6$) of mPEG₄₅-*b*-PDEGA₁₃ and PEG-*co*-PDEGA with 4%, 7%, 15%, and 29% DEGA fraction, respectively.

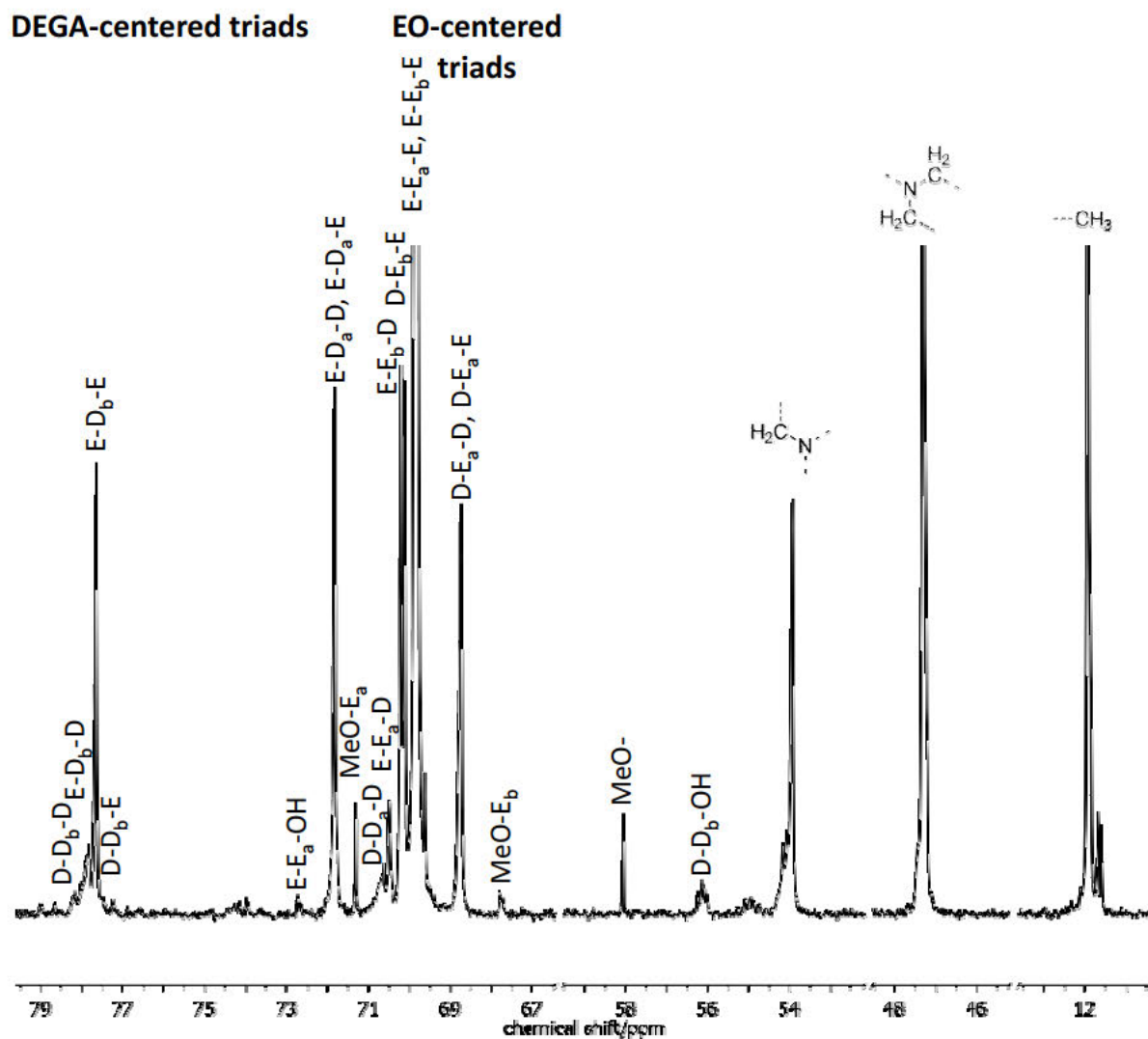


Figure S6. ^{13}C NMR spectrum ($\text{DMSO-}d_6$) of $\text{PEG}_{124}\text{-co-PDEGA}_{22}$ with triad assignment.

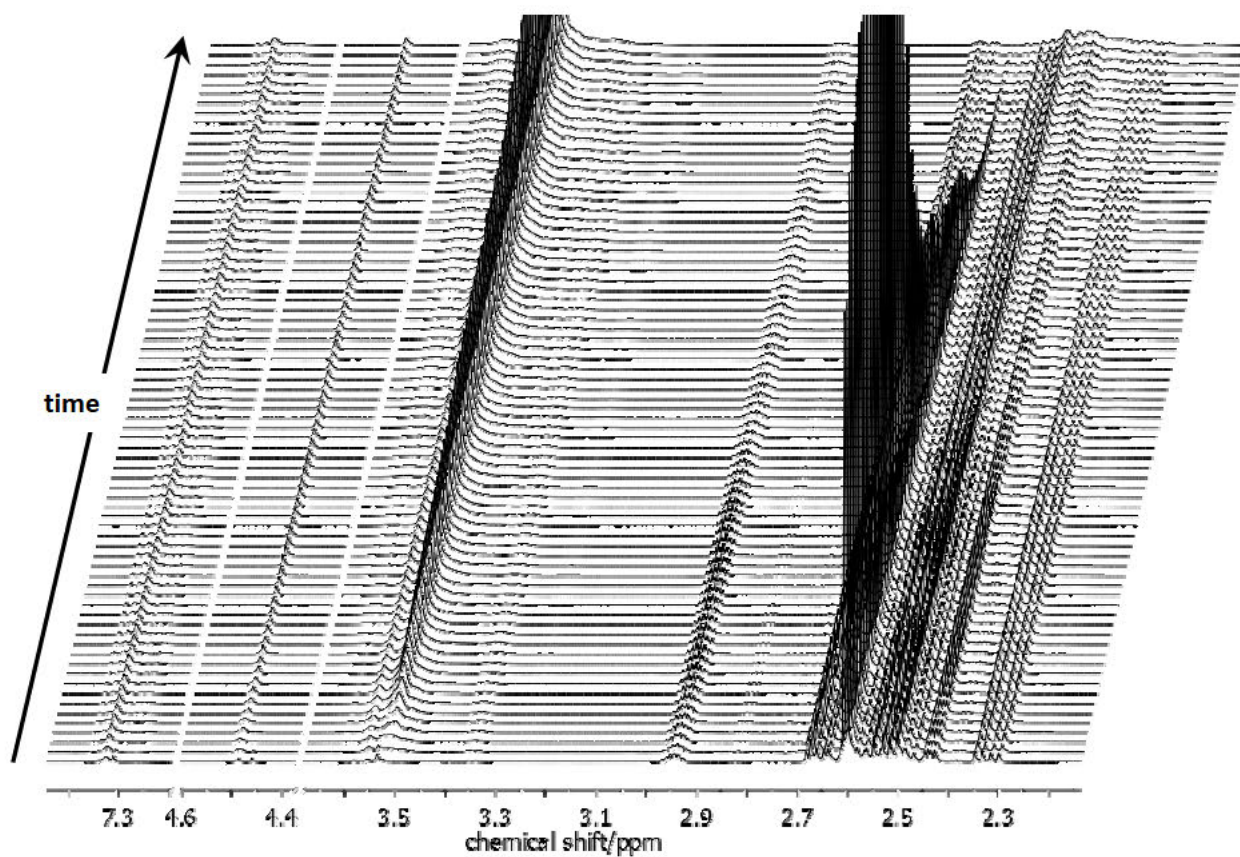


Figure S7. Selected spectra of online ^1H NMR measurements (400 MHz, $\text{DMSO-}d_6$), illustrating course of copolymerization of *N,N*-diethyl glycidyl amine (DEGA, 19%) and ethylene oxide (EO). Decrease of methine proton of DEGA (2.95 ppm) and of methylene protons of EO (2.6 ppm) as well as growth of polymer backbone (3.5 ppm) can be followed. Initiator signals are found at 7.35 ppm and 4.5 ppm and remain constant.

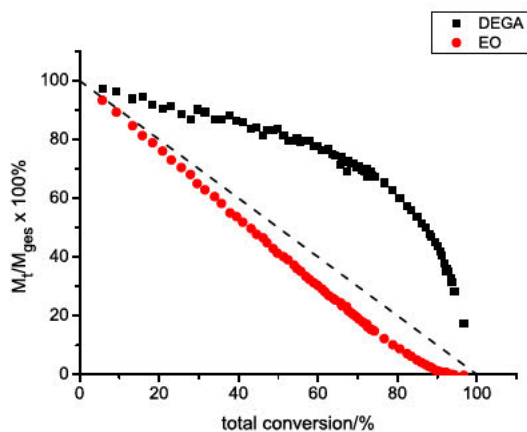


Figure S8. Percentage of initial monomer concentration of *N,N*-diethyl glycidyl amine (DEGA, black squares, 19%) and ethylene oxide (EO, red circles) versus total conversion for copolymerization in sealed NMR tube at 40 °C in DMSO-*d*₆.

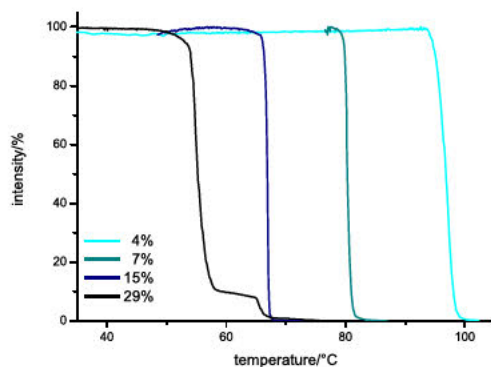


Figure S9. Transmitted laser light intensity versus solution temperature for aqueous solutions of PEG-*co*-PDEGA ($c = 20 \text{ mg mL}^{-1}$, heating rate 1 K min^{-1}) with varying DEGA fraction.

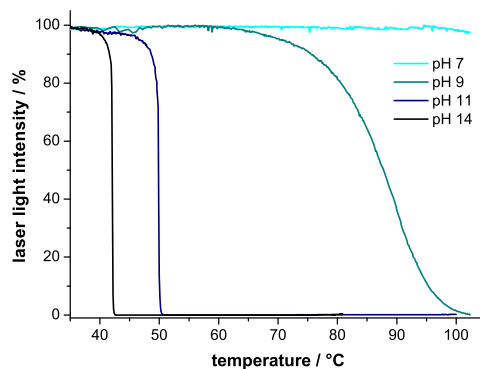


Figure S10. Transmitted laser light intensity versus solution temperature for aqueous solutions of PEG₅₈-co-PDEGA₂₄ ($c = 20 \text{ mg mL}^{-1}$, heating rate 1 K min^{-1}) at different pH values. Solutions with desired pH values were prepared by titration with concentrated HCl aq. and 50 wt% NaOH aq. The volumes added were in the range of 1-15 μL (added to 3 mL solution), so dilution effects were considered to be negligible.

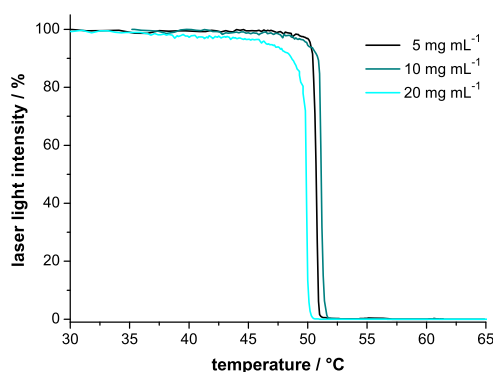


Figure S11. Transmitted laser light intensity versus solution temperature for aqueous solutions of PEG₅₈-co-PDEGA₂₄ (pH 11, heating rate 1 K min^{-1}) at varying concentrations (5, 10, and 20 mg mL^{-1}).

Table S1. Concentration- and pH-dependent cloud points of PEG₅₈-*co*-PDEGA₂₄.

concentration [mg mL ⁻¹]	pH	LCST [°C]
5	11	51
10	11	51
20	11	50
20	7	- #
20	9	88
20	10.5 [†]	55
20	11	50
20	14	42

[†] Solution prepared by dissolution of polymer in water.

No cloud point detected.

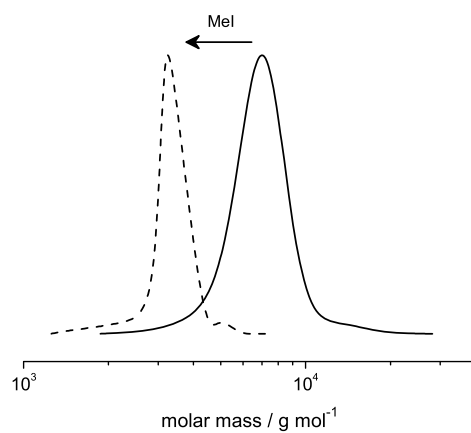


Figure S12. SEC elution traces of mPEG₁₁₃-*b*-PDEGA₂₂ before (solid line) and after (dashed line) quaternization with methyl iodide.

2.2) *N,N*-Diallylglycidylamine:

A Key Monomer for Amino-Functional Poly(ethylene glycol) Architectures

Valerie S. Reuss, Boris Obermeier, Carsten Dingels, Holger Frey

Published in Macromolecules **2012**, *45*, 4581-4589.

Abstract

The first application of *N,N*-diallylglycidylamine (DAGA) as a monomer for anionic ring-opening polymerization is presented. The monomer is obtained in a one-step procedure using epichlorohydrin and *N,N*-diallylamine. Both random and block copolymers consisting of poly(ethylene glycol) and poly(*N,N*-diallylglycidylamine) with adjusted DAGA ratios from 2.5 to 24% have been prepared, yielding well-defined materials with low polydispersities (M_w/M_n) in the range 1.04–1.19. Molecular weights ranged between 2600 and 10 300 g mol⁻¹. Isomerization of allylamine to enamine structures during polymerization depending on time, temperature, and counterion has been realized. The kinetics of the formation of the copolymer structure obtained by random copolymerization was investigated, using time-resolved ¹H NMR measurements and ¹³C NMR triad sequence analysis. A tapered character of the monomer incorporation was revealed in the course of the concurrent copolymerization of EO and DAGA. The thermal behavior of the copolymers in both bulk and aqueous solution has been studied, revealing LCSTs in the range 29–94 °C. Quantitative removal of protective groups via double-bond isomerization mediated by Wilkinson's catalyst and subsequent acidic hydrolysis yielded multiamino-functional PEG copolymers with tapered or block structure. Accessibility of liberated primary amines for further transformation was demonstrated in a model reaction by derivatization with acetic anhydride. In contrast to previous approaches, the DAGA monomer permits the synthesis of block copolymers with PEG block combined with a multiamino-functional polyether block.

Introduction

Poly(ethylene glycol) (PEG) and its derivatives represent a highly versatile class of polyethers, covering applications from fields as diverse as biomedicine to nonionic surfactants and soluble polymeric supports for catalysts and reagents.¹⁻¹⁶ Approved by the US-American Food and Drug Administration (FDA) for use in the human body,¹⁷ PEG combines excellent solubility in both water and organic solvents with biocompatibility; showing no immunogenicity, antigenicity, or toxicity.¹⁸ These properties are accompanied by high flexibility and pronounced hydration of the main chain. As a result, PEG has left behind its former task as a simple additive in cosmetic and skin care formulations, now being the “gold standard” for use in sophisticated biomedical applications such as “PEGylation” of pharmaceutically active drugs and peptides.^{18-32,67}

A drawback for both pharmaceutical and polymeric support-related applications is the low number of functional groups at the PEG backbone, namely the two end groups. Their nature can be varied by the choice of initiator, end-capping agent, or postpolymerization transformation reactions. As an example, amino end-functionalized PEG is accessible through the use of benzyl-protected 2-aminoethanol as an initiator and subsequent hydrogenation³³ and is also commercially available (e.g., Jeffamines).³⁴

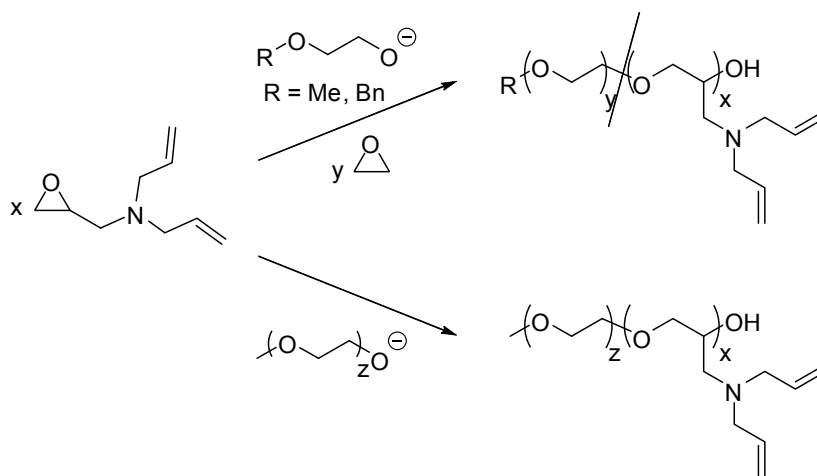
Multifunctionality can be realized by copolymerization of ethylene oxide (EO) with an epoxide derivative bearing a (protected) functional group, resulting in structures known as *mf*-PEGs (multifunctional PEGs).³⁵ The synthesis of functional aliphatic polyethers has been first reported by Taton et al.³⁶ in the mid-1990s, employing an acetal-protected glycidyl derivative (ethoxy ethyl glycidyl ether, EEGE), releasing hydroxyl groups at the chain upon acidic work-up to generate linear polyglycerol. This increased number of addressable moieties allows for the conjugation of an enlarged number of catalysts or active compounds, labels, and targeting molecules to a single polymer chain.³⁷

Few concepts for multiple incorporation of amino groups at a PEG-based backbone have been presented to date. Starting from anionic copolymerization of EO and allyl glycidyl ether (AGE), Koyama et al.³⁸ were the first to obtain amino functionalities via thiol–ene click of 2-aminoethanethiol to allylic double bonds, a methodology that has been adapted in many other published studies since.^{29,31,39} Employing the monomer-activated anionic polymerization concept,⁴⁰ Möller and co-workers⁴¹ recently obtained poly(glycidylamine) and copolymers thereof in a multistep

synthesis by nucleophilic substitution of poly(epichlorohydrin) with an azide and subsequent reduction.

As a further development of the concept of polymerization of protected glycidyl ether derivatives, the use of *N,N*-dibenzylamino glycidol (DBAG) as a comonomer in anionic ring-opening polymerization (AROP) has been introduced in a recent work by our group.⁴² Here, liberation of the amine is achieved by hydrogenation of the benzyl protecting groups, releasing the glycidylamine (GA) repeating units. Unfortunately, the success of this approach has been somewhat hampered by the heterogeneous nature of the deprotection reaction, not only resulting in prolonged reaction times and lowered yields but furthermore preventing the synthesis of amino-functional block copolymers PEG-*b*-PGA.

Herein, we present the first study of *N,N*-diallylglycidylamine (DAGA) as a comonomer for the straightforward preparation of well-defined *mf*-PEGs with varying content and incorporation sequence, including amino-functional block copolymers (Scheme 1).



Scheme 1. Synthetic Strategy for the Copolymerization of EO and DAGA (top), Diblock Copolymer Preparation of *m*PEG-*b*-PDAGA as well as PDAGA Homopolymer Synthesis (bottom) via Anionic Ring-Opening Polymerization.

The monomer can be prepared in a one-step procedure starting from commercially available reagents. This approach represents a major improvement of the above-mentioned concept of glycidyl amine derivatives and relies on an alternative deprotection route, providing fast access to copolymers with ethylene oxide and poly(ethylene glycol) monomethyl ether exhibiting multiple

amino functionalities. The block structures are interesting with regard to polymer-supported catalytic systems and for bioconjugation.

Experimental Section

Instrumentation

^1H NMR spectra (300 and 400 MHz) and ^{13}C NMR spectra (75.5 MHz) were recorded using a Bruker AC300 or a Bruker AMX400 spectrometer. All spectra were referenced internally to residual proton signals of the deuterated solvent. For SEC measurements in DMF (containing 0.25 g/L of lithium bromide as an additive) an Agilent 1100 Series was used as an integrated instrument, including a PSS HEMA column ($10^6/10^5/10^4$ g mol $^{-1}$), a UV (275 nm) detector, and a RI detector. Calibration was carried out using poly(ethylene oxide) standards provided by Polymer Standards Service. DSC measurements were performed using a PerkinElmer DSC 8500 with PerkinElmer CLN2 in the temperature range from -100 to 100 °C at heating rates of 10 K min $^{-1}$ under nitrogen. Cloud points were determined in deionized water at a concentration of 20 mg mL $^{-1}$ and observed by optical transmittance of a light beam ($\lambda = 670$ nm). The measurements were performed in a Tepper turbidimeter TP1. The intensities of the transmitted light were recorded versus the temperature of the sample cell. The heating/cooling rate was 1 K min $^{-1}$. The cloud point temperatures of the sharp transitions from translucent to opaque solutions were defined as the values measured at 50% transmittance.

Reagents

Poly(ethylene glycol) monomethyl ether (mPEG 5000, $M_n = 5000$ g mol $^{-1}$) was purchased from Fluka. Diallylamine, epichlorohydrin (99%), sodium hydroxide, and ethylene oxide (99.5%) as well as dimethyl sulfoxide (puriss, over molecular sieve), tetrahydrofuran (puriss, over molecular sieve), and toluene (puriss, over molecular sieve) were purchased from Aldrich. Deuterated chloroform- d_1 and DMSO- d_6 were purchased from Deutero GmbH. All other solvents and reagents were purchased from Acros Organics.

Synthesis of *N,N*-Diallylglycidylamine (DAGA: *N,N*-Diallyl(2,3-epoxypropyl)amine)

118 g of diallylamine (1.21 mol, 1 equiv) and 118 g of epichlorohydrin (1.28 mol, 1.05 equiv) were combined. A 50 wt % aqueous solution of 85 g of NaOH (2.12 mol, 1.75 equiv) was added, and the two-phase mixture was vigorously stirred overnight. After centrifugation (10 min, 4500 min $^{-1}$)

and careful separation of the layers, the organic layer was dried over MgSO_4 . Fractionating distillation from CaH_2 (8×10^{-2} mbar, 54°C) afforded the product as a colorless liquid. The monomer was stored under argon at 8°C and cryo-transferred from CaH_2 prior to polymerization. Yield: 80–91%. ^1H NMR (400 MHz, $\text{DMSO}-d_6$): δ [ppm] = 5.95–5.70 (m, 2H, $\text{CH}=\text{}$), 5.30–4.95 (m, 4H, $\text{CH}_2=\text{}$), 3.22–3.02 (m, 4H, $\text{N}-\text{CH}_2-\text{CH}=\text{}$), 3.01–2.95 (m, 1H, CH_{ring}), 2.70–2.62 (m, 2H, $\text{CH}'\text{H}''_{\text{ring}}$ and $\text{CH}'\text{H}''-\text{N}$), 2.45–2.40 (dd, 1H, $\text{CH}'\text{H}''_{\text{ring}}$), 2.38–2.29 (dd, 1H, $\text{CH}'\text{H}''-\text{N}$). ^{13}C NMR (75.5 MHz, CDCl_3): δ [ppm] = 135.37 ($\text{CH}=\text{}$), 117.66 ($\text{CH}_2=\text{}$), 57.34 (CH_2-N), 55.69 ($\text{N}-\text{CH}_2-\text{CH}=\text{}$), 50.72 (CH_{ring}), 45.22 ($\text{CH}_{2\text{ring}}$).

Homopolymerization

In a dry Schlenk flask under argon atmosphere, 21 mg of cesium hydroxide monohydrate (0.13 mmol, 1 equiv) was suspended in 5 mL of benzene. 10 mg of 2-methoxyethanol (0.13 mmol, 1 equiv) was added. Stirring at 60°C for 30 min and evacuation at 90°C for 3 h afforded the cesium alkoxide. 1 g of DAGA (6.5 mmol, 50 equiv) was added, and polymerization was performed at 90°C for 12 h. Polymerization was terminated by addition of 0.3 mL of methanol. Unreacted monomer and solvent were removed in high vacuum at 60°C under stirring. The polymer was dissolved in chloroform, filtrated to remove salts, and dried in high vacuum. Yield: 41%.

Block Copolymer Synthesis (mPEG-*b*-PDAGA)

2 g of mPEG 5000 (0.4 mmol, 1 equiv), 60 mg of cesium hydroxide monohydrate (0.36 mmol, 0.9 equiv), and 10 mL of benzene were added sequentially to a dry Schlenk flask under argon atmosphere. Stirring at 60°C for 30 min and evacuation at 90°C for 3 h afforded the partially deprotonated macroinitiator. The respective amount of DAGA was syringed in, and the reaction mixture was stirred for 12 h. After addition of 0.3 mL of methanol and cooling, the polymer was dissolved in chloroform and filtrated to remove salts. The solvents were removed under reduced pressure. Precipitation from methanol into cold diethyl ether and drying in high vacuum afforded the block copolymer. Yields >93%. For block copolymer synthesis using alternative deprotonating agents, mPEG was twice dissolved in benzene and dried at 70°C under high vacuum prior to addition of potassium methoxide or sodium hydride, respectively. The subsequent deprotonation and evacuation steps were carried out as described above.

Copolymerization of Ethylene Oxide with *N,N*-Diallylglycidylamine (PEG-*co*-PDAGA)

For $\text{PEG}_{95}\text{-CO-PDAGA}_5$: In a dry Schlenk flask under argon atmosphere, 177 mg of cesium hydroxide monohydrate (1.05 mmol, 1 equiv) was suspended in 5 mL of benzene. After addition of 80 mg of 2-methoxyethanol (1.05 mmol, 1 equiv) the mixture was stirred at 60°C for 30 min and evacuated at 90°C for 3 h, affording the cesium alkoxide. 5 mL of DMSO and ~30 mL of THF were

added to the evacuated flask. The flask was cooled to $-80\text{ }^{\circ}\text{C}$, and 5 mL of ethylene oxide (100 mmol, 95 equiv) was cryo-transferred from a graduated ampoule. 812 mg of DAGA (5.3 mmol, 5 equiv) was injected. Polymerization was performed at $40\text{ }^{\circ}\text{C}$ for 12 h. Copolymerization with 20% DAGA was performed without THF. Polymerizations were terminated by addition of methanol. For DAGA contents up to 10%, filtration, removal of THF under reduced pressure, and precipitation in cold diethyl ether resulted in the pure polymer. For higher DAGA contents, dialysis in methanol was carried out ($\text{MWCO} = 1000\text{ g mol}^{-1}$). Polymers were dried at $40\text{ }^{\circ}\text{C}$ in high vacuum or dissolved in water and lyophilized to give pale yellow to brownish yellow materials in good yields (>80%). Polymers were stored under argon at $-27\text{ }^{\circ}\text{C}$. Because of limited shelf life of the polymers and observed gelation effects, deprotection steps were carried out soon after synthesis.

Isomerization of Double Bonds

Under an argon atmosphere, 300 mg of diallyl-protected polymer was dissolved in 5 mL of dry toluene. The solution was degassed by three freeze–pump–thaw cycles. 2 mol % of Wilkinson’s catalyst was added followed by another three freeze–pump–thaw cycle. The mixture was refluxed for 2 h. After cooling, precipitation in cold diethyl ether and centrifugation afforded the polymer with completely isomerized double bonds. Yields: 85–90%.

Release of Amino Functionalities

The polymer with isomerized double bonds was dissolved in toluene and subsequently acidic ion-exchange resin (Dowex 50WX8), and water was added. While stirring at $85\text{ }^{\circ}\text{C}$ for 2 h, some liquid was distilled off the reaction mixture to allow propanal to escape and avoid possible imine formation. Filtration, removal of solvents under reduced pressure, precipitation from toluene into cold diethyl ether, and centrifugation afforded the amino-multifunctional materials in almost quantitative yields.

One-Pot Isomerization and Removal of Allyl Groups

The two deprotection steps can also be carried out in a one-pot procedure, omitting the purification step after isomerization of the allyl to propenyl moieties. Instead of precipitation of the polymer, water and acidic ion-exchange resin are added directly to the reaction mixture. The polymer is worked up in the same way as mentioned above, yielding the amino-multifunctional materials.

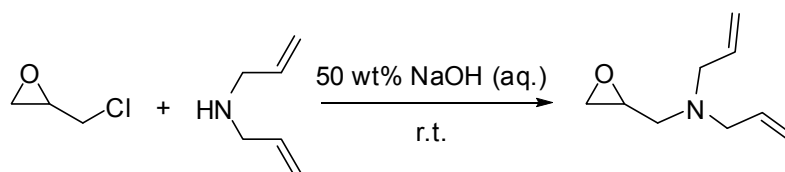
Derivatization of Amino Functionalities with Acetic Anhydride

The reaction was carried out according to a literature procedure.⁴²

Results and Discussion

Monomer Synthesis

The synthesis of allyl-protected comonomer *N,N*-diallylglycidylamine (DAGA) was accomplished in a facile one-step procedure (Scheme 2). Starting from commercially available epichlorohydrin and diallylamine in presence of a 50 wt % aqueous solution of sodium hydroxide, DAGA is obtained without observation of residual diallyl-3-chloro-2-hydroxypropylamine or isomerization of the double bonds in ^1H NMR spectroscopy. In addition, the aqueous conditions permit to avoid the use of organic solvents and thus reduce environmental impact and cost. By modification and optimization of a literature procedure,⁴³ good yields (>80%) were realized despite the rigorous monomer purification steps required for the ensuing oxyanionic polymerization. Detailed characterization including 2D NMR studies and mass spectrometry has been carried out (see Supporting Information). This compound has recently become commercially available.⁶⁸



Scheme 2. Synthesis of the Allyl-Protected Amino-Functional Epoxide Monomer *N,N*-Diallylglycidylamine (DAGA).

Synthesis of Block Copolymers mPEG-*b*-PDAGA

Preparation of the macroinitiators was achieved using commercially available mPEG ($M_n = 2000$ or 5000 g mol^{-1}) and cesium hydroxide monohydrate (Scheme 1) as an initiator system. Block copolymer synthesis was carried out at $90 \text{ }^\circ\text{C}$ for 12 h. Compared with the macroinitiator, SEC analysis showed a shift toward higher molecular weights as well as monomodal molecular weight distributions with low polydispersity indices in the range 1.04–1.11. As can be seen from Table 1 (runs 2–5), the obtained degrees of polymerization were usually somewhat lower than anticipated. This may be attributed to transfer reactions, a known limiting parameter in alkali metal-mediated anionic ring-opening polymerization of epoxides.^{42,44} A detailed study of transfer to the monomer has been carried out, based on NMR spectroscopy and SEC (for detailed discussion see Supporting

Information). Whereas chain transfer appears to play a limited role in block copolymer synthesis, its influence is small in the concurrent copolymerization of both comonomers.

Table 1. Characterization Data for Polymers comprised of Ethylene Oxide (EO) and *N,N*-Diallyl Glycidyl Amine (DAGA) obtained from ^1H NMR Spectroscopy and SEC.^a

#	composition _{NMR}	DAGA ^b /%	$M_{n,NMR}$ ^b /g mol ⁻¹	$M_{n,SEC}$ ^c /g mol ⁻¹	M_w/M_n ^c
1	PDAGA ₂₀	100	3000	1400	1.20
2	mPEG ₄₅ - <i>b</i> -PDAGA ₁₀	-	3500	3200	1.08
3	mPEG ₁₁₃ - <i>b</i> -PDAGA ₅	-	6000	4500	1.05
4	mPEG ₁₁₃ - <i>b</i> -PDAGA ₁₅	-	7300	5200	1.04
5	mPEG ₁₁₃ - <i>b</i> -PDAGA ₁₇	-	7600	6300	1.11
6	PEG ₁₃₆ - <i>CO</i> -PDAGA ₃	2	6500	5200	1.12
7	PEG ₉₈ - <i>CO</i> -PDAGA ₃	2.5	4700	3800	1.08
8	PEG ₁₅₄ - <i>CO</i> -PDAGA ₈	5	7400	5100	1.08
9	PEG ₁₆₀ - <i>CO</i> -PDAGA ₁₁	6	8800	5800	1.11
10	PEG ₁₁₃ - <i>CO</i> -PDAGA ₁₀	8	6500	3400	1.19
11	PEG ₄₂ - <i>CO</i> -PDAGA ₄	9	2600	1800	1.18
12	PEG ₁₂₈ - <i>CO</i> -PDAGA ₃₀	19	10300	3800	1.13
13	PEG ₉₀ - <i>CO</i> -PDAGA ₂₈	24	8200	2800	1.08

^aFor SEC elugrams see Figures S5 and S6 in the Supporting Information. ^bCalculated from ^1H NMR spectra. ^cDetermined by SEC-RI in DMF.

During block copolymer formation, partial isomerization of the double bonds from allyl to *cis*- and *trans*-propenyl moieties was observed. This behavior is known from allylamines under harsh basic conditions.⁴⁵⁻⁴⁷ The degree of isomerization was calculated using ^1H NMR, comparing the integrals of the signals representing all incorporated DAGA units (signals a and b in Figure 6, (1)), with those representing the propenyl groups (signal d in Figure 6, (1)). It was shown to depend on both temperature and counterion. We assume isomerization to take place at DAGA units positioned at the propagating chain end only (see online ^1H NMR kinetics section).

Using initiators deprotonated by cesium hydroxide monohydrate, the degree of isomerization increased with temperature, from 5% at 70 °C to 53% at 100 °C. This finding is in agreement with observations on double-bond isomerization in allyl glycidyl ether polymerization made by Lee et al.,⁴⁸ although one has to note that in the case of DAGA both *cis*- and *trans*-isomers are formed with no observable trend concerning a relationship between *cis/trans* ratio and temperature.

Maintaining the reaction temperature constant at 90 °C and using different deprotonating agents, viz. sodium hydride, potassium methoxide, and cesium hydroxide monohydrate, a

dependence of the degree of isomerization on the counterion was revealed. While both potassium and cesium led to an isomerization degree of 39%, the presence of the counterion sodium resulted in no change of double-bond structure at all according to ^1H NMR characterization. One may speculate whether this might be caused by sodium lacking any d-orbitals, thereby impeding excessive interaction of the alkali metal cation with the lone pair of nitrogen and π -orbitals of the double bond. From another point of view, the character of the ion pair alkali metal ion–alkoxide might serve as an explanation. Sodium (Na^+) is smaller and better solvated compared to its larger, less solvated homologues (K^+ , Cs^+). Because of lower interaction and larger distance between counterion and propagating chain end, one may assume that interaction of a sodium cation with terminal DAGA units is less likely, resulting in a pronounced decrease in tendency for isomerization.

By tuning both parameters—temperature and counterion—the amount of isomerized double bonds can be adjusted. Deprotection of amino groups carrying propenyl groups is achieved via acidic hydrolysis, leaving the remaining *N*-allyl moieties unaltered. Following this strategy, double functional polymers with adjustable number and ratio of primary amino groups to terminal allylic double bonds are easily obtained in one pot, offering an alternative to the hydroxy- and allyl-functional polyethers presented by Hawker and co-workers.⁴⁸

Concurrent Anionic Ring-Opening Polymerization of EO and DAGA

Based on initiation of the cesium salt of 2-methoxyethanol or 2-benzyloxyethanol, DAGA was copolymerized with EO concurrently. Analytical data of the obtained copolymers are summarized in Table 1. Determination of absolute molecular weights using ^1H NMR spectra revealed elevated molecular weights compared to the targeted values, especially when using 2-methoxyethanol as an initiator. This may be attributed to incomplete dissolution of the cesium alkoxide even in DMSO, resulting in a reduced actual initiator concentration. Because of a certain signal overlap, the error of NMR determination is estimated to be $\pm 10\%$. While keeping the number of repeating units constant, an increase in DAGA content corresponds to a higher molecular weight due to the mass of the side chains (e.g., 24 mol % DAGA add up to 52 wt %). Additionally, this leads to an increased hydrophobicity of the polymer chain as compared to the PEG standards used for SEC measurements. Thus, underestimation of molecular weights in SEC measurements becomes more pronounced with increasing DAGA fraction.

Online ^1H NMR Copolymerization Kinetics

In order to disclose the copolymer microstructure and distribution of functional groups at the backbone, online polymerization monitoring was carried out, recording ^1H NMR spectra of a reaction mixture in $\text{DMSO-}d_6$ in a conventional NMR tube sealed under high vacuum in intervals of 30 s.⁴² In order to permit precise determination of the degree of polymerization, 2-benzyloxyethanol was used as an initiator, providing five protons in the aromatic region well-suited for integration and referencing purposes. The polymerization was conducted in a preheated NMR spectrometer with a DAGA fraction of 16%. Within the course of preceding studies, copolymerization temperature was not found to exert any remarkable influence on relative reactivities of epoxide monomers in anionic ring-opening polymerization;^{33,42} hence, it was fixed to 40 °C in order to mimic polymerization conditions in the flask.

Monomer consumption and changes in the remaining monomer composition were followed by integration of the respective signals (Figure 1). EO consumption was monitored by integration of the methylene signal (4H, 2.61 ppm). DAGA conversion could be determined by comparison of the signal generated by the methine proton of the epoxide ring (e, 1H, 3.02–2.93 ppm) (representing monomeric DAGA) with the combined signal of methine protons of the double bond (a and b, 2H, 6.00–5.50 ppm), representing the total amount of DAGA present. Finally, growth of the polymer backbone was observed by an evolving signal at around 3.5 ppm.

The copolymerization was found to proceed rapidly at 40 °C, with >95% total conversion after 63 min (Figure 2). Because of the asymmetry of the sealed NMR tube, spinning is not possible in this method. Nevertheless, the obtained polymer exhibited a narrow molecular weight distribution ($M_w/M_n = 1.12$, DMF, RI detection, PEG standards; Figure S18), pointing to negligible mixing and diffusion issues. Furthermore, virtually nonexistent chain transfer can be assumed for these reaction conditions (cf. Supporting Information).

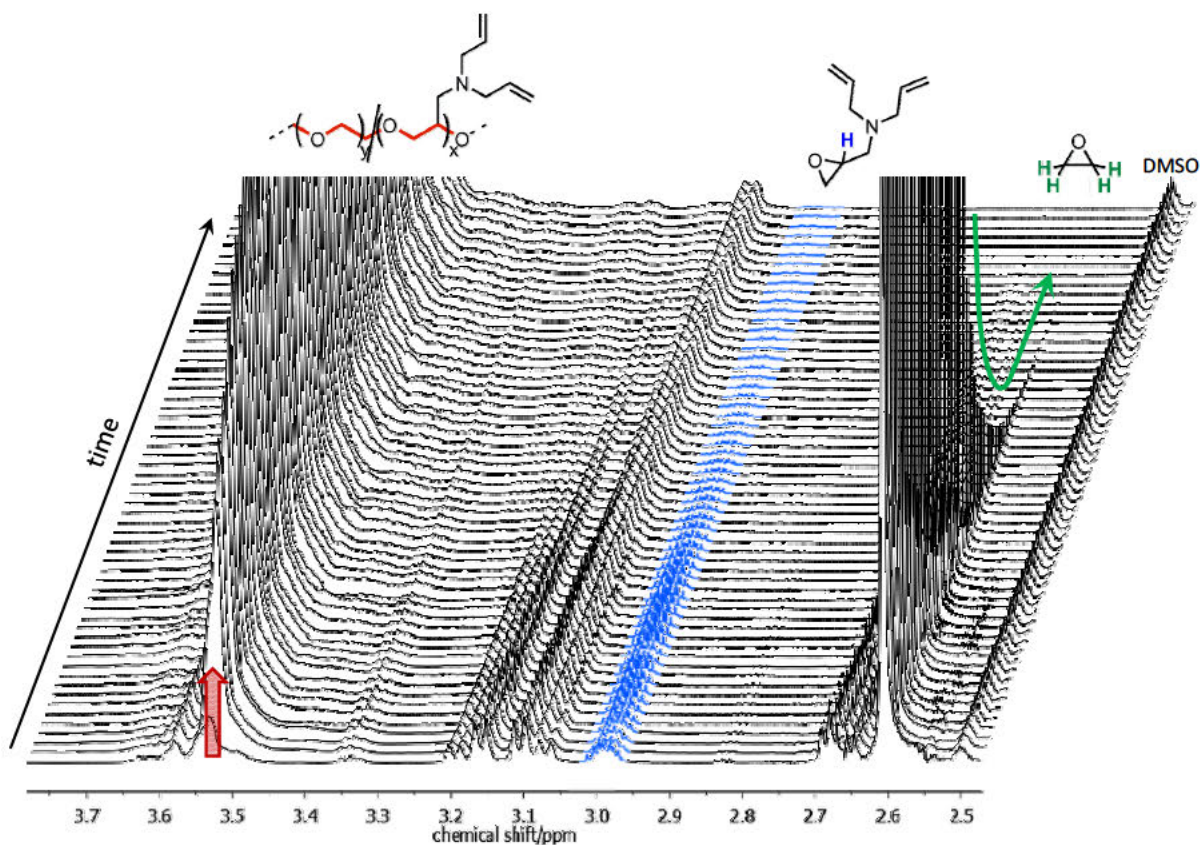


Figure 1. Time-resolved 400 MHz ^1H NMR spectra for random copolymerization of EO and DAGA (16%) at 40 °C with highlighted signals for polymer backbone and comonomers.

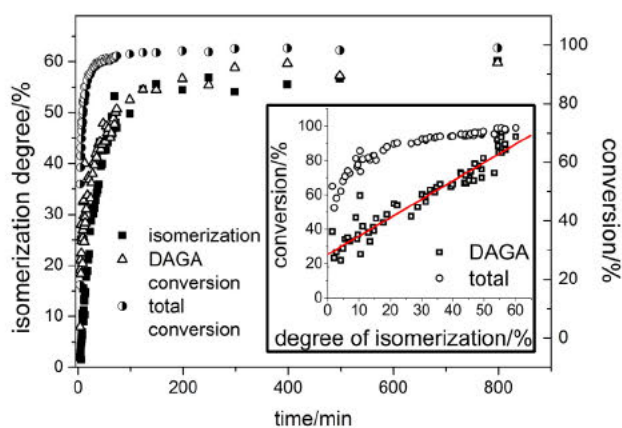


Figure 2. Monomer conversion and degree of isomerization versus time plots for copolymerization of ethylene oxide and *N,N*-diallylglycidylamine (16%) at 40 °C in DMSO- d_6 . Inset: plot of total and DAGA conversion versus isomerization degree. Spheres: total conversion; squares: DAGA conversion; red line: linear fit of experimental data of DAGA conversion.

Tracing the evolution of monomer feed composition (Figure 3) in the initial stages of polymerization, the data show that EO becomes incorporated into the growing polymer chain more rapidly than DAGA. The DAGA fraction remains slightly below the corresponding initial monomer feed ratio of 16%, reaching this value toward the end of the reaction. In conclusion, copolymers with a tapered structure are obtained.

Figure 3. Percentage of initial monomer concentration of ethylene oxide and *N,N*-diallylglycidylamine (16%) versus total conversion for copolymerization at 40 °C in DMSO-*d*₆.

Online monitoring of the polymerization also allows for a more detailed analysis of the 1,3-hydrogen shift, leading to isomerization of *N*-allyl to *N*-propenyl moieties. Comparing the emergence of isomerized double bonds with the conversion of the DAGA monomer over time, both processes seem to take place simultaneously (Figure 2). The linear relationship between the degree of isomerization and DAGA conversion (Figure 2, inset) is not found when comparing to total conversion of this copolymerization. Additionally, further heating of the reaction mixture does not change the degree of isomerization significantly. Accounting for the above-mentioned results on the influence of counterions on isomerization during block copolymer formation, it can be assumed that double-bond isomerization takes place at DAGA units located at the living terminus of a polymer chain only. We assume that interaction of comonomer allyl side chains with the alkali metal ions is involved in this process.

¹³C NMR Characterization of Copolymer Microstructure

Detailed characterization of the random copolymer microstructures also demands ¹³C NMR triad analysis. The relevant regions of the spectra are highlighted in Figure 4. On the left-hand side of the

figure, signals generated by the carbon atoms in DAGA (D)-centered triads are found while EO (E)-centered triads are located on the right (complete ^{13}C NMR data are available from the Supporting Information, Figure S7). Peak assignment was performed with reference to literature data on random EO/oxirane copolymers^{42,49-51} and comparison with block- and homopolymers as well as calculated spectra. Nomenclature of the carbon atoms was adopted from cited work,^{42,49-51} a and b representing first and second CH_2 groups of central monomer units, respectively. Upon incorporation of increasing DAGA amounts, signal splitting of the tertiary carbon peak at 77.5 ppm becomes increasingly pronounced, indicating a parallel existence of a mixture of possible triads. Taking a closer look at the triad distribution, their abundance can be roughly sorted in $\text{E-D-E} > \text{D-D-E} \cong \text{E-D-D} > \text{D-D-D}$, although inverse gated experiments were not carried out due to considerable signal overlap. This order equals the sequence one would expect from random or gradient copolymers. Together with an increasing intensity of the $\text{E-D}_a\text{-E}$ triad signal with increasing DAGA content, ^{13}C NMR supports absence of a copolymer composed of blocky segments.

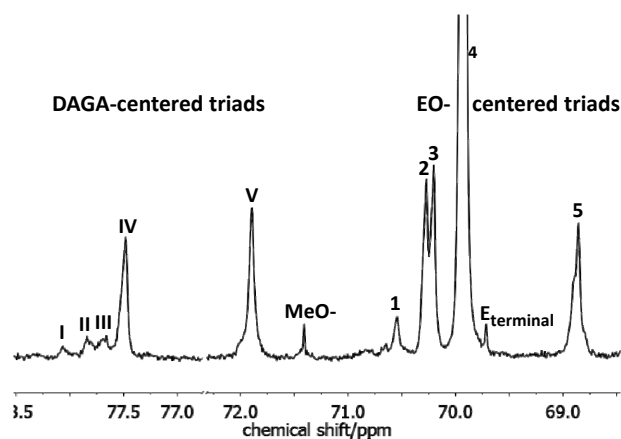


Figure 4. ^{13}C NMR spectrum (75.5 MHz, $\text{DMSO-}d_6$) of $\text{PEG}_{128}\text{-co-PDAGA}_{30}$ (19% comonomer; run 11, Table 1), regions characteristic for DAGA CH (I–IV) and CH_2 (V) backbone signals and EO CH_2 backbone signals. Signal assignment: (I) D-D_b-D, (II) D-D_b-E, (III) E-D_b-D, (IV) E-D_b-E, (V) E-D_a-E; (1) D-E_b-D, (2) D-E_b-E, (3) E-E_b-D, (4) E-E_a-E + E-E_b-E, (5) D-E_a-D + D-E_a-E; (MeO-) initiator signal, (E_{terminal}) E_b-OH.

Thermal Behavior

In order to further evaluate the properties of the copolymers PEG-co-PDAGA and to confirm the conclusions on the microstructure of the polymer chains, their thermal behavior in bulk and in

aqueous solution was studied by means of differential scanning calorimetry (DSC) and turbidimetric measurements.

PEG and its copolymers are known to exhibit lower critical solution temperature (LCST) behavior in water (Figure 5).^{13,52-62,69-71} The LCSTs found were in the range of 29–94 °C, depending on the amount of the apolar DAGA monomer in the chain (cf. Table 2). Plotting the cloud points of PEG-co-PDAGA copolymers over the incorporated DAGA fraction results in a linear correlation (Figure S9, Supporting Information). Thus, the temperature at which the sharp transition from translucent to opaque takes place can be tailored by variation of comonomer fractions in the polymer. Fitting of the experimental data and interpolation of the data to a comonomer content of 0%, i.e. PEG homopolymer, results in a theoretical cloud point of 89 °C. This value differs considerably from the literature value for PEG of comparable molecular weight.^{52,62} Taking analyses of ¹H NMR online kinetic measurements as well as previous work on LCST behavior of random PEG-based structures⁵⁴ into account, this can be understood as further support for our assumption that this shifted linear behavior is induced by a compositional drift in the chain.

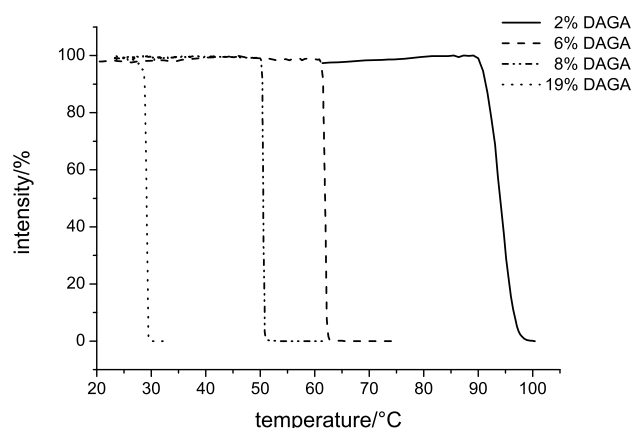


Figure 5. Transmitted laser light intensity plotted versus solution temperature for PEG-co-PDAGA copolymers in aqueous solution, $c = 20 \text{ mg mL}^{-1}$.

Concerning bulk properties, the PEG homopolymer is a highly crystalline material. Examining the behavior of PEG-co-PDAGA in bulk visually, going from 2% to 24% comonomer content, the materials' appearance changes from a powder to highly viscous liquids at room temperature. DSC measurements reveal gradually decreasing glass transition temperatures, melting temperatures, and melting enthalpies for increasing amounts of DAGA present in the polymer. An interesting feature of these measurements is that linear interpolation of the melting point data to a comonomer content of 0% is in excellent agreement with data reported for mPEG 5000 (Table 2).⁶³ If a block-type structure

had been obtained from the copolymerization reaction, one would expect a melting point for the PEG segments close to the melting point of PEG. The linear, gradual character of the decrease of the melting point is another indication that DAGA is incorporated throughout the polymer chain in a gradient manner, without the occurrence of prolonged stretches of EO repeating units.

Table 2. Thermal Properties of Copolymers PEG-co-PDAGA in Bulk and Aqueous Solution obtained from Differential Scanning Calorimetry (DSC) and Turbidimetry (/ Not Determined; – Not Existent).

composition _{NMR}	DAGA ^a /%	c.p. /°C	T _g ^c / °C	T _{rc} ^d / °C	T _m ^e / °C	ΔH ^f / J g ⁻¹
mPEG ₁₁₃	0	-- ^g	-65.0 ^h	--	53.2 ⁱ	195.1 ⁱ
PEG ₁₃₆ -CO-PDAGA ₃	2	94.0	/	/	/	/
PEG ₉₈ -CO-PDAGA ₃	2.5	/	-55.9	--	41.8	97.6
PEG ₁₆₀ -CO-PDAGA ₁₁	6	62.0	-61.7	--	36.8	64.9
PEG ₁₉₄ -CO-PDAGA ₁₄	7	/	-64.5	--	34.9	61.1
PEG ₁₁₃ -CO-PDAGA ₁₀	8	50.5	/	/	/	/
PEG ₁₂₈ -CO-PDAGA ₃₀	19	29.0	-69.2	-41.6	-5.0	19.4

^a Percentage of comonomer incorporated, determined from ¹H NMR. ^b c = 20 mg ml⁻¹. ^c Glass transition temperature. ^d Recrystallization temperature. ^e Melting temperature. ^f Melting enthalpy, determined via integration of the melting signal. ^g No cloud point observed under chosen conditions (20 mg mL⁻¹, 20-100°C, 1K min⁻¹). ^h Taken from the literature.⁶⁴ ⁱ Taken from the literature.⁶³

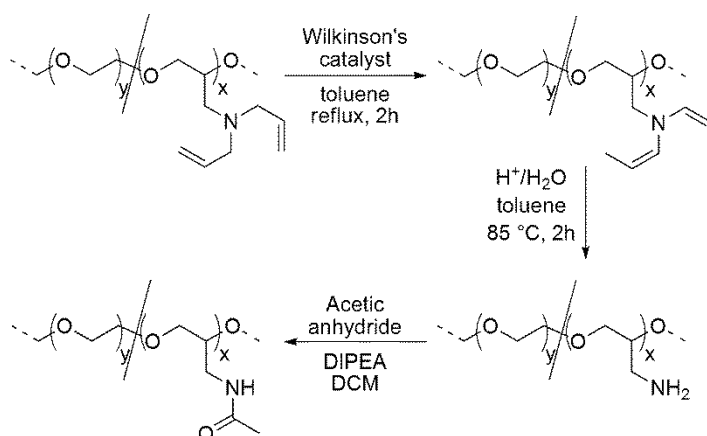
Deprotection and Release of Amino Functionalities

The general pathway for the cleavage of *N*-allyl protecting groups includes two steps (Scheme 3): Quantitative isomerization of the allylamine into an enamine, fostered by the favorable equilibrium between these systems and subsequent cleavage of the enamine upon hydrolysis.^{45,65} For both gradient and block copolymers, Wilkinson's catalyst [RhCl(PPh₃)₃] effected full isomerization of the double bonds, as concluded from ¹H NMR. Interestingly, only the *cis* isomer has been observed after this treatment. This might be explained by an initial coordination of the transition metal center of the complex to a nitrogen lone pair, followed by a 1,3-hydrogen shift via a π-allyl intermediate formed by oxidative addition of the allylic C–H bond to the metal and a consecutive final reductive elimination step.

Subsequent treatment of the material under acidic hydrolysis conditions results in formal substitution of all propenyl groups by hydrogen, thus yielding the desired amine functionalities at the

poly(ethylene glycol)–poly(glycidyl amine) (PEG–PGA) copolymer chain. It has proven beneficial to remove a small portion of the solvents via distillation in order to strip off evolving propanal from the reaction mixture, thus avoiding imine formation. Successful hydrolysis in high yields (>85%) can be deduced from ^1H NMR spectra due to the absence of allyl or propenyl signals (a–g; Figure 6), supported qualitatively by ninhydrin tests (Figure S8, Supporting Information).⁶⁶ Liberation of the amines, including isomerization and hydrolysis, can also be carried out in a one-pot procedure without necessity for an intermediate work-up of the isomerized polymer. Facile deprotection is considered a key feature of the new comonomer DAGA.

Accessibility of the primary amino groups at the PEG chains for further modification was demonstrated by derivatization with acetic anhydride. In ^1H NMR, the emergence of the additional methyl group could be observed. Comparison of SEC elugrams of PEG-co-PDAGA as well as PEG-co-PGA reacted with acetic anhydride results in preservation of the molecular weight and retained low polydispersity (Figure S10, Supporting Information).



Scheme 3. Synthetic Scheme for Isomerization and Cleavage of N-Allyl Protecting Groups as Well as Subsequent Reaction of Amino Groups with Acetic Anhydride.

Conclusions

We have described the first application of the allyl-protected amino-functional epoxide monomer *N,N*-diallylglycidylamine (DAGA) for use in anionic ring-opening copolymerization with ethylene oxide, resulting in well-defined random and block copolymer structures. The fraction of amino-functional comonomer was varied from 2.5 to 24%, and the resulting copolymer microstructure was studied by online ^1H NMR monitoring, ^{13}C NMR triad analysis, differential

scanning calorimetry, and turbidimetry. Formation of block-like structures could be excluded, although a certain gradient character of the composition was observed in the course of the copolymerization. Facile deprotection in a two-step one-pot procedure via isomerization of allylamine to enamine moieties and subsequent acidic hydrolysis was demonstrated, independent of the copolymer structure. The obtained primary amines were derivatized using acetic anhydride in a model reaction, proving accessibility for coupling reactions.

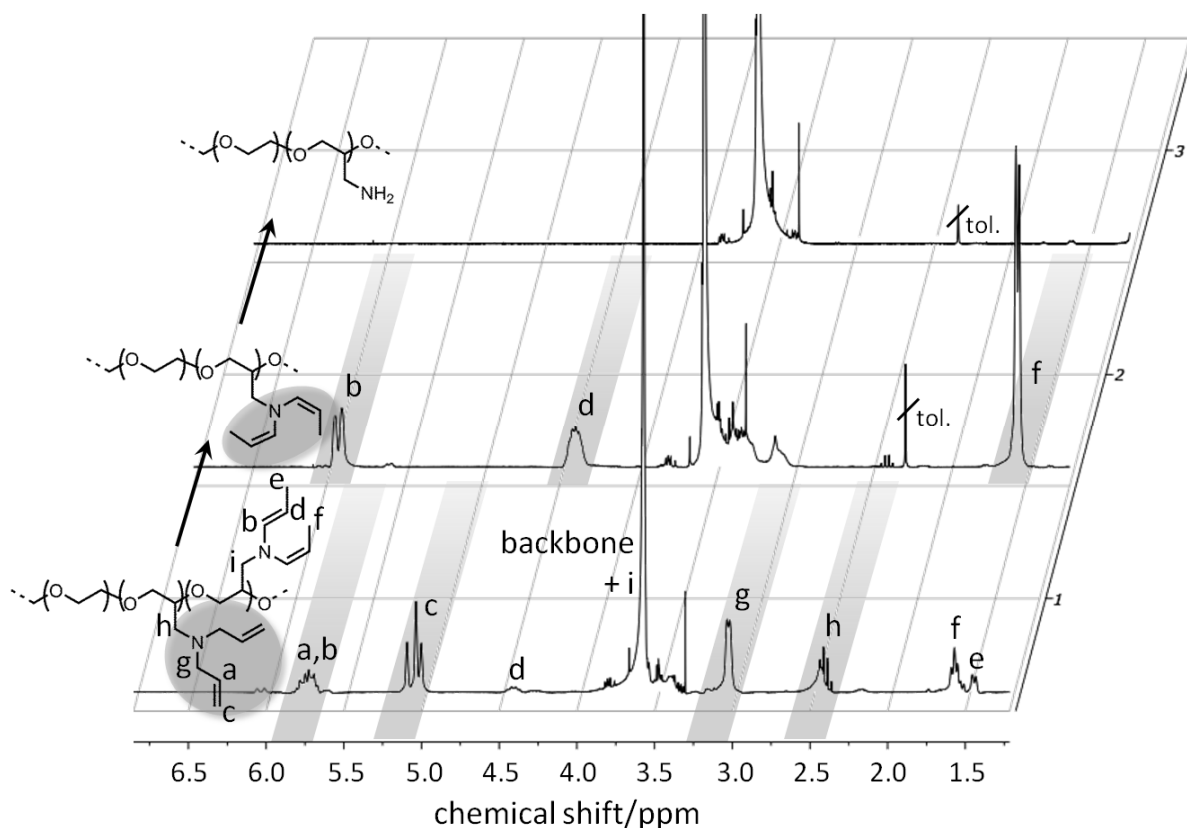


Figure 6. ^1H NMR spectra (300 MHz, CDCl_3) of a block copolymer of poly(ethylene glycol) monomethyl ether and *N,N*-diallylglycidylamine (1) after polymerization, (2) after isomerization of the double bonds with Wilkinson's catalyst ($\text{RhCl}(\text{PPh}_3)_3$), and (3) after liberation of the primary amino groups via acidic hydrolysis.

Compared to the earlier concept of *N,N*-dibenzyl protecting groups,⁴² this approach possesses major advantages for the preparation of multiamino-functional poly(ethylene glycol)s via protected glycidylamines: (i) the monomer, DAGA, can be obtained in a facile one-step procedure on a large scale, (ii) time for deprotection is reduced from 1 to 8 days to 4 h, (iii) yields improved from 30 to 50% to over 85%, and (iv) most importantly, the synthesis grants first time access not only to

gradient but also to block copolymers of ethylene oxide and glycidylamine with narrow polydispersities via living AROP.

The obtained materials offer intriguing potential regarding new architectural possibilities and applications in biomedicine as hybrid materials and cross-linkers. Furthermore, in the field of homogeneous polymer-supported catalysts and reagents, multiple amino groups may serve as anchors for active compounds, while the PEG block ensures easy separation of low-molecular-weight product and polymer-bound reagent via precipitation or dialysis.

Acknowledgment

We thank Dr. Mihail Mondeshki for NMR measurements and Dennis Sauer and Colin Drabe for technical assistance. V.S.R. and B.O. are grateful to the Fonds der Chemischen Industrie (FCI) for a fellowship and to the Graduate School "Materials Science in Mainz" for funding. V.S.R. acknowledges valuable financial support from the Gutenberg-Akademie der Johannes Gutenberg-Universität Mainz. C.D. is thankful to the Max Planck Graduate Center mit der Johannes Gutenberg-Universität Mainz for a fellowship.

References

- [1] Feng, C.; Lu, C.; Chen, Z.; Dong, N.; Shi, J.; Yang, G. *J. Heterocycl. Chem.* **2010**, *47*, 671-676.
- [2] Gravert, D. J.; Janda, K. D. *Chem. Rev.* **1997**, *97*, 489-510.
- [3] Huang, Y.; Lu, C.; Chen, Z.; Yang, G. *J. Heterocycl. Chem.* **2007**, *44*, 1421-1424.
- [4] Osburn, P. L.; Bergbreiter, D. E. *Prog. Polym. Sci.* **2001**, *26*, 2015-2081.
- [5] Porcheddu, A.; Ruda, Gian F.; Sega, A.; Taddei, M. *Eur. J. Org. Chem.* **2003**, *2003*, 907-912.
- [6] Rao, Z.; Peng, H.; Yang, G.; Chen, Z. *Comb. Chem. High Throughput Screening* **2006**, *9*, 743-746.
- [7] Toy, P. H.; Janda, K. D. *Acc. Chem. Res.* **2000**, *33*, 546-554.
- [8] Xiang, F.-Y.; Lu, C.-F.; Yang, G.-C.; Chen, Z.-X. *Chin. J. Chem.* **2008**, *26*, 543-546.
- [9] Yan, X.; Yu, J.; Ye, R.; Chen, Z.; Yang, G. *Lett. Org. Chem.* **2007**, *4*, 239-241.
- [10] Yang, G.; Chen, Z.; Zhang, H. *Green Chem.* **2003**, *5*, 441-442.
- [11] Yang, G.-C.; Chen, Z.-X.; Zhang, Z.-J. *React. Funct. Polym.* **2002**, *51*, 1-6.
- [12] Zhang, H.; Yang, G.; Chen, J.; Chen, Z. *Synthesis* **2004**, 3055-3059.
- [13] Dickerson, T. J.; Reed, N. N.; Janda, K. D. *Chem. Rev.* **2002**, *102*, 3325-3344.
- [14] Grinberg, S.; Kasyanov, V.; Srinivas, B. *React. Funct. Polym.* **1997**, *34*, 53-63.
- [15] Terashima, T.; Ouchi, M.; Ando, T.; Sawamoto, M. *Polym. J.* **2011**, *43*, 770-777.
- [16] Xiang, F.; Zhang, S.; Lu, C.; Chen, Z.; Yang, G. *Synth. Commun.* **2008**, *38*, 953-960.
- [17] Fuertges, F.; Abuchowski, A. *J. Controlled Release* **1990**, *11*, 139-148.
- [18] Pasut, G.; Veronese, F. M. *Adv. Drug Del. Rev.* **2009**, *61*, 1177-1188.
- [19] Levy, Y.; Hershfield, M. S.; Fernandez-Mejia, C.; Polmar, S. H.; Scudieri, D.; Berger, M.; Sorensen, R. U. *J. Pediatr.* **1988**, *113*, 312-317.
- [20] Graham, M. L. *Adv. Drug Del. Rev.* **2003**, *55*, 1293-1302.
- [21] Kinstler, O.; Molineux, G.; Treuheit, M.; Ladd, D.; Gegg, C. *Adv. Drug Del. Rev.* **2002**, *54*, 477-485.
- [22] Rajender Reddy, K.; Modi, M. W.; Pedder, S. *Adv. Drug Del. Rev.* **2002**, *54*, 571-586.
- [23] Wang, Y.-S.; Youngster, S.; Grace, M.; Bausch, J.; Bordens, R.; Wyss, D. F. *Adv. Drug Del. Rev.* **2002**, *54*, 547-570.
- [24] Knop, K.; Hoogenboom, R.; Fischer, D.; Schubert, U. S. *Angew. Chem. Int. Ed.* **2010**, *49*, 6288-6308.
- [25] Li, Z.; Chau, Y. *Bioconjugate Chem.* **2009**, *20*, 780-789.
- [26] Zhou, P.; Li, Z.; Chau, Y. *Eur. J. Pharm. Sci.* **2010**, *41*, 464-472.
- [27] Hrubý, M.; Koňák, Č.; Ulbrich, K. *J. Appl. Polym. Sci.* **2005**, *95*, 201-211.
- [28] Hrubý, M.; Koňák, Č.; Ulbrich, K. *J. Controlled Release* **2005**, *103*, 137-148.
- [29] Vetvicka, D.; Hruby, M.; Hovorka, O.; Etrych, T.; Vetrík, M.; Kovar, L.; Kovar, M.; Ulbrich, K.; Rihova, B. *Bioconjugate Chem.* **2009**, *20*, 2090-2097.
- [30] Koyama, Y.; Yamashita, M.; Iida-Tanaka, N.; Ito, T. *Biomacromolecules* **2006**, *7*, 1274-1279.
- [31] Sakae, M.; Ito, T.; Yoshihara, C.; Iida-Tanaka, N.; Yanagie, H.; Eriguchi, M.; Koyama, Y. *Biomed. Pharmacother.* **2008**, *62*, 448-453.
- [32] Yoshihara, C.; Shew, C.-Y.; Ito, T.; Koyama, Y. *Biophys. J.* **2010**, *98*, 1257-1266.
- [33] Mangold, C.; Wurm, F.; Obermeier, B.; Frey, H. *Macromolecules* **2010**, *43*, 8511-8518.
- [34] Jeffamines are distributed by Huntsman International LLC.
- [35] Obermeier, B.; Wurm, F.; Mangold, C.; Frey, H. *Angew. Chem. Int. Ed.* **2011**, *50*, 7988-7997.
- [36] Taton, D.; Le Borgne, A.; Sepulchre, M.; Spassky, N. *Macromol. Chem. Phys.* **1994**, *195*, 139-148.
- [37] Ringsdorf, H. *J. Polym. Sci. Polym. Symp.* **1975**, *51*, 135-153.
- [38] Koyama, Y.; Umehara, M.; Mizuno, A.; Itaba, M.; Yasukouchi, T.; Natsume, K.; Suginaka, A.; Watanabe, K. *Bioconjugate Chem.* **1996**, *7*, 298-301.

- [39] Obermeier, B.; Frey, H. *Bioconjugate Chem.* **2011**, *22*, 436-444.
- [40] Gervais, M.; Brocas, A.-L.; Cendejas, G.; Deffieux, A.; Carlotti, S. *Macromolecules* **2010**, *43*, 1778-1784.
- [41] Meyer, J.; Keul, H.; Möller, M. *Macromolecules* **2011**, *44*, 4082-4091.
- [42] Obermeier, B.; Wurm, F.; Frey, H. *Macromolecules* **2010**, *43*, 2244-2251.
- [43] Failla, L.; Massaroli, G.; Scuri, R.; Signorelli, G. *Farmaco Sci.* **1964**, *19*, 269-285.
- [44] Hans, M.; Keul, H.; Möller, M. *Polymer* **2009**, *50*, 1103-1108.
- [45] Escoubet, S.; Gastaldi, S.; Bertrand, M. *Eur. J. Org. Chem.* **2005**, *2005*, 3855-3873.
- [46] Price, C. C.; Snyder, W. E. *Tetrahedron Lett.* **1962**, *3*, 69-73.
- [47] Musorin, G. K. *Russ. J. Org. Chem.* **2003**, *39*, 915-918.
- [48] Lee, B. F.; Kade, M. J.; Chute, J. A.; Gupta, N.; Campos, L. M.; Fredrickson, G. H.; Kramer, E. J.; Lynd, N. A.; Hawker, C. J. *J. Polym. Sci., Part A: Polym. Chem.* **2011**, *49*, 4498-4504.
- [49] Hamaide, T.; Goux, A.; Llauro, M.-F.; Spitz, R.; Guyot, A. *Angew. Makromol. Chem.* **1996**, *237*, 55-77.
- [50] Heatley, F.; Yu, G.; Booth, C.; Blease, T. G. *Eur. Polym. J.* **1991**, *27*, 573-579.
- [51] Rejsek, V.; Sauvanier, D.; Billouard, C.; Desbois, P.; Deffieux, A.; Carlotti, S. *Macromolecules* **2007**, *40*, 6510-6514.
- [52] Saeki, S.; Kuwahara, N.; Nakata, M.; Kaneko, M. *Polymer* **1976**, *17*, 685-689.
- [53] Kjellander, R.; Florin, E. *J. Chem. Soc., Faraday Trans. 1* **1981**, *77*, 2053-2077.
- [54] Mangold, C.; Obermeier, B.; Wurm, F.; Frey, H. *Macromol. Rapid Commun.* **2011**, *32*, 1930-1934.
- [55] Louai, A.; Sarazin, D.; Pollet, G.; François, J.; Moreaux, F. *Polymer* **1991**, *32*, 703-712.
- [56] Persson, J.; Johansson, H.-O.; Tjerneld, F. *Ind. Eng. Chem. Res.* **2000**, *39*, 2788-2796.
- [57] Kurzbach, D.; Reh, M. N.; Hinderberger, D. *ChemPhysChem* **2011**, *12*, 3566-3572.
- [58] Dworak, A.; Trzebicka, B.; Walach, W.; Utrata, A.; Tsvetanov, C. *Macromol. Symp.* **2004**, *210*, 419-426.
- [59] Halacheva, S.; Rangelov, S.; Tsvetanov, C. *Macromolecules* **2006**, *39*, 6845-6852.
- [60] Dilip, M.; Griffin, S. T.; Spear, S. K.; Rodríguez, H.; Rijkssen, C.; Rogers, R. D. *Ind. Eng. Chem. Res.* **2010**, *49*, 2371-2379.
- [61] Dormidontova, E. E. *Macromolecules* **2004**, *37*, 7747-7761.
- [62] Bailey, F. E.; Callard, R. W. *J. Appl. Polym. Sci.* **1959**, *1*, 56-62.
- [63] Yan, J.; Ye, Z.; Chen, M.; Liu, Z.; Xiao, Y.; Zhang, Y.; Zhou, Y.; Tan, W.; Lang, M. *Biomacromolecules* **2011**, *12*, 2562-2572.
- [64] Brandrup, J.; Immergut, E. H.; Grulke, E. A., *Polymer Handbook*. 4th ed.; Wiley-Interscience: New York, 1999; p VI-253.
- [65] Krompiec, S.; Krompiec, M.; Penczek, R.; Ignasiak, H. *Coord. Chem. Rev.* **2008**, *252*, 1819-1841.
- [66] Schwetlick, K. In *Organikum* 21st ed.; Wiley-VCH: Weinheim, 2001; p 695.
- [67] Dingels, C.; Schömer, M.; Frey, H. *Chem. unserer Zeit* **2011**, *45*, 338-349.
- [68] *N,N*-Diallyl-*N*-[oxiran-2-ylmethyl]amine is available from Evoblocks, Inc. [catalog number EB14321].
- [69] Chen, H.; Jia, Z.; Yan, D.; Zhu, X. *Macromol. Chem. Phys.* **2007**, *208*, 1637-1645.
- [70] Jia, Z.; Chen, H.; Zhu, X.; Yan, D. *J. Am. Chem. Soc.* **2006**, *128*, 8144-8145.
- [71] Zhou, Y.; Yan, D.; Dong, W.; Tian, Y. *J. Phys. Chem. B* **2007**, *111*, 1262-1270.

Supporting Information

N,N-Diallylglycidylamine: A Key Monomer for Amino-Functional Poly(ethylene glycol) Architectures

Valerie S. Reuss, Boris Obermeier, Carsten Dingels, Holger Frey

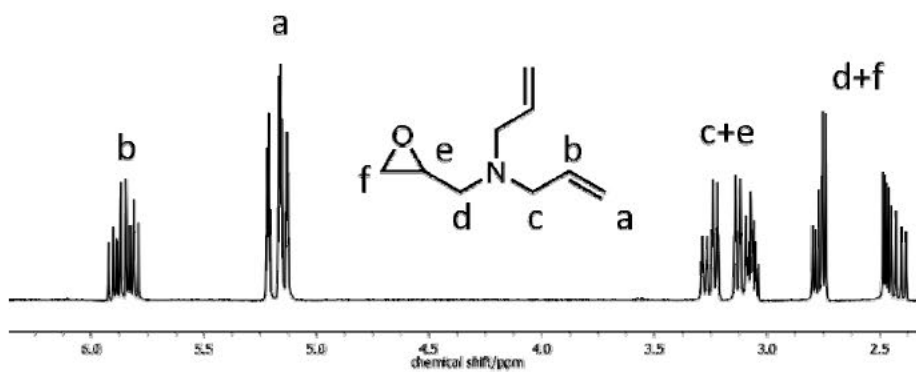


Figure S1. ^1H NMR spectrum (CDCl_3 , 300 MHz) of *N,N*-diallyl glycidyl amine including signal assignment.

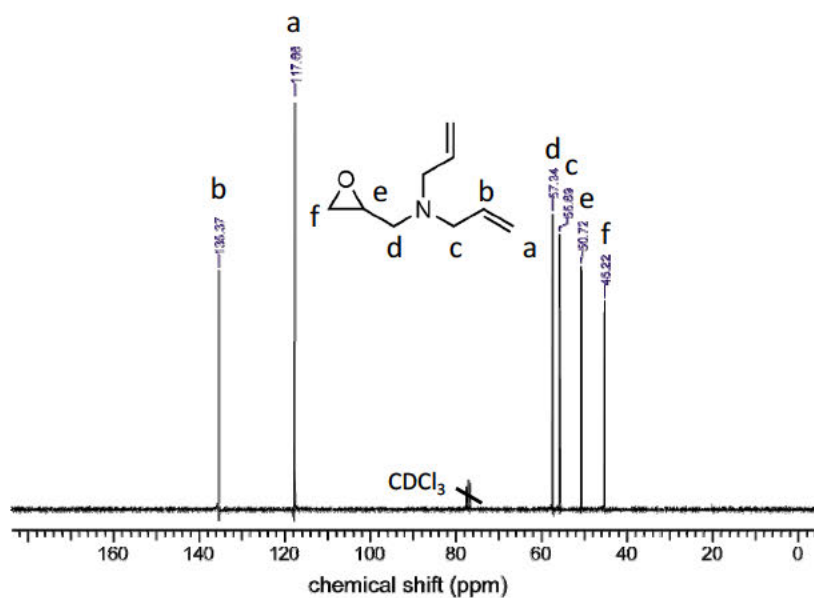


Figure S2. ^{13}C NMR spectrum (CDCl_3 , 75.5 MHz) of *N,N*-diallyl glycidyl amine including signal assignment.

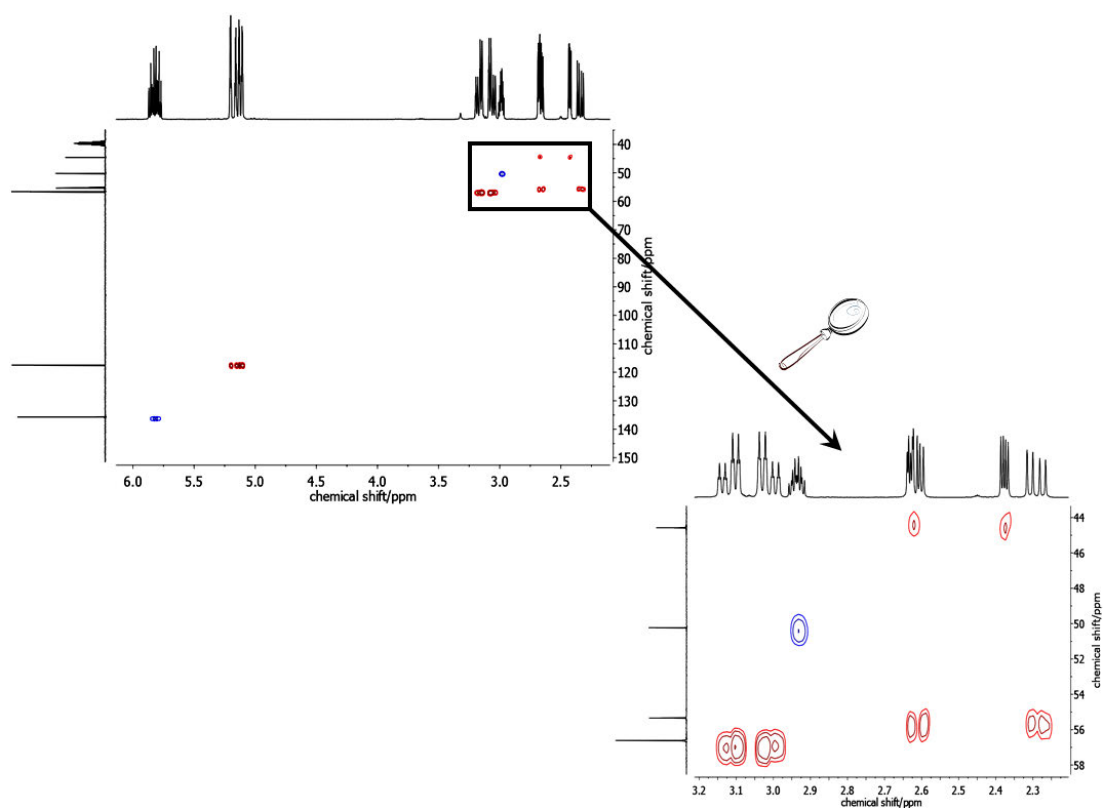


Figure S3. HSQC spectrum of *N,N*-diallyl glycidyl amine (in $\text{DMSO-}d_6$). Phase information is given by coloration of cross peaks (red: methylene, blue: methine).

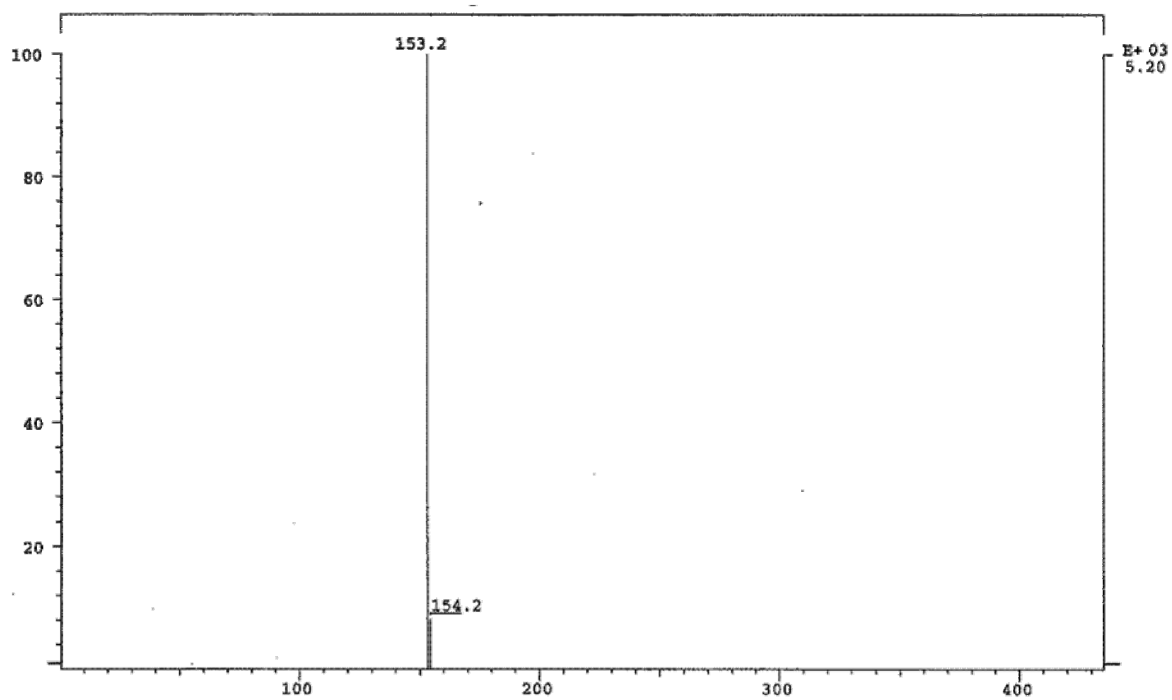


Figure S4. FD mass spectrum of *N,N*-diallyl glycidyl amine.

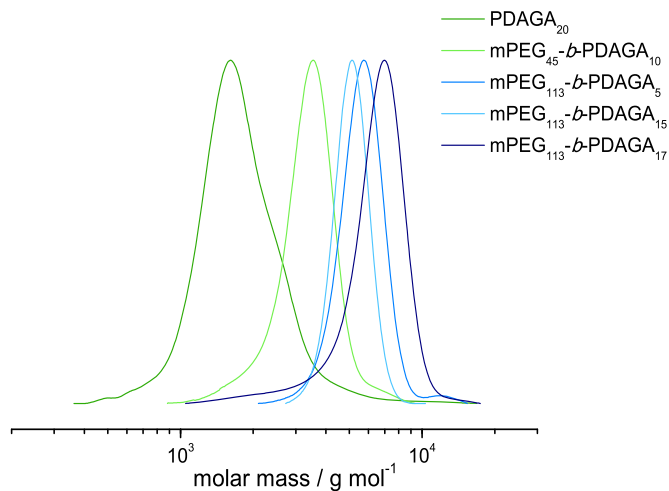


Figure S5. SEC elugrams of PDAGA homopolymer and mPEG-*b*-PDAGA diblock copolymers (in DMF, RI detection, PEG standards).

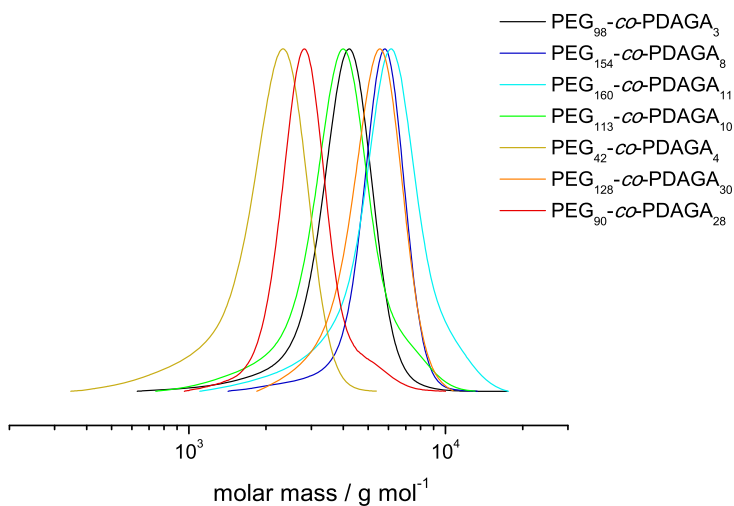


Figure S6. SEC elugrams of PEG-*co*-PDAGA random copolymers (in DMF, RI detection, PEG standards).

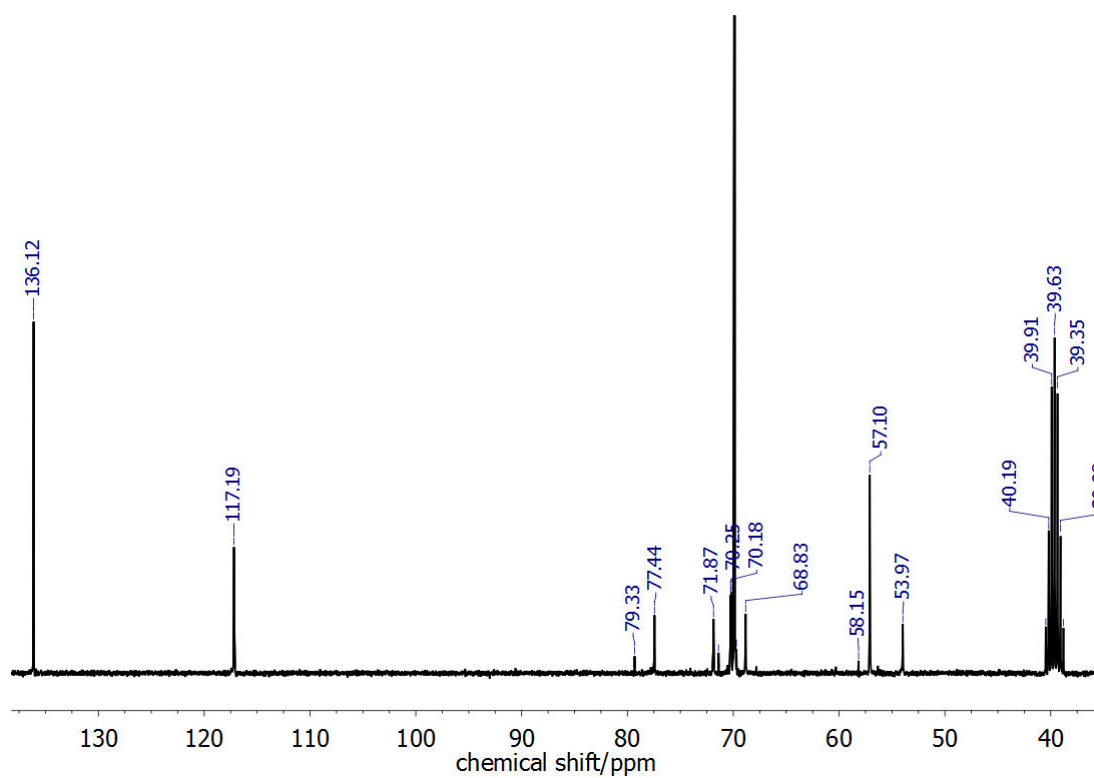


Figure S7. ^{13}C NMR spectrum (CDCl_3 , 75.5 MHz) of $\text{PEG}_{194}\text{-co-PDAGA}_{14}$.

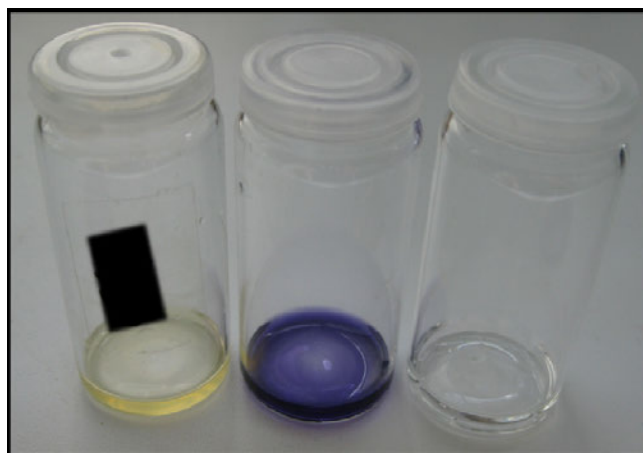


Figure S8. Qualitative proof of existence of amine groups via ninhydrin test. Left: polymer solution, right: ninhydrin solution, middle: mixture of both solutions after heating.

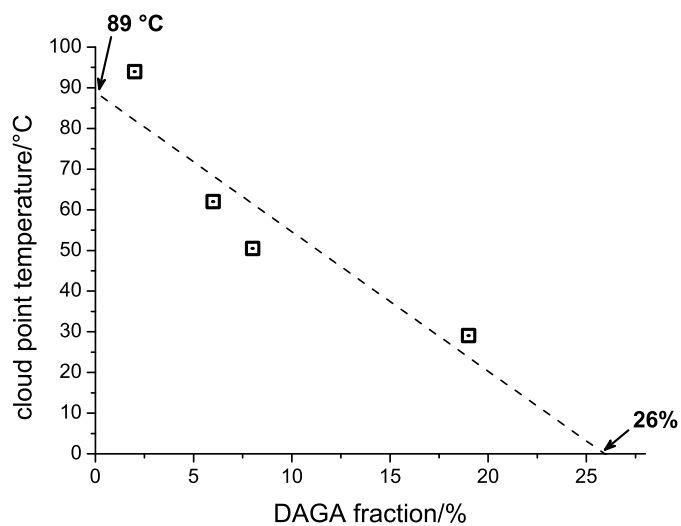


Figure S9. Cloud point temperature plotted versus DAGA fraction in respective copolymer PEG-*co*-PDAGA.

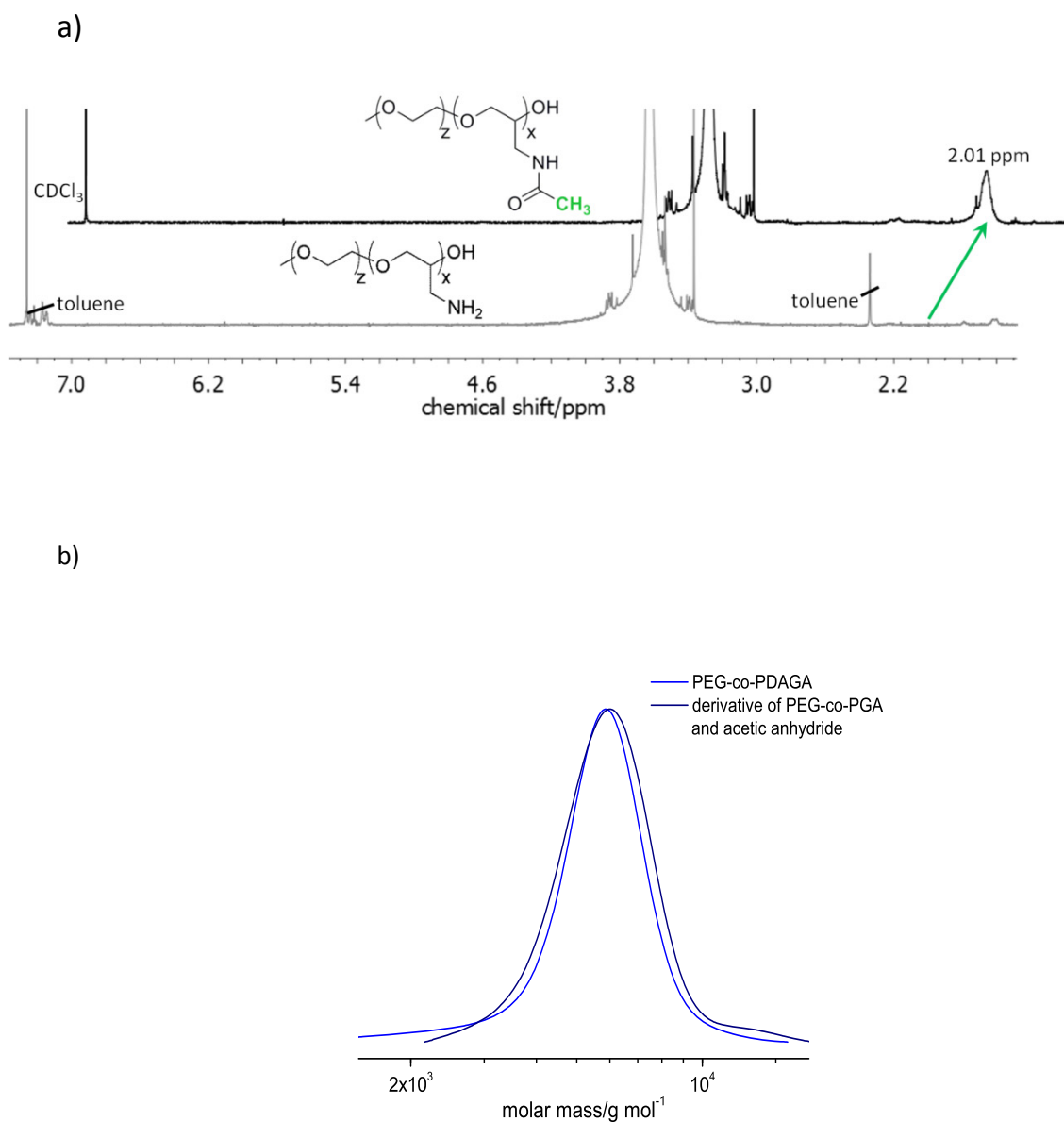


Figure S10. a) ¹H NMR spectra (CDCl₃, 300 MHz) of PEG-co-PGA before (bottom) and after reaction with acetic anhydride (top). b) Molecular weight distributions of copolymer PEG₁₃₆-CO-PDAGA₃ before (light blue) and after (dark blue) deprotection and derivatization with acetic anhydride obtained by SEC in DMF (RI detection, PEG standards). SEC data of PEG-co-PGA is not shown because of interaction of the free amino groups with the column material, resulting in unreliable elugrams.

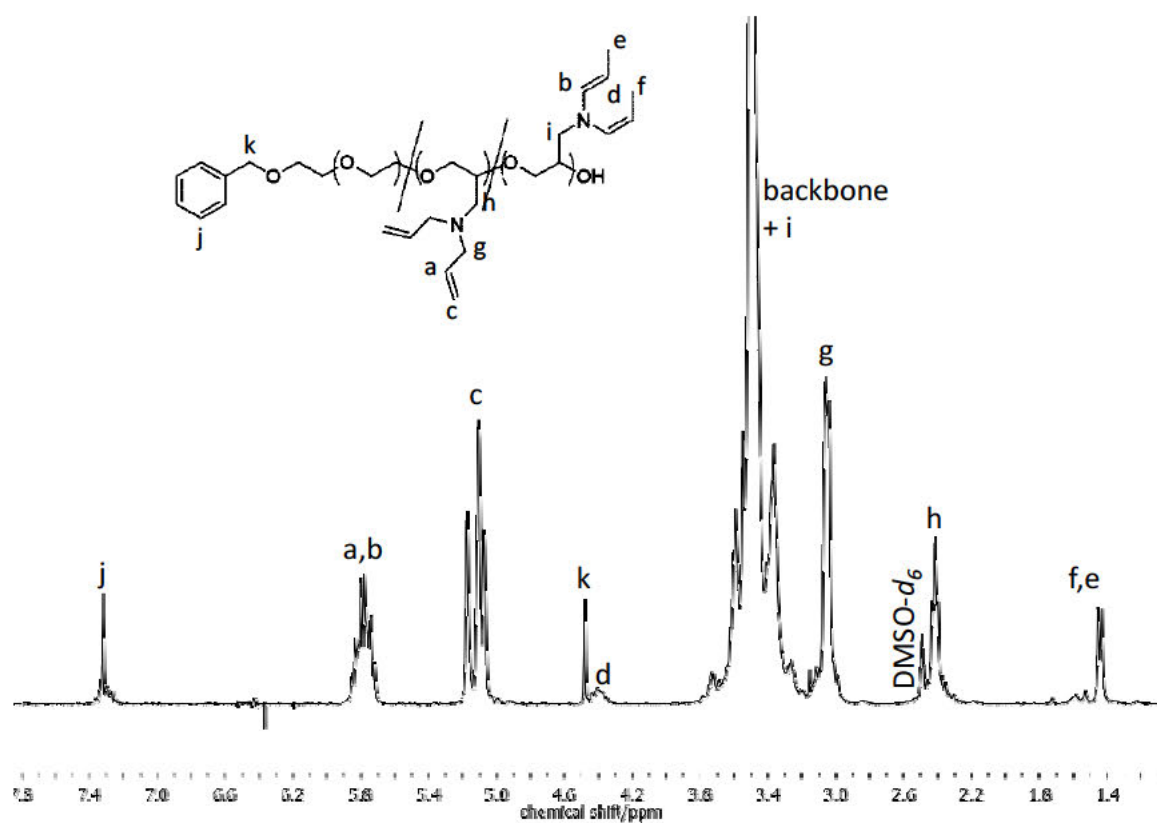


Figure S11. ^1H NMR spectrum (DMSO- d_6 , 300 MHz) of PEG₁₁₃-co-PDAGA₁₀ including signal assignment.

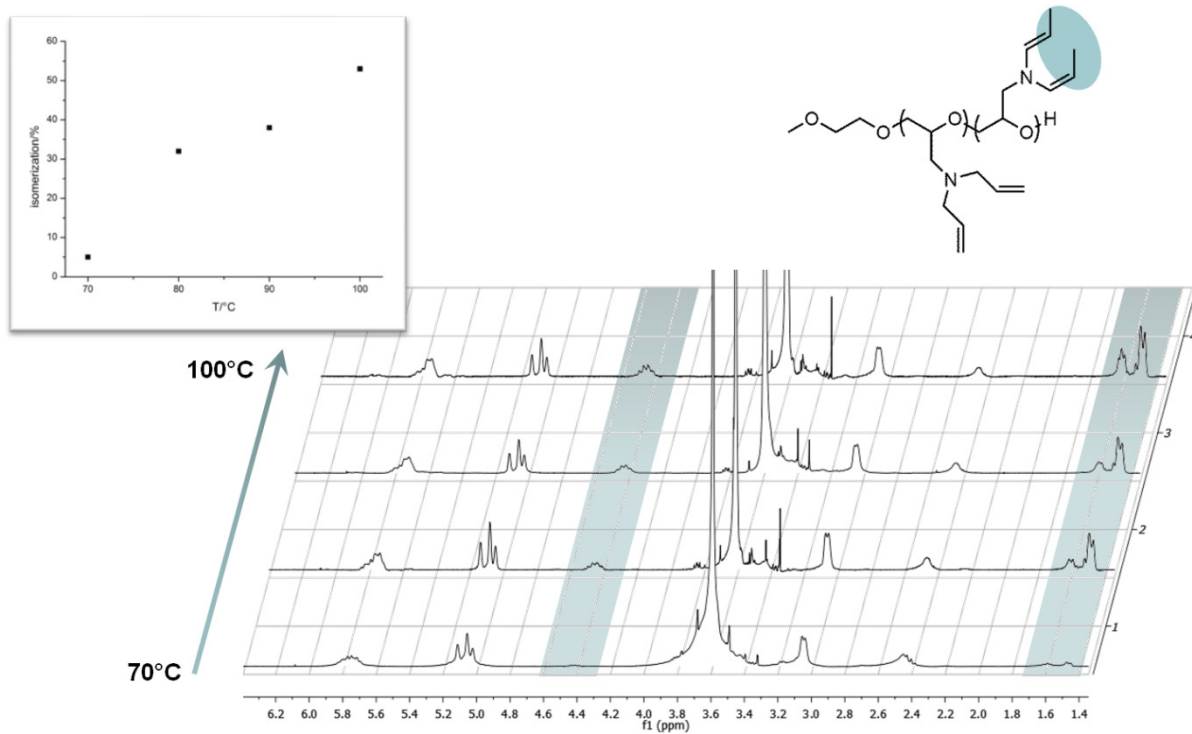


Figure S12. ¹H NMR spectra (CDCl₃, 300 MHz) of block copolymers mPEG₁₁₃-b-PDAGA₁₅ (theoretical composition) synthesized in bulk at 70, 80, 90, or 100 °C, respectively (from bottom to top). Signature proton signals of isomerized double bonds are highlighted. Inset: Percentage of isomerized double bonds at the corresponding polymerization temperature (70 °C: 5%, 80 °C: 32%, 90 °C: 38%; 100 °C: 53%).

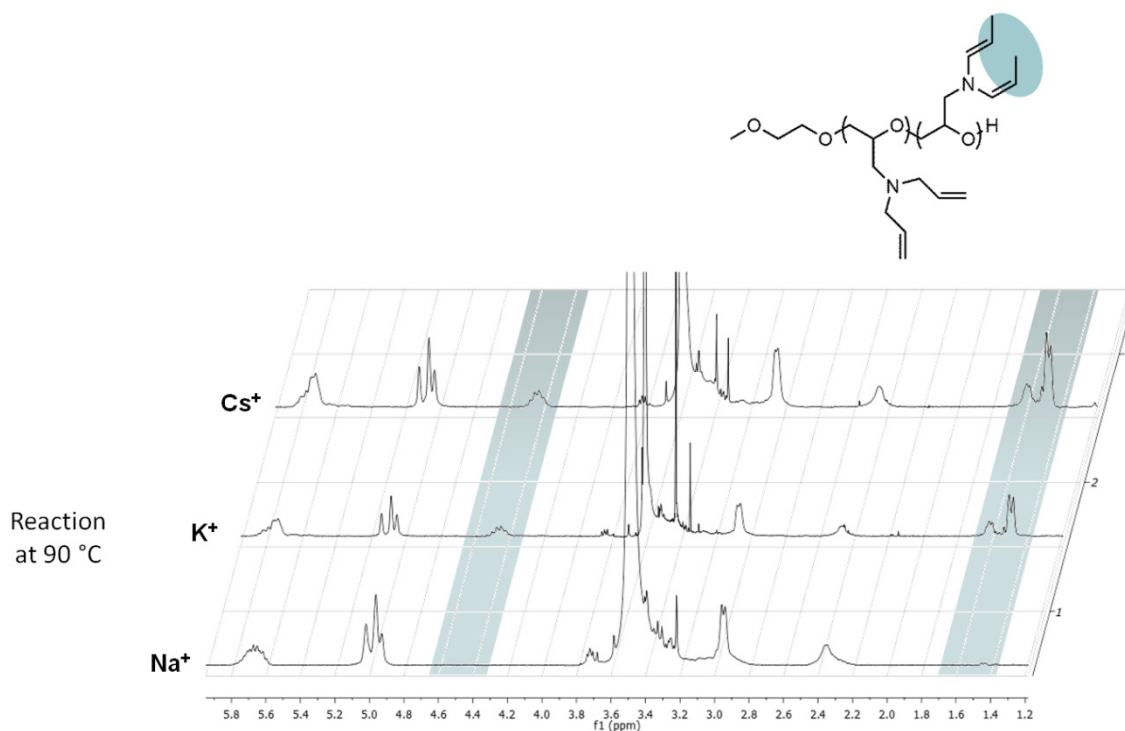


Figure S13. ¹H NMR spectra (CDCl₃, 300 MHz) of block copolymers mPEG₁₁₃-b-PDAGA₁₅ (theoretical composition) synthesized in bulk at 90 °C with sodium, potassium, and cesium as counterion, respectively (from bottom to top). Signature proton signals of isomerized double bonds are highlighted. Isomerization was determined to be 0% (Na⁺), 39% (K⁺), and 39% (Cs⁺).

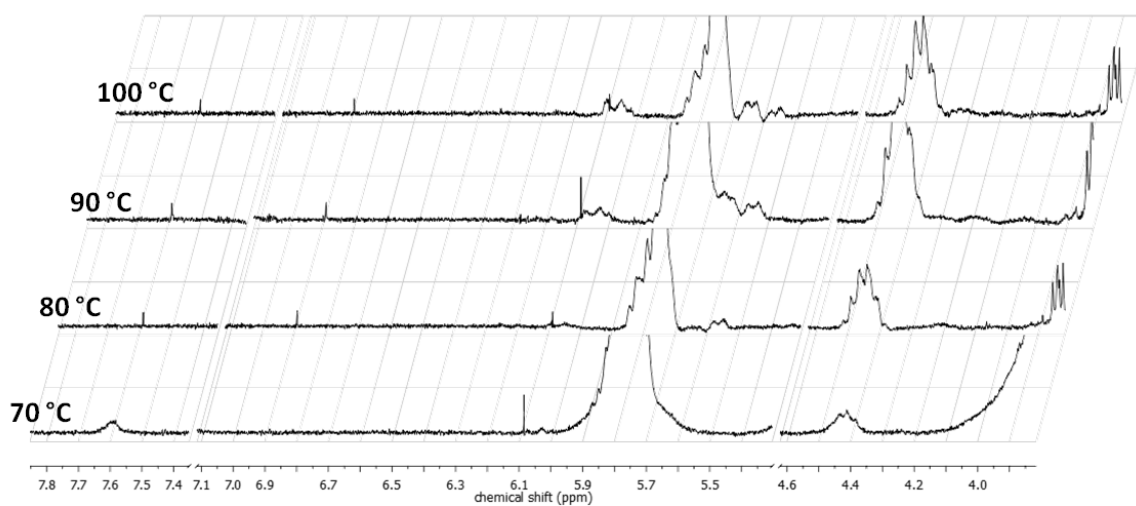


Figure S14. Zoomed in ¹H NMR spectra (CDCl₃, 300 MHz) of block copolymers mPEG₁₁₃-b-PDAGA₁₅ (theoretical composition) synthesized in bulk at 70, 80, 90, or 100 °C, respectively (from bottom to top).

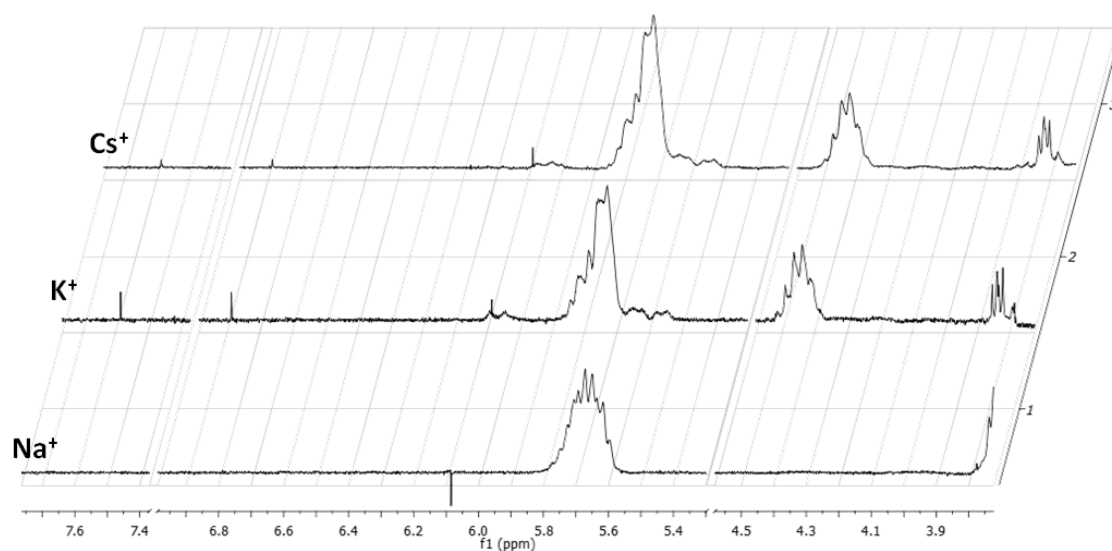


Figure S15. Zoomed in ^1H NMR spectra (CDCl_3 , 300 MHz) of block copolymers $\text{mPEG}_{113}\text{-}b\text{-PDAGA}_{15}$ (theoretical composition) synthesized in bulk at 90 °C with sodium, potassium, and cesium as counterion, respectively (from bottom to top).

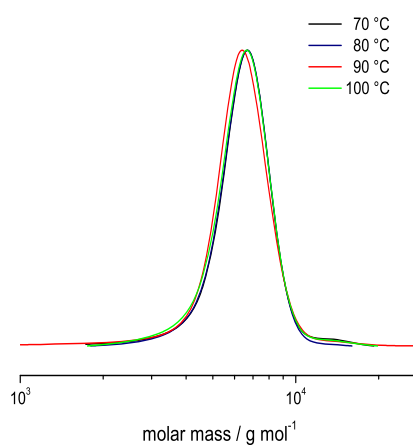


Figure S16. SEC elugrams (RI detection, DMF, PEG standards) of block copolymers $\text{mPEG}\text{-}b\text{-PDAGA}$ obtained at different temperatures.

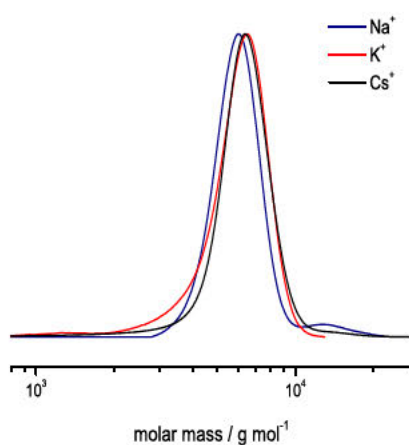


Figure S17. SEC elugrams (RI detection, DMF, PEG standards) of block copolymers mPEG-*b*-PDAGA obtained with different counterions.

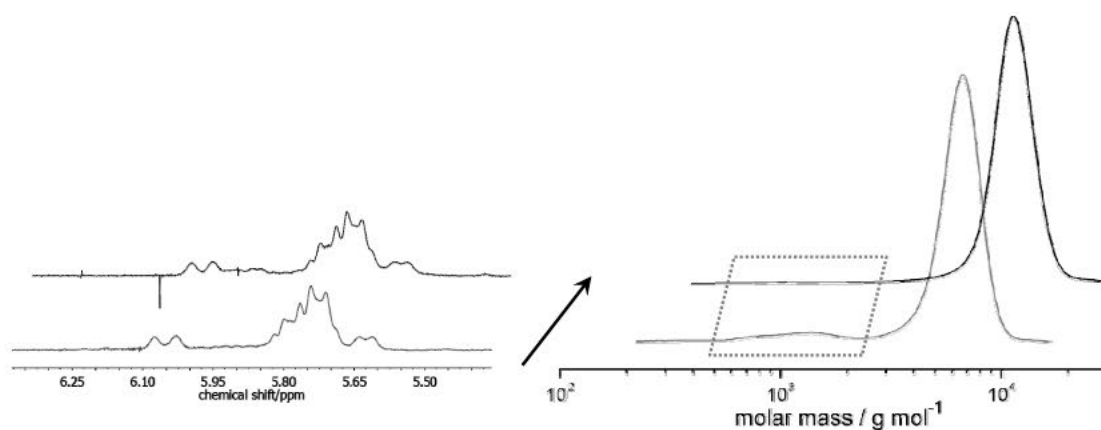
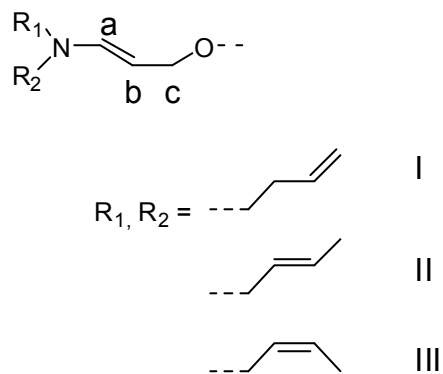


Figure S18. Zoom of ¹H NMR spectra (CDCl₃, 300 MHz) and SEC elugrams (DMF, PEG standards) of mPEG₁₁₃-*b*-PDAGA₇ before (grey, bottom) and after (black, top) precipitation in cold diethyl ether.

deuterated solvent	R ₁	R ₂	a* #	b* #	c* #
CDCl ₃	I	I	6.00	4.98	3.96
	I	II	6.55	4.99	4.04
	I	III	6.55	4.99	4.04
	II	II	7.42	4.96	4.12
	II	III	7.42	4.96	4.12
	III	III	7.42	4.96	4.12
DMSO- <i>d</i> ₆	I	I	6.17	5.00	3.80
	I	II	6.62	5.01	3.88
	I	III	6.62	5.01	3.88
	II	II	7.48	4.98	3.96
	II	III	7.48	4.98	3.96
	III	III	7.48	4.98	3.96



Shifts in ¹H NMR spectrum in ppm, calculated in deuterated solvents indicated in first column using ACD 9 H NMR predictor.

Table S1. Calculated ¹H NMR shifts in CDCl₃ and DMSO-*d*₆ of structure formed by chain transfer to monomer. Note that five different structures are possible dependent on the nature of the double bonds (I: allyl, II: *trans*-propenyl, III: *cis*-propenyl) at the chain-starting ring-opened DAGA monomer. Calculations have been made using ACD 9 H NMR predictor.

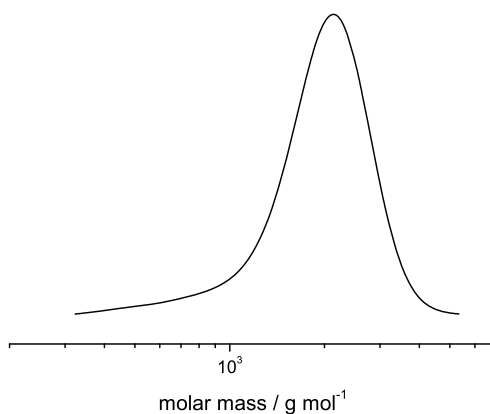


Figure S19. SEC elugram (RI detection, DMF, PEG standards) of polymer obtained without work-up from the online kinetic measurement of the concurrent polymerization of EO and DAGA initiated by cesium benzyloxyethoxide carried out in a sealed NMR tube in DMSO-*d*₆ at 40 °C without spinning.

Consideration of chain-transfer to monomer in polymerizations of DAGA:

1) In block copolymers mPEG-*b*-PDAGA:

The existence of chain-transfer to monomer reactions in the formation of block copolymers mPEG-*b*-PDAGA can be assumed for various reasons. First of all, the degree of polymerization of the second block, i.e. the PDAGA block, is always lower than anticipated. The formation of a side product of lower molecular weight can be deduced from SEC (Figure S18, bottom). This smaller by-product is removed via precipitation in cold diethyl ether (Figure S18, top), therefore it is most probably not bound to the mPEG 5000 precursor.

Confirmation of these findings using ^1H NMR spectroscopy is not straightforward, since the forming species are expected to show chemical shifts similar to those caused by the DAGA repeating units in the polymer (calculated chemical shifts using ACD 9 H NMR predictor; cf. Table S1, values in CDCl_3). The signal expected to emerge around 5 ppm (denoted “b*” in Table S1) will always be hidden under the signal of protons “c” of the copolymer, therefore this region is not shown in the zoomed-in ^1H NMR spectra in Figures S14 and S15. Taking a closer look at the ^1H NMR spectra of the block copolymers obtained at different temperatures and with different counterions (Figures S14 and S15), also no clear signal around 4 ppm can be detected (for proton denoted “c*” in Table S1). Some spectra contain a signal at 7.6 ppm, which might be assigned to proton “a*” in structures containing two *cis*- or *trans*-propenyl moieties bound to the terminal nitrogen atom, but a clear assignment of “c*” remains difficult.

Also, emerging “satellite” signals around the signal for protons “a” and “b” of the block copolymers in the range of 5.4 ppm to 6.1 ppm can be observed. Although predictions for chain-transfer products with *N,N*-diallylamine structure at the chain end ($R_1 = R_2 = \text{allyl}$) include a signal at these chemical shifts, we do not think it is caused by this event. We assign these “satellites” to DAGA repeating units with one allyl and one propenyl (*cis* or *trans*, respectively) moiety bound to nitrogen. The reasons are the following: i) these signals do not vanish after precipitation of the block copolymer, i.e. removal of low molecular weight side product (Figure S16); ii) these signals get more pronounced with increasing reaction temperature which causes increasing isomerization (Figure S14); iii) these signals are not visible in the block copolymer synthesized using sodium as counterion, which resulted in almost complete suppression of double bond isomerization.

2) In polymers obtained by concurrent polymerization of EO and DAGA, PEG-co-PDAGA:

In order to analyze occurrence of chain-transfer to monomer in concurrent polymerizations of EO and PDAGA, the products were investigated in more detail (^1H NMR spectrum in Figure S11) and expected shifts were calculated as described above (Table S1, in $\text{DMSO-}d_6$). Again, clear signal assignment of possible products of chain-transfer is complicated due to partial signal overlap. Yet, in the regions 3.8 - 4.0 ppm ("c*") as well as 6.2 – 6.6 ppm and at 7.5 ppm ("a*"), no signals are visible. Additionally, SEC elugrams of the obtained products do not show low molecular weight side products. Most importantly, the product of the ^1H NMR online measurement, obtained directly after polymerization of EO and DAGA initiated by cesium benzyloxyethoxide in $\text{DMSO-}d_6$ in a sealed NMR tube at 40 °C without spinning (no work-up), exhibits a monomodal molecular weight distribution with only a slight tailing (Figure S19).

3) MULTIFUNCTIONAL PEGs FOR SURFACE FUNCTIONALIZATION

3.1) Catechol-initiated Polyethers: Multifunctional Hydrophilic Ligands for PEGylation and Functionalization of Metal Oxide Nanoparticles

Valerie S. Wilms, Heiko Bauer, Christine Tonhauser, Anna-Maria Schilmann, Marc-Christian Müller, Wolfgang Tremel, Holger Frey

Submitted to Biomacromolecules.

Abstract

Bifunctional CA-PEG and multifunctional CA-PEG-PGA/PEVGE ligands for the functionalization and solubilization of nanoparticles were synthesized. Tunable polymers with polydispersities < 1.25 and molecular weights in the range $500\text{-}7,700\text{ g mol}^{-1}$ containing a catechol moiety for conjugation to metal oxide nanoparticles were prepared. Ligands were synthesized starting from the acetal-protected catechol initiator 2,2-dimethyl-1,3-benzodioxole-5-propanol (CA-OH) for oxyanionic polymerization. CA-OH was used for homopolymerization of ethylene oxide (EO) as well as copolymerization with functional epoxides *N,N*-diallyl glycidyl amine (DAGA), releasing primary amino groups and ethylene glycol vinyl glycidyl ether (EVGE), exhibiting a double bond for click-type reactions, to generate CA-PEG and CA-PEG-PGA/PEVGE. We demonstrate the potential of the functional ligands by binding to MnO nanoparticles. The PEGylated nanoparticles are highly stable in aqueous environment. Furthermore, addressability of the functional groups has been proven, e.g., by coupling with fluoresceine isothiocyanate (FITC), to allow for optical monitoring of the nanoparticle fate in biological systems.

Introduction

Nanoparticles of various 3d transition metal oxides have attracted enormous interest in both academia and industry due to their intriguing size-dependent set of properties.¹ They are suitable candidates for a vast variety of applications including drug delivery,² protein separation,³⁻⁵ magnetic hyperthermia,⁶ as well as magnetic resonance imaging (MRI) due to their superparamagnetic character.^{7,8} Early research focused on iron oxide nanoparticles consisting of magnetite (Fe_3O_4) and maghemite ($\gamma\text{-Fe}_2\text{O}_3$), being already used as *in vivo* T_2 contrast agents in MRI.^{2,9} In recent years, manganese oxide (MnO) nanoparticles have proven their potential for use as T_1 MRI contrast agents,¹⁰⁻¹² exhibiting a shortening of the longitudinal relaxation time resulting in a positive contrast.

Controlled MnO nanoparticle synthesis relies on a high temperature reaction of manganese oleate precursors,¹³ providing nanoparticles covered by hydrophobic ligands. Therefore, as-prepared nanoparticles are insoluble in water and a direct application of the unmodified particles into aqueous solutions would lead to particle aggregation and precipitation. All the worse, if applied directly to a living organism, these nanoparticle aggregates would pose an immediate threat to health, since they would clog up small blood vessels and obstruct a free blood circulation. Even if particle agglomeration could be prevented, unprotected inorganic nanoparticles are prone to opsonization, a defense process initiated by the innate immune system, in which certain serum proteins attach to the particle surface and initiate phagocytosis. Therefore, it is necessary to exchange the hydrophobic protection shell by hydrophilic ligands, that warrant not only a high colloidal stability in aqueous environment, but also prevent opsonization by serum proteins under physiological conditions.¹⁴ The latter is often referred to as “stealth effect”.^{15,16} Furthermore, the ultimate fate of nanoparticles within the body is determined by the interaction with the local environment inside biological systems, which depends not only on the particle size, but also on their surface properties, including morphology, charge and surface chemistry. As a consequence, efficient strategies for the synthesis of magnetic nanoparticles and their subsequent surface modification are necessary to meet the challenges of a later application in biomedicine.

Often simple cap exchange with bifunctional hydrophilic ligands is the method of choice. Bifunctionality in this case refers to the ligand being composed of two parts, the anchor group that tightly binds to the nanoparticle surface, and the hydrophilic tail responsible for solubilization and biocompatibility in polar media. Surface modification employing poly(ethylene glycol) (PEG) derivatives has been shown to increase circulation times in the blood while suppressing recognition and clearance by the RES. The “stealth effect”¹⁶ is accompanied by excellent water-solubility and

biocompatibility of PEG.^{17,18} In order to be able to replace the hydrophobic ligands on the MnO nanoparticle surface, the PEG ligands have to exhibit effective anchor groups. Typical anchor groups for metal oxides include carboxylates and phosphonates. An exceptionally powerful tool is the employment of bidentate catechol chelators, inspired by the amino acid L-DOPA, which is a key component in mussel adhesive proteins.¹⁹ This “non-innocent” functional group shows a strong affinity to high-valent metal oxide surfaces, even in aqueous and physiological environment.^{20,21}

So far, bifunctional PEG-catechol ligands have been synthesized mostly employing extensive protecting group and coupling chemistry.¹⁶ Almost exclusively, commercially available PEG derivatives were used, coupling the dopamine moiety to the polymer chain via an amide bond at the junction. Versatility of these strategies is clearly restricted: simple linear PEGs exhibit a very low number of functional groups, namely the two end-groups, which can be varied by the choice of initiator, post-polymerization transformation, or end-capping agent. Also there is only a limited product range of PEG compounds available on the market. This hampers implementation of additional moieties for attachment of, e.g., markers, targeting molecules, or drugs, on the nanoparticle ligand. One approach overcoming these drawbacks is the coupling of dopamine and other amines with a poly(acrylic acid) backbone via amide bonds, thereby creating brush structures with multiple anchor sites.^{4,22-25}

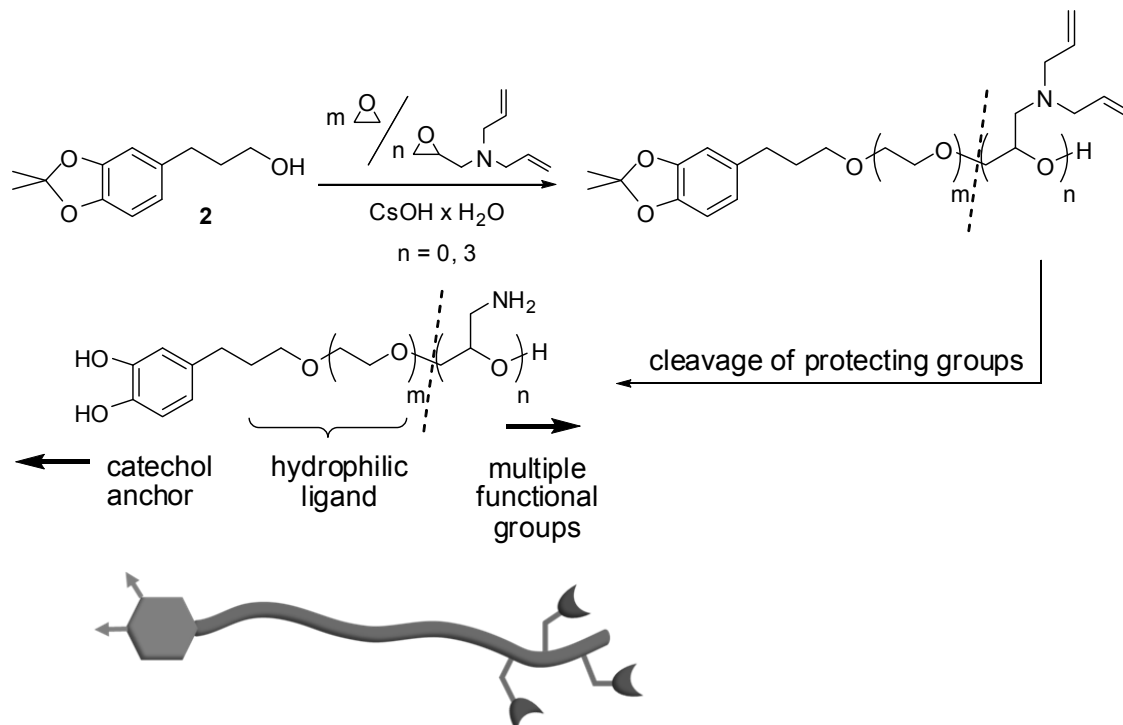
Multifunctionality of linear PEGs is realized by copolymerization of ethylene oxide (EO) with epoxide derivatives bearing functional groups, which might be protected, if necessary.²⁶ These structures have attracted enormous interest in recent years and have also become known as multifunctional PEGs (*mf*-PEGs).²⁷ First reports on functional aliphatic polyethers were published by Taton et al.²⁸ in 1994, employing an acetal protecting group strategy for release of hydroxyl groups along the chain after polymerization. Many variations of this concept have been developed since then, including the introduction of acetal-protected 1,2-diols,²⁹ allylic,^{30,31} and vinylic³² double bonds for click-type functionalization as well as benzyl-protected amines.³³ In a recent work by our group,³⁴ diallyl glycidyl amine (DAGA) has been introduced as a new protected amine-bearing monomer for the synthesis of multi-aminofunctional PEG-poly(glycidyl amine) (PEG-PGA) architectures. This monomer combines facile one-step synthesis, fast deprotection after polymerization, and access to any desired polyether structure with amino groups distributed either randomly or block-like along the macromolecule.

We here present the first use of a protected catechol initiator for anionic ring-opening polymerization (AROP) of ethylene oxide as well as copolymerization of EO with functional epoxides (**Scheme 1**). This strategy guarantees irreversible attachment of the anchor group to each single polymer chain via an aliphatic ether linkage. Well-defined bifunctional ligands with tailorable length

3.1) CATECHOL-PEGs

are obtained from the living polymerization of EO. Through the use of functional comonomers, viz. *N,N*-diallyl glycidyl amine (DAGA) and ethylene glycol vinyl glycidyl ether (EVGE), multiple functionalities at the polyether backbone are easily introduced during polymerization. This simultaneously leads to multifunctional PEGs (*mf*-PEGs) as well as to multifunctional ligands for metal oxide nanoparticle solubilization. The obtained ligands are comprised of an effective bidentate anchor group, a hydrophilic chain, as well as a tailored amount of functional groups at the polymer chain. Thus, a vast variety of possibilities for further functionalization of the polymer shell around the nanoparticle core are opened up. In the current work, the applicability of this approach is demonstrated using MnO nanoparticles. The amount of functional groups on each nanoparticle can be adjusted by mixing of bifunctional catechol-PEGs with multifunctional ligands. Because of the high binding affinity of the catechol motif, this approach embodies a new general concept for the functionalization of a large variety of metal and metal oxide surfaces.

Scheme 1. Polymerization of Epoxides using Acetonide-protected Catechol Initiator followed by Release of Catechol and Amine Moieties resulting in Multifunctional Hydrophilic Ligands for MnO Nanoparticle Functionalization.



Experimental Section

Instrumentation. ^1H NMR spectra (300 MHz and 400 MHz) and ^{13}C NMR spectra (75.5 MHz) were recorded using a Bruker AC300 or a Bruker AMX400 spectrometer. All spectra are referenced internally to residual proton signals of the deuterated solvent. For SEC measurements in DMF (containing 0.25 g/L of lithium bromide as an additive) an Agilent 1100 Series was used as an integrated instrument, including a PSS HEMA column ($10^6/10^5/10^4$ g mol $^{-1}$), a UV (275 nm), and a RI detector. Calibration was carried out using poly(ethylene oxide) standards provided by Polymer Standards Service. DSC measurements were performed using a PerkinElmer DSC 8500 with PerkinElmer CLN2 in the temperature range from – 100 to 100 °C at heating rates of 10 K min $^{-1}$ under nitrogen. Matrix-assisted laser desorption/ionization-time of flight (MALDI-ToF) measurements were performed on a Shimadzu Axima CFR MALDI-ToF mass spectrometer equipped with a nitrogen laser delivering 3 ns laser pulses at 337 nm. α -Cyano-4-hydroxycinnamic acid (CHCA) was used as a matrix, potassium trifluoroacetate (KTFA) was added to increase ion formation. All samples were prepared from methanol solutions. Dynamic light scattering measurements were carried out on a Zetasizer Nano from Malvern Instruments. The concentration was 100 $\mu\text{g}/\text{mL}$ as determined by flame atomic absorption spectroscopy on a Perkin-Elmer 5100 ZL apparatus, related to the total amount of manganese. Transmission electron microscope images were recorded on a Philips EM 420 instrument with an acceleration voltage of 120 kV. UV/Vis spectroscopy was carried out on a Perkin-Elmer Lambda 19 UV-vis/NIR spectrometer.

Reagents. 3,4-Dihydroxyhydrocinnamic acid (98%) and ethylene oxide (99.5%) as well as dimethylsulfoxide (puriss, over molecular sieves) were purchased from Aldrich. Deuterated chloroform- d_1 , DMSO- d_6 , and methanol- d_4 were purchased from Deutero GmbH. All other solvents and reagents were purchased from Acros Organics. *N,N*-Diallyl glycidyl amine (DAGA) was synthesized according to the literature.³⁴ For polymerizations, THF was dried using sodium/benzophenone and cryo-transferred into the reaction vessel. Epoxide comonomers were cryo-transferred from CaH_2 prior to polymerization. The MnO nanoparticle preparation has been described elsewhere.¹³ MnO nanoparticles with a size of approximately 18 nm have been used.

2,2-Dimethyl-1,3-benzodioxole-5-propanoic acid (catechol acetone-COOH, CA-COOH, 1a) and 2,2-dimethyl-1,3-benzodioxole-5-propanoic acid methyl ester (catechol acetone-COOMe, CA-COOMe, 1b)

The synthesis was carried out analogous to a literature procedure.^{35,36} In a three-neck round bottom flask equipped with a Soxhlet extractor with a reflux condenser, 3,4-dihydroxycinnamic acid (3.86 g, 21.2 mmol, 1 equiv.) and *p*-toluenesulfonic acid monohydrate (162 mg, 0.85 mmol, 0.04

equiv.) were dissolved in 250 ml benzene. The Soxhlet thimble was filled with CaCl_2 . 2,2-Dimethoxypropane (3.92 mL, 31.8 mmol, 1.5 equiv.) was syringed in and the reaction mixture was refluxed over night. The solution was concentrated to a volume of approximately 10 mL under reduced pressure. The solvent was not removed completely in order to avoid acetal hydrolysis in presence of atmospheric moisture. The crude product was purified via column chromatography (silica gel, petroleum ether : ethyl acetate = 7 : 3). ^1H NMR (300 MHz, CDCl_3) acid: δ [ppm] 6.66 – 6.61 (m, 3 H, H_{arom}), 2.87 (t, 2 H, $\text{CH}_2, \text{benzyl}$), 2.64 (t, 2 H, $\text{CH}_2\text{-COOH}$), 1.67 (s, 6 H, CH_3); ester: δ [ppm] 6.65 – 6.58 (m, 3 H, H_{arom}), 3.67 (s, 3 H, COOCH_3), 2.85 (t, 2 H, $\text{CH}_2, \text{benzyl}$), 2.58 (t, 2 H, $\text{CH}_2\text{-COOH}$), 1.65 (s, 6 H, CH_3).

2,2-Dimethyl-1,3-benzodioxole-5-propanol (catechol acetonide-OH, CA-OH, 2)

Both **1a** and **1b** could be used as starting material. The reaction is exemplified for use of pure **1a**: In a three-neck round bottom flask equipped with a reflux condenser and a dropping funnel, LiAlH_4 (0.79g, 20.8 mmol, 2.2 equiv.) was dissolved in 600 mL dry diethyl ether. CA-COOH (**1a**, 2.14 g, 9.6 mmol, 1 equiv.) was dissolved in 50 mL dry diethyl ether, transferred to the dropping funnel, and added dropwise to the flask in order to keep the diethyl ether refluxing without use of an external heat source. If the reaction did not start, a warm water bath was applied for 1 min. After completion of addition, the reaction mixture was stirred overnight. Excess of LiAlH_4 was decomposed by careful addition of ice water. Precipitated aluminium hydroxide was filtered off and washed thoroughly with diethyl ether. After drying over sodium sulphate, volatiles were removed under reduced pressure. Column chromatography (silica gel, petroleum ether : ethyl acetate = 3 : 7) gave the pure product which was stored at 8 °C. ^1H NMR (300 MHz, CDCl_3): δ [ppm] 6.66 – 6.59 (m, 3 H, H_{arom}), 3.67 (t, 2 H, CH_2OH), 2.62 (t, 2 H, $\text{CH}_2, \text{benzyl}$), 1.90 – 1.80 (m, 2 H, CH_2), 1.67 (s, 6 H, CH_3). ^{13}C NMR (75 MHz, CDCl_3): δ [ppm] 147.37 (O-C-CH-C), 145.45 (O-C-CH-CH), 134.90 (C- CH_2), 120.40 (O-C-CH-CH), 117.49 (C(CH_3) $_2$), 108.62 (O-C-CH-C), 107.89 (O-C-CH-CH), 62.13 ($\text{CH}_2\text{-OH}$), 34.41 (C- $\text{CH}_2\text{-CH}_2$), 31.78 (C- CH_2), 25.78 (CH_3).

Anionic ring-opening (co)polymerization of epoxides

Exemplified for CA-PEG $_{18}$: Under argon atmosphere, CA-OH (**2**, 232 mg, 1.11 mmol, 1 equiv.) and cesium hydroxide monohydrate (150 mg, 0.89 mmol, 0.8 equiv.) were suspended in 5 mL benzene and stirred for 30 min at 60 °C. The partially deprotonated initiator was dried under high vacuum at 55 °C for 12 h. Approximately 15 mL THF and 3 mL DMSO were added and the mixture was stirred for 15 min to ensure complete dissolution of the initiator. Ethylene oxide (1 mL, 20.0 mmol, 18 equiv.) was cryo-transferred to the reaction mixture via a graduated ampoule. In the case of concurrent copolymerization, the dry comonomer was syringed in at this moment. The polymerization was

carried out for 16 h at 55 °C. When block copolymers were synthesized, the comonomer was syringed in and the reaction was carried out for additional 12 h at 55 °C. The product was precipitated into cold diethyl ether and separated via centrifugation (0 °C, 4500 min⁻¹, 10 min). Yields: quantitative. ¹H NMR (CA-PEG, 300 MHz, CDCl₃): δ [ppm] 6.64 – 6.55 (m, 3 H, H_{arom}), 3.96 – 3.30 (m, backbone and CH₂-O-PEG), 2.58 (t, 2 H, CH_{2, benzyl}), 1.90 – 1.78 (m, 2 H, CH₂), 1.66 (s, 6 H, CH₃). ¹³C NMR (CA-PEG, 300 MHz, methanol-*d*₄): δ [ppm] 148.88 (O-C-CH-C), 146.96 (O-C-CH-CH), 136.50 (C-CH₂), 121.83 (C(CH₃)₂), 118.67 (C-CH-CH), 109.78 (C-CH-C), 108.94 (C-CH-CH), 73.74 (CH₂-O), 71.40 (backbone), 62.23 (CH₂-OH), 33.07 (C-CH₂), 32.92 (C-CH₂-CH₂), 26.14 (CH₃). For comonomer signal shifts refer to original literature.^{32,34}

Cleavage of acetonide protecting group (catechol-PEG, C-PEG)

CA-PEG-OH was stirred in 1 M HCl aq. for 3-12 h, letting evolving acetone escape from the solution. Water was removed under reduced pressure. After neutralization with ion-exchange resin, the polymer was precipitated from methanol into cold diethyl ether and separated via centrifugation (0 °C, 4500 min⁻¹, 10 min). Yields: quantitative. ¹H NMR (300 MHz, methanol-*d*₄): δ [ppm] 6.77 – 6.58 (m, 2 H, HO-C-CH), 6.75 – 6.40 (m, 1 H, CH), 3.95 – 3.35 (m, backbone and CH₂-O-PEG), 2.50 (t, 2 H, CH_{2, benzyl}), 1.92 – 1.66 (m, 2 H, CH₂). ¹³C NMR (300 MHz, methanol-*d*₄): δ [ppm] 146.25 (HO-C-CH-C), 144.47 (HO-C-CH-CH), 134.87 (C-CH₂), 120.82 (C-CH-CH), 116.79 (C-CH-C), 116.41 (C-CH-CH), 73.80 (CH₂-O), 71.23 (backbone), 62.20 (CH₂-OH), 32.76 (C-CH₂), 32.68 (C-CH₂-CH₂). Release of catechol moiety led to aggregation, SEC data is therefore not included.

Successive release of amino and catechol functionalities

N-allyl moieties were isomerized to *N*-propenyl groups according to the literature.³⁴ For catalyst removal, the polymer was precipitated from the reaction mixture in cold diethyl ether and separated by centrifugation. Subsequently, the primary amines were released by stirring an aqueous polymer solution with acidic ion-exchange resin (Dowex 50WX8) for 30 min at room temperature, followed by filtration and evaporation under reduced pressure. In the next step, the acetonide can be cleaved according to the protocol above. If successive release is not needed, the isomerized polymer can be worked up using 1 M HCl directly, releasing amines and catechol in one step.

Successive release of alkyhydroxy and catechol functionalities

This can be realized starting from CA-PEG-*co*-PEVGE copolymers. Stirring an aqueous polymer solution with acidic ion-exchange resin results in removal of vinyl ether groups. The acetonide can be cleaved by stirring in 1 M HCl (aq.).

Thiol-ene click of benzyl mercaptane to vinyl double bonds

200 mg of CA-PEG₁₅₆-co-PEVGE₄ was dissolved in 10 mL dry DMF under argon atmosphere. Recrystallized azobis(isobutyronitrile) (AIBN, 0.75 equiv. to double bonds) and benzyl mercaptane (10 equiv. to double bonds) were introduced to the flask. The mixture was degassed in three freeze-pump-thaw cycles and stirred at 75 °C for 12 h. Evaporation of the solvent, precipitation from THF in cold diethyl ether, and centrifugation (10 min, 4500 min⁻¹, 0 °C) gave the fully functionalized product.

Nanoparticle functionalization

50 mg polymer were dissolved in chloroform (20 mL). The oleate-capped MnO nanoparticles (10 mg) were dissolved in chloroform (20 mL) and added dropwise to the polymer solution. The solution was stirred over-night at room temperature and subsequently concentrated to 10 mL under reduced pressure. Particles were precipitated by addition of an equal amount of hexane followed by centrifugation (10 min, 9000 min⁻¹) and redissolved in 5 mL of acetone. After one cleaning step (again precipitation with hexane, centrifugation), particles were dissolved in MilliQ-water and sterile-filtered for further investigations.

Reaction with fluorescent dye

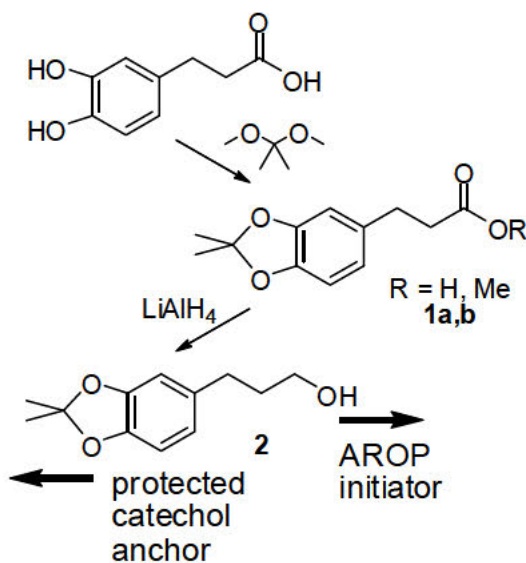
To couple amino functions to fluoresceine isothiocyanate (FITC), amino-functionalized particles were stirred overnight in a FITC-containing solution of chloroform (1 mg FITC per mg particles). After 24 h, the particles were washed, employing the procedure described above.

Results and Discussion

Synthesis of protected catechol initiator

A catechol derivative suitable as an initiator for oxyanionic polymerization has to fulfill two prerequisites: i) a free hydroxyl group for deprotonation and initiation is required, along with ii) protected catecholic hydroxyl groups in order to withstand the basic conditions of AROP unaltered. Both can be provided by 2,2-dimethyl-1,3-benzodioxole-5-propanol (CA-OH, **2**), which can be obtained in a two-step synthesis starting from dihydrocaffeic acid (**Scheme 2**).

Scheme 2. Synthesis of Acetonide-protected Catechol Initiator for Anionic Ring-Opening Polymerization of Epoxides.



Acetals are well-suited for the protection of hydroxyl functionalities during anionic polymerization, offering high stability under basic conditions while being cleaved conveniently upon acidic work-up. Compared to commercially available methylene acetal-bridged catechol derivatives, acetonide deprotection is much more facile, being possible in presence of 1 M aqueous HCl without the need for reagents like BBr_3 . Thus, formation of an acetonide was chosen for the *ortho*-positioned catecholic OH groups, resulting in a five-membered ring. This can be realized by refluxing dihydrocaffeic acid with 2,2-dimethoxypropane in benzene in presence of catalytic amounts of *para*-toluenesulfonic acid, resulting in a mixture of acetonide-protected acid (CA-COOH, **1a**) and methyl ester (CA-COOMe, **1b**). Full protection of the catechol hydroxyl groups can be deduced from ^1H NMR via integration of the prominent signal of the methyl protons of the resulting acetonide at high field. Purification via column chromatography ensures removal of the acidic catalyst in order to avoid the acid-catalyzed cleavage of the acetonide. In the second reaction step, the carboxyl acid and ester moieties are reduced to the respective alcohol (CA-OH, **2**), using an excess of lithium aluminum hydride. Opposed to standard conditions, evolving aluminum hydroxide is not reacted with acid but removed by filtration and thorough washing.

Anionic ring-opening polymerization of EO and epoxide comonomers

Having the protected monohydroxyfunctional catechol initiator CA-OH (**2**) at hand, bifunctional ligand synthesis is straightforward. Partial deprotonation using cesium hydroxide monohydrate is followed by a drying step in high vacuum. After dissolution, ethylene oxide is introduced into the reaction flask and the polymerization is carried out in a THF/DMSO mixture at 55 °C for 12 h. Low molecular weights in the range of 800 g mol⁻¹ to 1,600 g mol⁻¹ were targeted in order to compare the results to work previously done by Schladt and coworkers.¹² However, one has to keep in mind the structural difference to the catechol-functionalized polymers described here. In the cited work, amphiphilic PPO-PEO-PPO triblock copolymers were used in contrast to fully hydrophilic PEO polymers employed in the current study. Despite low degrees of polymerization with as few as seven EO repeating units, well-defined polymers with tailorable chain lengths and narrow molecular weight distributions below 1.22 were obtained (**Table 1**, **Figure 1**). Molecular weights were generally underestimated in SEC, which might be attributed to the initiator contributing less to the hydrodynamic radius of the molecule in DMF than a linear polymer chain of the same weight would. Unreacted initiator or non-catechol-functionalized PEG was not detected in mass spectrometry, making further chromatographic purification steps unnecessary.

Table 1. Characterization Data for Polymers initiated by CA-OH (**2**) comprised of Ethylene Oxide (EO) and *N,N*-Diallyl Glycidyl Amine (DAGA) or Ethylene Glycol Vinyl Glycidyl Ether (EVGE), respectively, obtained from ¹H NMR Spectroscopy and SEC.

composition _{NMR}	M _{n,NMR} ^a /g mol ⁻¹	M _{n,SEC} ^b /g mol ⁻¹	M _w / M _n ^b
CA-PEG _{6.5}	500	300	1.12
CA-PEG ₇	500	400	1.13
CA-PEG ₁₉	1050	800	1.22
CA-PEG ₂₈	1440	1100	1.11
CA-PEG ₃₂	1600	1000	1.15
CA-PEG ₁₆₀	7300	3100	1.14
CA-PEG ₁₉ - <i>b</i> -PDAGA ₃	1500	900	1.25
CA-PEG ₁₀₇ - <i>b</i> -PDAGA ₃	5400	3100	1.09
CA-PEG ₁₄₂ - <i>co</i> -PDAGA ₃	7000	3400	1.18
CA-PEG ₁₅₆ - <i>co</i> -PEVGE ₄	7700	3700	1.17
CA-PEG ₁₅₆ - <i>co</i> -PEVGE ₄ (TEC)	8100	4000	1.14

^a Calculated from ¹H NMR spectra. ^b Determined by SEC-RI in DMF.

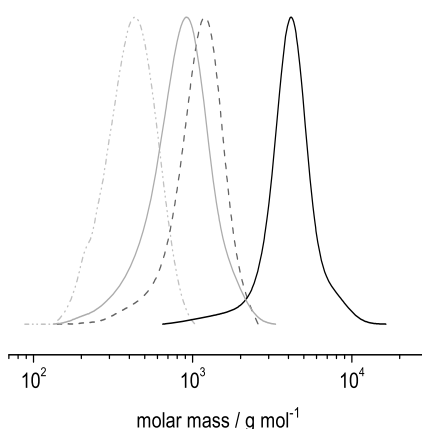
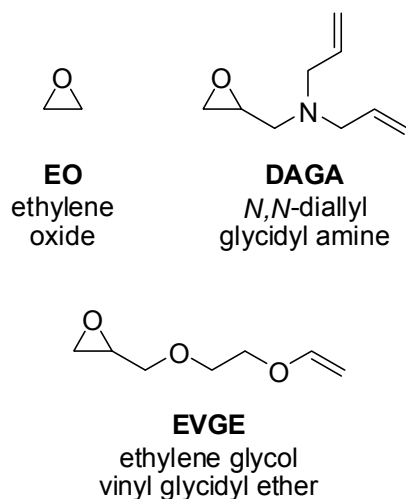


Figure 1. SEC traces (RI, DMF, PEG standards) of CA-PEG₇ (light gray, dash-dot-dot), CA-PEG₁₉ (light gray), CA-PEG₃₂ (gray, dashed), and CA-PEG₁₆₀ (black).

Introduction of additional functional groups can be realized easily by copolymerization of low percentages of functional epoxide comonomers such as *N,N*-diallyl glycidyl amine (DAGA, **Scheme 2**) with EO in a concurrent or step-wise fashion, yielding PEG-PDAGA gradient or block copolymers. In all cases, polydispersities remain low (< 1.25). Block copolymer formation yielding CA-PEG-*b*-PDAGA can be carried out either in a two-pot or in a one pot-two step procedure. In both cases, EO is polymerized first, thus the position of the DAGA units is fixed at the chain end. Gradient CA-PEG-*co*-PDAGA copolymers are obtained in one step via concurrent polymerization of EO and DAGA. DAGA has been found to possess a lower rate of insertion into the polymer chain than EO under similar conditions.³⁴ Hence, the probability to find a DAGA unit is again higher at the terminal chain end than near the catechol initiator, which may even be desired in the current context. Another functional comonomer used for catechol-initiated random copolymerization with EO is ethylene glycol vinyl glycidyl ether (EVGE, **Scheme 2**). In order to further ensure addressability of the functional groups, the length of the catechol-initiated *mf*-PEGs CA-PEG-PDAGA and CA-PEG-PEVGE has been chosen considerably longer than those of the bifunctional CA-PEGs. When a mixture of bifunctional CA-PEG and *mf*-CA-PEG is applied as ligands for MnO nanoparticles, the functional groups are believed to be extended outside of the polymer shell built by CA-PEG, avoiding possible steric hindrances caused by the dense PEG brush around the metal oxide nanoparticle core and facilitating further functionalization and targeting.³⁷ Because of the high EO fraction, water-solubility of all polymers is maintained over the whole temperature range.^{34,38}

Scheme 2. Epoxide Monomers Employed in Anionic Ring-Opening Polymerization Initiated by CA-OH (2).



Cleavage of protecting groups

In the bifunctional ligands CA-PEG obtained by polymerization of EO initiated with CA-OH (2), the catechol anchor group can be released by simple treatment with 1 M aqueous HCl solution for 3–12 h at room temperature. It is important to let evolving acetone escape from the solution in order to drive the reaction to completion. The successful deprotection can be followed via ^1H NMR spectroscopy through the disappearance of the methyl protons and a simultaneous shift of the protons in the aromatic region (Figure 2, gray arrows). The same effects are visible in ^{13}C NMR spectroscopy (**Figure S11**). In MALDI-ToF mass spectrometry, the formal removal of a C_3H_4 moiety is proven by a loss in molecular weight of 40 g mol^{-1} (**Figure 3**).

For both *mf*-PEG ligands, with additional protected amino groups introduced by use of DAGA monomers as well as vinyl-protected hydroxyl groups by use of EVGE in concurrent or successive polymerization with EO, respectively, cleavage of *N*-allyl or *O*-vinyl and acetonide moieties can be carried out successively. Treatment of the gradient or block copolymer CA-PEG-PDAGA with Wilkinson's catalyst³⁴ effects full isomerization of the double bonds to *cis*-propenyl moieties. Use of acidic ion-exchange resin in aqueous solution enables the targeted release of the amino or hydroxy groups, while leaving the more stable acetonide moiety unaltered. Monitoring via ^1H NMR spectroscopy reveals the selective removal of the propenyl or vinyl moieties (**Figures S8 and S10**). Release of the primary amines can be qualitatively proven via ninhydrin test and the appearance of the corresponding methine and methylene signals in ^{13}C NMR spectroscopy. Release of hydroxyl groups is proven by disappearance of the vinyl signals in ^1H NMR. The orthogonal character of the deprotection of catechol anchor and functional groups in the chain is an interesting feature, which

can be used, e.g., for the binding of active compounds at the chain before release of the catecholic anchor function. The bidentate anchor is then formed upon stirring with 1 M aqueous HCl solution, as described above. If separate deprotection of the monomer functionalities is not of interest, all functionalities can be released simultaneously upon stirring of the isomerized polymer with 1 M hydrochloric acid.

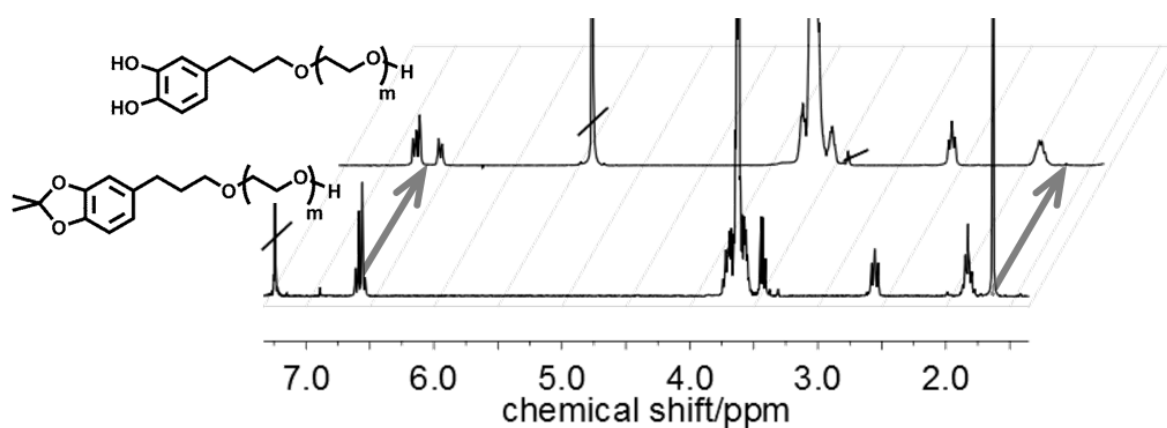


Figure 2. ^1H NMR spectra (300 MHz) of catechol-PEG before (CA-PEG₇-OH, bottom, CDCl₃) and after (C-PEG₇-OH, top, methanol-*d*₄) acidic cleavage of the acetonide protecting group. Disappearance of methyl protons as well as the shift of aromatic protons are highlighted with grey arrows.

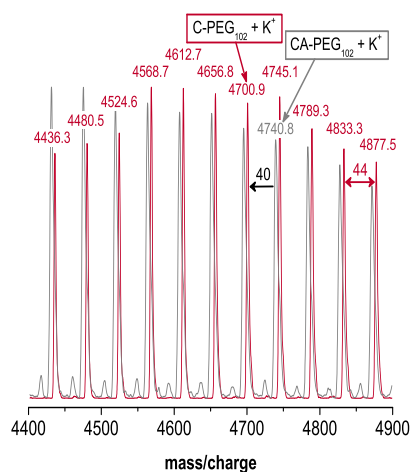


Figure 3. MALDI-ToF mass spectrum of CA-PEG₁₆₀ (gray) and C-PEG₁₆₀ (red) with exemplary assignment of peaks, confirming the loss of the protecting group (black arrow) and showing the repeating units (red arrow).

Thiol-ene click to vinyl double bonds

In addition to the selective release of OH functionalities at the backbone, in the case of EVGE comonomers these can be used for facile attachment of active compounds via thiol-ene chemistry. Successful click of benzyl mercaptane as a model compound to the polymer can be monitored by ^1H NMR with the appearance of the aromatic and benzylic signals at 7.3-7.1 ppm and 2.57 ppm, respectively. SEC reveals a shift to higher molecular weight (**Figure S9**), while narrow molecular weight distribution is retained (**Table 1**).

Nanoparticle functionalization

Bidentate ligands (CA-PEG). PEGylation of oleate-capped MnO nanoparticles with CA-PEG was achieved by a ligand exchange reaction in chloroform. Phase transfer to deionized water was possible, resulting in translucent solutions, remaining optically stable for weeks (Figure 4). Particle agglomeration in aqueous solution depending on PEG chain length was analyzed two weeks after synthesis via dynamic light scattering (DLS) and transmission electron microscopy (TEM). As expected, hydrodynamic radii decrease with decreasing chain length from $r_{\text{H}} = 41$ nm for CA-PEG₃₂ to $r_{\text{H}} = 36$ nm for CA-PEG₇. Best results were obtained with CA-PEG₃₂, showing no leaching or agglomeration. These undesired effects became more pronounced with decreasing PEG chain length. Only slight agglomeration was observed for CA-PEG₁₉. For CA-PEG₇, both agglomeration (> 60 nm) and presumably leaching of the nanoparticles, indicated by the presence of particles of $r_{\text{H}} = 13$ nm, could be observed. These trends are further supported by TEM images (Figure S16).

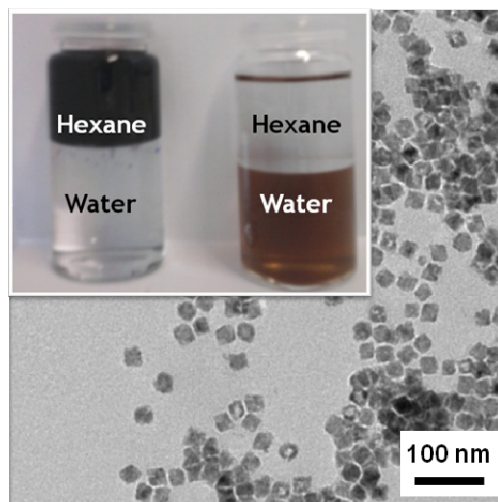


Figure 4. TEM image of MnO nanoparticles capped with C-PEG₁₆₀; the inset image demonstrates the phase transfer of nanoparticles from organic to aqueous phase.

Multifunctional ligands (CA-PEG-PGA). Following the DLS results of the bifunctional ligands, 10 mol% of CA-PEG was replaced by the multifunctional ligand CA-PEG₁₀₇-*b*-PGA₃ for mixed PEGylation of the nanoparticles. The increased chain length of the multifunctional ligand compared to CA-PEG₃₂ ensures addressability of the glycidyl amine repeating units. A coupling reaction of 50% of the amino moieties with the fluorescent dye FITC has been carried out as a proof of principle, allowing for optical monitoring of the fate of the nanoparticles in, e.g., cells. The remaining free amines are further available for the conjugation of drugs, antibodies, or siRNA. UV/Vis spectra of an aqueous solution of the FITC-functionalized nanoparticles show the expected signal at 495 nm, characteristic for fluoresceine bound to the nanoparticle.

Conclusions

This work describes the first use of 2,2-dimethyl-1,3-benzodioxole-5-propanol, a catechol-based initiator, for anionic ring-opening polymerization of epoxides. Bifunctional catechol-PEG ligands as well as multifunctional *mf*-catechol-PEGs using *N,N*-diallyl glycidyl amine (DAGA) and ethylene glycol vinyl glycidyl ether (EVGE) have been synthesized with tailored length and narrow molar mass distributions. Deprotection of primary amino and alcohol moieties from the monomers DAGA and EVGE, respectively, can be carried out separately, allowing for functionalization of the polymers before release of the catechol anchor. Furthermore, the vinyl double bond of the EVGE comonomer can serve as binding site for thiol-ene click reactions. Quantitative cleavage of the acetonide protecting group could be deduced from mass spectrometry. The following full accessibility of the catechol anchor group could be used for ligand exchange on MnO nanoparticles, resulting in water-solubility of the particles, a requirement for their use as T_1 contrast agents in MRI. Addressability of the functional groups on the nanoparticles was proven in a model reaction of the primary amines with fluoresceine isothiocyanate (FITC). *In vitro* cytotoxicity studies of the MnO nanoparticles modified with the multifunctional PEG structures are carried out in our groups at present and will be reported in due course. This work is the first example of a universal new route to multivalent ligands applicable for solubilization and functionalization of a broad range of metal oxide nanoparticles relying on a catechol-initiator approach in combination with the variety of copolymerizable functional epoxide comonomers available today, suitable for attachment of, e.g., targeting moieties. Through choice of comonomer and incorporated amount of comonomer, even stimuli-responsive nanoparticles should be obtainable.

Acknowledgment

The authors thank Dennis Sauer for technical assistance. V.S.W. is grateful to the Fonds der Chemischen Industrie for a scholarship and to the Gutenberg-Akademie for funding. V.S.W. and C.T. thank the Graduate School “Materials Science in Mainz” for valuable financial support. W.T. acknowledges partial funding from the Research Center Complex Materials (*COMATT*) and the Deutsche Forschungsgemeinschaft (DFG) within the priority program 1313 “Bio-Nano-Responses”.

References

- [1] Schladt, T. D.; Schneider, K.; Schild, H.; Tremel, W. *Dalton Trans.* **2011**, *40*, 6315-6343.
- [2] Qiao, R.; Yang, C.; Gao, M. *J. Mater. Chem.* **2009**, *19*, 6274-6293.
- [3] Gu, H.; Xu, K.; Xu, C.; Xu, B. *Chem. Commun.* **2006**, 941-949.
- [4] Shukoor, M. I.; Natalio, F.; Tahir, M. N.; Ksenofontov, V.; Therese, H. A.; Theato, P.; Schröder, H. C.; Müller, W. E. G.; Tremel, W. *Chem. Commun.* **2007**, 4677-4679.
- [5] Schröder, H. C.; Natalio, F.; Wiens, M.; Tahir, M. N.; Shukoor, M. I.; Tremel, W.; Belikov, S. I.; Krasko, A.; Müller, W. E. G. *Mol. Immunol.* **2008**, *45*, 945-953.
- [6] Bae, K. H.; Park, M.; Do, M. J.; Lee, N.; Ryu, J. H.; Kim, G. W.; Kim, C.; Park, T. G.; Hyeon, T. *ACS Nano* **2012**, *6*, 5266-5273.
- [7] Jun, Y.-W.; Lee, J.-H.; Cheon, J. *Angew. Chem. Int. Ed.* **2008**, *47*, 5122-5135.
- [8] Na, H. B.; Song, I. C.; Hyeon, T. *Adv. Mater.* **2009**, *21*, 2133-2148.
- [9] Prijic, S.; Sersa, G. *Radiol. Oncol.* **2011**, *45*, 1-16.
- [10] Na, H. B.; Lee, J. H.; An, K.; Park, Y. I.; Park, M.; Lee, I. S.; Nam, D.-H.; Kim, S. T.; Kim, S.-H.; Kim, S.-W.; Lim, K.-H.; Kim, K.-S.; Kim, S.-O.; Hyeon, T. *Angew. Chem. Int. Ed.* **2007**, *46*, 5397-5401.
- [11] Na, H. B.; Hyeon, T. *J. Mater. Chem.* **2009**, *19*, 6267-6273.
- [12] Schladt, T. D.; Schneider, K.; Shukoor, M. I.; Natalio, F.; Bauer, H.; Tahir, M. N.; Weber, S.; Schreiber, L. M.; Schröder, H. C.; Müller, W. E. G.; Tremel, W. *J. Mater. Chem.* **2010**, *20*, 8297-8304.
- [13] Schladt, T. D.; Graf, T.; Tremel, W. *Chem. Mater.* **2009**, *21*, 3183-3190.
- [14] Cedervall, T.; Lynch, I.; Lindman, S.; Berggård, T.; Thulin, E.; Nilsson, H.; Dawson, K. A.; Linse, S. *Proc. Natl. Acad. Sci. U.S.A.* **2007**, *104*, 2050-2055.
- [15] Michalet, X.; Pinaud, F. F.; Bentolila, L. A.; Tsay, J. M.; Doose, S.; Li, J. J.; Sundaresan, G.; Wu, A. M.; Gambhir, S. S.; Weiss, S. *Science* **2005**, *307*, 538-544.
- [16] Neoh, K. G.; Kang, E. T. *Polym. Chem.* **2011**, *2*, 747-759.
- [17] Jokerst, J. V.; Lobovkina, T.; Zare, R. N.; Gambhir, S. S. *Nanomedicine* **2011**, *6*, 715-728.
- [18] Flesch, C.; Unterfinger, Y.; Bourgeat-Lami, E.; Duguet, E.; Delaite, C.; Dumas, P. *Macromol. Rapid Commun.* **2005**, *26*, 1494-1498.
- [19] Waite, J. H.; Tanzer, M. L. *Science* **1981**, *212*, 1038-1040.
- [20] Lee, H.; Dellatore, S. M.; Miller, W. M.; Messersmith, P. B. *Science* **2007**, *318*, 426-430.
- [21] Latham, A. H.; Williams, M. E. *Acc. Chem. Res.* **2008**, *41*, 411-420.
- [22] Na, H. B.; Palui, G.; Rosenberg, J. T.; Ji, X.; Grant, S. C.; Mattoussi, H. *ACS Nano* **2012**, *6*, 389-399.
- [23] Schladt, T. D.; Shukoor, M. I.; Schneider, K.; Tahir, M. N.; Natalio, F.; Ament, I.; Becker, J.; Jochum, F. D.; Weber, S.; Köhler, O.; Theato, P.; Schreiber, L. M.; Sönnichsen, C.; Schröder, H. C.; Müller, W. E. G.; Tremel, W. *Angew. Chem. Int. Ed.* **2010**, *49*, 3976-3980.
- [24] Tahir, M. N.; Eberhardt, M.; Theato, P.; Faiß, S.; Janshoff, A.; Gorelik, T.; Kolb, U.; Tremel, W. *Angew. Chem. Int. Ed.* **2006**, *45*, 908-912.
- [25] Tahir, M. N.; Eberhardt, M.; Therese, H. A.; Kolb, U.; Theato, P.; Müller, W. E. G.; Schröder, H.-C.; Tremel, W. *Angew. Chem. Int. Ed.* **2006**, *45*, 4803-4809.
- [26] Mangold, C.; Wurm, F.; Frey, H. *Polym. Chem.* **2012**, *3*, 1714-1721.
- [27] Obermeier, B.; Wurm, F.; Mangold, C.; Frey, H. *Angew. Chem. Int. Ed.* **2011**, *50*, 7988-7997.
- [28] Taton, D.; Le Borgne, A.; Sepulchre, M.; Spassky, N. *Macromol. Chem. Phys.* **1994**, *195*, 139-148.
- [29] Mangold, C.; Wurm, F.; Obermeier, B.; Frey, H. *Macromolecules* **2010**, *43*, 8511-8518.
- [30] Koyama, Y.; Umehara, M.; Mizuno, A.; Itaba, M.; Yasukouchi, T.; Natsume, K.; Sugiyama, A.; Watanabe, K. *Bioconjugate Chem.* **1996**, *7*, 298-301.

3.1) CATECHOL-PEGs

- [31] Obermeier, B.; Frey, H. *Bioconjugate Chem.* **2011**, *22*, 436-444.
- [32] Mangold, C.; Dingels, C.; Obermeier, B.; Frey, H.; Wurm, F. *Macromolecules* **2011**, *44*, 6326-6334.
- [33] Obermeier, B.; Wurm, F.; Frey, H. *Macromolecules* **2010**, *43*, 2244-2251.
- [34] Reuss, V. S.; Obermeier, B.; Dingels, C.; Frey, H. *Macromolecules* **2012**, *45*, 4581-4589.
- [35] Liu, Z.; Hu, B.-H.; Messersmith, P. B. *Tetrahedron Lett.* **2008**, *49*, 5519-5521.
- [36] Messersmith, P. B.; Hu, B.-H.; Liu, Z [Northwestern University, Evanston, IL, USA]. Method of synthesizing acetonide-protected catechol-containing compounds and intermediates produced therein. US Patent Application Publication 2010/0087622 A1, April 8, 2010.
- [37] Torchilin, V. P. *Adv. Drug Del. Rev.* **2006**, *58*, 1532-1555.
- [38] Mangold, C.; Obermeier, B.; Wurm, F.; Frey, H. *Macromol. Rapid Commun.* **2011**, *32*, 1930-1934.

Supporting Information

Catechol-initiated Polyethers: Multifunctional Hydrophilic Ligands for PEGylation and Functionalization of Metal Oxide Nanoparticles

Valerie S. Wilms, Heiko Bauer, Christine Tonhauser, Anna-Maria Schilmann, Marc-Christian Müller, Wolfgang Tremel, Holger Frey

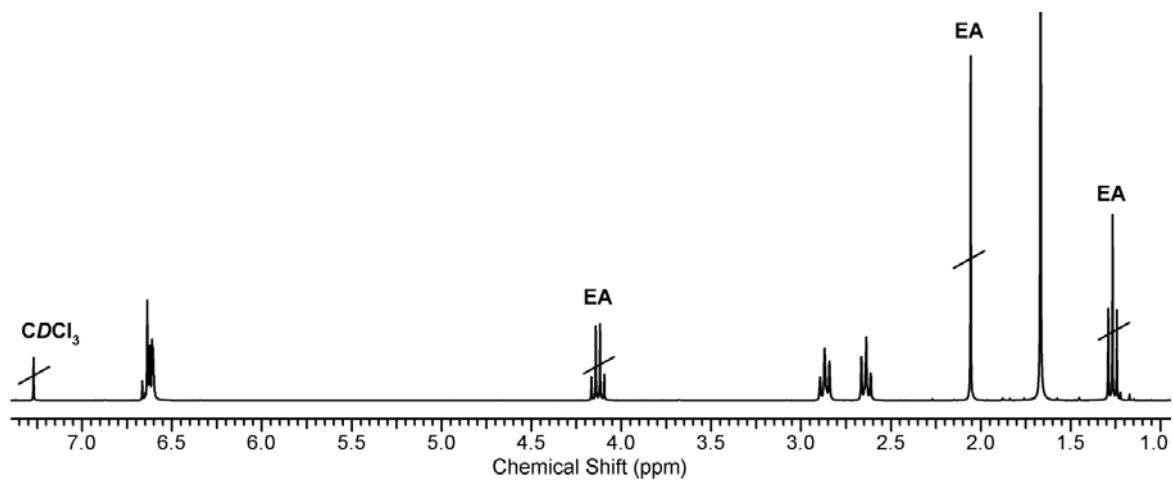


Figure S1. ¹H NMR spectrum (CDCl₃, 300 MHz) of 2,2-dimethyl-1,3-benzodioxole-5-propanoic acid (catechol acetonide-COOH, CA-COOH, **1a**; EA = ethyl acetate).

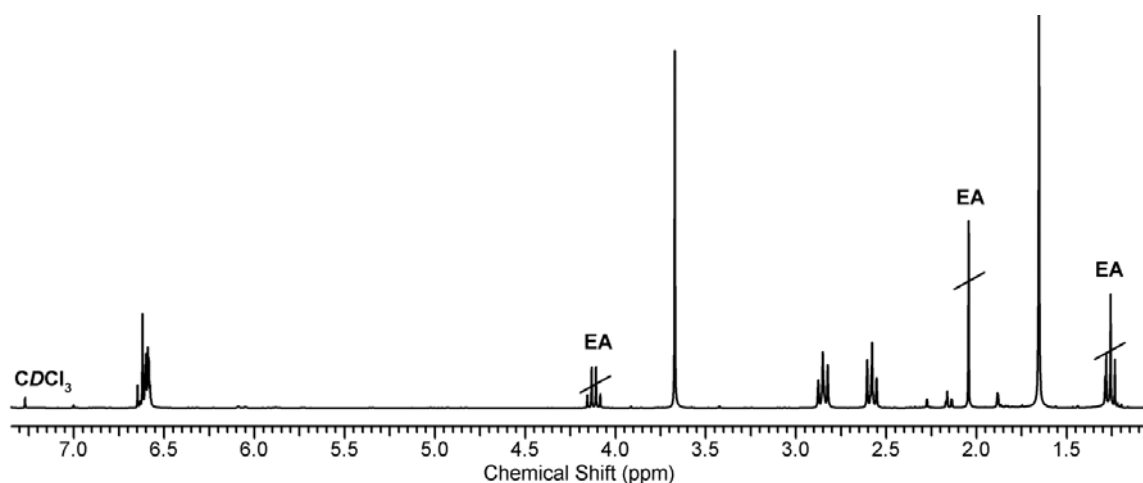


Figure S2. ¹H NMR spectrum (CDCl₃, 300 MHz) of 2,2-dimethyl-1,3-benzodioxole-5-propanoic acid methyl ester (catechol acetonide-COOMe, CA-COOMe, **1b**; EA = ethyl acetate).

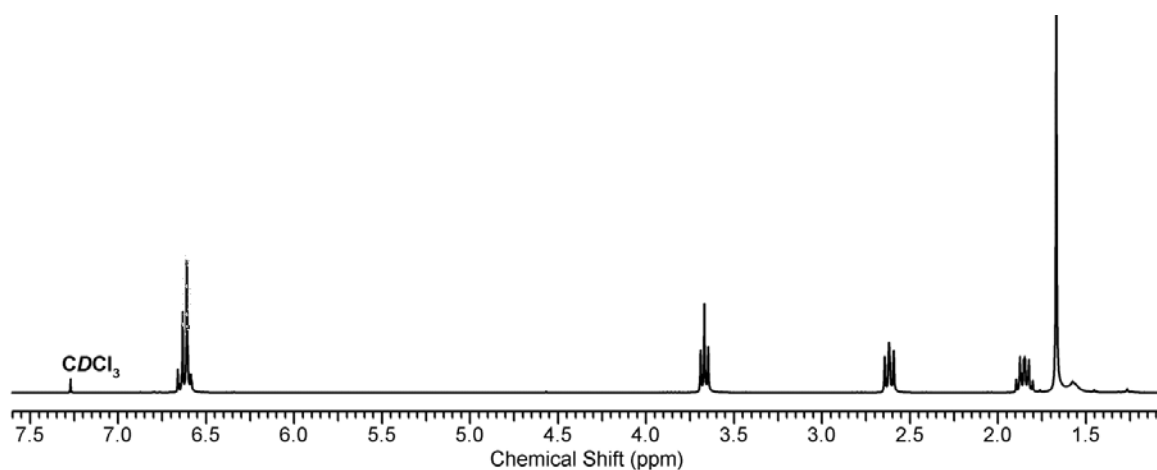


Figure S3. ¹H NMR spectrum (CDCl₃, 300 MHz) of 2,2-dimethyl-1,3-benzodioxole-5-propanol (catechol acetone-OH, CA-OH, **2**).

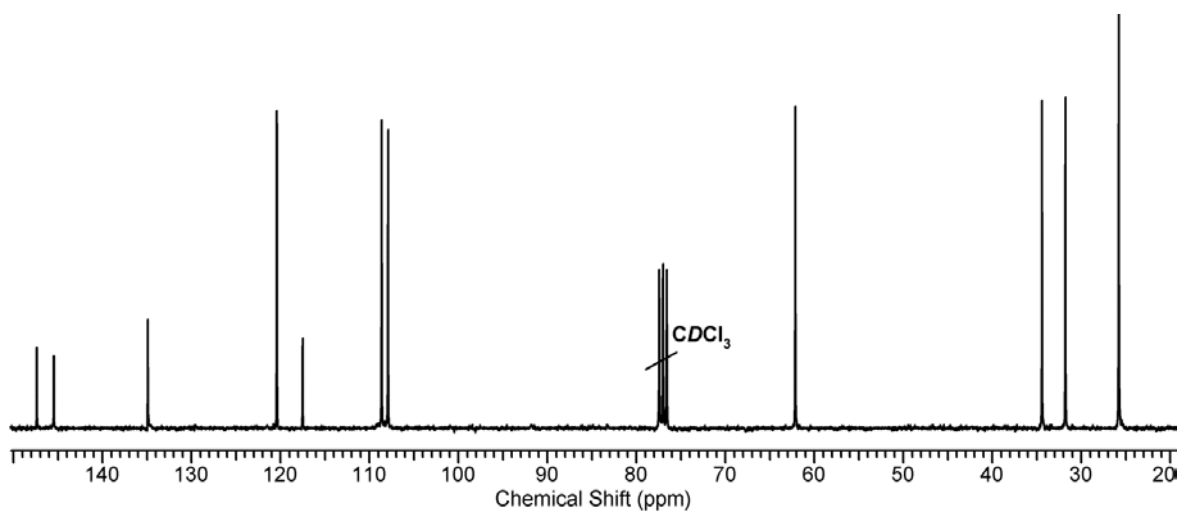


Figure S4. ¹³C NMR spectrum (CDCl₃, 75.5 MHz) of 2,2-dimethyl-1,3-benzodioxole-5-propanol (catechol acetone-OH, CA-OH, **2**).

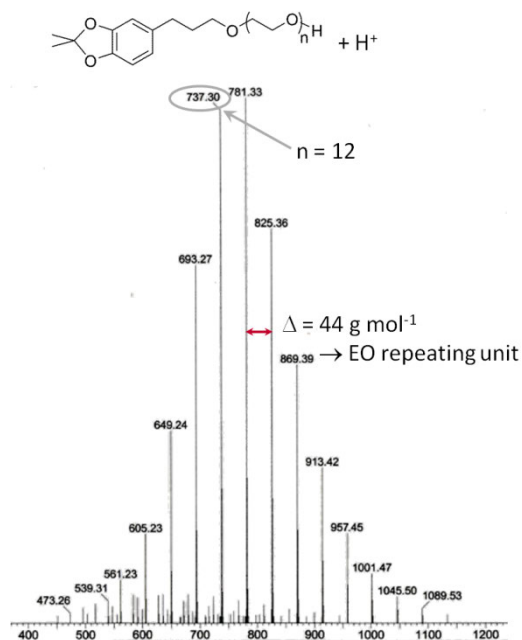


Figure S5. ESI mass spectrum of CA-PEG₇.

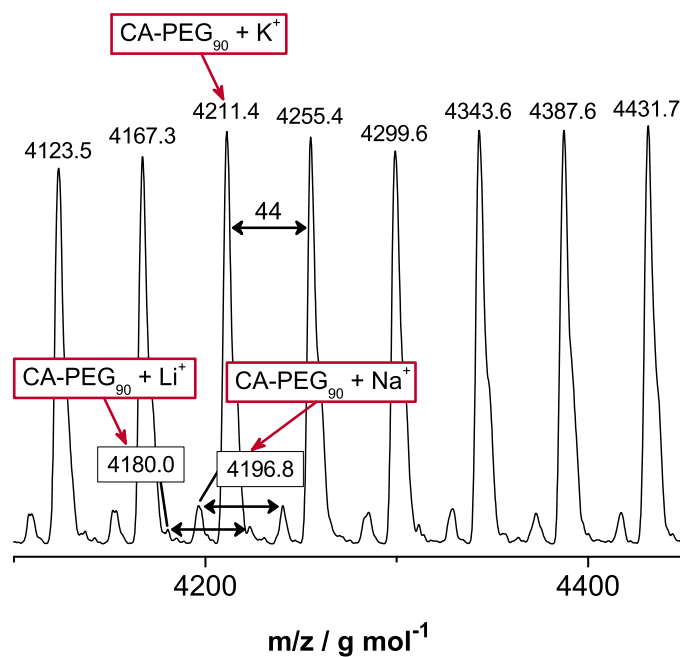


Figure S6. MALDI-ToF mass spectrum of CA-PEG₁₆₀ with partial assignment (linear mode, matrix: CHCA, ionization agent: KTFA). One repeating unit of EO (44 g mol^{-1}) is marked by black arrows. Main distribution corresponds to potassium adduct of the polymer, minor distributions can be assigned to sodium and lithium adducts of the polymer.

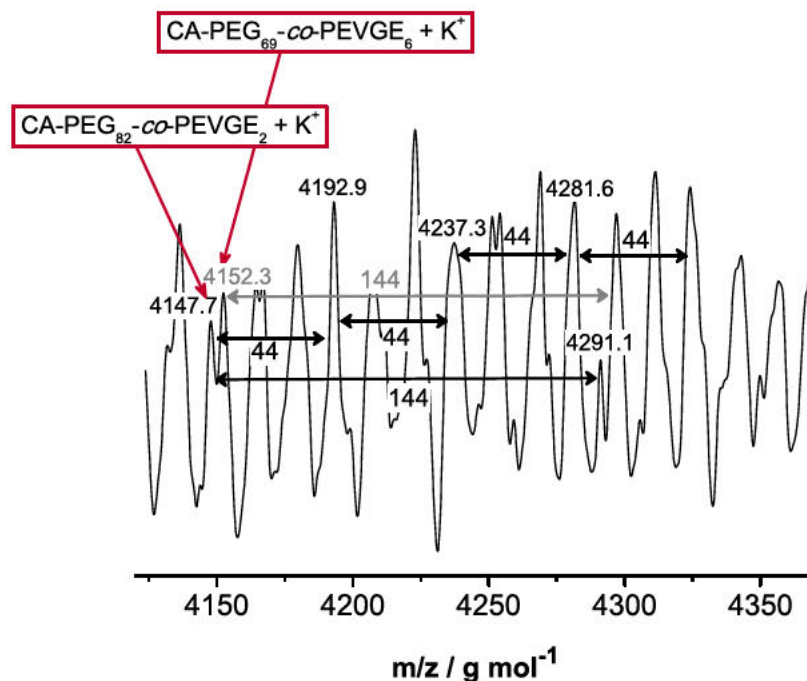


Figure S8. MALDI-ToF mass spectrum of CA-PEG₁₅₆-co-PEVGE₄ with partial assignment (linear mode, matrix: CHCA, ionization agent: KTFA). Incorporation of both monomers into the polymer can be deduced from the existence of two repeating units with 44 $g \text{ mol}^{-1}$ (EO) and 144 $g \text{ mol}^{-1}$ (EVGE). All signals can be assigned to linear combinations of EO and EVGE with the initiator attached and ionized by potassium or cesium, respectively.

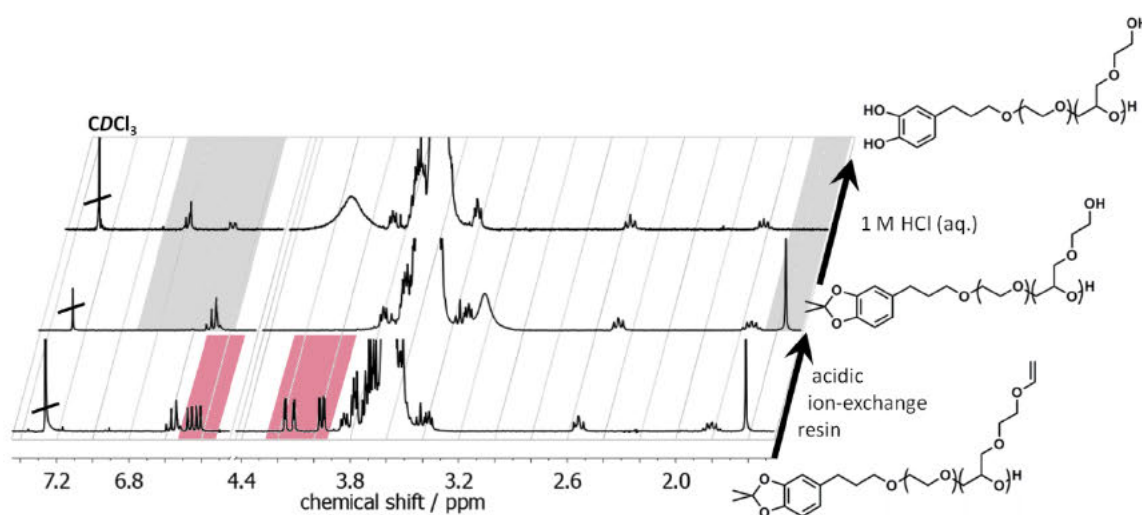


Figure S9. ¹H NMR spectra (CDCl₃, 300 MHz) of CA-PEG₁₅₆-co-PEVGE₄ before (bottom) and after cleavage of vinyl ether protecting groups (middle, relevant protons highlighted in red) as well as after subsequent release of catechol moiety (top, relevant protons highlighted in gray).

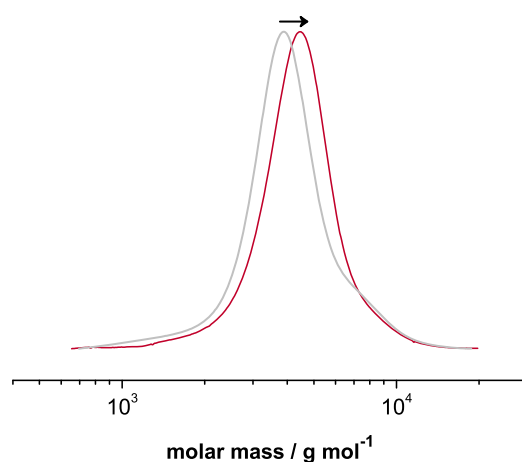


Figure S9. SEC traces of CA-PEG₁₅₆-co-PEVGE₄ before (gray) and after (red) thiol-ene click reaction with benzyl mercaptane. Molecular weight increases while narrow molecular weight distribution is retained.

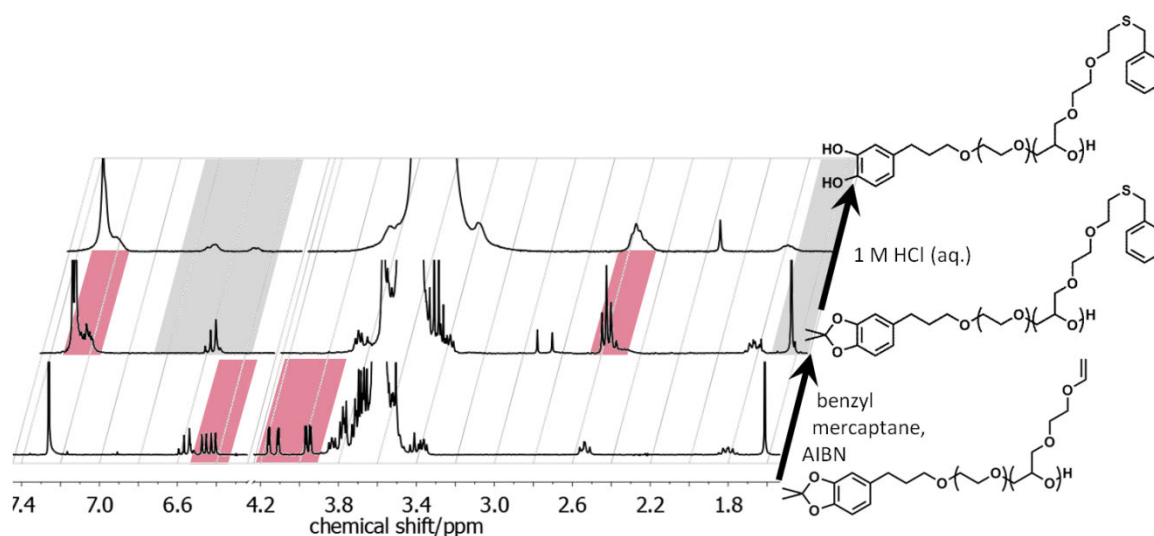


Figure S10. ¹H NMR spectra (CDCl₃, 300 MHz) of CA-PEG₁₅₆-co-PEVGE₄ before (bottom, vinyl protons highlighted in red) and after thiol-ene click reaction (middle, aromatic and benzyl protons highlighted in red) as well as after subsequent release of catechol moiety (top, relevant protons highlighted in gray).

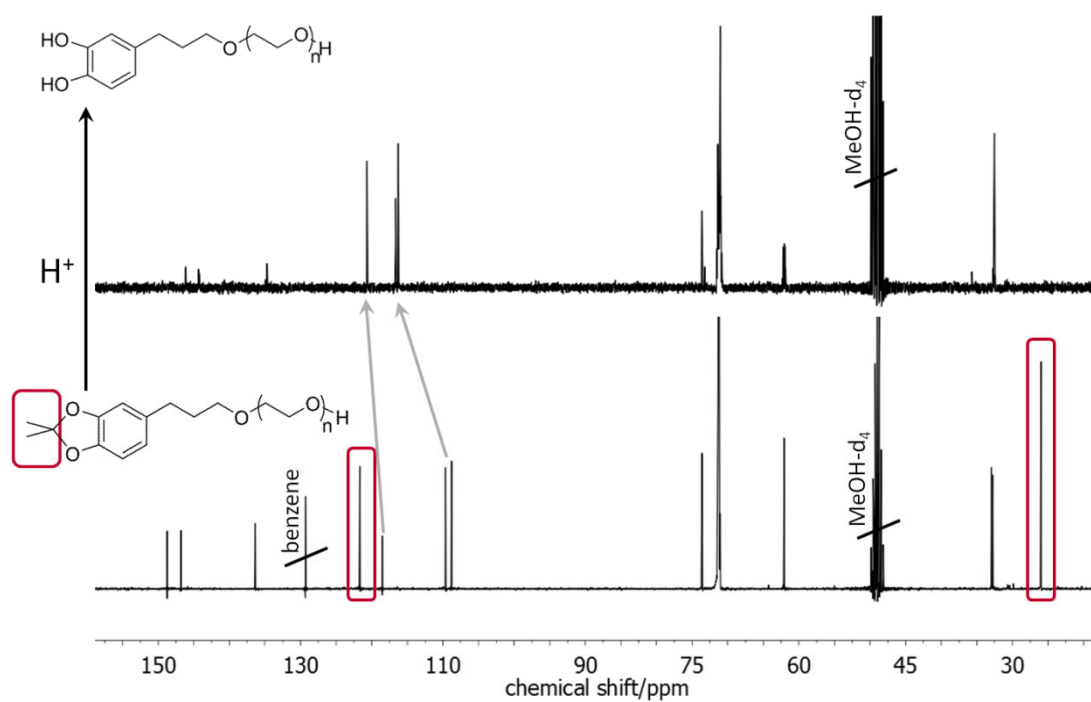


Figure S11. ^{13}C NMR spectra (methanol- d_4 , 75.5 MHz) of CA-PEG and C-PEG. Acetone protecting group carbon signals are highlighted in red. Gray arrows indicate shift of aromatic carbons upon deprotection.

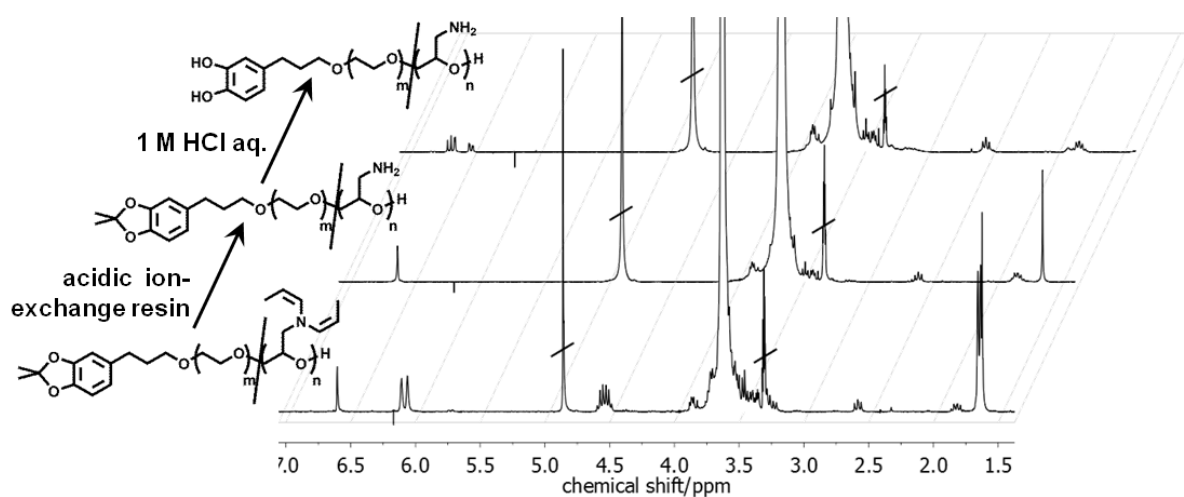


Figure S12. ^1H NMR spectra (methanol- d_4 , 300 MHz) of fully *cis*-isomerized CA-PEG $_{144}$ -*co*-PDAGA $_3$ (bottom), CA-PEG $_{144}$ -*co*-PGA $_3$ (middle), and C-PEG $_{144}$ -*co*-PGA $_3$ (top).

3.1) CATECHOL-PEGs

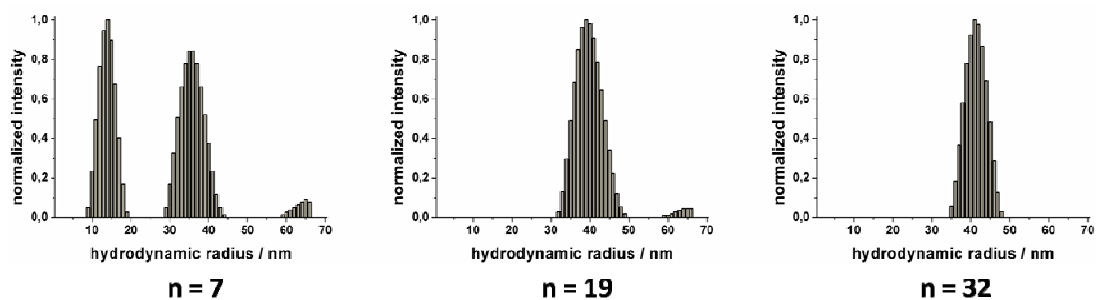


Figure S13. Dynamic light scattering results (MilliQ) of MnO nanoparticles capped with C-PEG_n ligands with n = 7, 19, and 32, respectively.

Figure S14. UV-Vis spectra of FITC, MnO nanoparticles with C-PEG ligands, and MnO nanoparticles with multifunctional ligands C-PEG-PGA labeled with FITC.

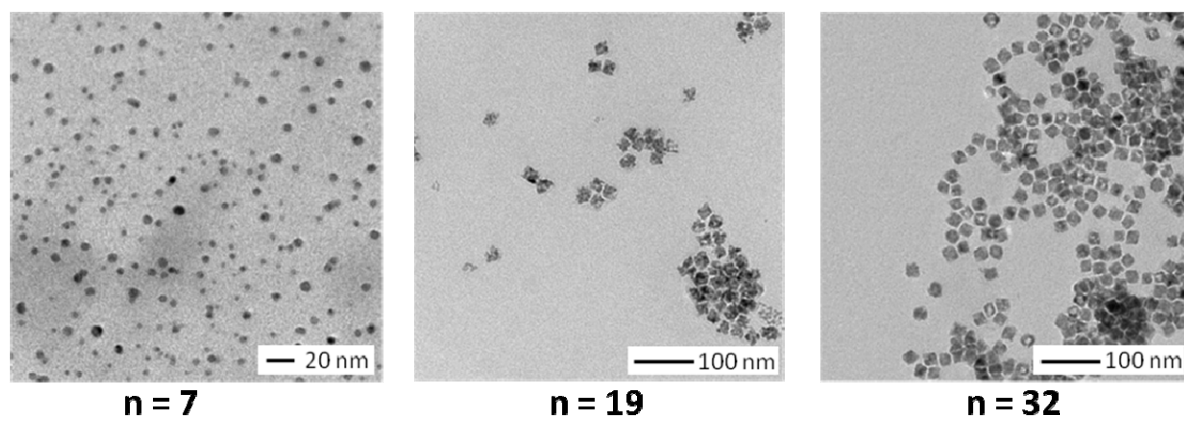


Figure S16. TEM results of MnO nanoparticles capped with C-PEG_n ligands with $n = 7$ (5.05 ± 1.43 nm), 19 (22.82 ± 3.51 nm), and 32 (20.31 ± 2.72 nm), respectively.

3.2) Novel Cationic Polyether Block Copolymers for Passivation and Functionalization of Glass Surfaces

Valerie S. Wilms, Jonathan Edgar, Carsten Sönnichsen, Holger Frey

To be submitted.

Abstract

Tailored polyether block copolymers with a cationically charged polyether block and a PEG block have been developed for the passivation and targeted functionalization of glass surfaces, suppressing unspecific fouling. For this means, block copolymers from poly(ethylene glycol) (PEG) and methylated, quaternized poly(*N,N*-diethyl glycidyl amine) (PqDEGA) with molecular weights in the range 5,500 – 10,200 g mol⁻¹ and PDI < 1.06 have been employed, anchoring via electrostatic interaction of cationic PqDEGA to negatively charged glass and shielding with the tethered PEG chain. These well-defined polymers could be obtained in a controlled manner from anionic ring-opening polymerization which enables precise tailoring of block lengths and functionalities. The potential of the polyether block copolymers for modification of the interaction of glass surfaces with adhering solutes has been tested on gold nanorods as a model system. Monitoring was simple, relying on the surface plasmon resonance of the metallic nanoparticles, visible in dark field microscopy. mPEG-*b*-PqDEGA diblock copolymers have been shown to attach electrostatically to glass and almost completely suppress gold nanorod adsorption. Tandem adhesion functionality has been introduced by use of the functional initiator 2-hydroxyethyl disulfide, leading to PqDEGA-*b*-PEG-S-S-PEG-*b*-PqDEGA triblock copolymers, able to attach to glass and specifically bind gold particles after reductive cleavage of the disulfide yielding thiol moieties at the chain end. By mixing this compound with passivating agent, directed binding of gold nanorods in the flow cells through strong Au-S interactions was possible. This study represents a first step in the development of glass flow cell-based assays for molecule recognition by use of gold nanorods as local refractive index sensors.

Introduction

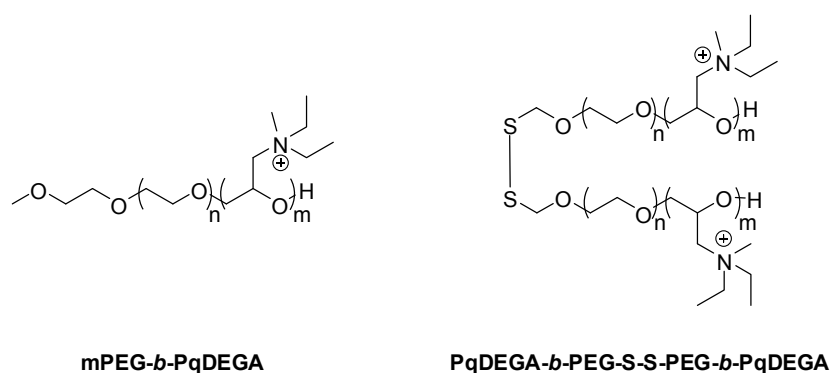
The behavior of polymers at interfaces is a field of extensive research, both basic and applied of nature. This includes the so-called “polymer brushes”, i.e., polymeric assemblies tethered at one end to a solid substrate, which consists of inorganic, organic, or polymeric material.¹ A high extent of control over chemical composition, film thickness, grafting density, and architecture of the macromolecular film is possible. Tethering is effected either through covalent attachment or physical adsorption via two methods, “grafting from” and “grafting to”. “Grafting from” involves surface-initiated polymerization from a substrate previously modified with initiators and calls for synthetic skills of the person interested in the respective surface. On the other hand, in the “grafting to”-approach, a preformed polymer with groups suitable for attachment to the respective surface is employed. Thus, synthetic and surface functionalization steps become separable and the latter can be carried out by institutions without elaborated chemical equipment as well. Compared to homopolymers and random copolymers, block copolymers are the most useful architectures in this context.

Poly(ethylene glycol) (PEG) has been investigated for use in a wide array of surface applications, e.g., for suppression of protein adsorption in aqueous environment, relying on steric stabilization and excluded-volume effects.² Attachment procedures include chemical derivatization of the surface with reactively functionalized PEG and adsorption of PEG-containing surfactants, also called Pluronics, to hydrophobic surfaces.¹ A simple, yet promising approach to functionalization of inorganic surfaces such as metal oxides or glass substrates is the combination of PEG with a polycation. The group of Textor has investigated in depth the comb copolymers poly(L-lysine)-*graft*-PEG (PLL-*g*-PEG) on titanium dioxide, silicon dioxide, and niobium pentoxide surfaces.²⁻⁸ Based on commercially available compounds, the PEG side chains were grafted to the existing PLL backbone via active ester chemistry. At pH 7.4, the amino moieties of the PLL are protonated, resulting in a polycationic comb backbone. At the same time, this pH value is markedly above the isoelectric point of the metal oxides, giving them a net negative charge. From an aqueous solution, PLL-*g*-PEG was shown to attach to the metal oxide surfaces, electrostatically attracted by the opposite charges present. The backbone was found to remain flat on the substrate, acting as an anchor, while the PEG chains reached perpendicularly into the solution, effecting protein-repellent behavior.^{2,4-8} In a related work, Ionov et al.⁹ utilized random poly(aminoethyl methacrylate)-*co*-poly(PEG methacrylate) (PAEMA-*co*-PPEGMA) copolymers obtained from free radical copolymerization for functionalization of glass surfaces. Permanent polycations irrespective of pH value of the surroundings, i.e., PPEGMA-*co*-poly(methacryloxyethyl

3.2) PEG-*b*-PqDEGA ON GLASS

trimethylammonium chloride) (PPEGMA-*co*-PMETAC) were employed by Iruthayaraj et al.¹⁰ on silica. Due to the uncontrolled nature of the polymer syntheses, the materials employed were not defined regarding distribution of the grafted chains and polydispersities, respectively, and additional functionalities were not explored.

Gold nanorods can be synthesized by straightforward protocols in high yields.¹¹⁻¹³ Amongst other applications, they can be used as “plasmonic rulers” in chemical sensing.¹⁴⁻¹⁸ The frequency of the surface plasmon resonance (SPR) of the noble metallic nanoparticles depends on many parameters, such as aspect ratio, interparticle distance, refractive index of the environment, and orientation.¹⁹ Hence, changes in these parameters can be monitored by the resonance frequency of the SPR and used for a variety of assays, capitalizing on the non-bleaching character of the nanorods.¹⁷ In order to obtain high signal-to-noise ratios (S/N), targeted binding of the gold nanorods has to be controllable, whilst non-specific binding to the glass substrate has to be prevented. Also thanks to the SPR of the gold nanorods, the number of adsorbed nanoparticles in a flow cell with a glass floor can be determined using dark-field microscopy.



mPEG-*b*-PqDEGA

PqDEGA-*b*-PEG-S-S-PEG-*b*-PqDEGA

Figure 1. Structures of block copolymers employed for attachment on glass surfaces in flow cells.

The synthesis of multifunctional PEGs (*mf*-PEGs)^{20,21} has attracted increasing interest in recent years, among them the multi-aminofunctional PEG copolymers from random or stepwise copolymerization of ethylene oxide (EO) with glycidyl amine derivatives.²²⁻²⁴ These polymers are employed in the current work, because the amino moieties can be quaternized to give cationic PEG polyelectrolyte block copolymers. The cationic block can attach to negatively charged surfaces while the PEG block has a shielding, anti-fouling effect, e.g., against uncontrolled adsorption of nanoparticles (Figure 2). Through the polymers' synthesis via anionic ring-opening polymerization (AROP), the obtained materials are well-defined. Polymerization degrees and molecular weight distributions can be controlled. Additional functionalities can be introduced via functional initiators,

capping agents, or other comonomers.²⁵ In this study, block copolymers PEG-*b*-poly(*N,N*-diethyl glycidyl amine) (PEG-*b*-PDEGA) are employed. The polymers can be methylated to give polyether polyelectrolytes with a quaternized, cationic PqDEGA block (Figure 1). Such, they are considered suitable candidates for attachment to negatively charged glass surfaces via electrostatic interaction. Interactions of other substances, such as gold nanorods, with the substrate shall be prevented by the shielding effect of the tethered PEG chain. Furthermore, functionalities for targeted attachment of gold rods to glass (Figure 2) are easily introduced due to the living character of the polymerization. In this work, a disulfide moiety has been chosen because of the strong character of the Au-S linkage (approx. 50 kcal mol⁻¹).²⁶ After reductive cleavage of the disulfide bond in the resulting triblock copolymers PqDEGA-*b*-PEG-S-S-PEG-*b*-PqDEGA, the resulting diblock copolymer is expected to bind via the cationic block to the glass surface, presenting its distal thiol bond to solutes. In the presence of gold rods, it may bind them covalent Au-S bonds, thereby anchoring the nanoparticles on the surface of the flow cell.

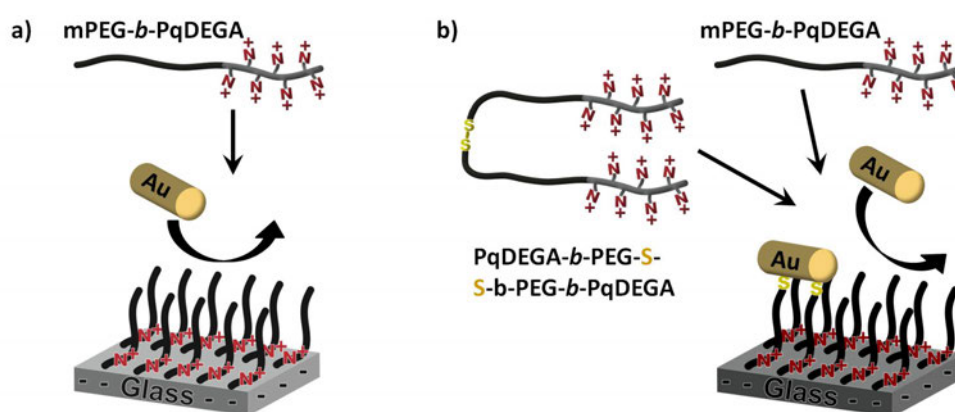


Figure 2. Schematic representation of a) passivation of the negatively charged glass surface of a flow cell against uncontrolled adhesion of gold nanorods by treatment with PEG-*b*-PqDEGA, and of b) functional passivation of a glass surface with a mixture of passivating PEG-*b*-PqDEGA and functional PqDEGA-*b*-PEG-S-S-PEG-*b*-PqDEGA, binding a targeted amount of gold nanorods by Au-S linkages.

Experimental Section

Instrumentation. ¹H NMR spectra (300 MHz) were recorded using a Bruker AC300 spectrometer. All spectra were referenced internally to residual proton signals of the deuterated solvent. For SEC measurements in DMF (containing 0.25 g/L of lithium bromide as an additive), an Agilent 1100 Series

was used as an integrated instrument, including a PSS HEMA column ($10^6/10^5/10^4$ g mol⁻¹), a UV (275 nm), and a RI detector. Calibration was carried out using poly(ethylene glycol) standards provided by Polymer Standards Service. Dark field microscopy was carried out using a Carl Zeiss Axio Observer D1 inverted optical microscope operated in dark field mode. Images were taken using a Plan-Apochromat 40x oil immersion objective and Canon EOS 5D mark II. The visible area in the microscope was 250 μ m x 350 μ m.

Passivation experiments were performed in a three-channel flow cell. Flow cells were constructed with two thin microscope slides separated by a thermoplastic sealing film (Nescofilm). Glass and sealing film were patterned using a laser cutter. The flow cell was constructed by heating the sealing film sandwiched between the two glass slides. The flow cell was then inserted into the holder for the microscope. Tubing for each channel was attached to the holder and ensured to be tightly fitting without cracking the slides. The flow for each channel was checked for leakages before the experiment was started. The channels were primed with a syringe and during the experiment, the flow was maintained by the siphon principle.

Materials. Poly(ethylene glycol) monomethyl ether (mPEG 5000, $M_n = 5000$ g mol⁻¹) was purchased from Fluka. Ethylene oxide (99.5%) was purchased from Aldrich. Deuterated chloroform-*d*₁ and DMSO-*d*₆ were purchased from Deutero GmbH. Hellmanex II cleaning concentrate was purchased from VWR. PLL (20,000 g mol⁻¹)-*g*-PEG (2,000 g mol⁻¹) with a grafting ratio of 3:4 was supplied by Surface Solutions (SuSoS). All other solvents and reagents were purchased from Acros Organics. *N,N*-Diethyl glycidyl amine (DEGA), mPEG-*b*-PDEGA, and quaternization with methyl iodide to give mPEG-*b*-PqDEGA were carried out according to the literature.^{24,27} Aqueous polymer solutions were filtered through a 0.2 μ m filter prior to the flow cell experiments.

Synthesis of PqDEGA-*b*-PEG-S-S-PEG-*b*-PqDEGA.

2-Hydroxyethyl disulfide (0.1 mL, 1 equiv.) was introduced into a Schlenk flask. Under an argon atmosphere, 5 mL benzene were added and the mixture was evacuated at room temperature until all volatiles were removed. This step was repeated twice, then the flask was kept under dynamic high vacuum for 3 d. For deprotonation, a solution of diphenylmethyl potassium (DPMK, 1 equiv.) in THF ($c = 0.501$ mol L⁻¹) was syringed in dropwise. The mixture was cooled to -80 °C and ethylene oxide was kryo-transferred first to a graduated ampoule and then into the flask. The polymerization was allowed to proceed for 24 h at 28 °C. The polymer PEG-S-S-PEG was purified via precipitation into cold diethyl ether. For polymerization of the DEGA blocks, 1 g of PEG-S-S-PEG was dissolved in benzene under argon atmosphere and dried at 28 °C for 16 h. Then, dry THF and DPMK (1 equiv.) were introduced into the flask. The solution was stirred for 45 min at 28 °C. Then, it was frozen in

liquid nitrogen and high vacuum was applied. The stop-cock was closed and DEGA was syringed in. Polymerization of the outer blocks was performed at 28 °C for 2 d. Quaternization of the amines to give PqDEGA-*b*-PEG-S-S-PEG-*b*-PqDEGA was carried out using methyl iodide in methanol solution according to the literature.^{24,27}

Gold Nanorods.

Gold nanorods were prepared according to a modified literature procedure.^{12,13} Briefly, 2 nm gold nanoparticle seeds were prepared by rapid addition of ice cold 0.01 M aqueous sodium borohydride solution to an aqueous solution of 0.1 mM HAuCl₄ (tetrachloroauric acid) and 25 mM C₁₆TABr (hexadecyltrimethyl ammonium bromide) under vigorous stirring. 10 μL of this seed solution was stirred into 10 mL of aqueous growth solution containing 0.1 M C₁₆TABr, 0.5 mM HAuCl₄, 0.6 mM ascorbic acid, and 70 μM AgNO₃. The reaction was allowed to proceed for one hour at 30 °C. The nanorods were separated from the excess surfactant by centrifugation (7500 rpm for 10 min, radius of centrifuge ~10 cm). Centrifugation was repeated twice, the supernatant was discarded each time and replaced with MilliQ water.

Flow Cell Experiments with Gold Nanorods: Passivation.

Each flow cell channel was rinsed with 5% v/v Hellmanex cleaning solution for 15 min and MilliQ water for 10 min. Then, the inner surface of each channel was imaged, with few or no objects present. In each flow cell channel, a solution of the passivating agent ($c = 25 \text{ mg mL}^{-1}$) was injected, allowed to flow for 4-5 min, and incubated for 1 h. One channel was always incubated with MilliQ water only, as a control. After rinsing with MilliQ water for 10 min, the inner surface of each channel was imaged. An aqueous solution of gold nanorods, 50x diluted from standard synthesis, was allowed to flow for 1-2 min, so each channel was full of nanorod solution. Subsequently, 0.1 M NaCl solution was injected into each channel and coating of the nanorods on the surface of the unpassivated control channel was monitored. Once a sufficient coverage was obtained, all channels were rinsed with MilliQ water for 10 min. After that, the inner surface of each channel was imaged.

Flow Cell Experiments with Gold Nanorods: Functional Passivation.

Each flow cell channel was rinsed with 2% v/v Hellmanex cleaning solution for 15 min and MilliQ water for 10 min. In each flow cell channel, a solution of the passivating agent (mPEG₁₁₃-*b*-PqDEGA₁₇, $c = 5 \text{ mg mL}^{-1}$) or the functional passivation solution (25 μL of mPEG₁₁₃-*b*-PqDEGA₁₇ solution, $c = 50 \text{ μg mL}^{-1}$, 292 μL of PqDEGA-*b*-PEG-S-S-PEG-*b*-PqDEGA solution, $c = 5 \text{ mg mL}^{-1}$, in 183 μL MilliQ water, pretreated with 10 equiv. *tris*(2-carboxyethyl)phosphine) was injected, allowed to flow for 4-5 min, and incubated for 1 h. One channel was incubated with MilliQ water only, as a control. After rinsing

with MilliQ water for 10 min, the inner surface of each channel was imaged. An aqueous solution of gold nanorods, 50x diluted from standard synthesis, was allowed to flow for 1-2 min, so each channel was full of nanorod solution, and incubated for 45 – 60 min. All channels were rinsed with MilliQ water for 10 min. After that, the inner surface of each channel was imaged.

Results and Discussion

Polymer Synthesis

In a single step, a series of block copolymers mPEG-*b*-PDEGA could be synthesized from mPEG macroinitiators, partially deprotonated by cesium hydroxide monohydrate.²⁴ mPEGs with 2000 g mol⁻¹ or 5000 g mol⁻¹ were employed. After removal of low-molecular-weight side products resulting from chain-transfer to monomer, well-defined amphiphilic materials with narrow molecular weight distributions were obtained (Table 1). Full methylation with methyl iodide in methanol, i.e., quaternization of the amines, gave double hydrophilic, polycationic mPEG-*b*-PqDEGA block copolymers (Figure 1).^{24,27} In SEC, shifts to lower apparent molecular weights and a lowering of polydispersities could be observed.

For the introduction of an additional functionality for interaction with gold nanorods a commercially available disulfide-containing initiator was used. 2-Hydroxyethyl disulfide was dried extensively before deprotonation because of a water content of the starting material of approximately 10 wt.%. Benzene was added for this purpose, known to form azeotropic mixtures with water. One has to be careful when drying this compound, since degradation was observed at elevated temperatures. Hence, temperatures for all steps were fixed in the range of room temperature to 28 °C at maximum. After deprotonation with one equivalent diphenylmethyl potassium (DPMK) in THF, which translates to a deprotonation degree of 50%, polymerization of EO was carried out in THF at 28 °C. DPMK was chosen, because it is a sterically hindered base and is believed not to attack the disulfide linkage, in contrast to otherwise employed reagents, such as potassium naphthalenide, which are reductively active species. The polymer was purified by precipitation into cold diethyl ether. Calculation of the degree of polymerization was not possible from ¹H NMR, since the initiator signals are part of the backbone signal around 3.5 ppm. Therefore, SEC molecular weight was employed for the determination. This value has to be handled with care due to the relative character of this measurement method.

Table 1. Characterization data for the block copolymers comprised of ethylene oxide and *N,N*-diethyl glycidyl amine (DEGA) or its methylated, quaternized derivative (qDEGA).

compound	M_n (NMR) [g mol ⁻¹]	M_n (GPC) [g mol ⁻¹]	M_n/M_w
mPEG ₄₅ - <i>b</i> -PDEGA ₁₃	3700	2900	1.07
mPEG ₁₁₃ - <i>b</i> -PDEGA ₁₃	6700	5800	1.08
mPEG ₁₁₃ - <i>b</i> -PDEGA ₂₂	7900	6600	1.07
mPEG ₄₅ - <i>b</i> -PqDEGA ₁₃	5500	2900	1.05
mPEG ₁₁₃ - <i>b</i> -PqDEGA ₁₂	8200	3300	1.06
mPEG ₁₁₃ - <i>b</i> -PqDEGA ₁₇	10200	3300	1.03
PEG ₂₉ -S-S-PEG ₂₉ ^a	-	2700	1.16
PDEGA ₄ - <i>b</i> -PEG ₂₉ -S-S-PEG ₂₉ - <i>b</i> -PDEGA ₄ ^b	-	5500	1.17
PqDEGA ₄ - <i>b</i> -PEG ₂₉ -S-S-PEG ₂₉ - <i>b</i> -PqDEGA ₄	-	2400 ^c	1.06

^a Polymerization degree of PEG calculated from molecular weight obtained by SEC, since initiator and end group signals are hidden by the polymer backbone in ¹H NMR. ^b Polymerization degree of PDEGA calculated from ratio of signals of PEG backbone/DEGA side chains in ¹H NMR. ^c This value has to be handled with care because of interaction of the charged macromolecule with the column material of the SEC.

Subsequently, polymerization of the outer PDEGA blocks was carried out in a second step. Again, deprotonation was effected by DPMK in THF, and DEGA was syringed into the evacuated flask. Increase of molecular weight could be easily followed via SEC. Polymerization degree of the outer DEGA blocks was calculated from the polymerization degree of EO from SEC values and the ratio of EO to DEGA units deduced from ¹H NMR (Figure 3, bottom).

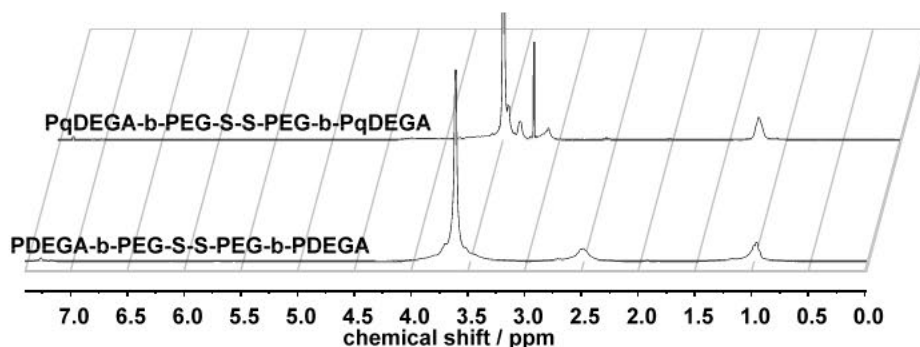


Figure 3. ¹H NMR spectra (300 MHz, CDCl₃) of the disulfide-containing block copolymers before (bottom, PDEGA-*b*-PEG-S-S-PEG-*b*-PDEGA) and after (top, PqDEGA-*b*-PEG-S-S-PEG-*b*-PqDEGA) quaternization with methyl iodide.

Quaternization of the DEGA units was possible in analogy to the diblock copolymers described above. In ^1H NMR spectra the signals of the protons of the ethylene groups were shifted to lower field, the methylene protons now being hidden under the polyether backbone (Figure 3, top). The newly attached methyl groups were now visible at 3.2 ppm. Complete methylation can be deduced from the ratio of methyl protons in ethyl and methyl groups attached to nitrogen, being 6:3.

Passivation of Glass Surfaces against Gold Nanorod Adhesion

In a first approach, the diblock copolymers mPEG-*b*-PqDEGA were tested for their ability to attach to glass surfaces, remain attached during flow, and suppress cluttering of those surfaces with gold nanorods. They were also compared to the commercially available passivating agent PLL-*g*-PEG. The experiments were carried out in a three channel flow cell setup. One channel was always treated with water as only “passivating agent”, as a positive control. Monitoring was possible through dark field microscopy capitalizing on the surface plasmon resonance of the metallic particles. Hence, the nanorods appear as red dots on a dark background.

The flow cells were first rinsed with Hellmanex solution in order to remove any contamination present and render the glass surfaces negatively charged (Figures 4 and 5, a). After a cleaning step with water, surface passivation with the respective polymers was carried out by incubation with aqueous polymer solutions and rinsing with water (Figures 4 and 5, b). In a final step, the cells were incubated with gold nanorod solution, NaCl solution was applied for immobilization of adsorbed particles, followed by a rinsing step (Figures 4 and 5, c). Adsorbed gold nanorods were counted, with decreasing numbers indicating improving passivation capabilities.

Copolymers with constant PqDEGA block length of a polymerization degree of 12 and a varying mPEG block length of 45 or 113 repeating units, i.e. 2000 g mol^{-1} or 5000 g mol^{-1} , were compared (Figure 4, middle and right). Both compounds were able to decrease adsorption of gold nanorods in comparison to approximately 453 visible particles in the water control channel. Increasing PEG length led to decreasing shielding in this case, with 11 visible particles for mPEG₄₅-*b*-PqDEGA₁₂ and approximately 260 visible particles for mPEG₁₁₃-*b*-PqDEGA₁₂. This significantly different effect might be explained by too weak adsorption of the short block with 12 qDEGA units, accompanied by steric repulsion of the longer PEG chains in the latter case, resulting in a too low surface density of the block copolymers and inferior passivation compared to the same PqDEGA anchor length but shorter PEG tail.

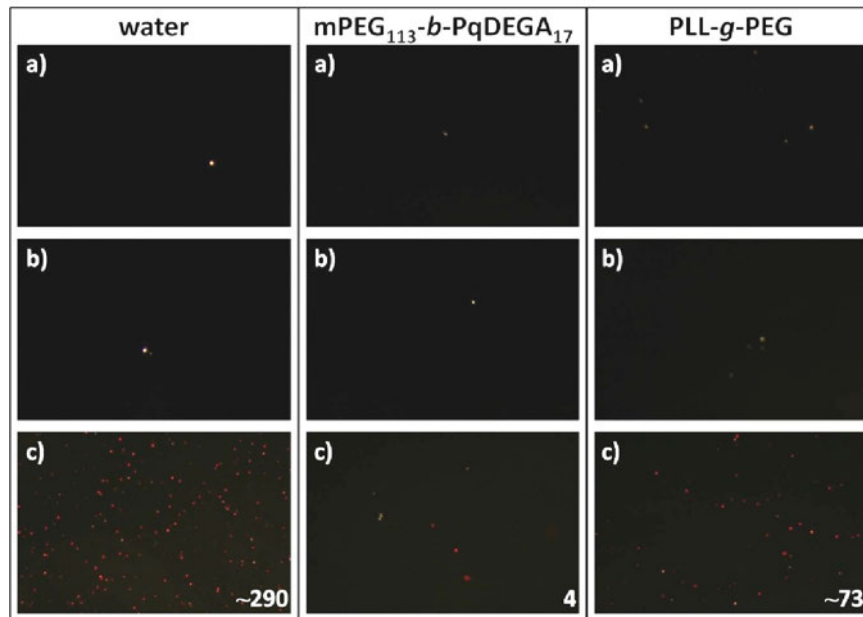


Figure 4. Images of glass surfaces in flow cells after a) rinsing with 5% v/v Hellmanex solution and MilliQ water, b) incubation with passivation agent indicated above and rinsing with MilliQ water, and c) incubation with gold nanorods and rinsing with MilliQ water, the numbers in the lower right corner indicate the number of gold nanorods present in the flow cell image.

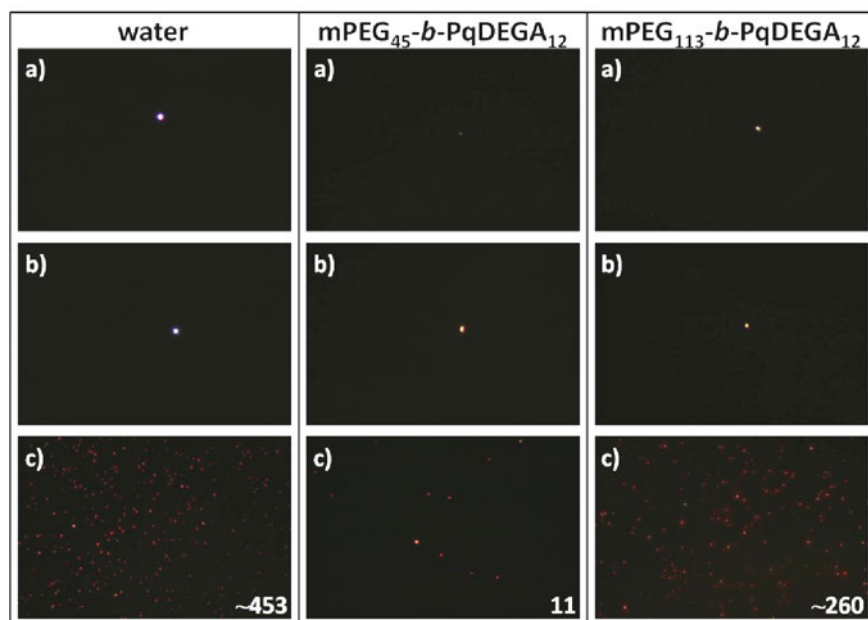


Figure 5. Images of glass surfaces in flow cells after a) rinsing with 5% v/v Hellmanex solution and MilliQ water, b) incubation with passivation agent indicated above and rinsing with MilliQ water, and c) incubation with gold nanorods and rinsing with MilliQ water, the numbers in the lower right corner indicate the number of gold nanorods present in the flow cell image.

Increase of the PqDEGA anchor length from 12 to 17 units was shown to be sufficient to effect nearly complete passivation of the glass surface against gold nanorod adhesion under the chosen conditions (Figure 5, middle). While in the water control channel, 290 adsorbed particles were detected, only 4 particles were visible after treatment of the glass with mPEG₁₁₃-*b*-PqDEGA₁₇. Comparison with the commercially available and highly established comb copolymer PLL-*g*-PEG (Figure 5, right) even revealed superior passivation properties of the newly available block copolymers.

Functional Passivation of Glass Surfaces

Glass-floored flow cells are potential platforms for assays, enabling e.g., the use of gold nanorods as local refractive index sensors revealing adsorption of chemical compounds or biomolecules. For this purpose, the glass surfaces have to be inert towards non-specific agglomeration of particles and molecules under surveillance, but the gold nanorods have to be bound tightly to the flow cell nevertheless. This can be accomplished using the polyether block copolymer approach, introducing a disulfide moiety via the initiator 2-hydroxyethyl disulfide. By pretreatment with *tris*(2-carboxyethyl)phosphine, the disulfide linkage is broken and the resulting thiols serve as strong binding unit to the gold surface via covalent Au-S bonds. The copolymer with the best passivating properties, as determined above, mPEG₁₁₃-*b*-PqDEGA₁₇, was thus mixed with the pretreated block copolymer PqDEGA-*b*-PEG-S-S-*b*-PqDEGA, to simultaneously suppress unwanted deposition and allow for binding of tailored amounts of gold nanorods with sensing capability.

The results of the comparison are depicted in Figure 6. The upper row, denoted with a), shows the flow cells after incubation with the passivating agents. Single spots seen here are merely dust particles, as they appear white through the ocular. The bottom row, denoted with b), shows the flow cells after incubation with gold nanorods and rinsing, i.e., the number of adsorbed nanoparticles, plus the dust particles mentioned before. Their color shown by the camera is affected by the settings and the removal of an IR filter.

The positive control channel, incubated with water only, can be seen on the left. The negative control channel, incubated with the passivating agent mPEG₁₁₃-*b*-PqDEGA₁₇, can be seen in the middle, showing less nanorods, but a considerably higher amount than in the passivation-only experiments above. This observation can be attributed to the lower polymer concentration applied in this case, about 1/5 compared to earlier experiments. For functional passivation, an aqueous solution containing a mixture of mPEG₁₁₃-*b*-PqDEGA₁₇ and PqDEGA-*b*-PEG-S-S-PEG-*b*-PqDEGA in a molar ratio

of approximately 1:2000 was employed. As expected, the number of now purposeful attached gold rods is elevated compared to the negative control experiment.

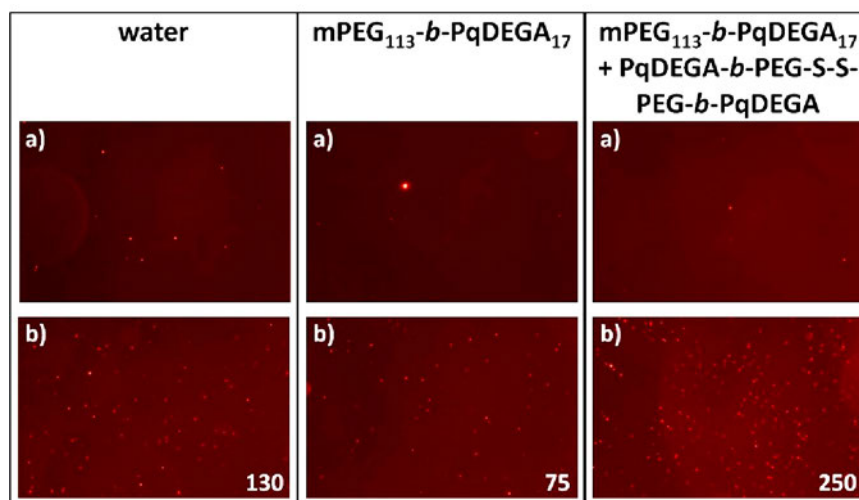


Figure 6. Images of glass surfaces in flow cells after a) rinsing with 5% v/v Hellmanex solution and MilliQ water, and incubation with passivation agent or mixture of passivation and functionalization agent indicated above, and b) after rinsing, incubation with gold nanorods and rinsing. The numbers in the lower right corner indicate the number of gold nanorods present in the flow cell image.

Conclusions

In this work, a polymer class that became available only recently,²⁴ i.e., block copolymers of poly(ethylene glycol) and methylated poly(*N,N*-diethyl glycidyl amine), PEG-*b*-PqDEGA, have been applied for the first time in the alteration of glass surface properties. The positively charged PqDEGA block serves as an anchor to the negatively charged glass surface, while the tethered PEG chains reach into aqueous solution and exert shielding influence. This effect has been studied in flow cells with the use of gold nanorods, monitoring their surface plasmon by dark field microscopy. By adjusting the block lengths and block length ratios of diblock copolymers mPEG-*b*-PqDEGA, the otherwise favored adsorption of gold nanorods on glass could be significantly reduced compared to positive controls incubated with water only, and even almost completely suppressed. Performance of the novel passivating agents has been shown to be superior to the commercially available blocking agent poly(*l*-lysine)-*graft*-PEG (PLL-*g*-PEG). Furthermore, additional functionality could be introduced through the use of the functional initiator 2-hydroxyethyl disulfide. The resulting scissile ABA triblock

copolymer PqDEGA-*b*-PEG-S-S-PEG-*b*-PqDEGA was able to attach to the glass by the outer A blocks. Pretreated with reducing agent, the disulfide linkage is cleaved to give terminal thiol moieties, enabling covalent linkage of the gold nanorods via Au-S bonds. This assumption was supported by elevated amounts of now purposefully attached gold particles in the flow cells treated with a mixture of functionalizing and passivating agent, compared to a negative control with the pure passivating agent. This approach is promising regarding the use of glass-floored flow cells as scaffolds for the design of assays for the sensing and recognition of a large variety of compounds, e.g., biomolecules, such as streptavidin.²⁸ These assays rely on the ability of a known amount of gold nanorods in a cell, displaying changes in the local refractive indices by alteration of their surface plasmon resonances, which can be visualized and measured in a dark field microscopy setup. Furthermore, the gold nanorods applied here only represent a model system for demonstration of the potential of the block copolymers for surface modification. These cationic polyether block copolymers are thought to be highly promising materials for passivation and functional passivation of metal oxide surfaces, controlling surface – solute interactions and bind targeted amounts of, e.g., proteins or DNA, onto them.

Acknowledgment. The authors thank Dennis Sauer for technical assistance. V.S.W. is grateful to the Fonds der Chemischen Industrie for a scholarship and thanks the Gutenberg-Akademie and the Graduate School “Materials Science in Mainz” for valuable financial support.

References

- [1] Azzaroni, O. J. *Polym. Sci., Part A: Polym. Chem.* **2012**, *50*, 3225-3258.
- [2] Kenausis, G. L.; Vörös, J.; Elbert, D. L.; Huang, N.; Hofer, R.; Ruiz-Taylor, L.; Textor, M.; Hubbell, J. A.; Spencer, N. D. *J. Phys. Chem. B* **2000**, *104*, 3298-3309.
- [3] Konradi, R.; Pidhatika, B.; Muhlebach, A.; Textor, M. *Langmuir* **2008**, *24*, 613-616.
- [4] Huang, N.-P.; De Paul, S. M.; Textor, M. *Biomacromolecules* **2011**, *12*, 4213-4220.
- [5] Huang, N.-P.; Michel, R.; Vörös, J.; Textor, M.; Hofer, R.; Rossi, A.; Elbert, D. L.; Hubbell, J. A.; Spencer, N. D. *Langmuir* **2001**, *17*, 489-498.
- [6] Huang, N.-P.; Vörös, J.; De Paul, S. M.; Textor, M.; Spencer, N. D. *Langmuir* **2002**, *18*, 220-230.
- [7] Michel, R.; Pasche, S.; Textor, M.; Castner, D. G. *Langmuir* **2005**, *21*, 12327-12332.
- [8] Pasche, S.; De Paul, S. M.; Vörös, J.; Spencer, N. D.; Textor, M. *Langmuir* **2003**, *19*, 9216-9225.
- [9] Ionov, L.; Synytska, A.; Kaul, E.; Diez, S. *Biomacromolecules* **2010**, *11*, 233-237.
- [10] Iruthayaraj, J.; Poptoshev, E.; Vareikis, A.; Makuska, R.; van der Wal, A.; Claesson, P. M. *Macromolecules* **2005**, *38*, 6152-6160.
- [11] Zijlstra, P.; Orrit, M. *Rep. Prog. Phys.* **2011**, *74*, 55.
- [12] Jana, N. R.; Gearheart, L.; Murphy, C. J. *Adv. Mater.* **2001**, *13*, 1389-1393.
- [13] Nikoobakht, B.; El-Sayed, M. A. *Chem. Mater.* **2003**, *15*, 1957-1962.
- [14] Ament, I.; Prasad, J.; Henkel, A.; Schmachtel, S.; Sönnichsen, C. *Nano Lett.* **2012**, *12*, 1092-1095.
- [15] Becker, J.; Trügler, A.; Jakab, A.; Hohenester, U.; Sönnichsen, C. *Plasmonics* **2010**, *5*, 161-167.
- [16] Sönnichsen, C.; Alivisatos, A. P. *Nano Lett.* **2004**, *5*, 301-304.
- [17] Sönnichsen, C.; Reinhard, B. M.; Liphardt, J.; Alivisatos, A. P. *Nat. Biotechnol.* **2005**, *23*, 741-745.
- [18] Leitner, M.; Henkel, A.; Sönnichsen, C.; Rosa, C. C.; Podoleanu, A. G. *Proc. SPIE* **2008**, *7139*, 71390T-71390T.
- [19] Alkilany, A. M.; Thompson, L. B.; Boulos, S. P.; Sisco, P. N.; Murphy, C. J. *Adv. Drug Del. Rev.* **2012**, *64*, 190-199.
- [20] Mangold, C.; Wurm, F.; Frey, H. *Polym. Chem.* **2012**, *3*, 1714-1721.
- [21] Obermeier, B.; Wurm, F.; Mangold, C.; Frey, H. *Angew. Chem. Int. Ed.* **2011**, *50*, 7988-7997.
- [22] Obermeier, B.; Wurm, F.; Frey, H. *Macromolecules* **2010**, *43*, 2244-2251.
- [23] Reuss, V. S.; Obermeier, B.; Dingels, C.; Frey, H. *Macromolecules* **2012**, *45*, 4581-4589.
- [24] Reuss, V. S.; Werre, M.; Frey, H. *Macromol. Rapid Commun.* **2012**, *33*, 1556-1561.
- [25] Wilms, V. S.; Bauer, H.; Tonhauser, C.; Schilman, A.-M.; Müller, M.-C.; Tremel, W.; Frey, H. *submitted*.
- [26] Di Felice, R.; Selloni, A. *J. Chem. Phys.* **2004**, *120*, 4906-4914.
- [27] Mongondry, P.; Bonnans-Plaisance, C.; Jean, M.; Tassin, J. F. *Macromol. Rapid Commun.* **2003**, *24*, 681-685.
- [28] Nusz, G. J.; Marinakos, S. M.; Curry, A. C.; Dahlin, A.; Hook, F.; Wax, A.; Chilkoti, A. *Anal. Chem.* **2008**, *80*, 984-989.

4) INVESTIGATION OF THERMORESPONSIVE POLYETHERS WITH EPR SPECTROSCOPY

4.1) How Structure-Related Collapse Mechanisms Determine Nanoscale Inhomogeneities in Thermoresponsive Polymers

Dennis Kurzbach, Martina Schömer, Valerie S. Wilms, Holger Frey, Dariush Hinderberger

Published in Macromolecules **2012**, *45*, 7535-7548.

Abstract

Continuous wave electron paramagnetic resonance (CW EPR) spectroscopy on the amphiphilic spin probe TEMPO in solutions of selectively chosen functional, thermoresponsive poly(propylene oxide) (PPO)- and poly(ethylene oxide) (PEO)-based copolymers of both linear and branched structure is used to elucidate their host-guest interactions and inverse phase transitions. Three different fundamental types of host-guest interactions between probes and polymers could be correlated to the phase transition mechanisms (supported by MD simulations), evidencing that these proceed via nanoscale inhomogeneities of the polymers. Due to their ability to host small amphiphilic guest molecules thermoresponsive copolymers are promising candidates for molecular transport applications. The host-guest interaction principles derived from our small amphiphilic spin probes may also aid in finding the “appropriate” design for the desired release property of a specific thermoresponsive polymer-based host-guest systems.

Introduction

In the last 20 years, thermoresponsive polymers that undergo coil-to-globule transitions above a certain critical temperature and their inverse phase behavior have been investigated intensively in numerous fields of science.¹⁻⁵ It has been shown that among other things the composition of a thermosensitive polymer can significantly affect its phase transition behavior.⁶⁻¹¹ That is, a high fraction of hydrophilic comonomers may lead to the incorporation of large amounts of water into aggregates of a thermoresponsive polymer above its collapse temperature, while it is generally shifted to lower temperatures by introducing hydrophobic comonomers.¹²⁻¹⁹ The potential use of thermosensitive macromolecules in molecular transport and drug delivery applications led to the synthesis of a large set of polymeric, LCST-exhibiting materials and to detailed investigation of their inverse phase transitions.¹⁹⁻²⁶ In this respect, it is important that specific analytical methods give rise to specific molecular information:²⁷⁻²⁹ macroscopic ensemble-averaging methods like dynamic light scattering (DLS) among other things yield valuable information about transition temperatures and ranges, while intrinsically local methods like magnetic resonance or fluorescence spectroscopy can also reveal details about, e.g., micellar configurations. Such, the combination of macroscopic and local methods in general can lead to a rather thorough understanding of thermoresponsive polymers.

We have previously shown that spin probing techniques in electron paramagnetic resonance (EPR) spectroscopy can deliver interesting and novel insights into local, static and dynamic properties of thermoresponsive systems.²⁷⁻³² This is mainly due to the intrinsically local character of EPR spectroscopy, which gives rise to sensitivity also to rather small nanoscale inhomogeneities in polymer solutions.³³⁻³⁶ Thus, conventional continuous wave (CW) EPR can detect nanoscopic apolar cavities, stemming from unimer collapse (coil-to-globule transition) or from aggregates of only a small number of polymer chains, even when these cavities are too small or too sparse to be detected by macroscopic methods (e.g. turbidity measurements). The observation of such small apolar cavities in aqueous media is possible, because small amounts of spin probe molecules of varying amphiphilicity/hydrophobicity can be spectrally discerned in dependence of their respective environment and thereby report on the occurrence of polar and apolar regions alike (see Figure 1). We have observed that such detected inhomogeneities are either *dynamic* or *static* on EPR time scales. In this context, the term *dynamic inhomogeneities* is a summary for the case of spin probe guest molecules exchanging between the medium (or polar, water-swollen regions) and the apolar cavities constituted of a collapsed polymer on a time scale of several nanoseconds ($\omega_{\text{exchange}} > 10^7 \text{ s}^{-1}$) only in a certain, restricted temperature range.^{28,29} (Note that in the following we refer to water-

depleted and polymer rich regions as apolar, since we observed that most of these regions feature a polarity comparable to chloroform. The aqueous phase is denoted as a polar region. To avoid confusion, chemical structures will be referred to as hydrophobic and hydrophilic in order to denote their polarity.) Such, dynamic inhomogeneities indicate significant morphological changes of collapsed polymer domains with temperature. In contrast, inhomogeneities that do not feature such a dynamic guest-exchange, can be viewed as being *static*, since they do not feature changes that are strong enough to influence the way of probe incorporation.^{27,29,37} While in principle fluorescence spectroscopy can yield information about the constitution of the environment of a probe molecule and about its nanoscale confinement similar to the information derivable from EPR spectroscopy, fluorescent probes are mostly constituted of rather large and rigid organic structures, which makes it difficult for them to detect inhomogeneities on length-scales of only a few nanometers.³⁸ EPR spin-probes like TEMPO (2,2,6,6-Tetramethylpiperidin-1-yl)oxyl) are small compared to most fluorescent probes and hence do not suffer this drawback. Furthermore, CW EPR features a very favorable timescale. For an experimental method to be sensitive to a certain process, the observation timescale must be faster than the timescale of the observed process³⁹ and rotational motions of a probe molecule on a sub-nanosecond timescale can easily be quantified by means of CW EPR. Such, also effects of only minor sterical confinement due to small apolar cavities that do not influence a probe's rotational mobility strongly can be observed. Fluorescence probing techniques are in the majority of cases sensitive for the nanosecond timescale only.⁴⁰ Yet note that e.g. for the exact elucidation of larger micellar configurations fluorescence spectroscopy is likely to be superior to CW EPR.⁴¹

However, recently simple CW EPR gave insights into the behavior of several different responsive polymer systems and their correlated inhomogeneities.⁴²⁻⁴⁵ Going beyond the description of individual case studies, we here aim at relating polymer constitution to molecular and nanoscale collapse properties.⁴⁶ We have selectively chosen responsive linear polymer systems based on ethylene oxide (EO) / *N,N*-diethyl glycidyl amine (DEGA) copolymers¹⁴ as well as linear and hyperbranched propylene oxide / glycidol copolymers^{13,15} to systematically vary the constitutional and topological properties of the thermoresponsive polymers (hyperbranched vs. linear / block vs. random copolymer with varying hydrophobicity of the comonomers). This allows us to elucidate how the thermally induced polymer collapse mechanisms depend on polymer topology and the chemical nature of the monomers. As is shown below, the respective collapse mechanisms, in return, determine the occurrence of dynamic or static nanoscale inhomogeneities.^{28,29} Hence, the recent developments in functional PEO, PPO and polyglycidol synthesis, which allow for specific manipulation of constitutional and topological characteristics of thermoresponsive systems, make these systems ideally suited for a systematic EPR study.^{13-15,19}

In the following, experimental results gained from spin probing ethylene oxide (EO)/ *N,N*-diethyl glycidyl amine (DEGA)^{14,47} copolymers and propylene oxide (PO) / glycidol (G)^{13,15} copolymers are presented first. We utilize the fact that the amphiphilic spin probe TEMPO ((2,2,6,6-tetramethylpiperidin-1-yl)oxyl) has a favorable partitioning coefficient between polar and apolar domains (between water and polystyrene of approx. 10^2 , see Ref. ⁴⁸) and hence detects apolar polymer regions when they occur (see Figure 1). Subsequently we discuss the collapse mechanisms of the different polymers, explaining the experimentally observed EPR data. Making use of all available EPR data, including also previously published work on poly(*N*-isopropylacrylamide) (PNIPAM) gels, dendronized polymers and Pluronic block copolymers,²⁷⁻³⁰ we develop relations between polymer constitution, collapse mechanism, aggregate properties and the characteristics of interaction with small amphiphiles. Given the manifold approaches to use responsive polymers for sensing or for the delivery of a large variety of molecules, in particular small to intermediate-sized, often amphiphilic drug molecules,⁴⁹⁻⁵¹ these *structure-function correlations* derived from our small amphiphilic spin probes may actually help identifying an “appropriate” design for the desired release or hosting property of polymer-based host-guest systems.

Results

Spin probing poly(propylene oxide)-polyglycidol (PPO-co-PG) copolymers

In Figure 2c) the high-field line of TEMPO in 1 wt% solutions of linear poly(propylene oxide-co-glycidol) random copolymers, **PPO-co-PG** (Figure 2a)) and their hyperbranched analogues **hbPPO-co-PG** (Figure 2b))¹³⁻¹⁵ is depicted as a function of temperature for varying glycidol comonomer content. We will focus on the TEMPO high-field transition throughout this article, since it contains all information necessary for the interpretation of all spectra presented here. Further, we denote a spectral species A that stems from TEMPO in an aqueous, polar environment and a species B that stems from TEMPO in a more apolar environment, e.g., a polymer micelle (see Figure 1). The Supporting Information contains a detailed description of the TEMPO spin-probing approach.

As can be observed in Figure 2c) and d), **PPO-co-PG** as well as **hbPPO-co-PG** lead to the occurrence of a spectral component in an apolar environment (i.e. a TEMPO species in an apolar environment) B at $T > 30$ °C for all polymer constitutions, as can be deduced from the hyperfine coupling constant of species B. The hyperfine coupling constant between the unpaired electron and the nitrogen nucleus of TEMPO, A_{iso} , of species B of $45.2 \pm 0.1 - 45.5 \pm 0.1$ MHz can be compared

with A_{iso} of TEMPO in chloroform and hence indicates water-depleted regions constituted primarily of collapsed polymer strands.^{39,40}

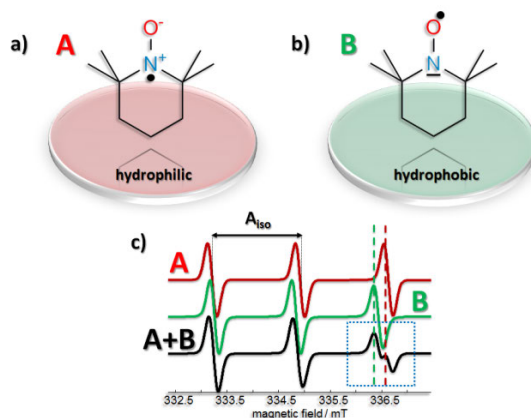


Figure 1. Origin of the spectral components of CW EPR spectra of TEMPO in a (nano-)phase separated system. a) Mesomeric structure of TEMPO in a polar environment. The unpaired electron is predominantly localized at the nitrogen atom. b) Mesomeric structure of TEMPO in an apolar environment. The unpaired electron is predominantly localized at the oxygen atom. Both cases indicate higher (a) or lower (b) unpaired electron spin density on the nitrogen c) Spectral components: stemming from TEMPO in a polar environment (A; red); stemming from TEMPO in an apolar environment (B; green); combined, bimodal spectrum (A+B; black). The dashed lines indicate the differences between the high-field transitions of species A and B. A_{iso} approximately corresponds to the separation of the zero crossings of two lines of a TEMPO CW EPR spectrum. The blue marked region of the spectrum (high-field transition) shows the most prominent effects, and hence we focus on this part of any CW EPR spectrum throughout this article.

Note that from the A_{iso} -values one can deduce that there are apolar, polymer-rich domains in the solution, since in an otherwise aqueous solution only a locally high density of polymer segments can form such apolar environments. Hence, the CW EPR data provide exclusive evidence for an increase of local polymer density through either aggregation or compaction of polymer strands (the latter is the predominant factor for **PPO-co-PG** as well as **hbPPO-co-PG**, as will be shown below). No other evidence is needed. The high-field line corresponding to species B does not shift its field position with temperature and thus can be correlated with a *static inhomogeneity*.

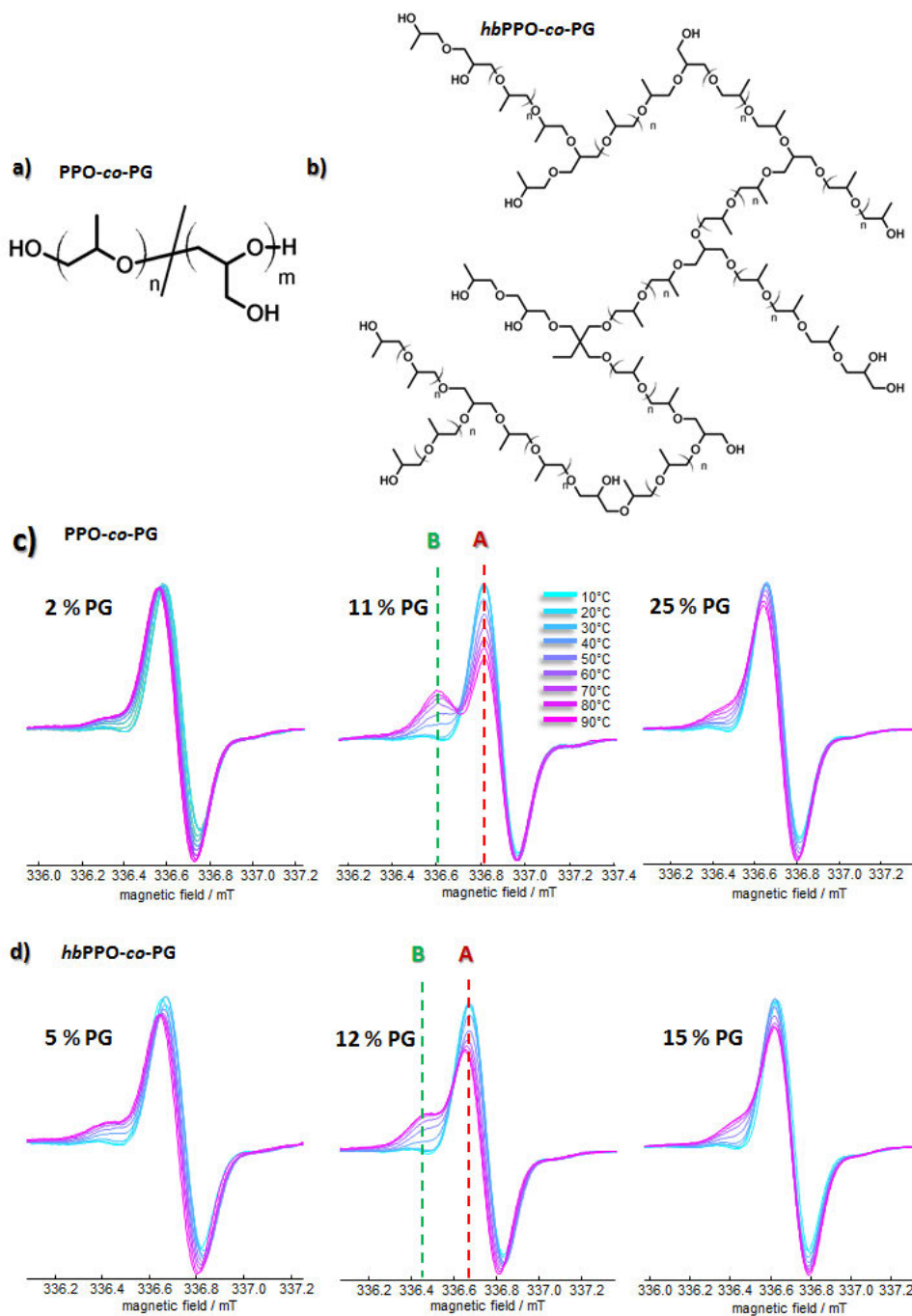


Figure 2. a) Molecular structure of **PPO-co-PG**. b) Molecular structure of **hbPPO-co-PG**. c) High-field lines from CW-EPR spectra of 1 wt% aqueous solutions of the polymers depicted in a) and 0.2 mM TEMPO. d) High-field lines from CW EPR spectra of 1 wt% aqueous solutions of the polymers depicted in b) and 0.2 mM TEMPO. For the complete spectra and for simulations see the Supporting Information. A_{iso} -values of species B are $45.2 \pm 0.1 \rightarrow 45.5 \pm 0.1$ MHz, depending on the glycidol content for both linear and hyperbranched cases. The red and green dashed lines indicate the constant field positions of the high-field transitions of the TEMPO species A and B.

This means that the TEMPO molecules do not diffuse in / out of polar and apolar regions (on EPR timescales) at any temperature, which would lead to averaging of the lines corresponding to species A and B and consequently to a temperature-dependent shift in A_{iso} , as will be shown in the next section. Contrary, the A_{iso} -values are equal within the error bounds at any temperature for a particular polymer constitution of **PPO-co-PG** and **hbPPO-co-PG**.

Yet, the spectral intensity of species B strongly depends on the glycidol content of the polymers. The maximum spectral fraction of species B, χ_B , is observed at 11% glycidol content for the linear polymers and at 12% for the hyperbranched polymers. Note that we varied the glycidol content in large steps of 5-15%, such that the maximum percentage of TEMPO uptake might in fact deviate from 11-12%. Above 25% and below 2% glycidol no significant contribution of a spectral component B could be observed in both cases, linear and hyperbranched polymers. In Figure 3 a) and b), the spectral fraction of the TEMPO species A, χ_A , is plotted versus the temperature for different fractions of glycidol (the full spectrum S_{exp} is simulated as a weighted sum of the individual species A and B: $S_{\text{exp}} = \chi_A S_A + (1 - \chi_A) S_B$.²⁴) Note that in order to yield feasible partitioning coefficients one actually should compare the fraction of TEMPO in solutions of the homo polymers PPO and PG and not the fraction of TEMPO in water with the fraction of TEMPO species B, since the hosting parameters between polymers and guest compounds in water are influenced by the hydrophobicity of the guests. However, for homo PG one only observes a TEMPO species that equals TEMPO in neat water and homo PPO is generally not soluble in water, only polymers of very low molecular weight are.⁵⁴ From the reduced number of spin probes in polar surroundings (χ_A) at a given temperature, concentration and percentage of glycidol in the case of **PPO-co-PG** compared to **hbPPO-co-PG**, it further follows that the linear polymers incorporate more TEMPO molecules than their hyperbranched analogues. For both types of molecular architectures, the first occurrence of the species B, indicating the onset of the collapse, is located between 30 °C and 40 °C. Remarkably, turbidity measurements of the same polymer reveal cloud points differing significantly from 30 °C – 40 °C (see Figure 3c)). Depending on the relative content of glycidol comonomers (i. e., glycerol building units), the “macroscopic” cloud point can shift from 20 °C to 80 °C. In Figure 3e) all the different cloud points are plotted versus the glycidol content for both types of architecture. To avoid confusion in the following we refer to the temperature of first occurrence of species B, which is detected by means of spin-probing EPR, as $T_{\text{c,EPR}}$. The cloud point, as detected by turbidity measurements is denoted as T_{c} . $T_{\text{c,EPR}}$ and T_{c} should clearly be discerned, since only $T_{\text{c,EPR}}$ reports on the occurrence of polymer-rich, apolar cavities in a system. T_{c} merely reports on the formation of large structures that can scatter incident light.

Spin probing poly(ethylene oxide)-*co*-poly(*N,N*-diethyl glycidyl amine) (PEO-*co*-PDEGA) copolymers

In contrast to **PPO-*co*-PG** and **hbPPO-*co*-PG**, polymer systems containing ethylene oxide and *N,N*-diethyl glycidyl amine repeating units (PEO-*co*-PDEGA) exhibit a significant dependence of A_{iso} on the polymer constitution. The EPR data and the hyperfine coupling constants gained from spin probing linear gradient polymers, **PEO-*co*-PDEGA**, and linear diblock copolymers, **PEO-*block*-PDEGA**, with different DEGA contents are presented in Figure 4 and 5. In this context ‘gradient’ means that the probability to find a DEGA monomer in **PEO-*co*-PDEGA** is not completely random, but changes gradually as one goes from one end of the chain to the other.^{14,47}

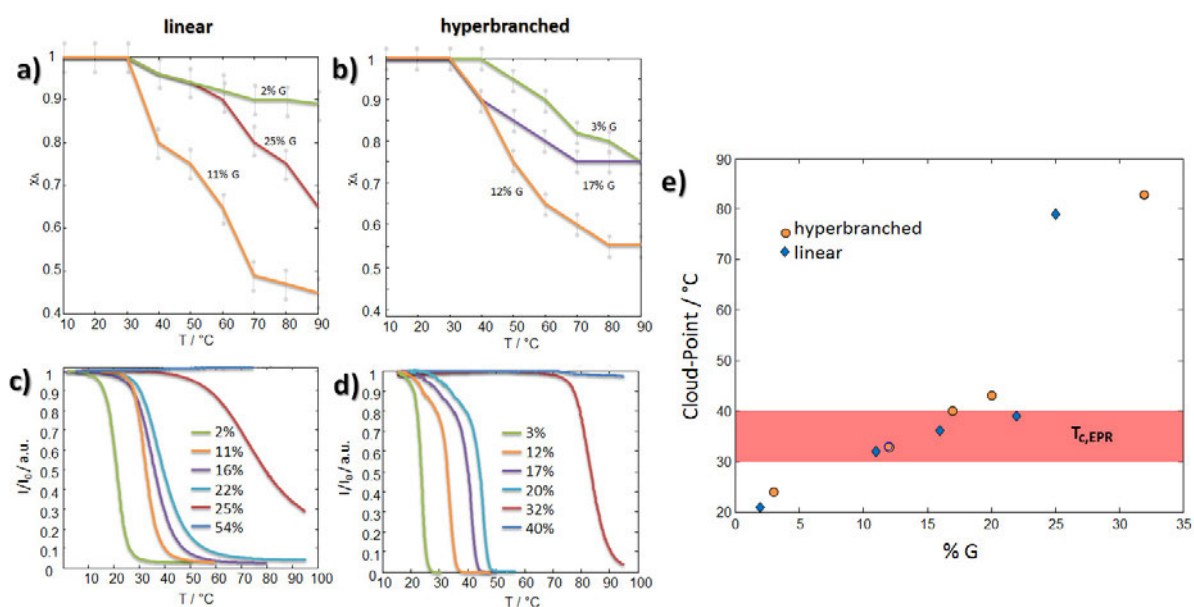


Figure 3. a) Temperature dependence of χ_A for **PPO-*co*-PG** with 2% (green), 11% (orange) and 25% (red) glycidol. b) Temperature dependence of χ_A for **hbPPO-*co*-PG** with 3% (green), 12% (orange) and 17% (violet) glycidol. c) Turbidity curves for **PPO-*co*-PG** with different amounts of glycidol. d) Turbidity curves for **hbPPO-*co*-PG** with different amounts of glycidol. e) Turbidity-derived cloud points, T_c , of linear (blue diamonds) and hyperbranched (yellow circles) PPO-*co*-PG plotted versus the glycidol content. The red bar indicates the narrow temperature-region, in which all the EPR-derived temperatures of first occurrence of species B, $T_{c,EPR}$, are located.

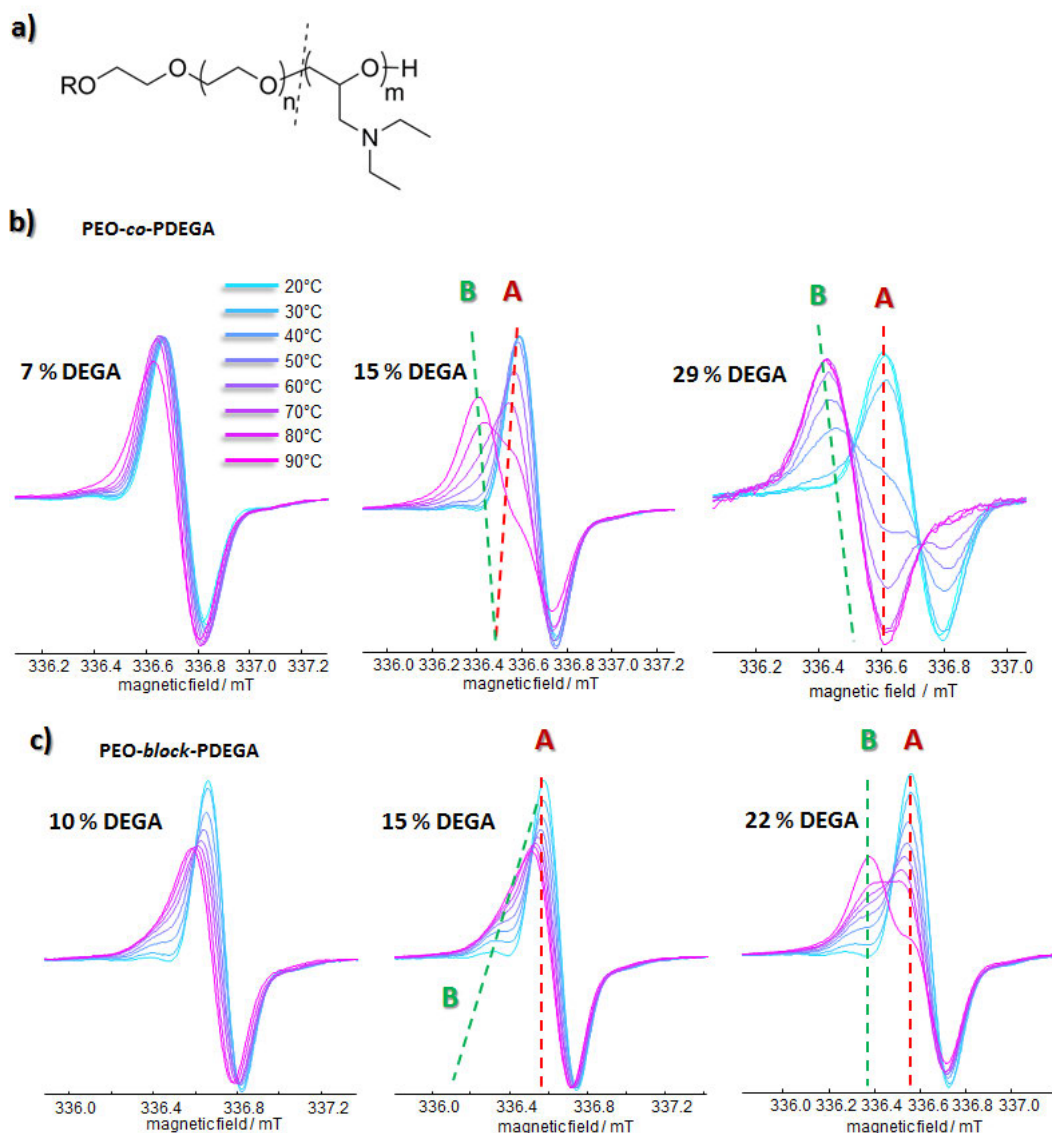


Figure 4. a) Molecular structure of PEO-co-PDEGA. b) High-field transition of TEMPO in 5 wt% aqueous solutions of gradient **PEO-co-PDEGA**. In the case of the copolymer with 7% DEGA, no significant temperature-dependent effects can be observed, yet a dynamic inhomogeneity at a DEGA content $\geq 15\%$ occurs. c) High-field transition of TEMPO in a 5 wt% aqueous solution of **PEO-block-PDEGA** with different percentages of DEGA. A DEGA content $\leq 15\%$ leads to the occurrence of dynamic inhomogeneities. At a DEGA content of 22% a static inhomogeneity occurs. The red and green dashed lines serve as a guide to the eye for following the temperature-dependent shift of the maximum of the high-field lines of species A and B. The exact positions of these lines (i.e. zero-crossings) are best extracted from spectral simulations (see the Supporting Information), since strong overlap makes a direct observation difficult, especially for 15% DEGA. However, following the peak positions of species B in the above graphic yields qualitative information about the development of A_{iso} . (Increasing A_{iso} -values lead to a high-field shift, decreasing A_{iso} -values to the opposite.)

For the slightly gradient copolymer with 15% DEGA (Figure 4b)), the hydrophobic TEMPO species B exhibits A_{iso} values that decrease with rising temperature, hence, species B senses increasing apolarity of the polymer-rich regions with increasing temperature. At 80 °C, A_{iso} reaches a constant value of 45.5 ± 0.1 MHz. In general, there are two possible explanations for a temperature-dependent shift of A_{iso} . Either the polarity of the direct environment of the spin-probes changes, likely due to conformational changes of polymer-rich regions, or the exchange rate (between medium and apolar cavity) of the spin probes becomes slower (decreasing A_{iso}) or faster (increasing A_{iso}). As will be shown in the Discussion section, the decrease in A_{iso} of species B for **PEO-co-PDEGA**-based systems can be traced back to a diminishing TEMPO exchange between apolar cavities and the surrounding medium as the temperature rises.

As will be shown in the Discussion section, the decrease in A_{iso} of species B for **PEO-co-PDEGA**-based systems can be traced back to a diminishing TEMPO exchange between apolar cavities and the surrounding medium as the temperature rises. Hence, this system features a *dynamic inhomogeneity*: probe exchange at temperatures slightly above the initial collapse of polymer segments, but no exchange at high temperatures near 90 °C, as can be judged from the constant A_{iso} between 80 °C and 90 °C.

At significantly lower DEGA contents ($\leq 7\%$ DEGA) a considerable formation of apolar regions, as a consequence of the high ratio of relatively (compared to PDEGA) hydrophilic PEO and weak hydrophobic interactions, could not be observed through our amphiphilic⁴⁸ tracer molecules, as can be seen from Figure 4 b). Turbidity data show an aggregation of **PEO-co-PDEGA** with $\leq 7\%$ DEGA at approx. 80 °C, where the CW EPR data also at least indicate a jump-wise reduction in A_{iso} . Note that the fact that one does not observe any significant apolar cavities by means of TEMPO spin-probing should not to be confused with the non-existence of such cavities. This only implies that the interaction between TEMPO and cavities **PEO-co-PDEGA** is not strong enough to influence the CW EPR spectra significantly, e.g. because the cavities contain a lot of residual water. One should nonetheless keep in mind, too, that an increasing turbidity of a solution does not necessarily coincide with a compaction of polymers.

For **PEO-block-PDEGA** a DEGA content of 10 and 15% leads to increasing hyperfine coupling constants for species B with increasing temperature, indicating that the probes experience a more polar environment at higher temperatures. In contrast, a DEGA block-content in **PEO-block-PDEGA** of 22% leads to the occurrence of static inhomogeneities as they are detected in the cases of **PPO-co-PG** and **hbPPO-co-PG**. Thus, small hydrophobic PDEGA-blocks in **PEO-block-PDEGA** can be correlated with *dynamic inhomogeneities* that feature guest exchange at higher temperatures, while large

hydrophobic PDEGA-blocks can be correlated with the complete suppression of guest exchange on EPR timescales.

Note that the cloud points, derived from turbidity measurements, as well as $T_{C,EPR}$, derived from CW EPR, are both independent of the concentrations of the samples in the range from 5 mg/mL to 20 mg/mL and can hence be directly compared in any case.⁴⁷ (CW EPR measurements are frequently carried out at rather high concentrations to increase the signal intensity.)

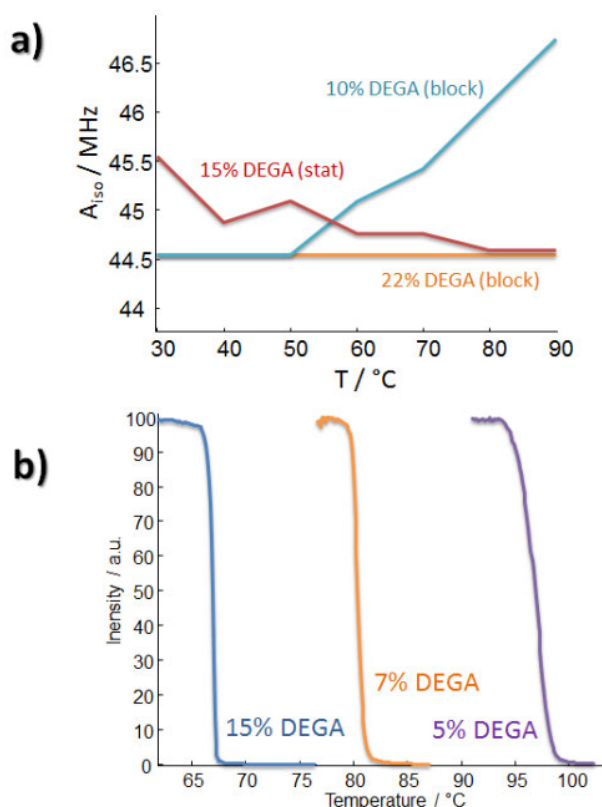


Figure 5. a) Temperature-dependence of TEMPO hyperfine splitting values of species B in different PEO-PDEGA copolymers. b) Turbidity data of **PEO-co-PDEGA** solutions with variable amount of DEGA.

Discussion

We now address the correlation of the polymer structure and architecture with the polymers' collapse mechanisms and three fundamental nanoscopic host-guest interaction schemes during temperature-induced collapses of thermoresponsive polymers and their aggregates (static inhomogeneity and dynamic inhomogeneity featuring exchange at high temperatures or at

temperatures slightly above the initial collapse of the polymers). A general point should be considered first, though: Spin probing with TEMPO yields indirect information about nanoscopic apolar and polar regions formed during collapse or the aggregation of polymers. However, it has been shown before for other classes of materials that *macroscopically*, i.e. by means of DLS etc., detected cloud points can differ significantly at a given concentration from EPR-derived $T_{c,EPR}$ (have in mind that the initial collapse of polymer segments, i.e. the temperature at which a TEMPO species B first occurs, is denoted as $T_{c,EPR}$), since the macroscopic aggregation or collapse transition of several polymer molecules does not necessarily coincide with the local occurrence of apolar, water-depleted regions, to which EPR measurements with TEMPO as spin probe are sensitive. Such nanoscopic apolar cavities often constitute only the onset of a macroscopic phase transition.²⁷⁻²⁹ Therefore, it is not surprising that the cloud points detected by turbidity measurements differ from the $T_{c,EPR}$ for **PEO-co-PDEGA**, **PPO-co-PG** and **hbPPO-co-PG** as observable in Figure 3 and 5. Interestingly though, the $T_{c,EPR}$ s are all located in the narrow temperature interval between 30 °C and 40 °C, while the turbidity-derived cloud points, T_c , range from approx. 20 °C to 80 °C for **PPO-co-PG** and **hbPPO-co-PG**, depending on the glycidol content, and for **PEO-co-PDEGA** T_c varies from 55 °C to 97 °C, depending on the DEGA content (see Figure 3e) and Table 1; note that as a consequence of intermolecular aggregation at $T_{c,EPR}$, as will be shown below, for PPO-co-PG slight changes in turbidity are observable between 30 °C and 40 °C, i.e. below T_c). This discrepancy between $T_{c,EPR}$ and T_c can satisfactorily be explained when taking into account that spin probe CW EPR is sensitive to *local* apolar cavities and the fact that the polymer classes investigated here (PPO-co-PG and PEO-co-PDEGA) locally, on the level of monomeric units and below, do not differ too much among each other although their overall topology or “randomness” might differ significantly. (E.g., PPO-co-PG polymers all feature linear segments of PPO of random length, while their overall topology might be linear or hyperbranched.) As a rule of thumb, one can state that the smaller and more hydrophobic a spin-probe, the more sensitive it is to smallest inhomogeneities in polymer solutions. Hence, the small and amphiphilic TEMPO leads to most poignant differences between $T_{c,EPR}$ and T_c , while e.g. frequently used, large spin-labeled stearic acids do not lead to such drastic differences, since they enter collapsed domains only after these have grown to a certain size.²⁹ Thus, deviations of $T_{c,EPR}$ from T_c are likely: the local collapse/aggregation of polymer segments as detected by CW EPR is only dependent on the local (i.e. a few nanometers) molecular structure, which – as explained above – is very similar for a particular set of comonomers, while the macroscopically detected collapse is also dependent on the overall topology of a polymer, which might vary. This conclusion is further substantiated by the observation that $T_{c,EPR}$ s do not depend on the concentration of the polymers.²⁹

Table 1. Turbidimetry-derived cloud points (T_c) of the different copolymers under investigation.

PPO- <i>co</i> -PG	$T_c/^\circ\text{C}$	hbPPO- <i>co</i> -PG	$T_c/^\circ\text{C}$	PEO- <i>co</i> -PDEGA	$T_c/^\circ\text{C}$	PEO- <i>b</i> -PDEGA	$T_c/^\circ\text{C}$
2% G	21	3% G	24	29% DEGA	55	22% DEGA	80
11% G	32	12% G	33	15% DEGA	67	15% DEGA	100
16% G	36	17% G	40	7% DEGA	81	10% DEGA	-
22% G	39	20% G	43	5% DEGA	97		
25% G	79	32% G	83				

Hence, it is not unexpected that the general tendency of T_c rising with increasing hydrophilicity of the copolymers (Figure 3e) and Table 1) is not reproduced by the CW EPR results. The rise of T_c with the mean hydrophilicity of a polymer can be attributed to the fact that turbidity-measurements are sensitive to pronounced aggregation of polymer strands and the formation of large supramolecular assemblies, which lead to light scattering: the aggregation propensity of macromolecules in aqueous solution of course is higher for polymers with larger fractions of hydrophobic comonomers. As a consequence, more hydrophobic copolymers aggregate at lower temperatures in order to minimize solvent exposure, as hydrogen-bonds between water and the alkylene-oxide units become weaker. Hence, the mean hydrophobicity of an amphiphilic copolymer is directly related to its cloud point, T_c . Turbidimetry detects an abrupt decrease of transmitted light intensity, as can be seen in Figure 3 and 5, while EPR detects a slowly and steadily increasing mole fraction of incorporated TEMPO probes in collapsed/aggregated PPO-*co*-PG and PEO-*co*-PDEGA polymers. This discrepancy can also be explained by the sensitivity of turbidimetry to the aggregation of polymers: Once the polymers reach the cloud point the solvent becomes poor for all the chains and together they form large aggregates. However, it has been shown that also a few nanoscopic cross-linking points between different chains are sufficient for a macroscopic phase-transition, although large segments of the chains might still be swollen.²⁸ The complete dehydration process, as observed through A_{iso} of all the monomers might therefore spread over a wide temperature range. On the one hand, an ongoing dehydration of the polymers does not influence the turbidity of a solution, if a large proportion of the chains is already aggregated. On the other hand, the propensity for incorporation of TEMPO rises with an increasing fraction of dehydrated polymer strands. Yet, note that the transmitted intensity of the PPO-*co*-PG polymer containing solutions decreases slightly already at temperatures below the drastic turbidity-increase, which indicates aggregation of several molecules below the cloud point and a slight deviation from step-like behavior of the macroscopic

phase-transition. In general one cannot deduce the shrinkage or compaction of a polymer from mere turbidity data. However, for the present case the observation of TEMPO enriched in apolar cavities is an unambiguous indication that the polymers are subject to compaction, since in an aqueous solution an apolar environment can only be based on a locally high concentration of polymer chains either through aggregation or micellization. The lack of correlation between turbidity data and polymer shrinkage is also experimentally reflected in the fact that for **PEO-block-PDEGA** with 10% DEGA does not become turbid while CW EPR clearly reports on the presence of apolar cavities in the polymer solution above $T_{c,EPR}$ (see Figure 4 and Table 1).

With this and the fact in mind that EPR yields information on local structural processes in polymers, we discuss in the following how the collapse mechanisms of the different polymers introduced in the Results section correlate with a particular type of nanoscale inhomogeneity and with the structural properties of a polymer.

Dynamic inhomogeneities as a consequence of a thermally induced two-step collapse mechanism of PEO-co-PDEGA

PEO-co-PDEGA with a DEGA content $\leq 7\%$ does not show any significant interaction with TEMPO, although turbidity data reveal a distinct cloud point (Figure 5b)). This can be understood taking into account that EO is, compared to DEGA, a rather hydrophilic comonomer, thus collapsed or aggregated structures constituted primarily of PEO are likely to contain a larger amount of water and are of lower density than aggregates of **PEO-co-PDEGA** with higher DEGA content. Thus, the local polarity inside a structure of collapsed/aggregated **PEO-co-PDEGA** becomes more and more similar to the polarity of the medium as the DEGA content decreases. Consequently, spin probes can diffuse in and out of **PEO-co-PDEGA** aggregates with a DEGA content of only $\leq 7\%$ fast, and hydrophobic interactions are weak, such that a shift in A_{iso} is not observable by CW EPR. This explanation is substantiated by the fact that increasing the DEGA content and the expected increase in aggregate density and hydrophobicity leads to significant effects on the TEMPO probes, as it can be observed for systems containing **PEO-co-PDEGA** with $\geq 15\%$ PDEGA: The dynamic inhomogeneity correlated with this system (spin probe exchange at temperatures slightly above $T_{c,EPR}$, but no exchange at further elevated temperatures, as depicted in Figure 4b)) can be explained by two processes:^{28, 30, 31}

1. An ongoing dehydration of the apolar cavities, formed above $T_{c,EPR}$, leads to a steady decrease of the polarity of the probes' environment and hence to a decrease in A_{iso} of species B with increasing temperature, ever more separating the spectral components of the TEMPO species A and B.

2. When dynamic exchange of the spin probes takes place on fast EPR time scales (normally $< 10^{-8}$ s), one observes an intermediate spectral line, averaged between the lines of the “pure” species A and “pure” species B. With increasing temperature above $T_{c,EPR}$ the volume fraction of collapsed regions or the density of the formed aggregates (due to ongoing dehydration) increases and hence dynamic probe exchange between apolar and polar regions becomes less probable. Consequently, the averaging between the spectral components A and B diminishes with rising temperature and A_{iso} shifts less and less, until a “static” value (of the mere species B) is reached, when no spin probe exchanges take place anymore on EPR timescales.

Taking into account that DEGA is a rather hydrophobic comonomer (homo PDEGA is insoluble in water) and that **PEO-co-PDEGA** can consequently be regarded as an amphiphilic copolymer, one can further identify the process behind the dynamic inhomogeneity discussed here: Amphiphilic random copolymers composed of more hydrophilic (here EO is more hydrophilic than DEGA) and more hydrophobic (here DEGA is more hydrophobic than EO) monomers feature conformations in aqueous solution, in which the hydrophobic monomers cluster due to hydrophobic attraction,⁵⁵⁻⁵⁷ while PEO-rich polymer segments are swollen and reach out into the medium (water is a good solvent for the EO monomers, but a poor solvent for the DEGA monomers; see Figure 6a)). In fact several groups reported the observation of small (i.e. unimeric or with low aggregation number) micelles of amphiphilic random copolymers in which the hydrophobic monomers form the micellar core and hydrophilic patches the corona (mesoglobules like in Figure 6a) on the left).⁵⁸⁻⁶⁰ The formation of such micelles however is competitive to intermolecular aggregation. Frequently it is observed that an increase in concentration⁶¹ or of the hydrophobicity of the small micelles (e.g. because the initially hydrophilic monomers pass through a critical solution temperature⁸ or because of changes in the chemical nature of the comonomers⁶²) leads to large-scale aggregation of the small micelles⁶³ or to the fusion of the small micelles and the subsequent formation of large aggregates with only one large core.⁶⁴ Swanson and co-workers furthermore showed that thermoresponsive polymers that randomly incorporate hydrophobic comonomers form intramolecular aggregates below the transition temperature, while large-scale aggregation takes place above the transition temperature.⁸⁶⁵ However, from mere CW EPR and turbidity measurements one cannot deduce the actual morphology of the structures formed during the phase-transition of **PEO-co-PDEGA**. Yet, judging from what is known about amphiphilic random copolymers, as stated above, we assume that the phase-transition proceeds via the formation of small micelles/aggregates constituted of one or only a small number of polymer strands and the subsequent formation of larger structures through aggregation of the small micelles/aggregates themselves, since such two-step processes have been observed a lot of times for amphiphilic copolymers like **PEO-co-PDEGA**. Hence, despite the actual morphology of the aggregates, we assume a two-step mechanism for the temperature-induced

phase-transition of **PEO-co-PDEGA**. In Figure 6a) such a mechanism is schematically depicted. Yet note that it only represents one of different possible two-step mechanisms and should hence only be regarded as clearly arranged visualization of a two-step phase-transition of **PEO-co-PDEGA**. Yet, the formation of unimer micelles like depicted in Figure 6a) (left and center) is well-known for hydrophilic polymers that feature small hydrophobic moieties, distributed along the chain. E.g. Borisov and Halperin have reported and physically described structures like depicted in Figure 6a) on the left already over 15 years ago and showed that bridging effects between these micelles can lead to the formation of larger multimeric structures.⁶⁶ Zhang, Winnik and Wu could furthermore show that the transition from a random coil state to such a core-shell structure proceeds via the formation of ordered coils. In this structure the hydrophobic monomers are concentrated in the center of a premicellar conformation, yet the polymer is still swollen, such that the hydrophobic monomers do not strongly cluster.⁶⁷ However, both reports emphasize that the formation of unimer micelles is only possible at rather low concentrations and that at higher concentrations the probability of interchain association is high. Such the proposed mechanism sketched in Figure 6 might be incomplete for the present case, since the polymer concentration for CW EPR was 5 wt%. Probably the first step of the phase-transition of **PEO-co-PDEGA** is in part the association of a small number of polymer chains that constitute a small micelle (small enough to not influence the turbidity of the solution significantly), but not the collapse of unimers. This micellization may well be facilitated by the nature of copolymerization of gradient copolymers like **PEO-co-PDEGA**, as short patches along the chains with only or mainly hydrophobic monomeric units may exist. Such, already at room temperature **PEO-co-PDEGA** may exist in a state in which DEGA monomers are clustered or spatially close, surrounded by PEO (Figure 6a) left-hand side). With increasing temperature, the PEO segments collapse too to form dense globules of only a small number of polymer chains. At even higher temperatures these globules subsequently aggregate to form larger objects, since water becomes more and more a poor solvent for PEO. An ongoing growth of hydrophobic cavities accompanied by the dehydration of PEO residues with rising temperature would arise in this scenario, which explains the observed CW EPR spectra of **PEO-co-PDEGA**. Molecular dynamics (MD) can be used to extract valuable information on polymeric systems.⁶⁸ Our MD simulations support the assumed collapse mechanism, since simulated aggregates of **PEO-co-PDEGA** with 15% PDEGA at 90 °C are constituted of collapsed globular unimer objects, formed from formerly (at 45 °C) individually collapsed unimers (Figure 6b)). Note that the data gained from MD simulations are only supporting the assumption of a two-step mechanism since they reproduce the picture one can deduce from the literature. However, the simulations should not be regarded as basis for argumentation, since MD simulations of such polymeric systems are likely to become trapped in local energetic minima, depending on the initial constitution of the simulated system and other factors. (Details on the simulations can be found in the Supporting Information.)

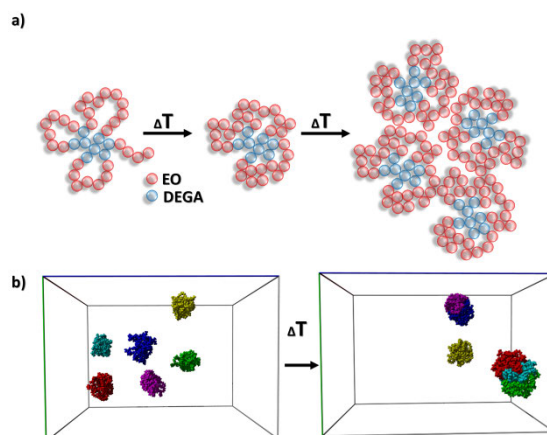


Figure 6. a) Proposed collapse mechanism for random **PEO-co-PDEGA** with a PDEGA content of 15% (EO: red, DEGA: blue). b) Aggregates of **PEO-co-PDEGA** with 15 % DEGA at 45 °C (left) and 90 °C (right), each after 4 ns of MD simulation. Different colors indicate different polymer strands. Supramolecular aggregates (right) are composed of spherical unimeric objects that occur already at lower temperatures (left).

Despite the exact micelle/aggregate morphology, the relatively sharp macroscopic phase-transition depicted in Figure 5b) should be attributed to the formation of large structures through aggregation of a large fraction of **PEO-co-PDEGA** since turbidity measurements are sensitive to the formation of large aggregates that scatter incident light (as explained above the cloud point is not necessarily correlated with the formation of apolar cavities, only with the formation of large structures). However, the complete collapse process of **PEO-co-PDEGA** covers a broader temperature range than the turbidity data indicate. This can be deduced from the CW EPR spectra that show significant changes in A_{iso} between 30°C and 90°C. Thus, $T_{c,EPR}$ should be attributed to the first step of the phase-transition in which apolar cavities are formed through micellization. The CW EPR data can hence be explained in accordance with the current knowledge about amphiphilic copolymers, which suggests a two-step collapse mechanism. The second explanation that was stated at the beginning of this section is in full agreement with a two-step phase transition: The probes can diffuse in and out of the small micelles/aggregates slightly above $T_{c,EPR}$ (first step: averaged A_{iso}), but cannot if the micelles/aggregates form much larger structures at higher temperatures above T_c (second step: constant A_{iso} of species B). Interestingly, dendronized polymers (so-called denpols: macromolecules that carry dendron side-groups at every repetition unit), which we have investigated earlier^{28,23,24} exhibit CW EPR spectra of TEMPO similar to the spectra for **PEO-co-PDEGA** with $\geq 15\%$ DEGA (Figure 4). This observation was ascribed to a complex collapse mechanism:²⁸ In the case of the thermoresponsive denpols, the dehydration of small parts of the polymer chains, subsequent

aggregation of several molecules and percolation of dehydrated regions. The macroscopically detected phase transition is very sharp in the cases of denpols, too. In both cases denpols and **PEO-co-PDEGA**, the observed spectra can be explained by an underlying two-step mechanism: Formation of small collapsed structures and aggregation upon temperature increase.

Static inhomogeneities in PEO-block-PDEGA explained by micellar configuration

For **PEO-block-PDEGA** with rather low PEO ($\leq 78\%$) content TEMPO spin probing reveals static inhomogeneities (i.e. no dynamic exchange at any temperature), while higher PEO contents ($\geq 85\%$) lead to dynamic inhomogeneities with static A_{iso} values of species B only at slightly elevated temperatures and increasing A_{iso} at higher temperatures. Two explanations could account for this apparently “reverse” behavior as compared to **PEO-co-PDEGA**. Either the aggregates’ conformations at higher temperature change and constitute a more polar environment for the spin probes or the spin probes in polymer-rich regions start to exchange fast with water-rich regions at higher temperatures and hence the A_{iso} values increase due to line-averaging. It is commonly observed for most thermoresponsive polymers⁶⁹⁻⁷¹ that rising temperatures lead to further deswelling of the polymer chains, which here would lead to a further decrease in hyperfine splitting. Hence, dynamic spin probe exchange is more likely an explanation for the increasing A_{iso} of TEMPO in systems containing **PEO-block-PDEGA** at temperatures above 50 °C.²⁹ One can refer to the common knowledge about amphiphilic block copolymers in order to understand the CW EPR spectra of **PEO-block-PDEGA**. Thermoresponsive amphiphilic diblock copolymers typically form micelles or other more complicated structures like lamellar with a core of hydrophobic monomers and a corona of hydrophilic monomers above T_c , where the hydrophobic blocks aggregate.⁷²⁻⁷⁴ In Figure 7a) the formation of a micelle is schematically depicted. Yet note that this sketch shall only aid to visualize the phase-transition of **PEO-block-PDEGA**, since by means of CW EPR and turbidimetry one cannot determine which morphology (micellar, lamellar, hexagonal etc.) the **PEO-block-PDEGA** aggregates actually have. Figure 7 shall demonstrate that, in aqueous solutions most known conformations of aggregates of amphiphilic diblock polymers consist of an inner segment that is constituted of the more hydrophobic blocks and an outer, solvent-exposed segment that consists of the more hydrophilic blocks. This should be kept in mind, although for the sake of simplicity we will refer to micelles of **PEO-block-PDEGA** in the following. Such, likely **PEO-block-PDEGA** with low PDEGA content leads to smaller micellar cores than **PEO-block-PDEGA** with high PDEGA content (Figure 7). These smaller cores, composed of DEGA blocks of **PEO-block-PDEGA** with a DEGA content $\leq 15\%$ consequently are also likely to have a lower density than cores of micelles of **PEO-block-PDEGA** with higher PDEGA content. Note that this phenomenon has been observed before for Pluronic block

copolymers.²⁹ The fact that one cannot observe any T_c for **PEO-block-PDEGA** with 10% DEGA, but a clear $T_{c,EPR}$, as well as a drastic difference between T_c and $T_{c,EPR}$ for 15% and 22% DEGA, furthermore indicates that the formed micelles are in general rather small (i.e. not large enough to influence the solution turbidity at $T_{c,EPR}$), substantiating the assumption of small micellar cores at low DEGA content and the notion of a nanoscale process. Small micellar cores give rise to exchange of TEMPO between the two environments at higher temperatures. With increasing thermal energy the translational displacement of the spin probes, $x_T = (6D_T\tau_T)^{1/2}$ with $D_T = kT/6\pi\eta R_H$,⁷⁵ (D_T is the translational diffusion coefficient and τ_T the characteristic diffusion time, all other abbreviations have their usual meaning.) becomes large enough for TEMPO to diffuse in and out of a small micelle. In contrast, high percentages of more hydrophobic comonomers (here $\geq 22\%$ DEGA) lead to denser and larger micelles¹⁰ and consequently prevent spin probe exchange through reduction of the diffusional freedom of TEMPO and a large distance from the micellar core to the medium. The values for x_T for different amounts of DEGA further indicate the correctness of this hypothesis: We calculated that the translational displacement is $x_T \approx 9$ nm for **PEO-block-PDEGA** with 22% DEGA and $x_T \approx 17$ nm for 10% DEGA at 80°C (for details on the calculation see the Supporting Information). Molecular dynamics simulations further support our explanation (Figure 7b)). At elevated temperature (90 °C), on average 2845.5 inter-chain contacts per chain are found for **PEO-block-PDEGA** with 10% DEGA and 3139.3 for 22% DEGA (at similar overall weight fractions). Assuming inter-chain contacts to be a measure for the density of a micelle, one could state that a micelle composed of only 10% DEGA actually is not as dense as a micelle composed of 22% DEGA. It should be noted that the simulations merely further support the picture we deduced above from other experimental sources, but are by no means a stand-alone basis for argumentation.

A somewhat similar temperature-dependent behavior has already been observed in aqueous solutions for some PEO-PPO-PEO (Pluronic) triblock copolymers.²⁹ Thus, it is likely that it is the block structure of Pluronics and of **PEO-block-PDEGA** and the consequently - compared to random copolymers - promoted ability to form micellar aggregates (or more complex structures as explained above) with the hydrophobic blocks located primarily in their center that leads to the occurrence of static inhomogeneities at low content of hydrophilic comonomers and to the occurrence of dynamic inhomogeneities at high content of hydrophilic comonomers. Such, the volume fraction of the hydrophobic blocks in the core of a micelle, constituted of a thermoresponsive polymer above the critical temperature, influences the density and size of formed micelles¹⁷ and consequently their ability to incorporate small amphiphiles like TEMPO.⁴⁸ In contrast, corresponding random copolymers with similar composition are likely to lead to collapse mechanisms as described for **PEO-co-PDEGA** and hence would yield dynamic inhomogeneities with probe exchange already slightly above $T_{c,EPR}$.

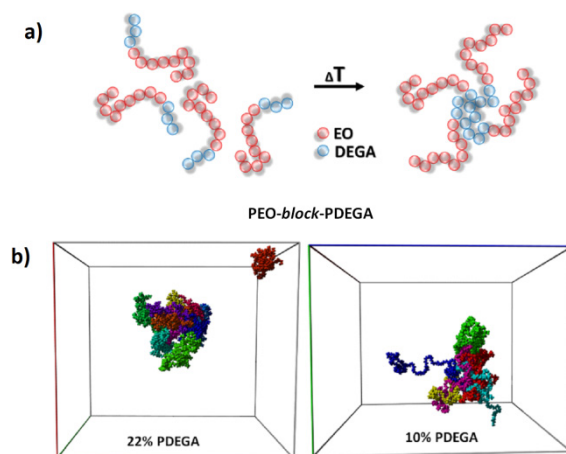


Figure 7. a) Formation of **PEO-*block*-PDEGA** micelles. The DEGA blocks (blue) are located in the micellar core. The PEO blocks (red) constitute the corona. b) Molecular dynamics simulations of micelles formed by **PEO-*block*-PDEGA** at 90°C with different DEGA content. The colors indicate different polymer chains.

Static inhomogeneities as a consequence of aggregation of **PPO-*co*-PG** and **hbPPO-*co*-PG**

In pronounced contrast to DEGA-containing systems, spin probing with TEMPO in aqueous solutions of **PPO-*co*-PG** and **hbPPO-*co*-PG** does not lead to the detection of dynamic inhomogeneities. On the contrary, A_{iso} -values remain constant (static inhomogeneities) at any temperature and comonomer ratio, which indicates that no significant changes on length scales of a few nanometers (the direct environment of TEMPO) take place in aggregates of PPO-*co*-PG. Interestingly, while A_{iso} does not change, the maximum of the mole fraction of the spectral species B, χ_{B} , varies significantly from 0 to ~ 0.6 , depending on the glycidol-content of **PPO-*co*-PG** and **hbPPO-*co*-PG**. We observe the maximum at 11% glycidol content for the linear polymers and at 12% for the hyperbranched polymers (Figure 3a) and b)). However, from the turbidity data shown in Figure 3c) and d) one can deduce that macroscopic aggregation takes place for all copolymers with a glycidol content $\leq 25\%$, with a steadily increasing tendency to aggregate earlier, as the glycidol content decreases. On the contrary we observe that χ_{B} decreases strongly at any given temperature if the glycidol content deviates from approx. 11-12%. (As stated in the Results section, we varied the glycidol content in steps of 5-15%, such the “real” maximum of χ_{B} might differ from 11-12%) Thus, it can be concluded that TEMPO does not equally penetrate all formed supramolecular aggregates present in solution. TEMPO is more and more likely to stay in the aqueous phase when the glycidol content deviates from 11-12% (in both cases: linear and hyperbranched PPO-*co*-PG copolymers).

Judging from the turbidity and the EPR data a likely explanation for this phenomenon is the following:

A) At low glycidol contents (below 11%) the aggregates are too dense to be penetrated by the TEMPO spin probes for two reasons: 1. With increasing glycidol content, the A_{iso} -values of the hydrophobically enclosed probes increase slightly, yet significantly (from 45.2 ± 0.1 MHz \rightarrow 45.5 ± 0.1 MHz), accounting for a higher water content of the aggregates (entrapped by glycidol monomers) at higher glycidol amounts and consequently for a lower polymer density. 2. CW EPR on **PPO-co-PG** with 16-doxyl stearic acid (16-DSA), a more hydrophobic spin-probe than TEMPO, revealed that these spin-labeled fatty acids are taken up by apolar cavities even when TEMPO stays primarily in the water-rich region, because of stronger hydrophobic interactions between DSA and the polymers. (See the Supporting Information.)

B) Above 12% glycidol content, the polymers' tendency to aggregate is low (as can be deduced from the turbidity measurements in Figure 3), thus the formed aggregates might be too loosely packed and too small to act as efficient hydrophobic hosts. The density of the formed aggregates at high glycidol content might also be too low for the TEMPO probes to interact strongly with hydrophobic comonomers of PPO-co-PG upon diffusion into aggregates, and consequently the effect on A_{iso} diminishes.

Concluding, there is an optimal content of glycidol for the incorporation of TEMPO in PPO-co-PG aggregates, since their molecular composition drastically influences their ability to interact with small guest molecules, as the PG content determines the aggregate density.

It is unexpected, though, that changing the polymer constitution from linear to hyperbranched (Figure 2a) and b)) does not lead to a fundamental change in the type of inhomogeneity, since the A_{iso} -values of incorporated spin probes in aggregates of **PPO-co-PG** and **hbPPO-co-PG** develops similarly with temperature in both cases. Also the maximum uptake was achieved with approx. 11-12% glycidol in both systems. However, the overall fraction of incorporated TEMPO molecules shrinks when changing the architecture from linear to hyperbranched (Figure 2 and 8). This observation can be explained when assuming that TEMPO is primarily enclosed into aggregates formed by several molecules (as will be shown below).

For the sake of simplicity we assume that unimers of **hbPPO-co-PG** are globular shaped (at least closer to globular than their linear analogues), although one cannot be completely sure about the exact topology.⁷⁶ Above T_c water becomes a poor solvent for PPO, but PPO-rich regions are not able to aggregate among themselves and to phase-separate completely to form the core of an aggregate as there are considerable structural constraints. In contrast, linear **PPO-co-PG** molecules can arrange

such that PPO-rich segments constitute an aggregate core and glycidol-rich segments build a rudimentary (the glycidol content is relatively low, $\leq 25\%$) layer on the surface of the hydrophobic aggregates, as depicted in Figure 8. Such, the volume-fraction of PPO-rich regions, marked red in Figure 8, should be higher for linear copolymer, compared to hyperbranched ones.

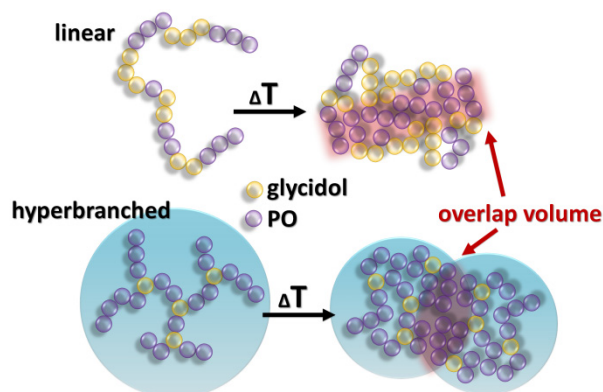


Figure 8. Proposed way of molecular aggregation of linear and hyperbranched PPO-co-PG thermoresponsive polymers (glycidol: yellow, propylene oxide: violet).

It is likely that aggregates of several molecules (as indicated in Figure 8), not mere collapsed PPO strands, are primarily constituting hydrophobic cavities in the case of PPO-co-PG, since CW EPR spectra of TEMPO in solutions of **PPO-co-PG** and in solutions of **hbPPO-co-PG** at a given glycidol content are very similar. If PPO-strand compaction (e.g. by coil-to-globule transition) were the primary mechanism behind the TEMPO incorporation the molecular architecture should lead to more pronounced differences in the CW EPR spectra. The exclusive occurrence of static inhomogeneities in systems containing PPO-co-PG can also be correlated with the slope of the turbidity curves in Figure 3. The turbidity data strongly suggest that the polymers aggregate already between 30 °C and 40 °C (although the drastic descent of transmitted intensity takes place at higher temperatures in many cases), i.e. in the same temperature range in which $T_{c,EPR}$ is located (Figure 3), since the transmitted light intensity decreases slightly already before T_c is reached. Above T_c the intensity decreases drastically. Hence, the onset of the formation of apolar cavities of **PPO-co-PG** and **hbPPO-co-PG** is already accompanied by intermolecular aggregation. This is likely to be a consequence of the small fraction of hydrophilic PG, which might be too small for the development of a dense layer of hydrophilic PG that surrounds the collapsed PPO. Such, PPO above $T_{c,EPR}$ tends to compensate the poor solvent (water) by aggregation with PPO segments of other polymer strands, which leads to large aggregates already at $T_{c,EPR}$. (Note that the cloud point only indicates the formation of large

aggregates, the formation of apolar cavities can only be deduced from $T_{c,EPR}$, which in the case of **PPO-co-PG** and **hbPPO-co-PG** coincides with the onset of changing turbidity.)

It should be noted that in the case of poly-NIPAM hydrogels solemnly static inhomogeneities are observed with CW EPR on TEMPO, too.²⁷ They appear similar to the spectra shown in Figure 2, yet, the molecular weights of the used three-dimensionally cross-linked hydrogels were very large (approx. 150-200 kDa). Thus initially formed apolar cavities are automatically embedded in an extensive network of polymer strands and are expected to be relatively large. Hence, an exchange of incorporated guest-molecules with the solvent and the occurrence of dynamic inhomogeneities are unlikely, since the distance to the medium that has to be bridged for guest-exchange to take place is too long. Such, although both systems appear similar when investigated with TEMPO spin probing and CW EPR, the actual reason behind the exclusive occurrence of static inhomogeneities in **PPO-co-PG**, **hbPPO-co-PG** and poly-NIPAM hydrogels may in fact be of different nature, because in the case of **PPO-co-PG** and **hbPPO-co-PG** molecular weights are only 1-4 kDa.

Comparison between PPO-co-PG and PEO-co-PDEGA

PPO-co-PG and **PEO-co-PDEGA** are of similar topology. They are linear, random (or slightly gradient-like)⁴⁷ copolymers composed of more hydrophilic and more hydrophobic comonomers. Yet, we observe that their nanoscale collapse behavior differs significantly, as depicted in Figures 6 and 8. While in **PPO-co-PG** several chains initially form aggregates with a PPO-rich core, the CW EPR data gained from **PEO-co-PDEGA** suggest an initial formation of small micelles and subsequent aggregation of the pre-formed globules. However, the proposed difference in collapse mechanism can be understood when taking into account that DEGA is even more hydrophobic than PO, which makes it less likely for DEGA-containing copolymers (at elevated temperatures in an aqueous environment) to rearrange in order to form collapsed structures with a single DEGA-rich core, since DEGA would intermediately be exposed to water. The DEGA units may in fact rather be trapped in small aggregates, and the poor solubility of DEGA in water prevents a further conformational rearrangement to form larger aggregates. This, in contrast, seems to be possible for **PPO-co-PG** polymers in water, since PPO is not as hydrophobic as PDEGA.

Conclusion: Relating Structure to Temperature-Response

CW EPR spectroscopy and spin probing with amphiphilic⁴⁸ TEMPO is a well-suited technique for the observation of temperature-dependent behavior of thermoresponsive polymers on the

molecular- and nanoscale. Using this method, one observes a system from a guest molecule's point of view. Such, insights into the supramolecular interactions between the spin probe guests and the host polymers can be deduced. Although other probes might also be used to investigate the phase-transition of thermoresponsive polymers,^{44,77} it is the handy and favorable partitioning coefficient of TEMPO between water-rich (polar) and water-depleted (apolar) regions and the rather large hyperfine coupling shifts up to 3 MHz, depending on the direct environment, that makes spin probing with TEMPO a convenient approach. It aids to elucidate not only the fraction of guest-molecules incorporated into collapsed polymer molecules, but also aggregates' configurations. Since spin-probing CW EPR is an intrinsically local technique it is also sensitive to smallest changes in the molecular environment of the probes. Such, we could show that $T_{c,EPR}$ of a thermoresponsive copolymer is independent of the ratio between more hydrophilic and more hydrophobic monomers. Local regions that are rich of only one of the comonomers always collapse in a very narrow temperature range, as the chemical composition of such rather homogeneous regions is independent of the overall composition of the copolymer in which they are embedded. In contrast, the macroscopic phase-transition of the polymers under investigation clearly depends on the polymer composition that influences the temperature-dependent large-scale aggregation. Yet, since the aggregation of thermoresponsive macromolecules in solution and their local dehydration do not take necessarily place in the same temperature range (since dehydration may take place in a much broader temperature range than aggregation) $T_{c,EPR}$ can deviate strongly from T_c . The EPR-based evidence on the collapse mechanisms can be substantiated by referring to MD simulations, well-known structural features of the respective polymers and prior, published, knowledge about amphiphilic polymers.

Since we have varied the structural and topological properties of selected thermoresponsive polymers (amphiphilic random copolymers with linear and hyperbranched architecture and amphiphilic block copolymers with different ratios of more hydrophobic to more hydrophilic comonomers and differing hydrophobicity/hydrophilicity of the respective comonomers) and investigated their inverse phase-transitions, one can relate these properties to certain collapse mechanisms and to corresponding inhomogeneities on the nanoscale:

The thermally induced aggregation of block-copolymers of hydrophilic and hydrophobic blocks (**PEO-block-PDEGA** and Pluronic) is fostered by the possibility to form micelles with the hydrophobic block primarily located in their core and the hydrophilic blocks enriched in the corona. Such, above $T_{c,EPR}$ initially relatively large and well-structured micelles are formed that do not allow for dynamic exchange of guest-molecules like TEMPO, which are incorporated into the micellar cores. However, if the fraction of hydrophobic blocks is small and the micellar cores are consequently small and of low

density (compared to polymers with higher fractions of hydrophobic blocks) guest exchange can take place at high temperatures, when the kinetic energy of the guests becomes large, such that the distance from the micellar core to the aqueous medium can be bridged. Thus, the occurrence of static inhomogeneities or of dynamic inhomogeneities, featuring guest-exchange at high temperatures can be regulated by adjusting the size of hydrophobic blocks in amphiphilic block copolymers.

The collapse mechanism of random copolymers as seen on the nanoscale depends crucially on the hydrophobicity/hydrophilicity of the employed comonomers. A small amount of strongly hydrophilic comonomers (which is not large enough to constitute a dense hydrophilic layer on the surface of collapsed polymer segments) next to a large fraction of relatively hydrophobic comonomers like in **PPO-co-PG** and **hbPPO-co-PG** leads to the exclusive occurrence of static inhomogeneities, because of a strong tendency to intermolecular aggregation and hence to the formation of large aggregates already at the onset of the nanoscale collapse of the polymers. The tendency to aggregate is determined by the amount of hydrophilic comonomers, though. The fraction of PG also determines the aggregates' interaction strength with small amphiphiles like TEMPO. Increasing amounts of glycidol in **PPO-co-PG** and **hbPPO-co-PG** reduce the propensity of aggregates to interact significantly with TEMPO. Rather small amounts of glycidol instead lead to aggregates that are too dense to be penetrated by TEMPO. The "loading capacity" of a system with a specific ratio of PPO to PG is further determined by the topology of the polymers. Hyperbranched polymers cannot incorporate as much TEMPO as their linear analogues.

On the contrary, a small amount of very hydrophobic comonomers like in **PEO-co-PDEGA** leads to the occurrence of dynamic inhomogeneities, featuring guest-exchange at temperatures slightly above the microscopic LCST, while exchange does not take place at further elevated temperatures. This can be understood taking into account that the strongly hydrophobic DEGA clusters in the center of small micelles/aggregates at $T_{c,EPR}$ to yield only rather small collapsed structures which allow for guest-exchange. With further increasing temperature and decreasing solubility of PEO these small globules form larger aggregates, which do not allow for guest exchange anymore. Hence, the occurrence of static or dynamic inhomogeneities in amphiphilic random copolymers can be controlled by the hydrophobicity of the respective comonomers.

Other factors might also determine the occurrence of a certain type of inhomogeneity. A) In PNIPAM hydrogels of large molecular weight the exclusive occurrence of static inhomogeneities can be attributed to the fact that the 3D network structure is so large that incorporated guest-molecules cannot diffuse in and out of the polymer. Further, the steric confinement of the gel-network does not allow for large scale rearrangements and hence promotes static guest incorporation. B) For

thermoresponsive dendronized polymers the occurrence of dynamic inhomogeneities is a consequence of a special two-step collapse mechanism: Local collapse of chain-segments followed by intermolecular aggregation.

Principles as stated above might help to find particular temperature-dependent properties, desired for certain applications of thermoresponsive polymers and, given the general importance of functional PEO and PPO, might facilitate their purposeful, application-oriented synthesis. TEMPO as a small amphiphilic molecule has important features like molecular structure and the ensuing physico-chemical properties in common with many drugs and can thus be regarded as a model compound for probing the applicability of thermoresponsive systems in actual drug delivery or in analytical/sensing research. On a more general level, we are convinced that with local methods like CW EPR, NMR, or fluorescence spectroscopy the set of “inhomogeneity design principles” stated here can be expanded to, e.g., bio-inspired systems and finally yield a data pool for the development of thermosensitivity-based drug-delivery (or similar) systems.

Experimental

Sample preparation.

In all cases, 0.2 mM aqueous TEMPO solutions were freshly prepared and the required amount of polymer was dissolved subsequently in the TEMPO solution. Afterwards, the solution was transferred to 3 mm outer diameter quartz tubes. All substances are commercially available or synthesized as reported earlier^{13-15, 47} and were used without further purification. Note that the pH of the solutions was left unchanged after dissolution of the polymers. Thus, PEO-co-PDEGA polymers were measured at pH 11. The pH-dependence of the CW EPR data is shown in the Supporting Information.

EPR Spectroscopy.

CW EPR spectra at X-band (~9.4 GHz) were measured on a MAgnettech (Berlin, Germany) MiniScope MS200 benchtop CW EPR spectrometer with a variable-temperature cooling/heating unit. The sample volume was always large enough to fill the complete resonator volume in the probehead (>300 μ L). Each sample was left at the particular temperature for exactly 5 minutes to equilibrate. Changes in mole fractions of species A or B after longer periods of time were not detected. Typical experimental parameters were: modulation amplitude of 0.06 mT and sweep width of 10 mT.

Data Analysis.

All spectral simulations were performed with home-written programs in MATLAB (The MathWorks, Inc.) employing the EasySpin toolbox for EPR spectroscopy.⁷⁸ Simulations of CW EPR spectra in fluid solution were performed by using a model, which is based on the fast-motion theory and a program developed by Freed and Fraenkel as implemented in EasySpin.⁷⁹ These simulations can account for the effect of intermediate or slow rotational diffusion of the radical on the EPR spectra. All reported values for hyperfine-coupling parameters and spectral fractions were obtained from simulating the experimental CW EPR spectra. The hyperfine-coupling constants are given in MHz throughout this article. 1 MHz corresponds to 0.0357 mT at a magnetic field of 336 mT. The evolution of the spin-probe concentration over time was determined by double integration of the spectra.

Acknowledgment

We thank Christian Bauer for technical support and Prof. Hans W. Spiess for continuing support. D.K. and V.S.W. acknowledge support by the Gutenberg Academy of the University of Mainz. M.S. and D.H. acknowledge support by the Max Planck Graduate Center with the University of Mainz (MPGC). V.S.W. is thankful to the Graduate School “Materials Science in Mainz” for financial support and to the “Fonds der Chemischen Industrie” for a scholarship. This work was financially supported by the Deutsche Forschungsgemeinschaft (DFG) under grant number HI 1094/2-1 and the MPGC.

Supporting Information Available. Spectral simulations and tabulated spin-Hamiltonian components. Details on MD simulations. Details on spin-probing CW EPR. CW-EPR on TEMPO/Pluronic solutions. Calculation of diffusional displacement.

References

- [1] Schmaljohann, D. *Advanced Drug Del. Rev.* **2006**, 58, 1655-1670.
- [2] Gil, E. S.; Hudson, S. M. *Prog. Polym. Sci.* **2004**, 29, 1173-1222.
- [3] Alarcón, C. d. I. H.; Pennadam, S.; Alexander, C. *Chem. Soc. Rev.* **2005**, 34, 276-285.
- [4] Wu, C.; Wang, X. *Phys. Rev. Lett.* **1998**, 80, 4092-4094.
- [5] Wu, C.; Zhou, S. *Macromolecules* **1995**, 28, 5388-5399.
- [6] Alexandridis, P.; Holzwarth, J. F.; Hatton, T. A. *Macromolecules* **1994**, 27, 2414-2425.
- [7] Skrabania, K.; Kristen, J.; Laschewsky, A.; Akdemir, Ö.; Hoth, A.; Lutz, J.-F. *Langmuir* **2007**, 23, 84-93.
- [8] Chee, C. K.; Rimmer, S.; Shaw, D. A.; Soutar, I.; Swanson, I. *Macromolecules* **2001**, 34, 7544-7549.
- [9] Katono, H.; Maruyama, A.; Sanui, K.; Ogata, N.; Okano, T.; Sakurai, Y. *J. Controlled Release* **1991**, 16, 215-228.
- [10] Zhao, J.; Zhang, G.; Pispas, S. *J. Poly. Sci. A: Poly. Chem.* **2009**, 47, 4099-4110.
- [11] Tanaka, F. *Macromolecules* **2000**, 33, 4249-4263.
- [12] Mangold, C.; Obermeier, B.; Wurm, F.; Frey, H. *Macromol. Rapid Commun.* **2011**, 32, 1930-1934.
- [13] Schömer, M.; Seiwert, J.; Frey, H. *ACS Macro Lett.* **2012**, 1, 858-891.
- [14] Reuss, V. S.; Obermeier, B.; Dingels, C.; Frey, H. *Macromolecules* **2012**, 45, 4581-4589.
- [15] Schömer, M.; Frey, H. *Macromolecules* **2012**, 45, 3039-3046.
- [16] Deshmukh, M. V.; Vaidya, A. A.; Kulkarni, M. G.; Rajamohanam, P. R.; Ganapathy, S. *Polymer* **2000**, 41, 7951-7960.
- [17] Alexandridis, P.; Hatton, T. A. *Colloids and Surfaces A* **1995**, 96, 1-46.
- [18] Chung, J. E.; Yokoyama, M.; Okana, T. *J. Controlled Release* **2000**, 65, 93-103.
- [19] Weber, C.; Hoogenboom, R.; Schubert, U. S. *Prog. Polym. Sci.* **2012**, 37, 686-714.
- [20] Obermeier, B.; Wurm, F.; Mangold, C.; Frey, H. *Angew. Chem. Int. Ed.* **2011**, 50, 7988-7997.
- [21] Lyon, L. A.; Meng, Z.; Singh, N.; Sorrell, C. D.; John, A. S. *Chem. Soc. Rev.* **2009**, 38, 865-874.
- [22] Ganta, S.; Devalapally, H.; Shahiwala, A.; Amiji, M. *J. Controlled Release* **2008**, 126, 187-204.
- [23] Zhou, Y.; Yan, D.; Dong, W.; Tian, Y. *J. Phys. Chem. B* **2007**, 111, 1262-1270.
- [24] Liu, R.; Fraylich, M.; Saunders, B. R. *Colloid. Polym. Sci.* **2009**, 287, 627-643.
- [25] Lutz, J.-F.; Akdemir, Ö.; Hoth, A. *J. Am. Chem. Soc.* **2008**, 128, 13046-13047.
- [26] Lutz, J.-F.; Hoth, A. *Macromolecules* **2006**, 39, 893-896.
- [27] Junk, M. J. N.; Jonas, U.; Hinderberger, D. *Small* **2008**, 4, 1485-1493.
- [28] Junk, M. J. N.; Li, W.; Schlüter, A. D.; Wegner, G.; Spiess, H. W.; Zhang, A.; Hinderberger, D. *Angew. Chem. Int. Ed.* **2010**, 122, 5818-5823.
- [29] Kurzbach, D.; Reh, M. N.; Hinderberger, D. *ChemPhysChem* **2011**, 12, 3566-3572.
- [30] Junk, M. J. N.; Li, W.; Schlüter, A. D.; Wegner, G.; Spiess, H. W.; Zhang, A.; Hinderberger, D. *Macromol. Chem. Phys.* **2011**, 212, 1229-1235.
- [31] Junk, M. J. N.; Li, W.; Schlüter, A. D.; Wegner, G.; Spiess, H. W.; Zhang, A.; Hinderberger, D. *J. Am. Chem. Soc.* **2011**, 133, 10832-10838.
- [32] Li, W.; Zhang, A.; Feldmann, K.; Walde, P.; Schlüter, A. D. *Macromolecules* **2008**, 41, 3659-3667.
- [33] Hinderberger, D. *Top. Curr. Chem.* **2012**, 321, 67-89.
- [34] Baute, D.; Goldfarb, D. *J. Phys. Chem. C* **2007**, 111, 10931-10940.
- [35] Ruthstein, S.; Raitsimring, A. M.; Bitton, R.; Frydman, V.; Godt, A.; Goldfarb, D. *Phys. Chem. Chem. Phys.* **2009**, 11, 148-160.
- [36] Martini, G.; Ciani, L. *Phys. Chem. Chem. Phys.* **2009**, 11, 211-254.

- [37] Importantly, a dynamic exchange of spin-probes, the diffusion of probes in and out of hydrophobic cavities, must not be mistaken for dynamic inhomogeneities.
- [38] Procházka, K.; Limpouchová, Z.; Uhlík, F.; Košovan, P.; Matejíček, P.; Štěpánek, M.; Mariusz Uchman; Jitka Kuldová; Šachl, R.; Humpolická, J.; Hof, M. *Adv. Polym. Sci.* **2010**, 241, 187-249.
- [39] Ottochian, A.; Leporini, D. *J. Non-Cryst. Solids* **2011**, 357, 298-301.
- [40] Thomas, D. D. *Biophys. J.* **1978**, 24, 439-462.
- [41] Winnik, F. M.; Davidson, A. R.; Hamer, G. K.; Kitano, H. *Macromolecules* **1992**, 25, 1876-1880.
- [42] Ionita, G.; Chechik, V. *Chem. Commun.* **2010**, 46, 8255-8257.
- [43] Caldararu, H.; Timmins, G. S.; Gilbert, B. C. *PCCP* **1999**, 1, 5689-5695.
- [44] Caragheorghopol, A.; Caldararu, H.; Dragutan, I.; Joela, H.; Brown, W. *Langmuir* **1997**, 13, 6912-6921.
- [45] Winnik, F. M.; Ottaviani, M. F.; Bossmann, S. H.; Garcia-Garibay, M.; Turro, N. J. *Macromolecules* **1992**, 25, 6007-6017.
- [46] Koberstein, J. T. *J. Polym. Sci. B: Polym. Phys.* **2004**, 42, 2942-2956.
- [47] Reuss, V. S.; Werre, M.; Frey, H. *Macromolecules* **2012**, DOI: 10.1021/ma300292m.
- [48] Ma, J. W.; Cunningham, M. F.; McAuley, K. B.; Keoshkerian, B.; Georges, M. K. *J. Polym. Sci. A: Polym. Chem.* **2001**, 39, 1081-1089.
- [49] Bemis, G. W.; Murcko, M. A. *J. Med. Chem.* **1999**, 42, 5095-5099.
- [50] Bemis, G. W.; Murcko, M. A. *J. Med. Chem.* **1996**, 39, 2887-2893.
- [51] Wishart, D. S.; Knox, C.; Guo, A. C.; Shrivastava, S.; Hassanali, M.; Stothard, P.; Chang, Z.; Woosley, J. *Nucleic Acids Res.* **2006**, 34, D668-D672.
- [52] Booth, C.; Attwood, D. *Macromol. Rapid. Commun.* **2000**, 21, 501-527.
- [53] Kjellander, R.; Florin, E. *J. Chem. Faraday Trans. 1* **1981**, 77, 2053-2077.
- [54] Halacheva, S.; Rangelov, S.; Tsvetanov, C.; Garamus, V. M. *Macromolecules* **2010**, 43, 772-781.
- [55] Wahlund, P. O.; Galaev, I. Y.; Kazakov, S. A.; Lozinsky, V. I.; Mattiasson, B. *Macromol. Biosci.* **2002**, 2, 33-42.
- [56] Berezkin, A. V.; Khalatur, P. G.; Khokhlov, A. R. *J. Chem. Phys.* **2003**, 118, 8049-8060.
- [57] Dill, K. A. *Protein Sci.* **1999**, 8, 1166-1180.
- [58] Siu, M.; Liu, H. Y.; Zhu, X. X.; Wu, C. *Macromolecules* **2003**, 36, 2103-2107.
- [59] Zhu, X.; Liu, M. *Langmuir* **2011**, 27, 12844-12850.
- [60] Morishima, Y.; Nomura, S.; Ikeda, T.; Seki, M.; Kamachi, M. *Macromolecules* **1995**, 28, 2874-2881.
- [61] Dutta, P.; Dey, J.; Ghosh, G.; Nayak, R. R. *Polymer* **2009**, 50, 1516-1525.
- [62] Pereira, R. V.; Gehlen, M. H. *Macromolecules* **2007**, 40, 2219-2223.
- [63] Dutta, P.; Dey, J.; Shome, A.; Das, P. K. *Int. J. Pharm.* **2011**, 414, 298-311.
- [64] Ogata, Y.; Iwano, M.; Mogi, T.; Makita, Y. *J. Polym. Sci. B: Polym. Phys.* **2011**, 49, 1651-1659.
- [65] Rimmer, S.; Soutar, I.; Swanson, L. *Polym. Int.* **2009**, 58, 273-278.
- [66] Borisov, O. V.; Halperin, A. *Macromolecules* **1996**, 29, 2612-2617.
- [67] Zhang, G.; Winnik, F. M.; Wu, C. *Phys. Rev. Lett.* **2003**, 90, 35506-1.
- [68] Puosi, F.; Leporini, D. *J. Chem. Phys.* **2012**, 136, 164901.
- [69] Lutz, J.-F.; Weichmann, K.; Hoth, Ö. A. A. *Macromolecules* **2007**, 40, 2503-2508.
- [70] Yoon, J. A.; Kowalewski, T.; Matyjaszewski, K. *Macromolecules* **2011**, 44, 2261-2268.
- [71] Alexandridis, P.; Nivaggiolo, T.; Hatton, T. A. *Langmuir* **1995**, 11, 1468-1476.
- [72] Mai, Y.; Eisenberg, A. *Chem. Soc. Rev.* **2012**, DOI: 10.1039/c2cs35115c.
- [73] Hamley, I. W., *The Physics of Block Copolymers*. Oxford University Press: New York, 1998.
- [74] Weiss, J.; Laschewsky, A. *Macromolecules* **2012**, 45, 4158-4165.

4.1) STRUCTURE-RELATED COLLAPSE

- [75] Atherton, N. M., *Principles of Electron Spin Resonance*. Ellis Harwood: New York, 1993.
- [76] Freire, J. J. *Adv. Polym. Sci.* **1999**, 143, 35-112.
- [77] Lucarini, M.; Pasquato, L. *Nanoscale* **2010**, 2, 668-676.
- [78] Stoll, S.; Schweiger, A. *J. Magn. Res.* **2006**, 178, 42-55.
- [79] Freed, J. H.; Fraenkel, G. K. *J. Chem. Phys.* **1983**, 39, 326-348.

Supporting Information

How Structure-Related Collapse Mechanisms Determine Nanoscale Inhomogeneities in Thermoresponsive Polymers

Dennis Kurzbach, Martina Schömer, Valerie S. Wilms, Holger Frey, Dariush Hinderberger

CW EPR SPECTRA AND CORRESPONDING SIMULATIONS

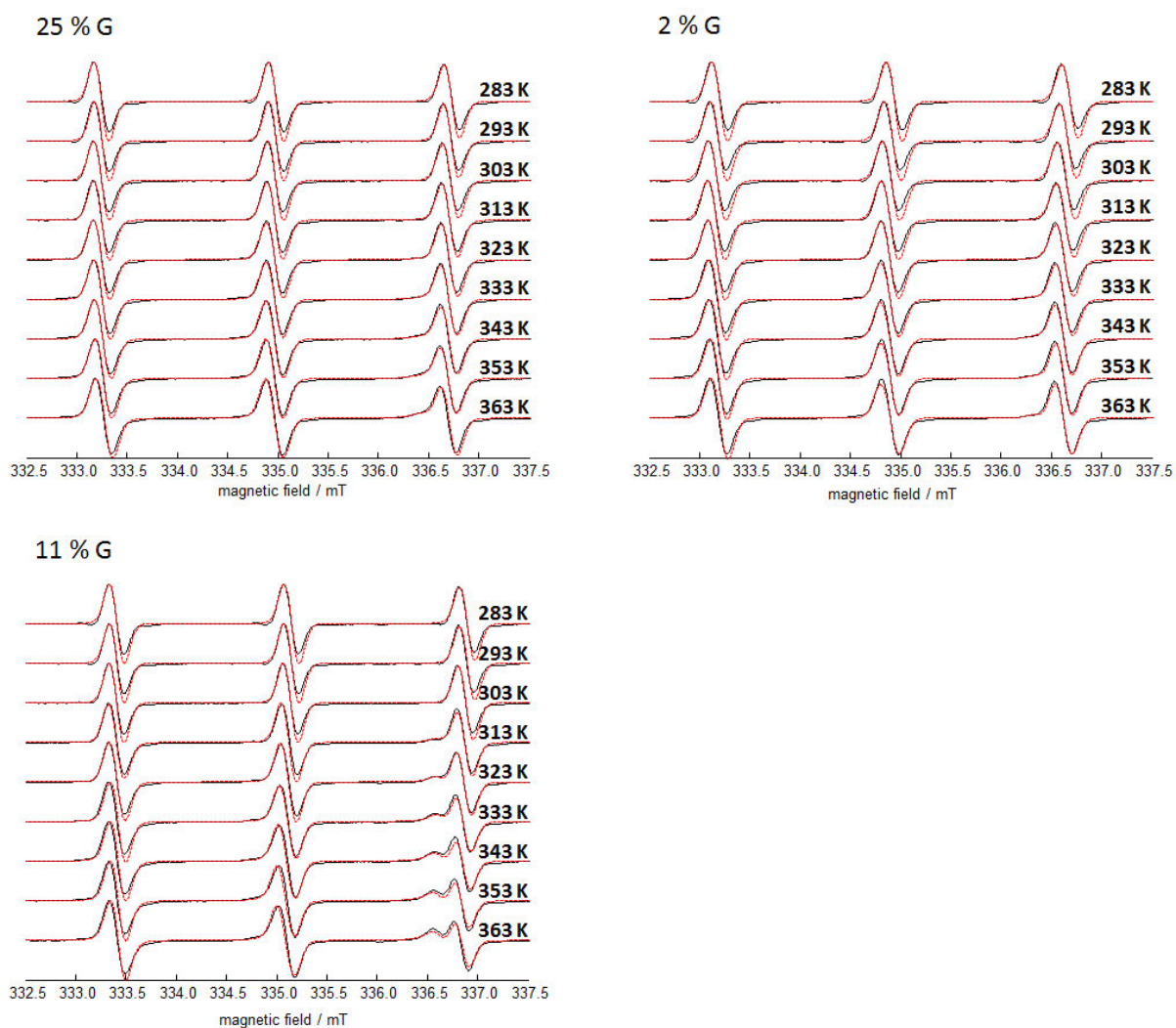


Figure S1. Full set of spectra (black) and corresponding spectral simulations (red) for 1 mM TEMPO in solution together with 1 wt % PPO-co-linPG.

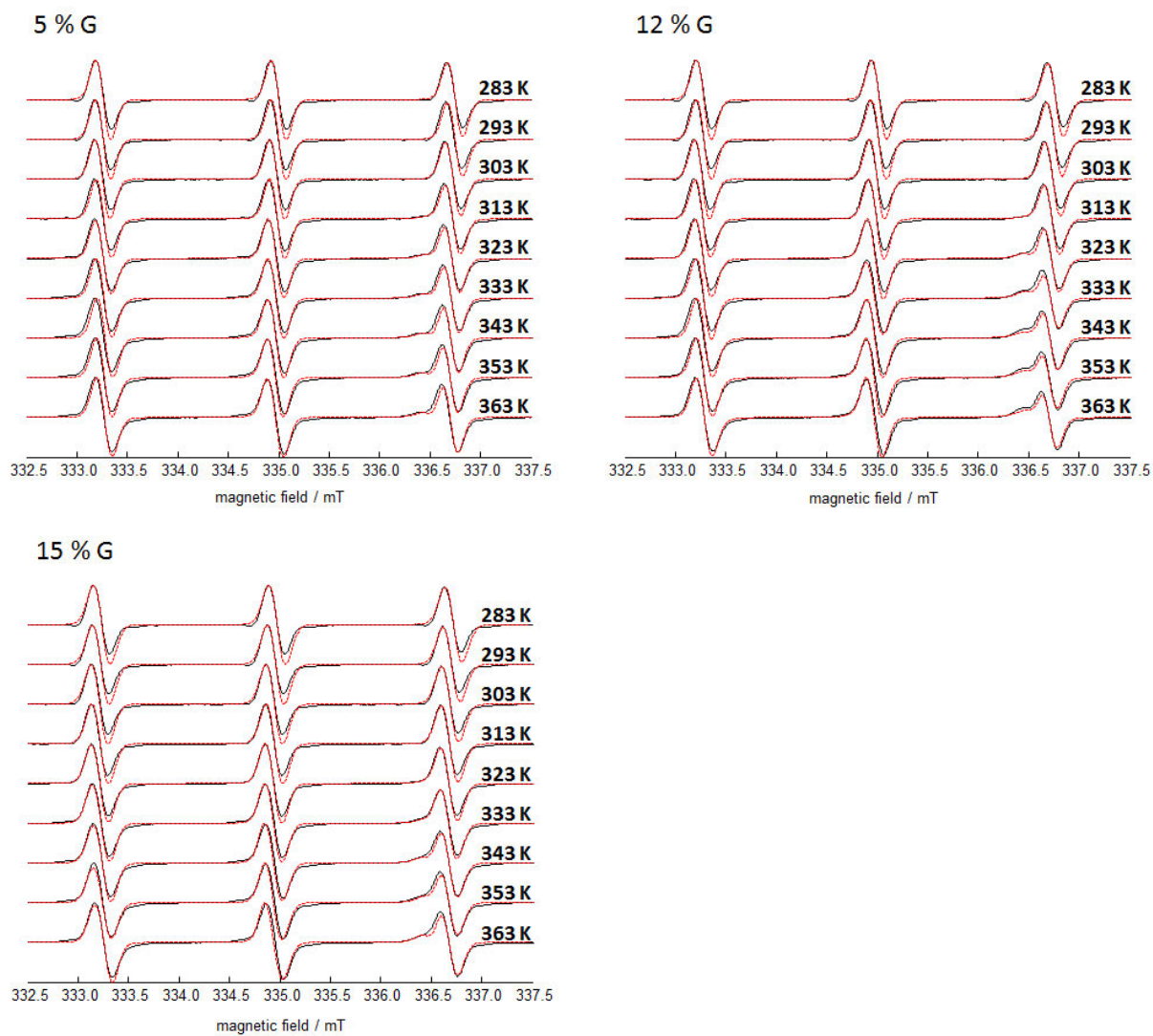


Figure S2. Full set of spectra (black) and corresponding spectral simulations (red) for 1 mM TEMPO in solution together with 1 wt % *hbPPO-co-PG*.

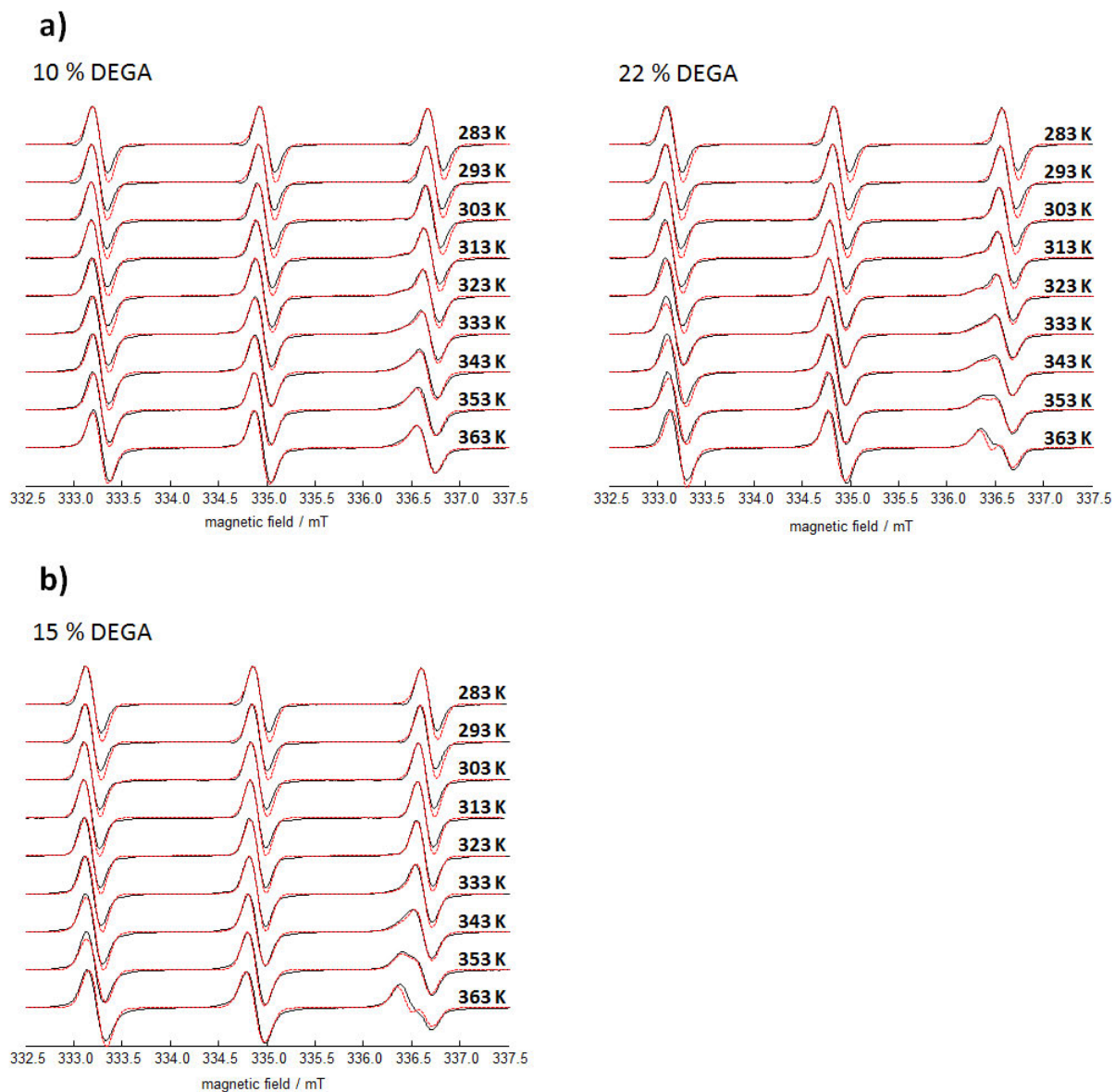


Figure S3. a) Full set of spectra (black) and corresponding spectral simulations (red) for 1 mM TEMPO in solution together with 5 wt % **PEO-block-PDEGA**. b) Full set of spectra (black) and corresponding spectral simulations (red) for 1 mM TEMPO in solution together with 5 wt % **PEO-co-PDEGA**.

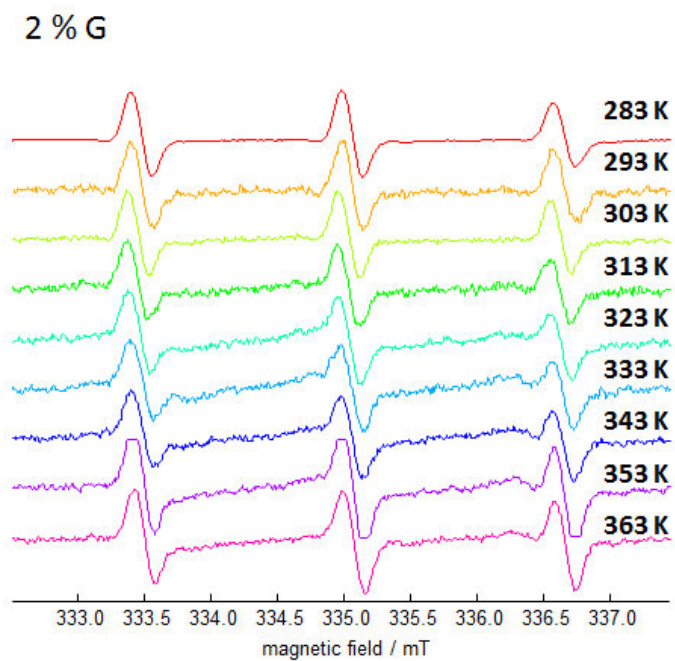


Figure S4. 1 wt % **PPO-co-PG** probed with 0.5 mM 16-DSA (doxyl-stearic acid). Broad lines clearly indicate an incorporation of the spin-probe into collapsed PPO-rich domains, although one cannot detect these with the less hydrophobic spin-probe TEMPO.

SELECTED SPECTRAL PARAMETERS

PPO-*co-lin*PG 25% G

	283 K	293 K	303 K	313 K	323 K	333 K	343 K	353 K	363 K
$g_{\text{iso}}(\text{A})$	2.0058	2.0058	2.0057	2.0057	2.0057	2.0056	2.0056	2.0056	2.0056
$A_{\text{iso}}(\text{A})/\text{MHz}$	48.93	48.76	48.76	48.60	48.60	48.43	48.43	48.26	48.26
$g_{\text{iso}}(\text{B})$			2.0062	2.0062	2.0062	2.0061	2.0060	2.0059	2.0059
$A_{\text{iso}}(\text{B})/\text{MHz}$			45.26	45.26	45.26	45.26	45.26	45.26	45.26

*hb*PPO-*co*-PG 12% G

	283 K	293 K	303 K	313 K	323 K	333 K	343 K	353 K	363 K
$g_{\text{iso}}(\text{A})$	2.0058	2.0058	2.0058	2.0057	2.0057	2.0056	2.0056	2.0056	2.0056
$A_{\text{iso}}(\text{A})/\text{MHz}$	48.93	48.76	48.76	48.59	48.59	48.43	48.26	48.26	48.26
$g_{\text{iso}}(\text{B})$			2.0062	2.0062	2.0062	2.0061	2.0061	2.0061	2.0061
$A_{\text{iso}}(\text{B}) \text{ MHz}$			45.54	44.88	44.76	45.43	45.09	45.26	45.26

PEO-*block*-PDEGA 10% DEGA

	283 K	293 K	303 K	313 K	323 K	333 K	343 K	353 K	363 K
$g_{\text{iso}}(\text{A})$	2.0059	2.0059	2.0058	2.0057	2.0057	2.0057	2.0056	2.0056	2.0056
$A_{\text{iso}}(\text{A})/\text{MHz}$	48.76	48.76	48.76	48.43	48.10	47.93	47.60	47.60	47.60
$g_{\text{iso}}(\text{B})$				2.0062	2.0062	2.0062	2.0062	2.0061	2.0061
$A_{\text{iso}}(\text{B}) \text{ MHz}$				44.54	44.54	45.10	45.43	46.10	46.76

Molecular Dynamic Simulations

MD-simulations were performed using the YASARA software-package. The AMBER 03 force field was employed with periodic boundary conditions.¹ Non-bonded interactions were cut off at 10.5 Å. Long-range Coulombic interactions were treated by a smoothed particle-mesh Ewald method.² Models of the simulated block-polymers were built using YASARA and semi-quantum-mechanically parameterized (YAPAC-AM1). The models of the polymers were built according to the polymers used for the experimental studies. For PEO-*block*-PDEGA with 10% 13 DEGA units and 113 EO units were attached in a linear manner. For PEO-*block*-PDEGA with 22% 22 DEGA units and 113 EO units were

used. PEO-*co*-PDEGA was modeled as random copolymer with a random distribution of DEGA monomers, although it is known to be slightly gradient-like. 22 DEGA units very randomly distributed between 124 EO units. The obtained linear structures were subsequently randomly distorted. The random model structures were subject to energy minimization in vacuum, subsequently randomly placed in the simulation box and solvated by water at pH = 12 (104532 water molecules (PEO-*co*-PDEGA 15% DEGA), 85178 water molecules (PEO-*block*-PDEGA 22% DEGA) and 93412 water molecules (PEO-*block*-PDEGA 10% DEGA)), and again minimized (steepest descent minimization followed by simulated annealing). The chosen time increment was 1 fs. After energy-minimization and equilibration for 10 ns at 25°C in order to yield a energetically acceptable structures, MD trajectories of 5.0 ns length were accumulated at 25°C and 90°C for the three systems. Intermolecular forces were recalculated at every second simulation sub-step. Temperature rescaling was employed with a set-temperature of 25°C or 90°C. The box dimensions (cubic of 120 - 150 Å side length) were controlled so as to yield a solvent pressure of 1 bar. Snapshots of the simulations were taken every 2000 fs. The average number of inter-chain contacts was calculated by counting per-chain inter-atomic distances shorter than 0.5 nm, excluding intramolecular distances, for every snapshot. Note that the described method is likely to yield structures that fluctuate around local energetic minima, as explained in the main text and data should be interpreted with caution.

The Spin Probing Approach for Responsive Polymers

The stable free radical TEMPO (2,2,6,6-tetramethylpiperidin-1-yl)oxyl) is an amphiphilic spin probe. If confined hydrophobic regions in an otherwise aqueous environment are available, it is partitioned between these aqueous and the hydrophobic environments. Since the electron spin population (density) at the nitrogen nucleus of TEMPO depends on the polarity of the molecule's direct environment, the hyperfine interaction or, more precisely, the coupling between the electron spin and the nuclear spin of ^{14}N of the nitroxide moiety (see Figure 1) is sensitive to environmental polarity, too. Such, a partitioning of TEMPO between regions of different hydrophobicity gives rise to a spectral contrast between a TEMPO species *A* in the hydrophilic regions and a species *B* located in the hydrophobic regions. Thus, the mole fraction of species *B*,

$$\chi_B = n_B / \sum_{i=1} n_i$$

is a relative measure of the hydrophobic volume present in a system. Further, the isotropic hyperfine coupling constant, A_{iso} , of species *B* is a measure for the hydrophobicity of the hydrophobic environment.³ Such, by adding TEMPO to an aqueous solution of a thermoresponsive polymer and by following the temperature dependence of its CW EPR spectrum, one can detect the occurrence and

polarity of hydrophobic cavities of any kind. These cavities form during the temperature-induced collapse of polymer strands and the amphiphilic spin probe is incorporated to some extent. This happens regardless of the precise collapse mechanism, whether e.g. one has a unimer collapse⁴, micellization⁵, 3D-network collapse⁶ etc. It should be noted that the hyperfine tensor, \mathbf{A}_i , of the effective spin-Hamiltonian

$$H = H_{\text{Electron-Zeeman}} + H_{\text{Hyperfine}} = \frac{\beta_e}{\hbar} \mathbf{B}^T \mathbf{g} \mathbf{S} + \sum_{i=1}^N \mathbf{S}^T \mathbf{A}_i \mathbf{I}_i$$

is completely independent of the g-tensor, \mathbf{g} , which describes the field position of the spectrum at a given frequency. \mathbf{g} typically shifts to lower field-positions with increasing hydrophobicity of a spin's environment.⁷ Hence, as depicted in Figure 1c), the most prominent effects can be observed at the high-field line of a nitroxide spectrum, where A- (larger) and g-(to lower fields) shifts add up. We hence focus on this line throughout this article.

Supplementary CW EPR

In Figure S5 the temperature-dependent development of the high-field transition of TEMPO in a 5 wt% solution of different Pluronic PEO-PPO-PEO triblock copolymers (40 % PEO: F64 / 50 % PEO: P105 / 70 % PEO: F127 / 80 % PEO: F108) is shown. With increasing PEO content, the high-field lines of species B shift to higher fields indicating dynamic spin-probe exchange at high temperatures, as it was observed more clearly for 10 wt % solutions before.⁸ Such low PEO content leads to static inhomogeneities, while high PEO content leads to dynamic inhomogeneities featuring dynamic exchange at high temperatures. Hence, Pluronic and PEO-*block*-PDEGA have the transition from static to dynamic inhomogeneities with increasing content of hydrophilic comonomers in common.

Since PEO-*co*-PDEGA has been investigated at pH 11, we also performed pH-dependent measurements. As expected the interaction between PEO-*co*-PDEGA with a DEGA content of 29 % and 0.2 mM TEMPO decreases with decreasing pH, due to the protonation of the DEGA amino-group at low pH (see Figure S6). With increasing pH the separation between species A and B increases, yet if there is a significant effect on TEMPO, one can always observe a dynamic inhomogeneity. Thus, the type of inhomogeneity seems not to be affected by the solution pH. Note that the microscopic LCST is dependent on the pH, which is in full agreement with the assumption that the local collapse of a polymer strand is solemnly dependent on the direct chemical environment, which of course changes as the amines become protonated, but which remains constant if only the fraction of comonomers is varied, as shown in the main text.

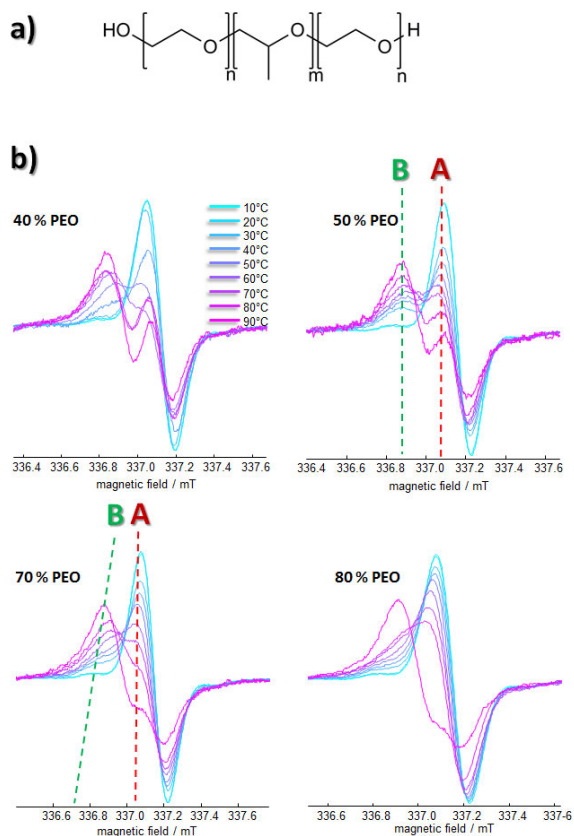


Figure S5. a) Molecular structure of Pluronic triblock copolymers. b) High-field transitions of TEMPO in 5 wt % aqueous solutions of Pluronic triblock copolymers with differing percentage of the PEO blocks. Note that spectra obtained from 10 wt% solutions have already been published and show slightly different temperature-dependent developments.⁸ The red and green dashed lines indicate the positions of the TEMPO-species A and B in cases of static (50% PEO) and dynamic (70% PEO) inhomogeneities.

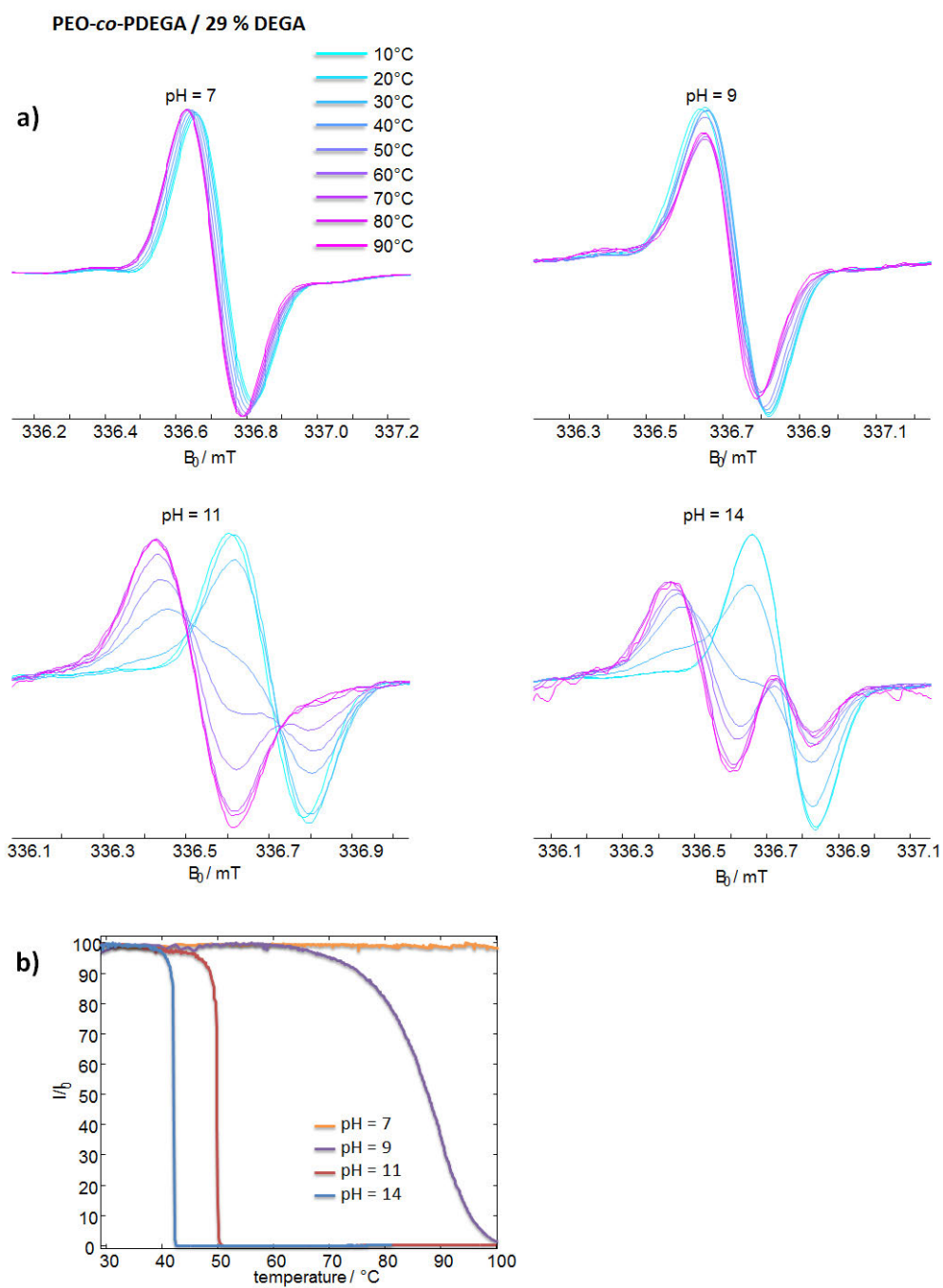


Figure S6. a) TEMPO spin probing CW EPR on **PEO-co-PDEGA** with a DEGA content of 29 % in dependence of the solution pH. b) Turbidity measurements corresponding to the CW EPR data in a).

Calculation of Diffusional Displacement

The mean-square diffusional displacement, $\langle x^2 \rangle$, of a molecule is generally described by:

$$\langle x^2 \rangle = 6D_T\tau_t.$$

It can be shown that for equal line-width and spectral contribution of the two TEMPO-species A and B the translational displacement of species B can be calculated by:

$$\langle x^2 \rangle \leq z \frac{R_{H,R}^3}{R_{H,T}}$$

$$z = \frac{8}{6} \cdot \frac{t}{\tau_c}$$

$$t = 8 \frac{1}{T_2} \frac{1}{10(\Delta\omega)^2}$$

assuming no extra line-broadening due to dynamic exchange.^{9,10} $R_{H,T}$ is the translational and $R_{H,R}$ the rotational hydrodynamic radius. For TEMPO in aqueous solution the ratio $\frac{R_{H,R}^3}{R_{H,T}} = 0.08$. t denotes the reduced lifetime, τ_c the rotational correlation time, $\frac{1}{T_2}$ the spectral width of the spectral components and $\Delta\omega$ the spectral separation of the two lines. For **PEO-block-PDEGA** with 22% PDEGA $\tau_c = 0.3 \text{ ns}$; $\Delta\omega = 5.0 \text{ MHz}$; $1/T_2 = 5.9 \text{ MHz}$ at 80 °C, as extracted from spectral simulations. For PEO-*block*-PDEGA with 10% PDEGA at 80 °C $\tau_c = 0.2 \text{ ns}$; $\Delta\omega = 2.9 \text{ MHz}$; $1/T_2 = 5.3 \text{ MHz}$. Thus, for 22% PDEGA $\sqrt{\langle x^2 \rangle} \approx 9 \text{ nm}$ and for 10% PDEGA $\sqrt{\langle x^2 \rangle} \approx 17 \text{ nm}$.

- [1] Krieger, E.; Darden, T.; Nabuurs, S. B.; Finkelstein, A.; Vriend, G. *Proteins* **2004**, 57, 678-683.
- [2] Essmann, U.; Perera, L.; Berkowitz, M. L.; Darden, T.; Lee, H.; Pedersen, L. G. *J. Chem. Phys.* **1995**, 103, 8577-8593.
- [3] Knauer, B. R.; Napier, J. J. *J. Am. Chem. Soc.* **1976**, 98, 4395-4400.
- [4] Wu, C.; Zhou, S. *Macromolecules* **1995**, 28, 5388-5399.
- [5] Alexandridis, P.; Hatton, T. A. *Colloids and Surfaces A* **1995**, 96, 1-46.
- [6] Junk, M. J. N.; Jonas, U.; Hinderberger, D. *Small* **2008**, 4, 1485-1493.
- [7] Weil, J. A.; Bolton, J. R.; Weitz, J. E., *Electron paramagnetic resonance: Elementary theory and applications*. Wiley-interscience: New York, 2007; Vol. 2.
- [8] Kurzbach, D.; Reh, M. N.; Hinderberger, D. *ChemPhysChem* **2011**, 12, 3566-3572.
- [9] Atherton, N. M., *Principles of Electron Spin Resonance*. Ellis Harwood: New York, 1993.
- [10] Junk, M. J. N.; Li, W.; Schlüter, A. D.; Wegner, G.; Spiess, H. W.; Zhang, A.; Hinderberger, D. *Angew. Chem. Int. Ed.* **2010**, 122, 5818-5823.

4.2) Impact of Amino-Functionalization on PEG Response to External Stimuli

Dennis Kurzbach, Valerie S. Wilms, Holger Frey, Dariush Hinderberger

Submitted to Angewandte Chemie.

Abstract

Amino-functionalization of PEG (poly(ethylene glycol)-*co*-poly(*N,N*-diethyl glycidyl amine)) leads to complex, stimuli-induced phase-transition behavior as revealed by a combination of continuous wave EPR and turbidimetry. Depending on the topology, specific two-step phase transition processes can be achieved, which either exhibit high degrees of cooperativity (tapered) or continuous growth (block) during nanoscale aggregation prior to precipitation.

In recent years, astonishing developments have been achieved in the field of polymers for therapeutic purposes, i.e. the use of polymer-based systems for application in targeted drug delivery.¹ In this context one of the most promising structures is poly(ethylene glycol) (PEG), since it does not exhibit immunogenicity, antigenicity and toxicity.² However, until recently the applicability of PEG was limited by its lack of functional groups, prohibiting e.g. drug conjugation. Recent developments in anionic ring-opening polymerization opened up new routes towards functionalized PEG, allowing for versatile usage in modern therapeutic strategies.³ Drug accumulation in tumor tissue based on hyperthermia or pH irregularity becomes possible by tuning the stimuli responsiveness of functional PEG.⁴ It is apparent that many properties of these state-of-the-art structures are so far undiscovered and that there is demand for innovative experimental techniques and theoretical concepts to gather deeper understanding of their complex response to external stimuli. This is a necessary prerequisite for purposeful synthesis and directed application of systems for polymer therapeutics.

In this work, we aim at showing that the newly available⁵ slightly tapered copolymer poly(ethylene glycol)-*co*-poly(*N,N*-diethyl glycidyl amine) (PEG-*co*-PDEGA; see Figure 1a)) and its block-structured analogue PEG-*b*-PDEGA exhibit surprising temperature- and pH-dependences in the temperature range around human body temperature, between 25 °C and 45 °C. The latter temperature represents the upper limit of therapeutic hyperthermia, which highlights the potential importance for medical applications.⁶ Here, we show that the combination of intrinsically local continuous wave electron paramagnetic resonance (CW EPR) spectroscopy and macroscopic turbidimetry reveals an astonishing versatility and complexity of the temperature-induced inverse phase transition of PEG-*co*-PDEGA and PEG-*b*-PDEGA. We find that the polymers form soluble nanoaggregates capable of incorporating large amounts of amphiphilic guest molecules between 20 °C and 30 °C, with the number of incorporated guests depending on the solution pH. Macroscopically observable large-scale aggregation and subsequent precipitation takes place at significantly higher temperatures (approx. 50 °C higher). While PEG-*b*-PDEGA nanoscopically features a more continuous phase transition (non-first order, like it is known for homoPEG⁷), PEG-*co*-PDEGA surprisingly exhibits a high degree of cooperativity indicating a first order nanophase transition.^{4b,8} The cloud points of the latter system can furthermore be tuned, largely independent of the nanoaggregate formation by adjusting the environmental pH. Thus, the amino-functionalization of PEG leads to the emergence of intriguing phase transition modes of an otherwise rather simple and widely used polymer that are highly interesting from a materials science and physicochemical point of view.

To gain deeper understanding of the temperature-dependence of the nanoscale solution behavior of PEG-*co*-PDEGA (comprising 29% DEGA and a molecular weight of 3300 g mol⁻¹) and PEG-*b*-PDEGA (comprising 22% DEGA and a molecular weight of 6600 g mol⁻¹), we performed temperature-dependent CW EPR measurements at different pH on 0.2 mM of the small and (like most drugs⁹) amphiphilic spin probe TEMPO ((2,2,6,6-tetramethylpiperidin-1-yl)oxyl). The probe reports the occurrence of collapsed, polymer-rich domains on the nanoscale (the polymer concentration was 5 wt%).¹⁰ If TEMPO becomes partitioned between such a domain and the aqueous environment, one observes two spectral signatures, from probes in the aqueous environment (species A) and in water-depleted, collapsed/polymer-rich domains (species B). The fraction of TEMPO incorporated into polymer-rich domains can be quantified by its mole fraction $\chi_B = n_B / \sum_i n_i$ (see the Supporting Information for a detailed description of the CW EPR spin-probing approach). As can be observed in Figure 1b), in solutions of PEG-*co*-PDEGA, species B occurs (rising χ_B) in the narrow temperature range between 20 °C and 30 °C at pH 9, 11 and 14. Only at pH 7, the contribution of species B is very small, such that it is hard to determine the temperature range in which species B occurs. However, in any case, PEG-*co*-PDEGA shows a thermal response and collapses when exposed to heat, as proven by $\chi_B > 0$ (Note that linear homo-PEG does not give rise to any changes in χ_B or turbidity^[5a] in the observed temperature range at the used molecular weights and concentrations). Yet the fraction of species B at a given temperature varies drastically with pH, as a consequence of changing hosting parameters with changing degree of DEGA protonation. Interestingly, for pH 11, $\chi_B = 1$ at 90 °C, which translates to complete uptake of TEMPO probes. At the concentrations used, this has so far not been observed for any other thermoresponsive system that has been investigated by means of CW EPR.^{10a,11}

When inspecting the degree of protonation, the narrowness of the temperature range in which collapsed domains initially occur (between pH 9 and 14 between 20 °C and 30 °C) is quite unexpected, since changes in pH alter the chemical structure of the polymer. Assuming a pK_a of approx. 11 for tertiary amines one can estimate that at pH 7 nearly all amines are protonated. At pH 9 around 1% of the amines are deprotonated, at pH 11 around 50% and at pH 14 nearly 100%. Thus, one would expect differences in hydration energy and hence on the collapse temperature. This is qualitatively not the case here. In this context it is important to note that spin-probing CW EPR is only dependent on local structures on length scales of a few nanometers. Hence, since at any pH (varying) fractions of non-protonated DEGA units are distributed along the polymer chains, it is very likely that the local polymer collapse on length scales below approx. 2 nm is always triggered by chemically equivalent segments of deprotonated PDEGA and PEG (similar phenomena have been observed recently^{10a,11}). This explanation is also in good agreement with the fact that with increasing degree of protonation (decreasing pH), the average values for χ_B decrease.¹²

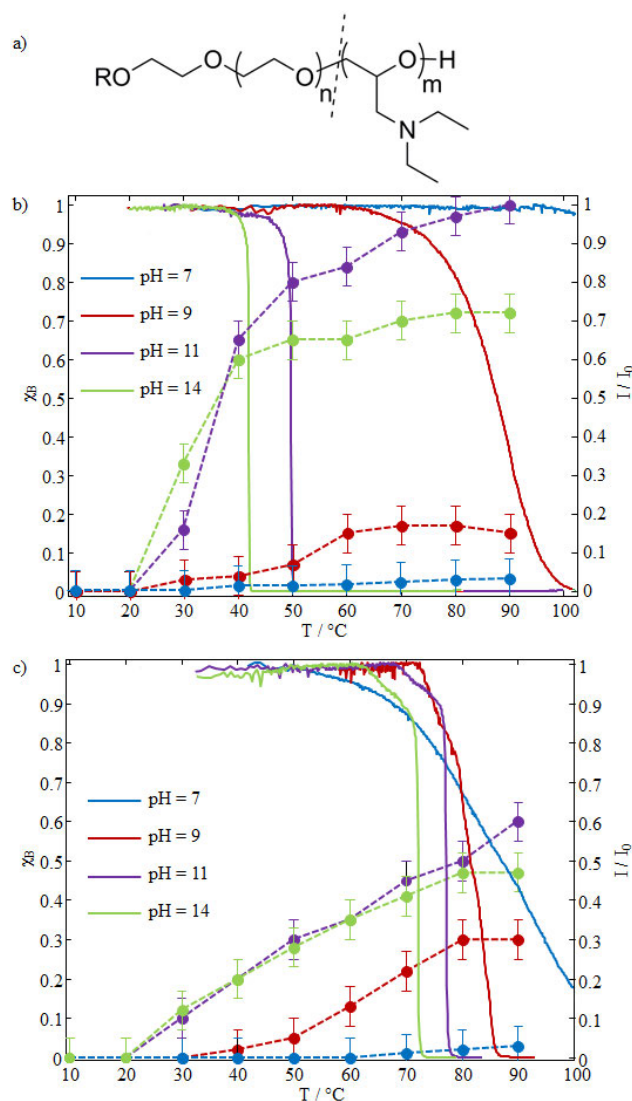


Figure 1. a) Molecular structure of PEG-co-PDEGA/ PEG-b-PDEGA. b) The fraction of TEMPO incorporated into collapsed PEG-co-PDEGA domains, χ_B , as a function of temperature for different pH (dots connected by dashed lines). The corresponding turbidity measurements of the solutions (transmitted light intensity, I/I_0 , respectively) are shown as solid lines. All measurements were performed at 5 wt% polymer concentration. c) The fraction of TEMPO incorporated into collapsed PEG-b-PDEGA domains, χ_B , and the transmitted intensity as a function of temperature for different pH (the concentration was 5 wt% in all cases). Error bars stem from uncertainties in spectral simulations (see the Supporting Information).

Intriguingly, the turbidity of the PEG-co-PDEGA solutions remains unchanged if the temperature does not exceed 40 $^\circ\text{C}$, although structures appear that are large enough to host a significant amount of TEMPO as the temperature rises above 20-30 $^\circ\text{C}$: more than 50% of the probe molecules at pH 11 and 14; see Figure 1b). Thus, one can conclude that PEG-co-PDEGA forms small nanoaggregates

(likely of globular shape¹¹) or similar structures that are too small to scatter light and that remain dissolved at intermediate temperatures (no increase in turbidity was observed for longer waiting periods). The mean-square diffusional displacement of the TEMPO probes at 40 °C is $\sqrt{\langle x_T^2 \rangle} = 3.5$ nm at pH 11 and $\sqrt{\langle x_T^2 \rangle} = 2.8$ nm at pH 14 (see ref. ¹³ and the Supporting Information for details on the calculation). In addition, we do not observe dynamic probe exchange between the collapsed domains and the solvent-exposed regions. Taken together, one can estimate the size of the aggregates to be < 5 nm.

In this context, the sigmoidal and steep development of the χ_B functions is clearly indicative of a high degree of cooperativity of nanoaggregate formation.⁸ Since dehydration of PEG typically is a non-cooperative process^{4b,7} we assume as underlying reason for the observed cooperativity that some of the randomly distributed deprotonated DEGA moieties (which are quite hydrophobic¹¹) can always be found on the surface of any collapsed structure of PEG-co-PDEGA. Such surface moieties of increased concentration may well facilitate the attraction of still swollen PEG-co-PDEGA. Such, a cooperative and for the nanoscale sharp transition can be observed, making it even more interesting that the nanoaggregates remain dissolved below 40 °C. The above explanation is also in agreement with the fact that at pH 9 no cooperative aggregation can be observed: too many DEGA units are charged for an effective hydrophobic attraction of nearby polymers.

Only as the temperature rises above 42 °C, the turbidity of the PEG-co-PDEGA solutions increases at pH 14, indicating metastability of the nanoaggregates (see Figure 1b)). Yet, at 30 °C no changes in turbidity were observed over hours. The cloud point, T_c , in contrast to the nanoaggregate formation, is dependent on the solution pH to a certain degree and can be shifted from 42 °C at pH 14 to 85 °C at pH 9. Note that the cloud points are largely independent of the polymer concentration as well as the temperature of first occurrence of TEMPO species B; see ref. ¹¹. At pH 7 changes in turbidity could not be detected, likely as a consequence of charged DEGA groups keeping the polymer solvated and elongated. Since no abrupt changes in χ_B can be observed at the cloud points at different pH, one can deduce that the initially formed nanoscopic aggregates cluster to form large structures at T_c and do not rearrange into other conformations. Since T_c decreases with increasing pH, it is at hand to assume that deprotonation of the DEGA units and accompanying loss of coordinating water molecules leads to lower solvation energy of the PEG-co-PDEGA nanoaggregates (the loss of solvating water with increasing pH is also reflected in the CW EPR spectra, as shown in the Supporting Information). Note that also this second transition step, the clustering of nanoaggregates, exhibits a high degree of cooperativity at pH 11 and 14, likely again due to surface-exposed DEGA moieties.

The picture of the temperature-induced phase transition of PEG-*co*-PDEGA that arises from our data is schematically depicted in Figure 2a). In a first step metastable nanoaggregates occur, which remain dissolved, the solution remains clear. These are depicted with the hydrophobic DEGA units clustered in the center, which is a likely conformation for amphiphilic random copolymers.^{11,14} If the temperature is further increased, the nanoscopic aggregates cluster in a second step to form large structures that precipitate. The first step takes place in a confined temperature range with respect to pH, while the second is stronger dependent on pH. Interestingly, both steps of the phase transition of PEG-*co*-PDEGA are very sharp at pH 11 and 14, while conventional PEG normally features a rather broad transition range.^{4b} This is indicative for a high degree of cooperativity and highlights the impact of amino-functionalization on the physicochemical properties of PEG.

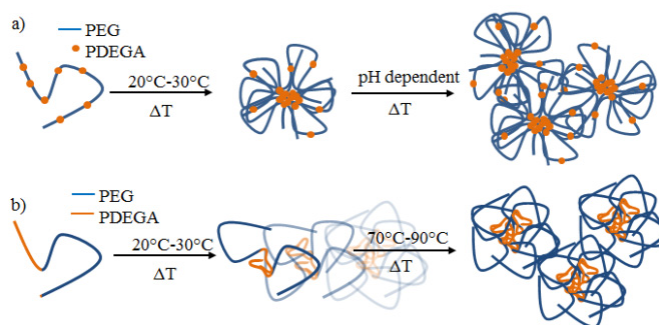


Figure 2. a) Schematic depiction of the temperature-triggered phase-transition of PEG-*co*-PDEGA. Initially small aggregates are formed and remain dissolved. This step takes place between 20 °C and 30 °C. In a second step the aggregates aggregate to form large structures. The aggregation temperature can be shifted from 42 °C to 85 °C by adjusting the pH. b) Schematic depiction of the temperature-triggered phase-transition of PEG-*b*-PDEGA above 20 °C-30 °C micelles grow steadily until they aggregate between 70 °C and 90 °C.

Like for PEG-*co*-PDEGA the nanoscale collapse of its block-structured analogue, PEG-*b*-PDEGA, sets in between 20 °C and 30 °C at pH 9, 11 and 14. Yet in contrast to PEG-*co*-PDEGA, χ_B grows steadily until a temperature of 80 °C is reached (Figure 1c)), indicating a non-cooperative nanophase separation. Collapsed domains grow steadily, resulting in a growing volume fraction of water-depleted regions that entrap TEMPO molecules. Notably, again no changes in turbidity can be observed until higher temperatures are reached, suggesting that the formed objects are of small nanoscopic size and remain solvated at intermediate temperatures ($\sqrt{\langle x_T^2 \rangle} \approx 3$ nm for species B in both cases of pH 11 and 14 at 80 °C). Only between 70 °C and 90 °C, these nanoaggregates cluster to

form larger structures, as can be deduced from the turbidimetry curves in Figure 1c). The turbidity does not decrease as steeply with temperature as for PEG-*co*-PDEGA at pH 11 and 14 (initially small slope of I/I_0), indicating a lower degree of cooperativity not only of the nanoscale collapse (see the slopes of the χ_B functions), but also of the macroscopically detectable aggregation step in the case of block architecture. This lack in cooperativity of the phase transition and the more “PEG-like” behavior of PEG-*b*-PDEGA is likely a consequence of the block architecture: DEGA blocks form the core of PEG-*b*-PDEGA aggregates (probably unimers initially), while the PEG blocks build the corona (depicted in Figure 2b); also see references^{11,15}). Such, the DEGA units are screened by the PEG coronas not allowing for effective attraction of swollen PEG-*b*-PDEGA molecules (for the local collapse) or nanoaggregates (for macroscopic aggregation), hampering DEGA-mediated cooperativity. This is also in good agreement with the observation that the average fraction of incorporated TEMPO is much smaller for PEG-*b*-PDEGA than for PEG-*co*-PDEGA, since different aggregate conformations are very likely to yield differently favorable environments for TEMPO probes. Note that this is in good agreement with our earlier observation that more densely packed structures like ordered core-shell-type micelles incorporate less amphiphiles than randomly arranged aggregates of amphiphilic random copolymers.¹¹ At pH 7, no significant interaction between TEMPO and PEG-*b*-PDEGA can be observed by means of CW EPR, but a very broad turbidity transition that crosses the other three turbidity functions (Figure 1c)). This phenomenon is a consequence of the formation of inverse micelles: since at pH 7 most of the DEGA units are charged, they constitute the corona of PEG-*b*-PDEGA aggregates, while PEG forms the core and now triggers the thermal response. Thus, a broad temperature range of the transition is observed, as it is typical for PEG.^{4b,7}

It is noteworthy that the onset of the nanophase separation (EPR) and the macroscopically visible aggregation of PEG-*b*-PDEGA (turbidity) are separated by more than 50 °C. In a very wide temperature range the block-copolymer forms nanoaggregates that remain dissolved while for PEG-*co*-PDEGA the nanoscopic and macroscopic collapse temperatures are significantly closer (see Figure 1). To the best of our knowledge, such drastic differences between the nanoscale collapse of a polymer and the macroscopic aggregation has not been achieved to date. The general phase transition mode of PEG-*b*-PDEGA is schematically shown in Figure 2b). As for its slightly tapered analogue the phase transition begins in the narrow temperature range between 20 °C and 30 °C at any pH. Yet in contrast, PEG-*b*-PDEGA aggregates grow steadily, until the cloud point is reached, at which the aggregates themselves cluster and precipitate.

Hosting amphiphilic structures like TEMPO without precipitation is a desirable property of polymers for drug transport through body fluid. Drugs could be transported in solution while not being subject to proteolytic degradation. Obviously PEG-*co*-PDEGA and PEG-*b*-PDEGA are good

examples of the versatility of functional PEG for future drug-delivery applications. Furthermore, the second step of the temperature-induced phase transition of these versatile structures could be exploited to accumulate polymer-drug conjugates in tissue that is subject to hyperthermia and/or pH irregularities, although in the present state precipitation within the temperature range achievable through hyperthermia is only observed at pH 14. This discrepancy, however, may well be overcome by adjusting the molecular weight of the polymer or by incorporating a higher fraction of DEGA units, which is currently on the agenda in our labs.

Altogether we have shown that amino-functionalization of PEG in combination with a specific copolymer topology can lead to the emergence of previously unexpected physicochemical properties that allow for precise manipulation of very complex phase-transition modes by adjusting the environmental conditions. Our study shows that extensive understanding of the phase behavior of advanced stimuli-responsive polymers, which is necessary to estimate the in vivo behavior of a drug hosting system, demands for the combination of macroscopic methods with intrinsically local observation techniques.

References

- [1] R. Duncan, *Nat. Drug Discovery Rev.* **2003**, *2*, 347-360.
- [2] a) B. Obermeier, F. Wurm, C. Mangold, H. Frey, *Angew. Chem. Int. Ed.* **2011**, *50*, 7988-7997; b) C. Weber, R. Hoogenboom, U. S. Schubert, *Prog. Polym. Sci.* **2012**, *37*, 686-714; c) K. Knop, R. Hoogenboom, D. Fischer, U. S. Schubert, *Angew. Chem. Int. Ed.* **2010**, *49*, 6288-6308; d) C. Mangold, F. Wurm, H. Frey, *Polym. Chem.* **2012**, *3*, 1714-1721.
- [3] C. Barner-Kowollik, J.-F. Lutz, S. Perrier, *Polym. Chem.* **2012**, *3*, 1677-1679.
- [4] a) M. Schömer, J. Seiwert, H. Frey, *ACS Macro Lett.* **2012**, *1*; b) V. Aseyev, H. Tenhu, F. M. Winnik, *Adv. Polym. Sci.* **2011**, *242*, 29-89.
- [5] a) V. S. Reuss, B. Obermeier, C. Dingels, H. Frey, *Macromolecules* **2012**, *45*, 4581-4589; b) V. S. Reuss, M. Werre, H. Frey, *Macromol. Rapid Commun.* **2012**, *33*, 1556-1561.
- [6] G. M. Hahn, *Cancer Res.* **1979**, *39*, 2264-2268.
- [7] A. Matsuyama, F. Tanaka, *Phys. Rev. Lett.* **1990**, *65*, 341-344.
- [8] K. E. v. Holde, W. C. Johnson, P. S. Ho, *Principles of Physical Biochemistry*, Prentice Hall, New Jersey, **1998**.
- [9] a) G. W. Bemis, M. A. Murcko, *J. Med. Chem.* **1996**, *39*, 2887-2893; b) G. W. Bemis, M. A. Murcko, *J. Med. Chem.* **1999**, *42*, 5095-5099; c) D. S. Wishart, C. Knox, A. C. Guo, S. Shrivastava, M. Hassanali, P. Stothard, Z. Chang, J. Woosley, *Nucleic Acid Research* **2006**, *34*, D668-D672.
- [10] a) D. Kurzbach, M. N. Reh, D. Hinderberger, *ChemPhysChem* **2011**, *12*, 3566-3572; b) M. J. N. Junk, U. Jonas, D. Hinderberger, *Small* **2008**, *4*, 1485-1493; c) M. J. N. Junk, W. Li, A. D. Schlüter, G. Wegner, H. W. Spiess, A. Zhang, D. Hinderberger, *Macromol. Chem. Phys.* **2011**, *212*, 1229-1235.
- [11] D. Kurzbach, M. Schömer, V. S. Wilms, H. Frey, D. Hinderberger, *Macromolecules* **2012**, *45*, 7535-7548.
- [12] The efficiency of TEMPO hosting is determined by the hydrophobicity of the host structure and its density. Protonation of DEGA thereby likely reduces the density of PEG-co-PDEGA aggregates. Too low or too high density leads to less pronounced TEMPO incorporation, since either hydrophobic interactions are too weak or TEMPO cannot penetrate the host structure.
- [13] M. J. N. Junk, W. Li, A. D. Schlüter, G. Wegner, H. W. Spiess, A. Zhang, D. Hinderberger, *Angew. Chem. Int. Ed.* **2010**, *49*, 8755-8759.
- [14] a) C. K. Chee, S. Rimmer, D. A. Shaw, I. Soutar, I. Swanson, *Macromolecules* **2001**, *34*, 7544-7549; b) G. Zhang, F. M. Winnik, C. Wu, *Phys. Rev. Lett.* **2003**, *90*, 35506-35501; c) O. V. Borisov, A. Halperin, *Macromolecules* **1996**, *29*, 2612-2617.

Supporting Information

Impact of Amino-Functionalization on PEG Response to External Stimuli

Dennis Kurzbach, Valerie S. Wilms, Holger Frey, Dariush Hinderberger

Experimental

Sample Preparation.

In all cases, 0.2 mM aqueous TEMPO solutions were freshly prepared and the required amount of polymer was dissolved subsequently in the TEMPO solution. Afterwards, the solution was transferred to 3 mm outer diameter quartz tubes. All substances are commercially available or synthesized as reported earlier^[1] and were used without further purification.

EPR Spectroscopy.

CW EPR spectra at X-band (~9.4 GHz) were measured on a Magnostech (Berlin, Germany) MiniScope MS200 benchtop CW EPR spectrometer with a variable-temperature cooling/heating unit. The sample volume was always large enough to fill the complete resonator volume in the probehead (>300 μ L). Each sample was left at the particular temperature for exactly 5 minutes to equilibrate. Changes in mole fractions of species A or B after longer periods of time were not detected. Typical experimental parameters were: modulation amplitude of 0.06 mT and sweep width of 10 mT.

Data Analysis.

All spectral simulations were performed with home-written programs in MATLAB (The MathWorks, Inc.) employing the EasySpin toolbox for EPR spectroscopy.^[2] Simulations of CW EPR spectra in fluid solution were performed by using a model, which is based on the fast-motion theory and a program developed by Freed and Fraenkel as implemented in EasySpin.^[3] These simulations can account for the effect of intermediate or slow rotational diffusion of the radical on the EPR spectra. All reported values for hyperfine-coupling parameters and spectral fractions were obtained from simulating the experimental CW EPR spectra. The hyperfine-coupling constants are given in MHz throughout this article. 1 MHz corresponds to 0.0357 mT at a magnetic field of 336 mT. The evolution of the spin-probe concentration over time was determined by double integration of the spectra. Typical simulation values were, depending on pH, temperature and polymer architecture: $g_{\text{iso,A}} = 2.0056 - 2.0059$; $A_{\text{iso,A}} = 47.6 - 48.7$ MHz; $\tau_{\text{c,A}} = 0.01 - 0.02$ ns; $g_{\text{iso,B}} = 2.0061 - 2.0062$; $A_{\text{iso,B}} = 44.5 - 46.75$ MHz; $\tau_{\text{c,B}} = 0.16 - 0.25$ ns.

CW EPR Spin-Probing: Approach and Experimental Data

The stable free radical TEMPO (2,2,6,6-tetramethylpiperidin-1-yl)oxyl) is an amphiphilic spin probe. If confined hydrophobic regions in an otherwise aqueous environment are available, it is partitioned between these aqueous and the hydrophobic environments. Since the electron spin population (density) at the nitrogen nucleus of TEMPO depends on the polarity of the molecule's

direct environment, the hyperfine interaction or, more precisely, the coupling between the electron spin and the nuclear spin of ^{14}N of the nitroxide moiety (see Figure S1a)) is sensitive to environmental polarity, too. Such, a partitioning of TEMPO between regions of different hydrophobicity gives rise to a spectral contrast between a TEMPO species A in the hydrophilic regions and a species B located in the hydrophobic regions as shown in Figure S1b). The mole fraction of species B,

$$\chi_B = n_B / \sum_{i=1} n_i$$

is a relative measure of the hydrophobic volume present in a system. Further, the isotropic hyperfine coupling constant, A_{iso} , of species B is a measure for the hydrophobicity of the hydrophobic environment.^[4] Such, by adding TEMPO to an aqueous solution of a thermoresponsive polymer and by following the temperature dependence of its CW EPR spectrum, one can detect the occurrence and polarity of hydrophobic cavities of any kind. These cavities form during the temperature-induced collapse of polymer strands and the amphiphilic spin probe is incorporated to some extent. This happens regardless of the precise collapse mechanism, whether e.g. one has a unimer collapse^[5], micellization^[6], 3D-network collapse^[7] etc. It should be noted that the hyperfine tensor, \mathbf{A}_i , of the effective spin-Hamiltonian

$$H = H_{Electron-Zeeman} + H_{Hyperfine} = \frac{\beta_e}{\hbar} \mathbf{B}^T \mathbf{g} \mathbf{S} + \sum_{i=1}^N \mathbf{S}^T \mathbf{A}_i \mathbf{I}_i$$

is completely independent of the g-tensor, \mathbf{g} , which describes the field position of the spectrum at a given frequency. \mathbf{g} typically shifts to lower field-positions with increasing hydrophobicity of a spin's environment.^[8] Hence, as depicted in Figure S1, the most prominent effects can be observed at the high-field line of a nitroxide spectrum, where A- (larger) and g-(to lower fields) shifts add up. We hence focus on this line throughout this article.

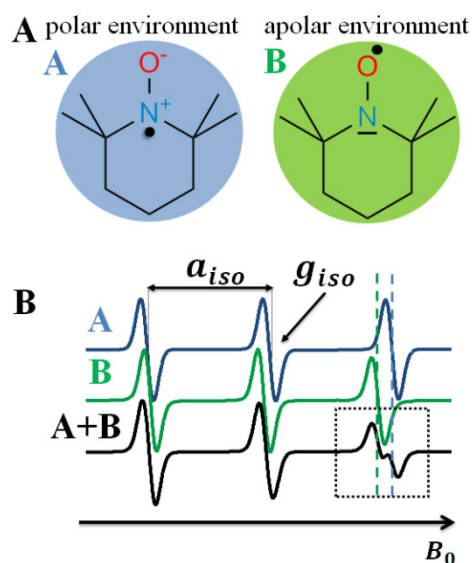


Figure S1. a) Mesomeric structures of TEMPO in polar and apolar media. b) The constitution of two-component CW EPR spectra of TEMPO species A and B. The most prominent effects occur at the high-field transition of the CW EPR spectra.

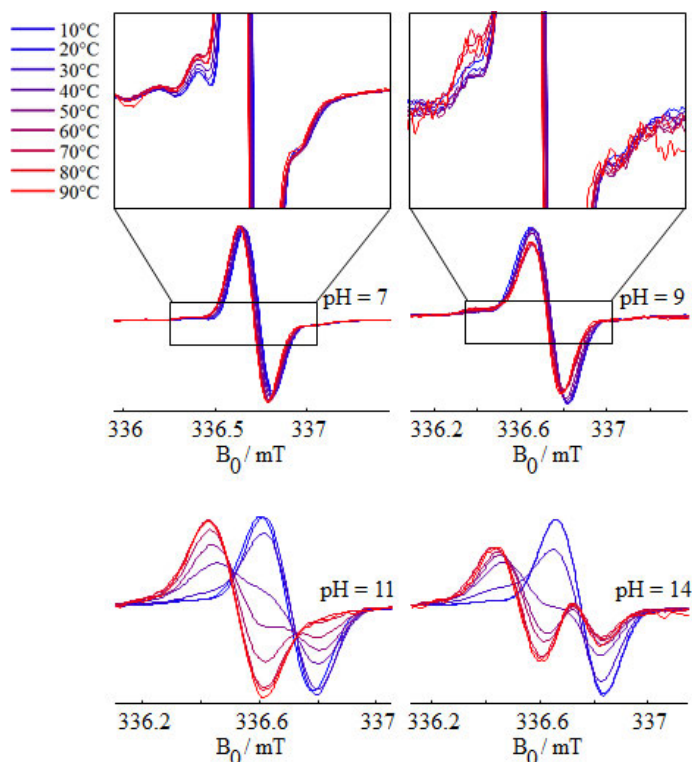


Figure S2. The development of the high-field transition of 0.2 mM TEMPO in solution with 5 wt% PEG-co-PDEGA with temperature at pH 7, 9, 11 and 14. Note that with increasing pH the lines stemming from species A and B separate more and more indicating stronger dehydration of PEG-co-PDEGA with increasing pH.

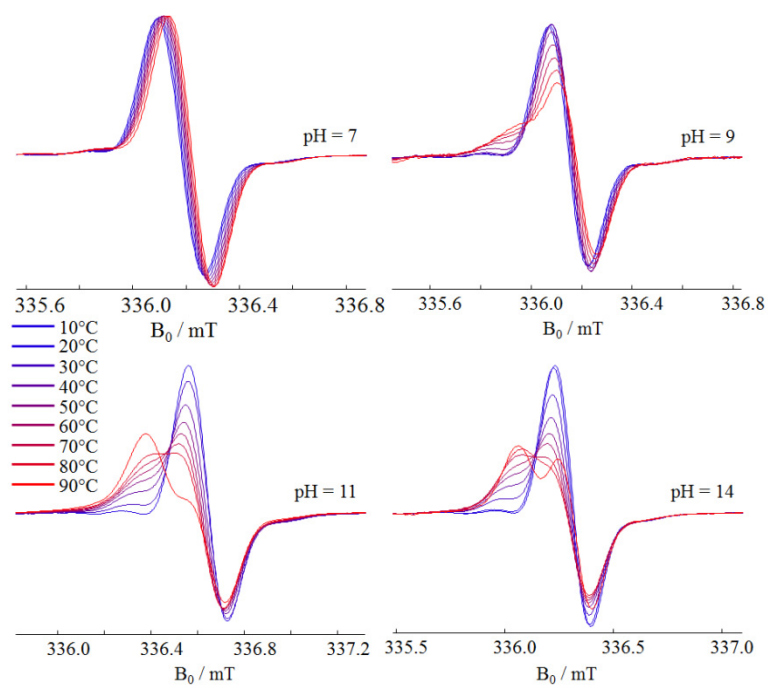


Figure S3. The development of the high-field transition of 0.2 mM TEMPO in solution with 5 wt% PEG-b-PDEGA with temperature at pH 7, 9, 11 and 14.

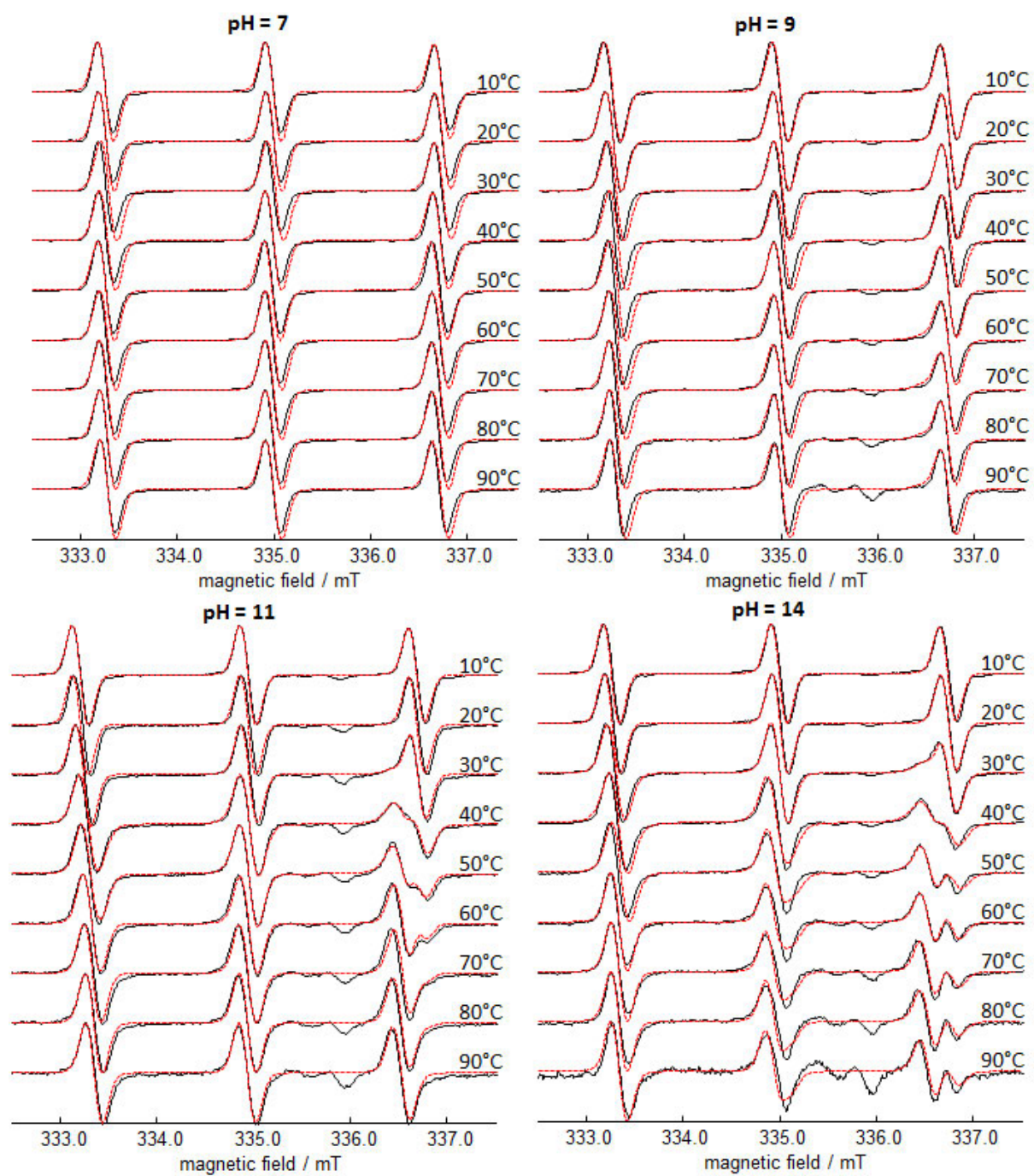


Figure S4. Experimental CW EPR spectra (black) and corresponding spectral simulations (red) between 10 °C and 90 °C at pH 7, 9, 11 and 14 of PEG-co-PDEGA.

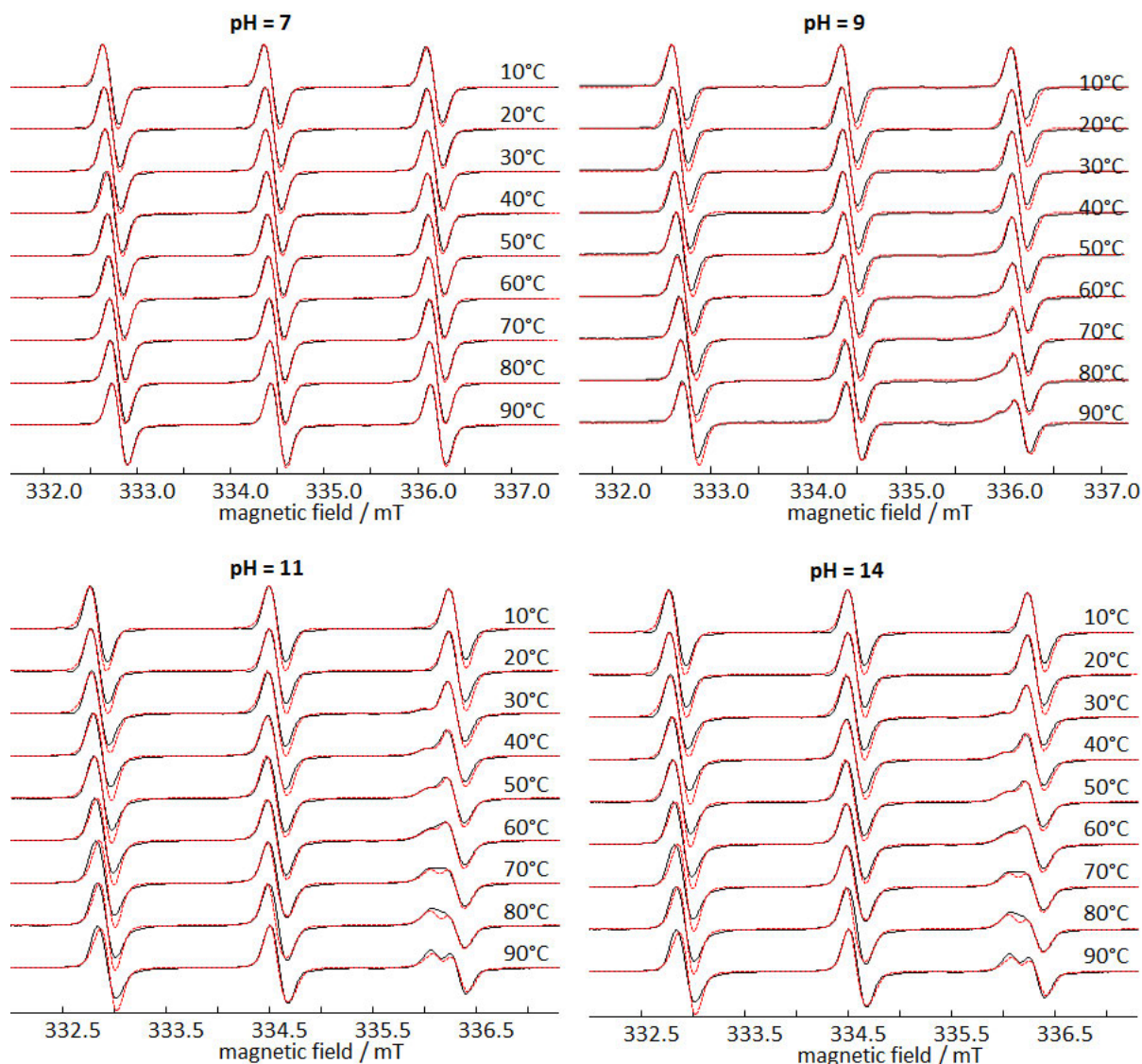


Figure S5. Experimental CW EPR spectra (black) and corresponding spectral simulations (red) between 10 °C and 90 °C at pH 7, 9, 11 and 14 of PEG-*b*-PDEGA.

- [1] a) M. Schömer, H. Frey, *Macromolecules* **2012**, 3039-3046; b) M. Schömer, J. Seiwert, H. Frey, *ACS Macro Lett.* **2012**, 1; c) V. S. Reuss, B. Obermeier, C. Dingels, H. Frey, *Macromolecules* **2012**, 45, 4581-4589; d) V. S. Reuss, M. Werre, H. Frey, *Macromol. Rapid Commun.* **2012**, 33, 1556-1561.
- [2] S. Stoll, A. Schweiger, *J. Magn. Res.* **2006**, 178, 42-55.
- [3] J. H. Freed, G. K. Fraenkel, *J. Chem. Phys.* **1983**, 39, 326-348.
- [4] B. R. Knauer, J. J. Napier, *J. Am. Chem. Soc.* **1976**, 98, 4395-4400.
- [5] C. Wu, S. Zhou, *Macromolecules* **1995**, 28, 5388-5399.
- [6] P. Alexandridis, T. A. Hatton, *Colloids Surf., A* **1995**, 96, 1-46.
- [7] M. J. N. Junk, U. Jonas, D. Hinderberger, *Small* **2008**, 4, 1485-1493.
- [8] J. A. Weil, J. R. Bolton, J. E. Weitz, *Electron paramagnetic resonance: Elementary theory and applications*, Vol. 2, Wiley-interscience, New York, **2007**.

5) CYCLIC POLYMERS

5.1) Efficient Approach to Poly(ethylene glycol) Macrocycles via Ring-Closing Metathesis

Valerie S. Reuss and Holger Frey

Published as Polymer Preprint 2011, Symposium Proceeding.

Introduction

Scientific interest in cyclic polymers¹⁻³ arose more than half a century ago with the discovery of cyclic viral^{4,5} and mitochondrial⁶ DNA. A variety of macrocycles can be obtained via ring-closing strategies. They can be classified as α, ω -homodifunctional bimolecular, α, ω -homodifunctional unimolecular, or α, ω -heterodifunctional unimolecular. Disadvantages of bimolecular ring-closure strategies include stoichiometry issues as well as the fact that the preliminary intermolecular coupling reaction, followed by the intramolecular cyclization reaction, is considerably slowed down by the dilution required for cyclization. Thus, unimolecular ring-closure is the reactive pathway of choice, eliminating the problems resulting from inexact stoichiometry and the inaugurating intermolecular coupling reaction. High dilution employed to avoid oligomerization can be used without decreasing the cyclization rate.

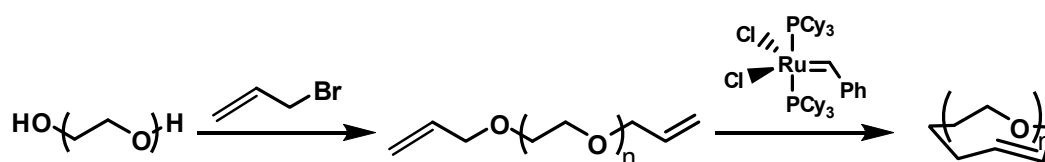
Here, we present the synthesis of macrocycles of poly(ethylene glycol) (PEG), a polymer with high potential for application in bioconjugation due to its water solubility and biocompatibility. Cyclization is achieved via ring-closing metathesis, a unimolecular ring-closure reaction tolerant toward a large variety of functional groups (**Scheme 1**).⁷⁻¹² Thus, this step can serve as a general model reaction for the macrocyclization of poly(ether) copolymers with incorporated functional monomers, leading to functional cyclic poly(ether)s. Furthermore, the generated double bond moiety in the macrocycle offers various possibilities for the defined synthesis of monofunctional PEG cycles, e.g., by thiol-ene click reaction.

Experimental

Materials. All reagents and solvents were purchased from Acros Organics or Sigma-Aldrich and used without further purification unless otherwise stated. Allyl bromide was purified according to literature procedures.¹³ Dichloromethane was dried over calcium hydride and degassed in two freeze – pump – thaw cycles. Deuterated solvents were purchased from Deutero GmbH and stored over molecular sieves (3Å).

Instrumentation. ¹H NMR spectra (300 MHz) and ¹³C NMR spectra (75.5 MHz) were recorded using a Bruker AC 300. All spectra were referenced internally to residual proton signals of the deuterated solvent. SEC measurements were carried out in dimethylformamide (DMF) containing 0.25 g/L of lithium bromide. An Agilent 1100 Series GPC Setup (gel permeation chromatography) was

used as an integrated instrument, including a PSS HEMA column ($10^6/10^5/10^4$ g/mol), a UV (254 nm), and a RI detector. Calibration was achieved using poly(ethylene glycol) standards provided by Polymer Standards Service. The eluent was used at 50 °C and at a flow rate of 1 mL/min. MALDI-ToF MS measurements were performed on a Shimadzu Axima CFR MALDI-ToF MS mass spectrometer, equipped with a nitrogen laser delivering 3 ns laser pulses at 337 nm. Dithranol (1,8-dihydroxy-9(10H)-anthracetone, 97%), was used as a matrix. Potassium triflate (98%) was added for ion formation. Good results were obtained for samples prepared from chloroform solution by mixing matrix (10 mg/mL), polymer (10 mg/mL), and salt (0.1 N solution) in a ratio of 10:1:1. A volume of 3 μ L sample solution was deposited on the MALDI target and allowed to dry at room temperature for 15 min prior to the measurement.



Scheme 1. Synthesis of cyclic PEG via ring-closing metathesis.

Synthesis of α , ω -Bisallylpoly(ethylene glycol). In a round-bottom flask, 1 g of α , ω -bishydroxypoly(ethylene glycol) ($M_w = 2000, 4000, 6000, \text{ or } 8000$ g/mol) was dissolved in 5 mL toluene. Allyl bromide (10 equiv. per OH group) and 0.75 g grinded sodium hydroxide were added. After stirring over night at 50 °C, the reaction mixture was filtered and washed twice with toluene. The solvent was evaporated under reduced pressure and the remaining solid dissolved in 10 mL water. Subsequently, 250 mg sodium chloride were added and the solution was extracted with dichloromethane (4 x 5 mL). The combined organic phases were washed with 5 mL water and dried over anhydrous sodium sulfate. The solvent was removed under reduced pressure and the product was purified by precipitation in cold diethyl ether. $^1\text{H-NMR}$ (300 MHz, $\text{DMSO-}d_6$): δ [ppm] = 5.94 – 5.81 (CH, 2 H, m), 5.27 – 5.12 ($=\text{CH}_2$, 4 H, m), 3.94 (O- CH_2 -CH, 4 H, d), 3.80 – 3.10 (CH_2 backbone, m) . $^{13}\text{C-NMR}$ (75.5 MHz, $\text{DMSO-}d_6$): δ [ppm] = 135.29 (CH), 116.24 ($=\text{CH}_2$), 71.04 (O- CH_2 -CH), 69.79 (CH_2 backbone), 69.02 (CH_2 -O-allyl) .

General Procedure for Macrocyclization via Ring-Closing Metathesis. Cyclization was carried out under an argon atmosphere. In a 1 L Schlenk flask, 500 mL of dichloromethane were degassed. Subsequently, α , ω -bisallylpoly(ethylene glycol) (100 mg, 1 equiv.) and Grubbs Catalyst 1st generation (benzylidene-bis(tricyclohexylphosphine)dichlororuthenium, 2 equiv.) were added. After refluxing

over 48 h, 3 mL ethyl vinyl ether were added and the solvent removed under reduced pressure. In order to remove catalyst, the polymer was precipitated in cold diethyl ether and isolated via centrifugation.

Purification of Cyclic Poly(ethylene glycol). The fraction of linear oligomers was determined using integration of the respective SEC elugrams. Isolation of the PEG macrocycles using α -cyclodextrin was carried out according to the literature.¹⁴

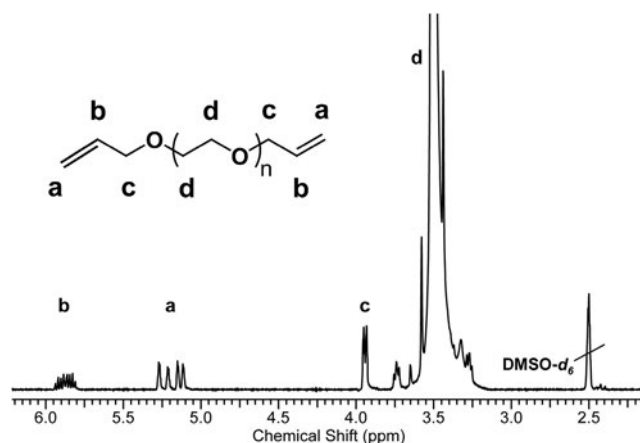


Figure 1. ^1H NMR spectrum (300 MHz, $\text{DMSO-}d_6$) of α, ω -bisallylpoly(ethylene glycol).

Results and Discussion

α, ω -Bisallylpoly(ethylene glycol). Quantitative allylation of the polymer end groups is a prerequisite for a successful, high-yield cyclization reaction. This has been achieved reacting the respective polymer with a 10-fold excess of allyl bromide in presence of sodium hydroxide in toluene, capitalizing on the ability of PEG to function as an emulsifier and phase transfer agent itself, superseding the use of phase transfer catalysts.

The absence of hydroxyl terminated PEG chains could be proven by ^1H and ^{13}C NMR spectroscopy as well as MALDI–ToF mass spectrometry. The ^1H NMR spectrum of one polymer of the series can be seen in **Figure 1**. In line with expectation, SEC shows a slight increase in molecular weight (**Figure 2**).

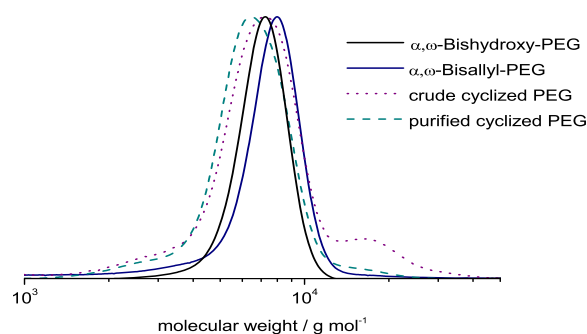


Figure 2. SEC traces (DMF, RI detection, PEG standards) of α,ω -bishydroxypoly(ethylene glycol), α,ω -bisallylpoly(ethylene glycol), crude, and purified cyclized polyethylene glycol.

Macrocyclization via Ring-Closing Metathesis. The ring-closure reaction was carried out in analogy to the conditions applied in the synthesis of cyclic poly(tetrahydrofuran).⁹ Successful ring-closure can be deduced from size exclusion chromatography. Since cyclic polymers exhibit a smaller hydrodynamic volume than their linear counterparts, their apparent molecular weight determined via SEC decreases during this reaction, see **Figure 2**. The crude cyclization product still contains linear dimers of the precursor polymer, as can be deduced from the high molecular weight shoulder. The percentage of these side products can be estimated using the integral of the SEC elugrams, being in the range 8 – 20% depending on the ring size.

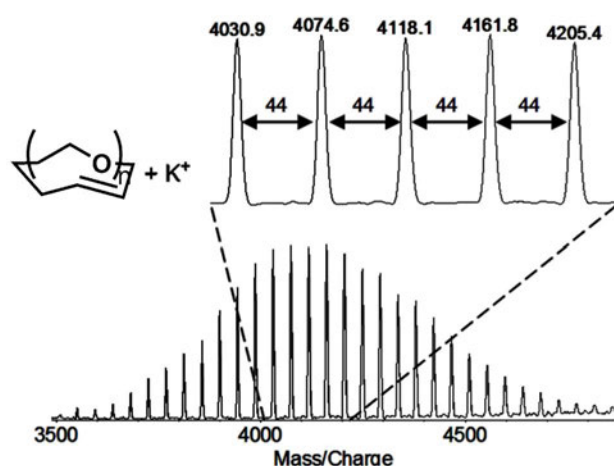


Figure 3. MALDI-ToF spectrum of purified cyclized poly(ethylene glycol) (SEC: $M_n = 5900$ g/mol; $M_w/M_n = 1.14$).

Purification of Cyclic Poly(ethylene glycol). The linear side products, both oligomerized precursor polymers and unreacted starting material, can be readily removed using α -cyclodextrin (α -CD), a cyclic sugar derivative forming inclusion complexes with linear poly(ethylene glycol).¹⁵ Successful purification can be followed by SEC (**Figure 2**).

Subsequent to the purification step, ring-closure can be verified in MALDI-ToF mass spectrometry, proving conversion of the linear precursor to a monocyclic product (**Figure 3**).

Conclusions

The synthesis of cyclic poly(ethylene glycol) of different ring sizes bearing one double bond moiety in the ring could be accomplished. Cyclization as well as removal of linear side products using α -cyclodextrin could be qualitatively and quantitatively proven by size exclusion chromatography and MALDI-ToF mass spectrometry. This strategy provides defined monofunctional PEG macrocycles, which can be applied in conjugation chemistry. Furthermore, it can serve as a model pathway for ring-closure of functionalized poly(ether) copolymers in general.

Acknowledgment

V.S.R. is grateful to the Fonds der Chemischen Industrie (FCI) for a fellowship and to the Gutenberg-Akademie der Johannes Gutenberg-Universität Mainz as well as the Gesellschaft Deutscher Chemiker (GDCh) for financial support.

References

- [1] Laurent, B. A.; Grayson, S. M. *Chem. Soc. Rev.* **2009**, *38*, 2202.
- [2] Deffieux, A.; Borsali, R., Controlled Synthesis and Properties of Cyclic Polymers. In *Macromolecular Engineering*, Matyjaszewski, K.; Gnanou, Y.; Leibler, L., Eds. Wiley-VCH Verlag GmbH & Co. KG: Weinheim, 2007; pp 875.
- [3] Endo, K. *Adv. Polym. Sci.* **2008**, *217*, 121.
- [4] Dulbecco, R.; Vogt, M. *Proc. Natl. Acad. Sci. U. S. A.* **1963**, *50*, 236.
- [5] Weil, R.; Vinograd, J. *Proc. Natl. Acad. Sci. U. S. A.* **1963**, *50*, 730.
- [6] Clayton, D. A.; Vinograd, J. *Nature* **1967**, *216*, 652.
- [7] Honda, S.; Yamamoto, T.; Tezuka, Y. *J. Am. Chem. Soc.* **2010**, *132*, 10251.
- [8] Xie, M.; Shi, J.; Ding, L.; Li, J.; Han, H.; Zhang, Y. *J. Polym. Sci., Part A: Polym. Chem.* **2009**, *47*, 3022.
- [9] Tezuka, Y.; Ohtsuka, T.; Adachi, K.; Komiya, R.; Ohno, N.; Okui, N. *Macromol. Rapid Commun.* **2008**, *29*, 1237.
- [10] Adachi, K.; Honda, S.; Hayashi, S.; Tezuka, Y. *Macromolecules* **2008**, *41*, 7898.
- [11] Hayashi, S.; Adachi, K.; Tezuka, Y. *Chem. Lett.* **2007**, *36*, 982.
- [12] Tezuka, Y.; Komiya, R. *Macromolecules* **2002**, *35*, 8667.
- [13] Perrin, D. D.; Armarego, W. L. F. In *Purification of Laboratory Chemicals* Pergamon Press: Oxford, **1988**.
- [14] Singla, S.; Zhao, T.; Beckham, H. W. *Macromolecules* **2003**, *36*, 6945.
- [15] Harada, A.; Li, J.; Kamachi, M. *Macromolecules* **1993**, *26*, 5698.

APPENDIX

A.1) Multihydroxy-Functional Polysilanes via an Acetal Protecting Group Strategy

Valerie S. Reuss and Holger Frey

Reproduced from Macromolecules **2010**, *43*, 8462-8467.

Multihydroxy-Functional Polysilanes via an Acetal
Protecting Group Strategy

Valerie S. Reuss and Holger Frey*

Department of Organic Chemistry, Johannes Gutenberg-Universität Mainz, Duesbergweg 10-14, 55099 Mainz, Germany

Received July 25, 2010; Revised Manuscript Received September 10, 2010

ABSTRACT: A new acetal-protected monomer for Wurtz-type coupling to polysilanes, dichloro(3-(2,2-dimethyl-1,3-dioxolane-4-yloxy)propyl)methylsilane, referred to as dichloro(isopropylidene glyceryl propyl ether)methylsilane (DCIMS), has been introduced to synthesize a series of protected linear polysilane copolymers, poly[di-*n*-hexylsilane-*co*-(isopropylidene glyceryl propyl ether)methylsilane] (P(DHS-*co*-IMS)) via alkali-mediated reductive Wurtz-type coupling. The acetal protecting group proved stable under the harsh polymerization conditions. Differential scanning calorimetry combined with ^1H , ^{13}C , and ^{29}Si NMR measurements confirmed composition and random structure of the obtained copolymers. After separation of the cyclic fraction, this route yielded defined linear polysilane copolymers with monomodal molecular weight distributions (2000–98700 g mol $^{-1}$ (SEC)) and polydispersities in the range 1.61–2.60. Subsequent cleavage of the acetal protecting groups under acidic conditions resulted in the multihydroxy-functional polysilanes poly[di-*n*-hexylsilane-*co*-(glyceryl propyl ether)methylsilane] (P(DHS-*co*-GMS)).

Introduction

Polysilanes, $^{1-3}$ sometimes called polysilylenes, consist of a one-dimensional silicon backbone with organic substituents and exhibit extraordinary electronic and photophysical properties such as UV absorption, 2 thermochromism, 4 solvatochromism, 5 and electroluminescence, 6 caused by the delocalization of the σ -electrons along the Si-chain. Because of these unique characteristics, polysilanes have attracted broad attention in academia and industry in the last 2 decades. They can be used as functional materials in semiconductors, radical photoinitiators, precursors for silicon carbide syntheses, and sensors. 6 Variation of substituents and copolymerization of different dichlorodiorganosilanes SiCl_2R_2 offers countless possibilities for tailoring chemical and physical properties, e.g., solubility, morphology, and optical characteristics. $^{7-9}$ Optically active polysilanes have been obtained by polymerizing monomers with enantiopure chiral side groups, 10 which, among other things, can be used for chiroptical switching and memory systems for data storage. 11 Functional polysilanes have rarely been described, since the main synthetic route to polysilanes via sodium-mediated reductive Wurtz coupling of SiCl_2R_2 is inherently intolerant toward functional groups. 12 Oftentimes, post-polymerization functionalization sequences have to be employed.

In consequence, only few functional polyorganosilanes are known to date. For example, trimethylammonium moieties bound to phenethyl substituents have been reported by Seki et al. 13 Aromatic hydroxyl functionalities at polysilanes have been introduced by way of trimethoxysilane protected phenols by Horiguchi et al. 14 Möller and co-workers 15 employed polymer modification reactions including hydrosilylation with unsaturated polysilane substituents to generate aliphatic hydroxyl substituents.

Ether moieties are known to be stable under the harsh polymerization conditions of the Wurtz coupling reaction. $^{16-21}$ Thus, ether-substituted polysilanes can be obtained from the

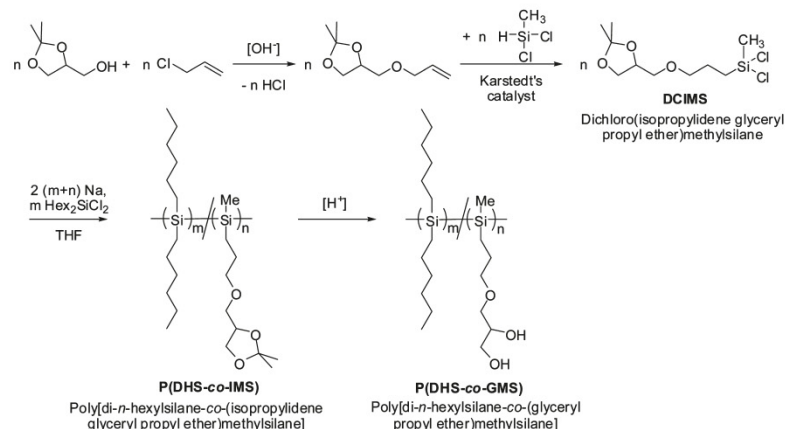
corresponding dichlorosilane monomers directly. However, it is crucial that the position of the ether moiety is chosen at least three methylene units away from the silicon backbone to avoid possible β -elimination of the electron-withdrawing group during polymerization. 21 The obtained polymers show enhanced solubility in polar solvents such as alcohols and ethers. These mostly viscous substances do not exhibit the typical bulk properties of poly(di-*n*-alkylsilanes), namely crystallization and formation of a columnar mesophase. For instance, poly(di-*n*-hexylsilane) (PDHS), soluble in nonpolar organic solvents only, approximates a trans-planar conformation of the backbone at room temperature. 22 At 45 °C, a transition to a liquid-crystalline, hexagonal columnar mesophase (hcm) with conformational disorder of the side chains takes place, which can be followed by calorimetric measurements (DSC) or UV spectroscopy as well as many other techniques.

The preparation of polar polysilanes containing randomly distributed OH groups at the backbone has remained a challenge to date, mostly because of the inherently sensitive chemistry entailed by the synthetic approaches. Such materials could provide fascinating potential in the field of polysilane-based networks or hydrogels with unusual electrooptical properties. Multiple hydroxyl moieties attached to the linear polymer chain should also provide intriguing possibilities for further functionalization sequences and the synthesis of complex macromolecular architectures.

Here we present the synthesis and characterization of multihydroxy-functional polysilane copolymers (Scheme 1). To the best of our knowledge, the employed sequential acetal protecting group strategy has not been used in polysilane synthesis to date. The protected substituents of a new monomer, dichloro(3-(2,2-dimethyl-1,3-dioxolane-4-yloxy)propyl)methylsilane, which will be referred to as dichloro(isopropylidene glyceryl propyl ether)methylsilane (DCIMS) for reasons of simplicity and clarity, release the desired functional groups upon deprotection, thus offering numerous pathways to entirely new polysilane-based materials.

*Corresponding author. E-mail: hfrey@uni-mainz.de.

Scheme 1. Synthesis of P(DHS-co-IMS) and P(DHS-co-GMS) Copolymers



Experimental Section

Instrumentation. ^1H NMR spectra (300 MHz) and ^{13}C NMR spectra (75.5 MHz) were recorded using a Bruker AC 300. All spectra were referenced internally to residual proton signals of the deuterated solvent. ^{29}Si NMR spectra (79.5 MHz) were obtained on a Bruker AMX 400. Size exclusion chromatography (SEC) measurements were performed on a setup consisting of a Waters 717 plus Autosampler, a TSP Spectra Series P 100 pump, and three PSS-HEMA-5 μL -columns with 100, 1000, and 10000 Å pore diameter, respectively. THF was used as an eluent at 30 °C and at a flow rate of 1 mL/min. UV absorptions were detected by a SpectraSYSTEM UV2000. The specific refractive index increment (dn/dc) was measured at 30 °C, using an Optilab DSP interferometric refractometer (also RI detector) and determined with the Wyatt ASTRA IV software (Version 4.90.08). Calibration was carried out using poly(styrene) standards provided by Polymer Standards Service. DSC measurements were carried out using a Perkin-Elmer DSC 7 with a Perkin-Elmer thermal analysis controller TAC7/DX in the temperature range of -100 to $+100$ °C using heating rates of 40 and 20 K/min for the copolymer samples and 40 and 5 K/min for the PDHS sample. The melting points of indium ($T_m = 156.6$ °C) and Millipore water ($T_m = 0$ °C) were used for calibration. Polarized light microscopy was carried out using a Leitz Ortholux II POL-BK microscope with crossed polarizers. Sodium dispersions were prepared using an EuroTurrax T20b homogenizer purchased from IKA Labortechnik.

Materials. All reagents and solvents were purchased from Acros Organics or Sigma-Aldrich and used without further purification unless otherwise stated. Solvents for the polymerizations (THF, xylene) were purified according to literature procedures.²³ Dry chlorobenzene over molecular sieves was purchased from Fluka. Karstedt's catalyst, platinum(0)-divinyltetramethyldisiloxane complex (in xylene, 2.1–2.4% Pt), and dichlorodi-*n*-hexylsilane (DCDHS) were obtained from ABCR GmbH & Co. KG. DCDHS was purified by fractionating distillation prior to use. Allyl solketyl ether was prepared according to the literature.²⁴ Deuterated solvents were purchased from Deutero GmbH and stored over molecular sieves (3 Å).

Monomer Preparation: Dichloro(isopropylidene glyceryl propyl ether)methylsilane (DCIMS). The synthesis was carried out under argon atmosphere. Allyl solketyl ether (2.60 g, 15.1 mmol, 1 equiv) was placed in a Schlenk flask. Chlorobenzene (3.5 mL), 90 μL of Karstedt's catalyst solution, and 3.5 mL of dichloromethylsilane (33.5 mmol, 2.2 equiv) were added via syringe.

After stirring at room temperature overnight, excess dichloromethylsilane and chlorobenzene were removed under reduced pressure. Fractional distillation (105 °C/0.001 mbar) yielded 2.36 g (54%) of colorless oil. ^1H NMR (300 MHz, CDCl_3): δ [ppm] = 4.28 (quintuplet, 1 H, $^3J = 9$ Hz, CH), 4.07 (dd, 1 H, $J_{AB} = 9$ Hz, $^3J = 6$ Hz, CH-CH'H''-O-C(CH₃)₂), 3.74 (dd, 1 H, $J_{AB} = 9$ Hz, $^3J = 6$ Hz, CH-CH'H''-O-C(CH₃)₂), 3.56–3.42 (m, 4 H, CH₂-O-CH₂), 1.85–1.75 (m, 2 H, Si-CH₂-CH₂), 1.43 (s, 3 H, CH₃), 1.37 (s, 3 H, CH₃), 1.20–1.14 (m, 2 H, Si-CH₂), 0.79 (s, 3 H, Si-CH₃). ^{13}C NMR (75.5 MHz, CDCl_3): δ [ppm] = 109.37 (s, C(CH₃)₂), 74.65 (s, CH), 72.64 (s, Si-(CH₂)₂-CH₂), 71.80 (s, CH₂-O-CH₂-CH), 66.73 (s, CH-CH₂-O-C(CH₃)₂), 26.70 (s, CH₃), 25.36 (s, CH₃), 22.63 (s, Si-CH₂-CH₂), 18.00 (s, Si-CH₂), 5.11 (s, Si-CH₃).

General Procedures for the Copolymerization of DCIMS and DCDHS. In a glovebox, 0.828 g (36 mmol, 2 equiv) sodium and 20 mL xylene were placed in a Schlenk flask, transferred to the vacuum line, and heated to 135 °C. The mixture was transformed into a fine dispersion using a preheated homogenizer (EuroTurrax T20b, IKA Labortechnik). After evaporation of xylene in high vacuum, 20 mL of THF and 0.018 mol of dichlorodiorganosilane were added via syringe. The mixture turned purple after 30 min and was stirred vigorously for 22 h at room temperature. The reaction was then quenched with 120 mL of methanol. The precipitated polymer was filtered, washed with water and methanol, and dried in high vacuum. The cyclic fraction was separated via fractional precipitation from THF/2-propanol. Yields: 21–50%. ^1H NMR (300 MHz, CDCl_3): δ [ppm] = 4.35–4.15 (CH), 4.15–3.95 (CH-CH'H''-O-C(CH₃)₂), 3.85–3.65 (CH-CH'H''-O-C(CH₃)₂), 3.65–3.20 (CH₂-O-CH₂), 1.80–1.55 (CH₃-Si-CH₂-CH₂), 1.55–0.50 (C(CH₃)₂, Si-(CH₂)₄-CH₃, and CH₃-Si-CH₂), 0.40–0.25 (Si-CH₃). ^{13}C NMR (75.5 MHz, CDCl_3): δ [ppm] = 109.13 (C(CH₃)₂), 74.54 (CH), 71.94 (Si-(CH₂)₂-CH₂-O), 67.80 (O-CH₂-CH), 67.02 (CH-CH₂-O-C(CH₃)₂), 34.28 (Si-(CH₂)₂-CH₂-Pr), 31.72 (Si-(CH₂)₃-CH₂-Et), 27.42 (Si-CH₂-CH₂-Bu), 26.66 (C(CH₃)₃), 25.49 (Si-CH₂-CH₂-CH₂-O), 25.28 (C(CH₃)₃), 22.74 (Si-(CH₂)₄-CH₂-Me), 14.95 (Si-CH₂-(CH₂)₂-O), 14.00 (Si-(CH₂)₅-CH₃), 10.41 (Si-CH₂-CH₂-Bu), -3.34 (Si-CH₃). ^{29}Si NMR (79.5 MHz, CDCl_3): δ [ppm] = -24.5 to -27.0 (Hex-Si), -29.5 to -32.5 (MeSiR).

Cleavage of Acetal Protecting Groups. In a round-bottom flask, 400 mg P(DHS-co-IMS) were dissolved in 400 mL THF (dest.). Subsequently, 12 mL of trifluoroacetic acid and 8 mL of water were added. After refluxing for 72 h, the solution was neutralized with saturated K₂CO₃ solution and filtered. The volatiles were removed under reduced pressure. The residue was

dispersed in chloroform, filtered, and the solvent removed under reduced pressure. Yields: $\geq 95\%$. $^1\text{H NMR}$ (300 MHz, CDCl_3): δ [ppm] = 3.95–3.80 ($\text{CH}-\text{OH}$), 3.75–3.65 ($\text{CH}-\text{CH}'\text{H}''-\text{OH}$), 3.65–3.55 ($\text{O}-\text{CH}'\text{H}''-\text{CH}$), 3.55–3.25 ($\text{CH}-\text{CH}'\text{H}''-\text{OH}$, $\text{O}-\text{CH}'\text{H}''-\text{CH}$, and $\text{Si}-(\text{CH}_2)_2-\text{CH}_2-\text{O}$), 1.85–1.55 ($\text{CH}_3-\text{Si}-\text{CH}_2-\text{CH}_2$), 1.55–0.60 ($\text{Si}-(\text{CH}_2)_4-\text{CH}_3$, and $\text{CH}_3-\text{Si}-\text{CH}_2$), 0.45–0.25 ($\text{Si}-\text{CH}_3$).

Results and Discussion

Monomer Synthesis. In order to obtain multihydroxy-functional polysilanes, a monomer containing a protected hydroxyl group had to be designed that both withstands the conditions of the polysilane formation in the Wurtz-type coupling reaction and can be deprotected easily subsequent to polymer synthesis. The accordingly developed synthetic strategy affording the new acetal protected monomer dichloro(isopropylidene glyceryl propyl ether)methylsilane (DCIMS) for Wurtz-type polymerization is shown in Scheme 1. The isopropylidene acetal group is stable toward most reaction conditions except for protic media and Lewis acids. Therefore, it serves as an ideal candidate for survival of the reductive conditions during polysilane formation and subsequent acidic cleavage to release the desired hydroxyl functionalities and acetone.

Starting from allyl chloride and solketal ((2,2-dimethyl-1,3-dioxolane-4-yl)methanol), the monomer was synthesized in two steps. First, the corresponding allyl solketyl ether was obtained by Williamson ether synthesis, followed by a hydrosilylation reaction with dichloromethylsilane in presence of Karstedt's catalyst, platinum(0)-divinyltetramethyldisiloxane, resulting in the desired acetal protected silane with a yield of 54% after optimization of reaction conditions. The hydrosilylation product was purified by fractional distillation, which was difficult due to the formation of side products at elevated temperatures ($\geq 140^\circ\text{C}$), indicated by a color change to dark yellow or brown, diminishing yield and purity of the obtained monomer. This phenomenon is well-known in silane chemistry and has already been reported for dichlorosilane monomers containing ether linkages.^{17,21} This detrimental behavior has been proposed to be caused by inter- and intramolecular reactions of the polar $\text{Si}-\text{Cl}$ bonds with the oxygen atoms in the substituents, leading to thermodynamically favored $\text{Si}-\text{O}$ bonds as well as $\text{C}-\text{Cl}$ compounds. Only freshly distilled DCIMS was used for all further reactions and characterization due to the limited shelf life of the monomer. After 2 days storage under argon at 6°C , the liquid turned dark yellow to brown, indicating the side reactions described above taking place. An NMR spectrum of the new monomer is shown in Figure 1 and detailed in the Supporting Information.

Polymer Synthesis. The dichlorosilanes were polymerized using a dispersion of sodium in THF at room temperature. This approach was chosen because of the superior yields compared to classical Wurtz coupling polymerization with molten sodium in refluxing toluene¹⁵ (Table 1). The dispersion was prepared in analogy to the method described by Jones and co-workers,²⁵ replacing toluene with xylene because of the higher boiling point of this solvent. This prevents solidification of sodium contacting the inserted homogenizer, which is externally preheated to approximately 200°C for this reason. Furthermore, this change of solvent obviously reduces the danger of solvent vapor ignition.

Polymer Characterization. The polysilanes were obtained as colorless, crystalline to amorphous, highly viscous compounds. The characterization data of the obtained P(DHS-*co*-IMS) copolymers and the respective homopolymers are listed in Table 1. The corresponding SEC elugrams can be

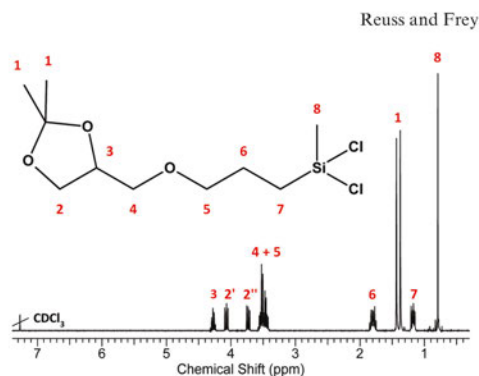


Figure 1. $^1\text{H NMR}$ spectrum (CDCl_3 , 300 MHz) of dichloro(isopropylidene glyceryl propyl ether)methylsilane (DCIMS) and peak assignment.

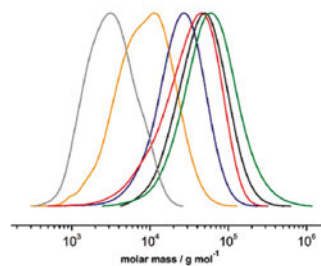


Figure 2. SEC elugrams of the polysilane copolymer series (THF, PS standards): PDHS (red); P(DHS-*co*-IMS) (6%, green; 11%, blue; 17%, black; 40%, yellow); PIMS (gray).

Table 1. Characterization Data for Polysilane Homo- and Copolymers

polymer	solvent	content ^a / %	M_w ^b / g mol^{-1}	PDI ^b	yield ^c / %
PDHS	toluene	0 (0)	98 700	2.60	17
	THF	0 (0)	60 700	2.34	58
P(DHS- <i>co</i> -IMS)	toluene	7 (10)	51 900	2.09	1
	THF	6 (10)	63 100	2.00	47
		11 (20)	30 700	1.60	24
		17 (30)	57 900	1.72	21
PIMS	THF	40 (50)	11 700	1.93	34
		100 (100)	2000	1.30	50 ^d
		100 (100)	4000	1.61	10

^a DCIMS content determined via $^1\text{H NMR}$ spectroscopy after separation of the cyclic fraction by fractionating precipitation. The value in parentheses denotes the DCIMS fraction in the monomer feed. ^b Determined by SEC in THF, polystyrene standards, RI detection. ^c After separation of the cyclic fraction by fractionating precipitation. ^d Separation of the cyclic from the linear fraction not possible due to similar molecular weights. ^e Polymer synthesis was carried out using C_8K in THF at room temperature.²⁶

seen in Figure 2, showing monomodal distributions with polydispersities in the range 1.61–2.60, which represent typical values for polysilane structures. Molecular weights were in the range 2000–98700 g mol^{-1} .

With increasing DCIMS fraction, the preparation of copolymers with high molecular weight became increasingly difficult. This might be due to an alteration of the solution equilibrium at the sodium surface by the polar substituents, similar to the previously reported effect observed after adding ethylene glycol (glyme) or diethylene glycol dimethyl

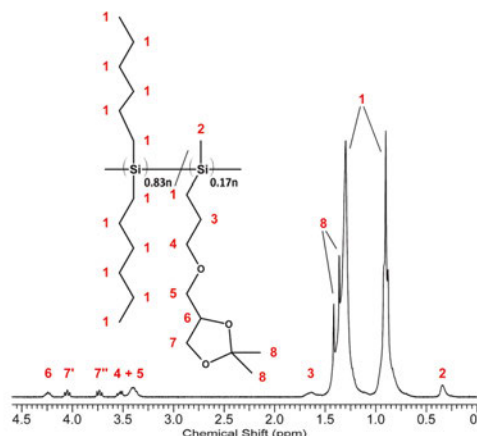


Figure 3. ^1H NMR spectrum (CDCl_3 , 300 MHz) of P(DHS-*co*-IMS) (17% IMS content) and peak assignment.

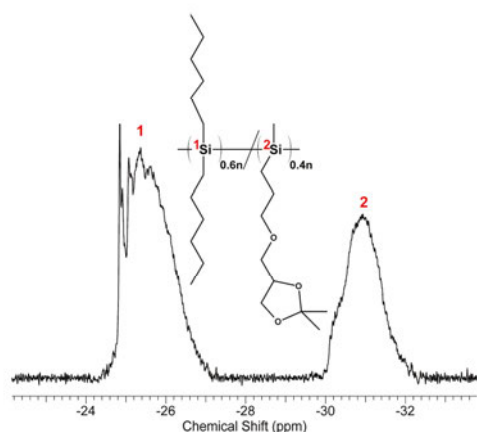


Figure 4. Inverse gated ^{29}Si NMR spectrum (CDCl_3 , 79.5 MHz) of P(DHS-*co*-IMS) (40% IMS content) and peak assignment.

ether (diglyme) to the heterogeneous reaction mixture of a poly(dialkylsilane) synthesis, resulting in a rapid reduction of molecular weight of the product.²⁷

The assignment of the ^1H and ^{13}C NMR signals of the protected polysilane copolymers P(DHS-*co*-IMS) was performed in analogy to the monomer spectra, taking the upfield shift of the units directly bound to the silicon backbone induced by the removal of the electron-withdrawing chlorine atoms into account, see Figure 3 and the Supporting Information.

^{29}Si NMR spectroscopy is a powerful tool for the determination of the microstructure of polysilane copolymers with respect to the distribution of comonomer units in the backbone. The spectrum of a copolymer with 40% DCIMS content is exemplarily shown in Figure 4. Two broad signals at -24.5 to -27 ppm and -30 to -32.5 ppm can be seen. Only a small sharp signal at -24.85 ppm is visible, induced by longer runs of directly connected di-*n*-hexylsilane repeating units. The intensity of this signal decreases with increasing comonomer content (5%

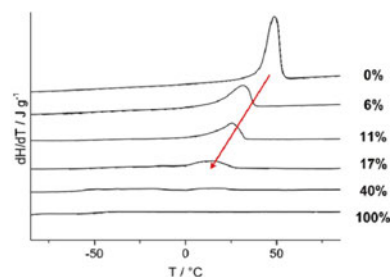


Figure 5. DSC traces of the second heating run for P(DHS-*co*-IMS) copolymers with IMS fractions from 0 to 100%, as denoted to the right of each trace. The arrow indicates the decrease of the transition temperature to the conformationally disordered mesophase with increasing fraction of IMS.

for the observed polymer). The asymmetry of the (isopropylidene glyceryl propyl ether)methylsilane building blocks adjacent to the other di-*n*-hexylsilane units generates the broad signal at -24.5 to -27 ppm, which possesses a considerably higher intensity than the sharp signal of the homoruns. This indicates a predominantly random composition of the P(DHS-*co*-IMS) copolymers interrupted by few di-*n*-hexylsilane homosequences only. The observed broad resonance around -31 ppm supports this conclusion, since it can be assigned to the IMS units. The chemical shift of the silicon atoms incorporated in polysilanes is influenced by the chain conformation and therefore by steric effects of the substituents. If a large steric constraint is imposed on the Si atom, a downfield shift can be observed.²⁸ According to the ^{29}Si NMR spectrum, repeat units emerging from DCIMS are sterically less demanding than di-*n*-hexylsilane units, presumably due to the monosubstitution of the DCIMS with the bulky side chain. Surprisingly, the sterically less demanding monomer DCIMS seems to be present at a higher percentage in the cyclic than in the linear fraction, comparing ^1H NMR spectra of the samples before and after work-up. The remaining difference between monomer feed ratio and incorporation ratio, existent even before separation of the cyclic oligomers, can be explained by slow decomposition of DCIMS monomer during the extended reaction time (22 h) by the side reactions discussed above.

Polysilanes with symmetric alkyl side chain substitution pattern have long been known to exhibit unusual mesomorphic behavior, forming conformationally disordered mesophases with hexagonal columnar order. Thus, it was an intriguing issue in the context of this work to investigate the thermal properties of the obtained P(DHS-*co*-IMS) copolymers with IMS fractions ranging from 0 to 100%, using differential scanning calorimetry (DSC). The main differences in properties could be seen with the naked eye, the PDHS being a crystalline powder, while incorporation of IMS generally led to a colorless, viscous material. The corresponding DSC traces of the copolymers with varying fractions of IMS are depicted in Figure 5, and the corresponding calorimetric data are listed in Table 2. While pure PDHS shows the typical endothermic phase transition from crystalline to a liquid-crystalline hexagonal columnar mesophase at 45 °C,²² a gradual decrease of the transition temperature as well as transition enthalpy is observed for the P(DHS-*co*-IMS) copolymers. This is caused by the comonomer-induced irregularities and consequent disturbance of the crystalline order in comparison to PDHS. The gradual character of the decrease of both transition temperature and enthalpy with increasing comonomer fraction represents another confirmation for the existence of random P(DHS-*co*-IMS) copolymers. To exclude the possibility of PDHS homopolymer fractions in the copolymer samples

Table 2. Calorimetric Data for Polysilane Homo- and Copolymers (DSC)

polymer	fraction ^a /%	T_g ^b /°C	T_p ^b /°C	ΔH^c /J g ⁻¹
PDHS	0		45	92
P(DHS-co-IMS)	7	-46	31	54
	11	-48	26	32
	17	-47	15	16
	40	-58		
P(DHS-co-GMS)	17	-46	29	17
PIMS	100	-48		

^aDCIMS fraction determined via ¹H NMR spectroscopy after separation of the cyclic fraction by fractional precipitation. ^bPeak temperature of the endothermic transition observed in the second heating run of the DSC measurements. ^cEnthalpy of the endothermic transition determined via DSC (second heating run). The determination of the exact enthalpy is impeded by the broadness of the phase transition.

causing an error in DSC characterization, 50 wt % mixtures of PDHS and P(DHS-co-IMS) with 17 and 40% IMS fraction, respectively, were also measured. The DSC traces showed the combined thermal behavior of both components and immiscibility due to crystallization, indicating once more absence of PDHS homopolymer in the copolymer samples.

Remarkably, copolymers with IMS fractions up to 17% are still capable of forming mesophases above the respective transition temperature. The anisotropic character was confirmed by polarized light microscopy using crossed polarizers, demonstrating birefringence above the disordering temperature. The observed phase transition is fully reversible, showing the expected hysteresis of the transition temperatures due to kinetically controlled nucleation. Furthermore, a glass transition temperature of approximately -48 °C was observed after incorporation of DCIMS monomer in a polysilane sample, indicating an increasing amorphous fraction. In line with expectation, P(DHS-co-IMS) samples with more than 40% IMS fraction were not able to form a mesophase and were obtained as amorphous isotropic materials above the glass transition temperature, as confirmed by polarized light microscopy. The thermal behavior of the materials after deprotection will be discussed below.

Cleavage of Acetal Protecting Groups. The deprotection is exemplified here for the copolymer containing 17% DCIMS. Since the polysilane backbone has been described as acid-sensitive,²⁹ mild conditions were initially employed to cleave the acetal protecting groups of the polysilane copolymers while avoiding degradation of the polysilane chain. Systems consisting of 1 M HCl, concentrated HCl, BCl₃, and the acidic ion-exchanger Dowex 50WX8 did not prove successful. Release of the hydroxyl groups was eventually achieved by refluxing the respective copolymer in THF and water with trifluoroacetic acid for 72 h. The difficulties in deprotection may be explained by the pronounced shielding effect of the nonpolar, superiorly soluble *n*-hexyl substituents. The cleavage of 90% of the protecting groups was proven by ¹H NMR spectroscopy by the disappearance of the respective methyl protons (see Supporting Information). SEC analysis yielded a shift in molecular weight from $M_w(\text{protected}) = 57900 \text{ g mol}^{-1}$ to $M_w(\text{deprotected}) = 45000 \text{ g mol}^{-1}$, a value smaller than the estimated M_w based on the loss of the protecting groups. This is tentatively explained by the interactions between the released hydroxyl groups and the polar SEC column material, causing a slower elution of the deprotected polymer and a smaller apparent molecular weight. No degradation of the polysilane main chain took place, confirmed by virtually unaltered polydispersities (1.72 and 1.73, respectively). The obtained glycerol-functional polysilanes show remarkable stability versus acids and solubility in polar solvents, such as 2-propanol, which cannot be used for precipitation any more.

Concerning the thermal properties of the deprotected compounds, it had been expected that the phase transition temperature to the mesophase would be at comparable or lowered temperatures upon deprotection due to the hydroxyl moieties, which are immiscible with the nonpolar surroundings, thereby destabilizing the crystalline packing. Comparing the DSC traces of the polymer before and after deprotection, it can be noted that the glass transition temperature T_g remains almost constant, while the phase transition temperature to the thermotropic mesophase increases by 14 K to 29 °C. This leads to the conclusion that the stability of the crystalline order has been increased by release of the hydroxyl moieties. Shortening of the substituents and loss of sterically demanding cyclic units after deprotection may disturb the packing of the chains less than in the case of the protected comonomer. Furthermore, formation of hydrogen bonds between the hydroxyl moieties and the subsequent order stabilizing effect through noncovalent interactions may have a similar influence.

Conclusions

The synthesis of a novel functional dichlorosilane monomer, dichloro(isopropylidene glyceryl propyl ether)methylsilane, and its subsequent copolymerization with dichloro*n*-hexylsilane, yielding linear, functional polysilanes of moderate polydispersity has been accomplished. The random character of the copolymer series has been confirmed using NMR spectroscopy and is also reflected by the thermal properties observed by DSC measurements. The acetal protecting group strategy has been successfully employed to obtain a series of polysilane copolymers bearing hydroxyl moieties. This pathway provides versatile access to new multifunctional polysilanes and unusual polysilane-based structures, such as hydrogels and polysilane nanoparticles. Work in this direction is currently in progress.

Acknowledgment. The authors of this paper thank the COMATT (Rhineland-Palatinate) initiative for financial support. V.S.R. is grateful to the Fonds der Chemischen Industrie (FCI) for a fellowship and to the Graduate School of Excellence MAINZ for financial support.

Supporting Information Available: Figures showing polymer samples, NMR spectra and signal assignment, and additional DSC traces and an equation showing the calculation of the IMS content. This material is available free of charge via the Internet at <http://pubs.acs.org>.

References and Notes

- Miller, R. D.; Michl, J. *Chem. Rev.* **1989**, *89*, 1359–1410.
- West, R. *J. Organomet. Chem.* **1986**, *300*, 327–346.
- Matyjaszewski, K.; Cypriak, M.; Frey, H.; Hrkach, J.; Kim, H. K.; Möller, M.; Ruel, K.; White, M. *J. Macromol. Sci., Pure Appl. Chem.* **1991**, *28*, 1151–1176.
- Mark, J. E.; Allcock, H. R.; West, R., *Inorganic polymers*, 2nd ed.; Oxford Univ. Press: Oxford, U.K., 2005; p XIV, 338 S.
- Oka, K.; Fujie, N.; Nakanishi, S.; Takata, T.; West, R.; Dohmaru, T. *J. Organomet. Chem.* **2000**, *611*, 45–51.
- West, R.; Menescal, R.; Asuke, T.; Eveland, J. *J. Inorg. Organomet. Polym.* **1992**, *2*, 29–45.
- Naito, M.; Fujiki, M. *Soft Matter* **2008**, *4*, 211–223.
- Frey, H.; Möller, M.; Matyjaszewski, K. *Macromolecules* **1994**, *27*, 1814–1818.
- Frey, H.; Möller, M.; Turetskii, A.; Lotz, B.; Matyjaszewski, K. *Macromolecules* **1995**, *28*, 5498–5506.
- Fujiki, M. *Macromol. Rapid Commun.* **2001**, *22*, 539–563.
- Ohira, A.; Okoshi, K.; Fujiki, M.; Kunitake, M.; Naito, M.; Hagihara, T. *Adv. Mater.* **2004**, *16*, 1645–1650.
- Koe, J. *Polym. Int.* **2009**, *58*, 255–260.

Article

Macromolecules, Vol. 43, No. 20, 2010 **8467**

- (13) Seki, T.; Tamaki, T.; Ueno, K. *Macromolecules* **1992**, *25*, 3825–3826.
- (14) Horiguchi, R.; Onishi, Y.; Hayase, S. *Macromolecules* **1988**, *21*, 304–309.
- (15) Schwegler, L. A.; Meyer-Pundsack, C.; Möller, M. *J. Polym. Sci., Part A: Polym. Chem.* **2000**, *38*, 2306–2318.
- (16) Schwegler, L. A.; Möller, M.; Schmitz, P.; Gruler, H.; Müller, J.; Pietralla, M. *Macromol. Chem. Phys.* **1998**, *199*, 1865–1871.
- (17) Schwegler, L. A.; Möller, M. *Macromol. Chem. Phys.* **1998**, *199*, 1859–1864.
- (18) Frey, H.; Out, G. J. J.; Möller, M.; Greszta, D.; Matyjaszewski, K. *Macromolecules* **1993**, *26*, 6231–6236.
- (19) Kani, R.; Nakano, Y.; Majima, Y.; Hayase, S.; Yuan, C.-H.; West, R. *Macromolecules* **1994**, *27*, 1911–1914.
- (20) Van Walree, C. A.; Cleij, T. J.; Zwikker, J. W.; Jenneskens, L. W. *Macromolecules* **1995**, *28*, 8696–8698.
- (21) Hrkach, J. S.; Matyjaszewski, K. *J. Polym. Sci., Part A: Polym. Chem.* **1994**, *32*, 1949–1956.
- (22) Winokur, M. J.; West, R. *Macromolecules* **2003**, *36*, 7338–7347.
- (23) Perrin, D. D.; Armarego, W. L. F. In *Purification of Laboratory Chemicals*, 3rd ed.; Pergamon Press: Oxford, U.K., 1988.
- (24) Hirth, G.; Saroka, H.; Bannwarth, W.; Barner, R. *Helv. Chim. Acta* **1983**, *66*, 1210–1240.
- (25) Holder, S. J.; Achilleos, M.; Jones, R. G. *Macromolecules* **2005**, *38*, 1633–1639.
- (26) Cleij, T. J.; Jenneskens, L. W. *Macromol. Chem. Phys.* **2000**, *201*, 1742–1747.
- (27) Zeigler, J. M. *Polym. Prepr.* **1986**, *27*, 109.
- (28) Wolff, A. R.; Maxka, J.; West, R. *J. Polym. Sci., Part A: Polym. Chem.* **1988**, *26*, 713–720.
- (29) Hayase, S. *Endeavour* **1995**, *19*, 125–131.

Supporting Information for

Multihydroxy-Functional Polysilanes via an Acetal Protecting Group Strategy

*Valerie S. Reuss and Holger Frey**

Department of Organic Chemistry, Johannes Gutenberg-Universität Mainz, Duesbergweg 10-14, 55099
Mainz, Germany

* Corresponding author. E-mail: hfrey@uni-mainz.de.

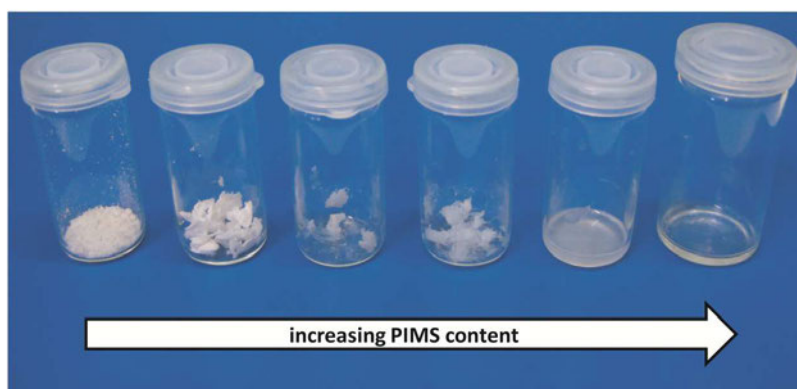


Figure S1. Random poly[di-*n*-hexylsilane-*co*-(isopropylidene glyceryl propyl ether)methylsilane] copolymers (P(DHS-*co*-IMS)) from left to right with IMS contents of 0%, 6%, 11%, 17%, 40%, and 100%, respectively, as determined by ^1H NMR.

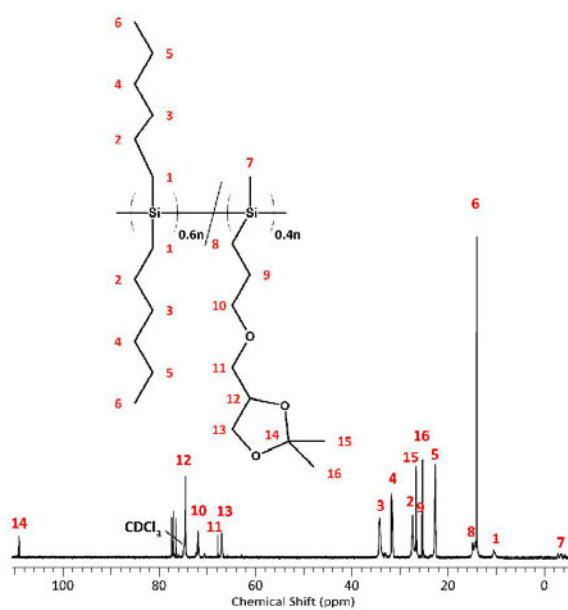


Figure S2. ^{13}C NMR spectrum (CDCl_3 , 75.5 MHz) of P(DHS-*co*-IMS) (40% IMS content) and peak assignment.

$$\%_{IMS} = 100 \cdot \left(\frac{\text{Integral}(1+8) - 8}{26} + 1 \right)^{-1}$$

Formula S1. Calculation of IMS content in P(DHS-*co*-IMS) copolymers based on ^1H NMR spectra.

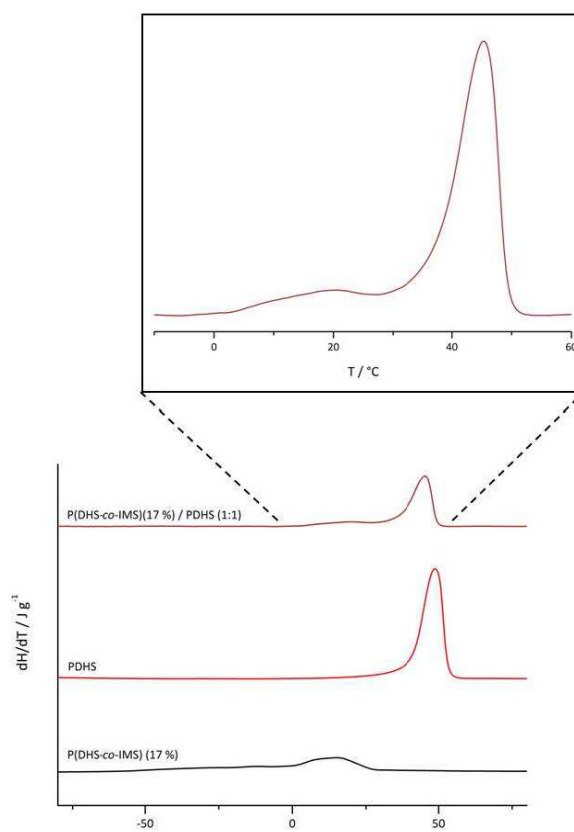


Figure S4. DSC traces of P(DHS-*co*-IMS) (17% IMS content, bottom), PDHS (middle), and a 50 wt% mixture of both compounds (top).

CURRICULUM VITAE

